Pyridone-substituted Pyridyl imines as Functionalised ligands in Coordination Chemistry and Catalysis

Thesis submitted for the degree of Doctor of Philosophy at University of Leicester

2018

Mona H Alhalafi

Department of Chemistry

Pyridone-substituted Pyridyl imines as Functionalised Ligands in Coordination Chemistry and Catalysis

Mona H Alhalafi

Abstract

In this thesis, the synthesis and coordination chemistry of a series of novel NNN and NN proton responsive ligands are described. All the ligands and complexes have been characterized by a combination of multinuclear NMR spectroscopic techniques, mass spectrometry, IR spectroscopy and by single crystal X-ray diffraction studies.

Chapter 1 presents an introduction to functional ligands/complexes and their applications in catalysis.

In Chapter 2, the synthesis and characterisation of a series of OH-functionalised NNN pincer ligands are discussed. The coordination chemistry of these pyridone-substituted pyridyl-imines towards platinum group metals is thoroughly investigated. It is envisaged that these ligands can remain protonated or undergo deprotonation reactions on coordination to give complexes of the type **L1**PdX (X = Cl, OAc), [**HL1**PdCl][X] (X = Cl, PF_6, OTf), **HL1**RuCl$_2$(PPh$_3$) and [**HL1**PtCl][PtCl$_3$(DMSO)]. Additionally, the reactivity of the palladium chloride complexes towards stoichiometric amounts of AgPF$_6$ is explored with a view to introducing two electron donor ligands (L) to the coordination sphere of the metal centre, including acetonitrile and 3,5-lutidine.

In Chapter 3, the synthesis and reactions of two classes of OH-functionalised NN-bidentate ligands towards group 10 metal salts of Pd(II), Pt(II) and Ni(II) including Pd(OAc)$_2$, (MeCN)$_2$PdCl$_2$ (DMSO)$_2$PtCl$_2$ and (DME)NiBr$_2$ are described. A thorough investigation is performed to ascertain the preferred coordination mode and charge on the heterocyclic unit of the NN-ligand. In addition, the reactivity of a selection of the palladium complexes towards some two electron donor ligands (L), including acetonitrile and triphenylphosphine is also studied. Furthermore, the reactions of a selection of the resulting compounds towards acids and bases is investigated to explore their proton responsiveness.

In Chapter 4, the NNN-Ru and -Pd complexes developed in Chapter 2 have been used as catalysts in transfer hydrogenation. Additionally, the NN-nickel complexes described in Chapter 3 have been investigated as pre-catalysts in ethylene oligo-/polymerisation. In both these types of catalysis the effect of the pendant OH group on the particular transformation is probed.

Chapter 5 details the experimental work carried out in Chapters 2-4.

Acknowledgements

I would like to express my gratitude to my supervisor Dr. Gregory Solan for his supervision, inspiring guidance, help, patience and encouragement during the last four years. Thank you for supporting and backing me up no matter what decision I have made and provide plenty of advice and make me feel at home; thank you for being my supervisor. I would also like to thank Professor Eric Hope for his guidance, motivation, patience and helpful discussions throughout this research in the last four years. I also would like to thank Dr. Gerry Griffith, Mr. Kuldip Singh and Mr. Mike Lee for their support with NMR spectroscopy, X-ray crystallography and mass spectroscopy.

I also want to thank all friends I made in the last four years here: Amina, Martyna, Raissa, Rena, Jinting and Rusul. Thank you for supporting me. Thank you for making the lab hour's motivation and friendly environment. I also thank my best friend Budoor Allehyani for her encouragement.

I want to thank my family for their emotional support and their constant encouragement and motivation throughtout my studies. I want to especially thank my brother Ali for making this achievement possible for me because he shouldered the responsibilities after my father passed away, and my sister Zahra for her constant support. I only wish my dad was still alive to see me completing my PhD. I do hope that all of you will be proud of me.

Finally, I would like to thank my dear husband Mohammed, for his support, encouragement and above all in believing in my ability to complete this PhD. Thank you very much, I could have done it without you. Also I thank my lovely daughter (Tala) for being so patient with me. You made me happy when I was sad and relived the stress with your nice words (I Love you mum). Thank you to all my family for supporting me in any possible way.

Contents

Abbreviations

°	degrees
Å	angstrom(0.1 nm)
Ar	aromatic
ASAP	atmospheric solids analysis probe
TOFMS	time-of-flight mass spectrometry
ESI	electrospray ionisation
FAB	fast atom bombardment
HRMS	high resolution mass spectroscopy
MS	mass spectroscopy
MHz	mega Hertz
m/z	mass/charge ratio
h	hours
g	grams
IR	infra-red
^{i}Pr	iso-propyl
OMe	methoxy
TMA	trimethylaluminium
MAO	methylaluminoxane
ESAC	ethylaluminum sesquichloride
DCM	dichloromethane
THF	tetrahydrofuran
MeCN	acetonitrile
HOAc	acetic acid
OAc	acetate
DME	dimethyl ether ethylene glycol
m	multiplet
d	doublet
dd	doublet of doublet
t	triplet
s	singlet
sept.	septet
py	pyridine
ppm	parts per million
OTf	triflate
Me	methyl
NMR	nuclear magnetic resonance
δ	chemical shift
m.p.	melting point
eq.	equivalents

NaCl	sodium chloride
NaH	sodium hydride
Cat.	catalyst
M^+	Molecular ion
MeOH	methanol
$CHCl_3$	chloroform
Ru	ruthenium
OH	hydroxyl
TH	Transfer hydrogenation
Bipy	bipyridine
$AgPF_6$	silver hexafluorophosphate
AgOTf	silver triflate
Me_2Py	3,5-dimethylpyridine
PPh_3	triphenylphosphine
KPF_6	potassium hexafluorophosphate
HBr	hydrobromic acid
NEt_3	triethylamine
Ag_2O	silver oxide
Pd	palladium
Ni	nickel
Pt	platnium

Chapter One

Introduction

1.0 Introduction

1.1 Functionalised Ligands

Among the various approaches being employed worldwide to improve and enhance the applications of transition metal complexes, the functionalisation of ligands has received much attention.[1] Functionalisation is the process of adding new functions, features, capabilities or properties to a inorganic compound by introducing functional groups to the periphery of a ligand that undergoes coordination to the metal centre. In general, functionalisation is performed by attaching the desired group to a compound via a chemical bond. In coordination chemistry, a functionalised ligand relates to a ligand bearing a functional group that remains pendant or partially interacting on coordination to the metal centre. This functional group is then able to impart different properties to the metal complex depending on a variety of factors. Two key reviews have been published on the subject of ligand functionalization.[1,2] The following highlights some of the functions this class of ligand could display in addition to the conventional binding to the metal.

1. Proton responsive ligands are capable of undergoing a change in properties on gaining or losing one or more protons. The proton responsiveness of a ligand can either increase or reduce the scope of the ligand to act as a donor, which allows access to a wider range of ligand properties than can be provided by a classical unresponsive spectator ligand.

2. Ligands with a hydrogen-bonding functionality imply partial proton transfer to or from a suitable partner.

3. Electro-responsive ligands are capable of gaining or losing one or more electrons and hence are able to undergo a change of properties. These ligands can participate in multi-electron reactions such as one electron transfers to or from the metal and to or from the ligand.

4. Photo-responsive ligands are capable of undergoing changes in properties upon irradiation.

5. Ligands that have molecular recognition.

Considering the above-mentioned points, different research groups have focused their work on optimizing and improving catalytic processes based on this ligand

functionalization approach. In particular, some notable advances in the area include i) the reduction in the number of steps in a multistep chemical reaction and ii) the improved separation of a catalyst at the end of a chemical reaction. The control or switching of catalytic properties such as reactivity and solubility are one of the strategies that has been employed for this purpose.[3]

With regard to proton responsive ligands, a ligand is expected to become a poorer σ-donor or a better π-acceptor upon protonation because of the increase in the positive charge or the decrease in the negative charge on the ligand. For example, the monoanionic NH_2 ligand acts as a strong donor to a metal due to the contribution from both σ- and π-electrons while the neutral NH_3 counterpart is a weaker donor and as it has no π-donor component.[1]

The impact of Periana and co-workers[4] research on CH-functionalization of methane to methanol provides an excellent illustration of the use of proton responsive ligands in catalytic reactions. In their study, they found that using strong acidic media, helps to generate the product methanol, by protonation or by formation of a bisulfate ester and hence it prevents further oxidation, ultimately to carbon dioxide. They employed platinum complex **1** for the study in which the ligand is capable of binding to the metal using two of its nitrogen donors of the bipyrimidine ligand while the free nitrogen lone pairs can bind with protons (Figure 1.1). This feature helps to modify the ligand properties by enhancing its π-acceptor capacity. In addition, it prevents the loss of the ligand from the metal in the harsh acidic environment, which normally happens with conventional ligands lacking proton acceptor sites.
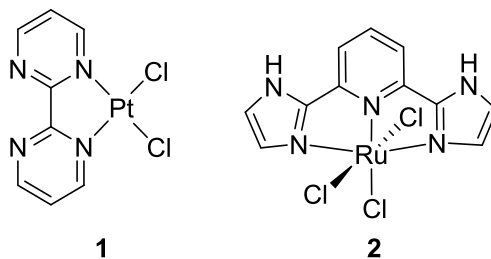
Figure 1.1: Proton responsive complexes, **1** and **2**, developed by Periana and co-workers

In 2010, the same group reported the use of ruthenium complex **2** for investigating the reverse strategy (Figure 1.1).[5] In this study, they employed a strong base instead of an

acid, as the medium for the CH activation reactions. In this complex, the ligand has labile protons that can be removed in a strongly basic environment. This deprotonation has the effect of improving the donor power of the ligand and speeds up the rate of CH activation in the system.

Hydroxy (OH) and amine (R_2NH or RNH_2) groups have the capability to undergo hydrogen bonding which is often considered a key function in organic catalysis and molecular recognition catalysis. The presence of hydrogen bonding groups within the periphery of the ligand can support a metal in binding a substrate by allowing these groups to interact with substrates while they simultaneously coordinate to the metal. Notably, iridium-(FH) complex **3** is only accessible when the ligand contains a hydrogen bonding amine group (Figure 1.2).[6]

3
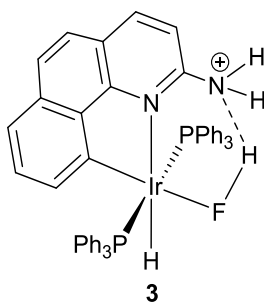
Figure 1.2: Stabilisation of an H-F ligand through FH⋯N hydrogen bonding in **3**

1.2 OH-Functionalised Ligands

In recent years, functionalised ligands have received considerable attention due to their capability to influence the properties of metal complexes and impart enhanced performance.[1] Among the various functional groups available, the hydroxy (OH) group is of particular interest due to its interesting properties such as its ability to undergo hydrogen bonding to stabilise certain structures, to impart water solubility, to be involved in acid-base reactions to allow pH switchability and, in its deprotonated state, to coordinate to metals as a strong donor. For example Shvo's[7,8] and Knolker's[9,10] catalysts (**4** and **5**) both contain hydroxy groups on modified cyclopentadienyl ligands which are found to perform as bifunctional catalysts (Figure 1.3). The M-H centre and the hydroxy group on the ligand can transfer hydride and protons, respectively, and hence can be used as catalysts for transfer hydrogenation reactions.[11-14] Both catalysts were able to show good catalytic activity when applied to outer sphere hydrogen transfer. Further work has

also been carried out using Shvo's catalyst for regio-selective oxidation of internal alkenes to alcohols.[15]
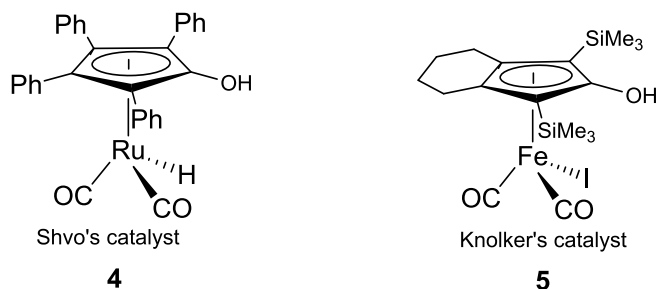
Figure 1.3: Shov's and Knolker's ruthenium (**4**) and iron (**5**) catalysts.

Recently, complexes bearing pyridine-like N-heterocyclic ligands substituted with hydroxyl groups have gained much attention due to the fascinating properties of the hydroxyl group and excellent coordination ability of the pyridine-like N-heterocyclic ligands.[16,17] Both Himeda *et al.*[16] and Yamaguchi *et al.*[17] have demonstrated the efficacy of these hydroxyl-substituted pyridine-like ligands in catalytic hydrogenation and dehydrogenation processes. Both groups have highlighted the added catalytic benefit of incorporating pyridinol ligands into metal complexes as applied to catalysis.
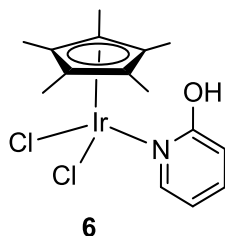
Figure 1.4: Cp*Ir-hydroxypyridine complex **6**.

Iridium complex **6**, which contains a 2-hydroxypyridine ligand, has shown a much higher catalytic activity for the dehydrogenation of secondary alcohols than complexes with 3- or 4-hydroxypyridine (Figure 1.4).[18,19] Indeed, **6** yielded a maximum turnover number (TON) of 2120 for dehydrogenation of 1-phenylethanol while the activity towards primary alcohols was found to be low. Later the same group reported the first homogeneous catalytic system for the efficient reversible and repetitive dehydrogenation-hydrogenation reaction of nitrogen heterocycles using a simple Cp*Ir-dipyridonate complex (**7a**) and its substituted derivatives (**7b-7c**) as the catalyst (Scheme 1.1).[20]
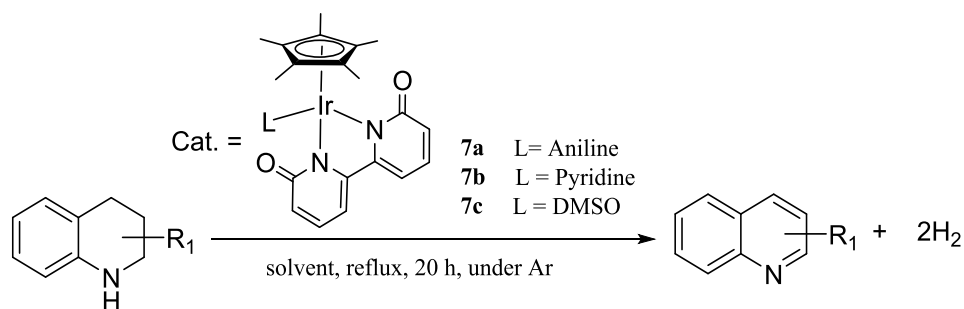
Scheme 1.1: Dehydrogenation of 1,2,3,4-tetrahydroquinolines catalysed by dipyridonate-bearing Cp*Ir complexes **7**.

In 2017, the same group reported a dicationic iridium complex **8** bearing a pyridinol-functionalised N-heterocyclic carbene ligand (Figure 1.5).[21] This complex has been used in dehydrogenation reactions of secondary and primary alcohols in aqueous media to give ketones. In addition, its use in the dehydrogenation of a primary alcohol to give carboxylic acids in aqueous media has been reported. Moreover, they found that using this complex as a catalyst without base in dehydrogenative transformation of primary alcohols to the carboxylic acids reactions showed higher catalytic activity.
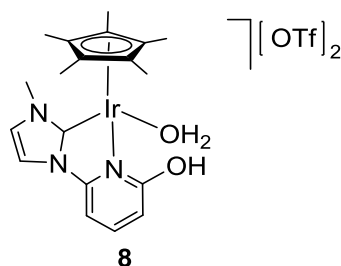
Figure 1.5: Dicationic iridium complex **8**.

Since the discovery of the antitumor properties of some platinum amine complexes, a range of complexes bearing pyridinol-based ligands and their derivatives have been screened for their antitumor activity.[22-24] More recently, the applications of these complexes have been exploited in diverse fields such as catalysis and photochemistry. Breit *et al*. reported a new idea for the construction of bidentate ligands employing self-assembly through hydrogen bonding via the pyridinol-pyridone units of the two phosphine ligands in complex **9** (Figure 1.5).[25] This type of complex proved highly active and regio-selective as a catalyst for the n-selective hydroformylation of terminal alkenes.
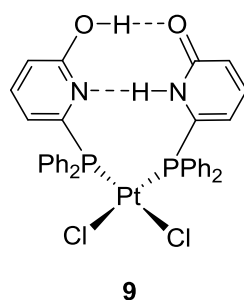
Figure 1.5: Platinum complex, **9**, bearing phosphine-pyridinol/pyridone ligands

Clearly, OH functionalisation of pyridine-based ligands discussed above can lead to some positive effects in catalytic reactions. Central to the role of these ligands is their adaptability in the form of tautomerisation and ease of deprotonation. To understand these specific features the next section explores them in more detail.

1.3.1 Pyridinol-Pyridone tautomerism

Tautomers are constitutional isomers of organic compounds that readily interconvert. 2-pyridinol is a simple but interesting hydroxy substituted aromatic N-heterocyclic ligand that displays lactam-lactim tautomerism between 2-hydroxypyridine (2-pyridinol: the hydroxyl or lactim form) and 2-oxopyrimidine (2-pyridone: the oxo or lactam form) (Scheme 1.2). The lactam form occurs in the crystal structure of 2-pyridone and in crystals of related molecules such as 2-thiopyridone,[26] but the lactim form occurs in crystals of 6-chloro-2-hydroxypyridine.[27] It should be noted that in a 1:1 molecular complex of 2-pyridone and 6-chloro-2-hydroxypyridine,[28] each molecule has the tautomeric form that exists in its own crystal structure. Beak suggested that for 2-pyridone in the vapour state, the lactim form has a slightly lower free energy and hence is favoured.[29] However, in solution form, the lactam form is favoured. Hence, it is concluded that the two forms, the lactam and the lactim exists in random equilibrium and are favoured depending on the conditions of the compound. Similar tautomerism between hydroxyl- and oxo- forms can be expected to exist between 4-hydroxypyridine and 4-oxopyrimidine.
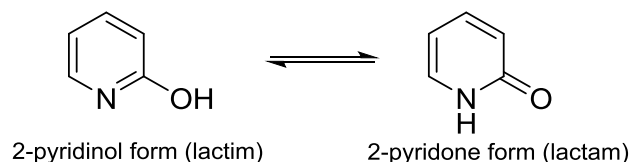
Scheme 1.2: Lactim-lactam tautomerism between 2-hydroxypyridine (2-pyridinol) and 2-oxopyrimidine (2-pyridone).[26]

1.3.2 Pyridinol-Pyridonate interconversions and effects

As mentioned earlier, the presence of a hydroxyl group allows pH switchability to the complex through acid-base equilibria. This can affect the electronic properties of the complexes along with their polarity and water solubility. Himeda *et al.* have developed a novel concept for the design of a catalyst by tuning the acid-base equilibrium between pyridinol and pyridonate for the hydrogenation of CO_2/bicarbonate in water.[30] They first introduced proton responsive ligands such as 4,4'-dihydroxy-2,2'-bipyridine and 4,7-dihydroxy-1,10-phenanthroline, which can form an acid-base equilibrium in the reaction solution (Scheme 1.3). The two key features of this catalytic system are, firstly catalytic activation by electronic effects and secondly catalyst recycling by tuning its water solubility. The inter-conversion between pyridinol and pyridonate leads to simultaneous changes in both electronic and polar properties of the catalyst. Specifically, the hydroxyl form shows moderate electron donating ability and polarity, while the oxyanion form generated by the deprotonation of the hydroxyl form shows strong electron donating ability and polarity. They have also considered that this catalytic system is closely associated with the change in the pH (i.e. from basic solution to acidic solution or vice versa) of the reaction solution during the course of the reaction. The pH change leads to the tuning of the preferred catalyst form; in the reaction step, the catalyst exists as the homogeneous, active and water-soluble oxyanion form, while in the separation step the catalyst exists as the heterogeneous, inactive and water-insoluble hydroxyl form. This property is advantageous for heterogeneous catalysis (i.e. the simplicity of catalyst separation), biocatalysis (i.e. aqueous reaction and pH dependence) and for homogeneous catalysis (i.e. high catalytic performance).
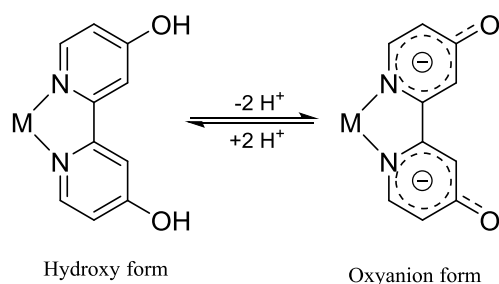
Scheme 1.3: Acid-base equilibrium between hydroxy and oxyanion form.

In 2012, Yamaguchi *et al.*[31] reported two cationic complexes **10** and **11** which were readily soluble in water, however, upon deprotonation these resulted into neutral complexes **10'** and **11'** respectively, which were soluble in organic solvents and sparingly soluble in water. The water soluble metal complex was used for the dehydrogenation of alcohols in aqueous media, which resulted in high yields of aldehydes or ketones with 1 mol% catalyst. The aqueous solution of the catalyst can be reused by simply adding hexane to extract the product, followed by separation. The aqueous phase containing the catalyst can be reused at least eight times without a significant decrease in the catalytic activity. In addition, complex **11'** has been used as a catalyst in perhydrogenation and perdehydrogenation of fused bicyclic N‑heterocycles.[20]
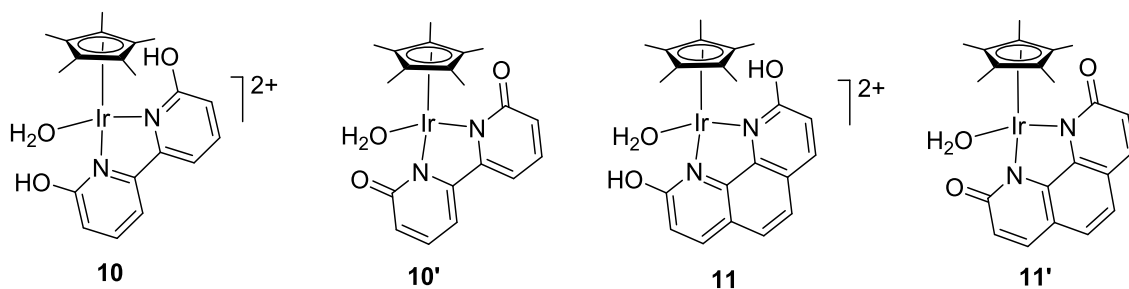
Figure 1.6: Cationic and neutral form of iridium complexes **10, 10'** and **11, 11'**.

Complex **12** was reported by Kelson and Phengsy which had the pyridonate acting as a N-bound monodentate ligand (Figure 1.7).[32] This complex was used for the transfer hydrogenation of ketones in isopropanol, which resulted in high yields (up to 99%) of the alcohol products with an average turnover frequency of up to 780 h^{-1}. In the case of acetophenone, a turnover number of over 1000 was obtained.
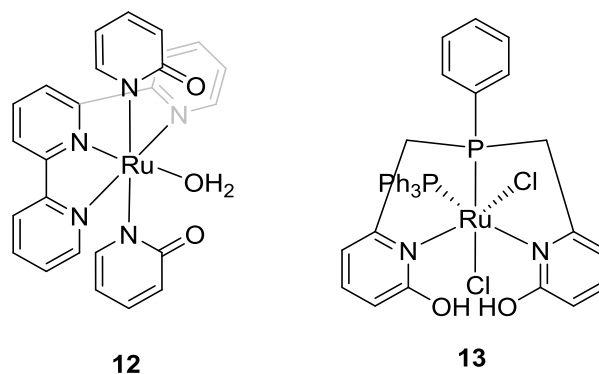
Figure 1.7: NNN-Ru(II) complexes **12** and **13** bearing pyridonate and pyridinol ligands

Ruthenium complex **13** (Figure 1.7) has been reported by Achard *et al*. and contains pyridinol groups as part of a tridentate NPN ligand.[33] This complex has been used for the transformation of primary alcohols to esters and for the hydrogenation of carbon dioxide to formic acid.[33] Moreover, it has been used in the cross coupling of alcohols to form α–alkylated ketones.[34] In their studies they found that the complex exhibited good catalytic activity with up to 99% yield of the product.

Undoubtedly, this area of ligand-assisted catalysis will further evolve in future due to the intriguing properties of functional ligands and in particular hydroxy-pyridines. There is much scope for understanding their applications with respect to palladium-based catalysis as this area is slightly underexplored, however, these complexes have been widely employed in many other applications such as medicinal chemistry, in particular towards anti-tumour treatments.[35] In 1981, Kong and Rochon,[35] who were investigating the anti-tumour properties of platinum-pyrimidine complexes, reported similar palladium complexes. Among the range of complexes, **14** was described as having a pyridinol-based ligand and was suggested to coordinate to palladium via the O atom in the pyridone form (Figure 1.8). Later, the same complex was applied to the preparation of carbonic/carbonate esters by Watanabe and Masunaga *et al*.[36-40] They have also used the same complex as a catalyst for the Wacker reaction in a separate study.[41]
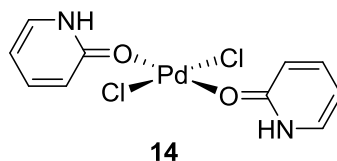
Figure 1.8: Palladium(II) dichloride complex **14** bearing two O-bound 2-pyridones

10

In 2005, Huq et al.[42] reported the N-bound pyridinol isomer of **14**, complex **15** (Figure 1.9). Complex **15** has been investigated for anti-tumour activity against the human ovarian cancer cell lines and it was found that these compounds have significant anti-tumour activity although less than cisplatin. Complex **15** has also been applied in Sonogashira coupling for indole synthesis.[43] Cheng et al.[44] have reported a trinuclear palladium complex **16** bearing N-bound 2-hydroxypyridine, which was found to exhibit significant anticancer activity against the cell lines A2780 (Figure 1.9).
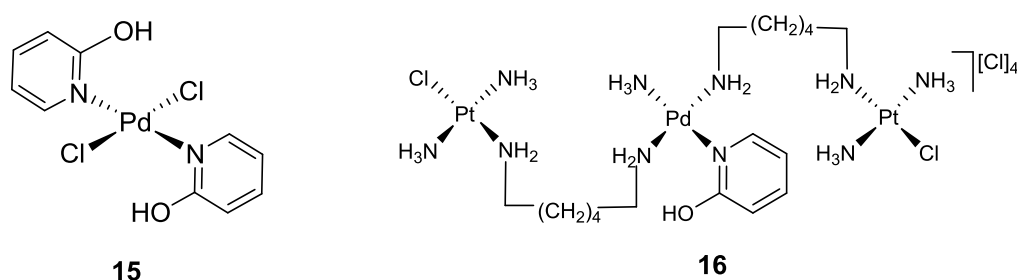
Figure 1.9: Palladium complexes, **15** and **16**, bearing N-bound pyridinols

A binuclear head-to-head Pd(II) complex with 2-pyridonate as a bridging ligand has been described by Matsumoto et al. (Figure 1.10).[45] The head-to-head (HH) structure (**17**) was confirmed by a single crystal X-ray diffraction study. The head-to-tail (HT) isomer (**18**) could not be isolated as it was not stable under the reaction conditions because of the rapid HT to HH isomerization and could only be observed in solution. This is fascinating as it demonstrates the lability of the 2-pyridonate in its binding to the two palladium centers thus switching between 'head-to-head' and 'head-to-tail' isomers.
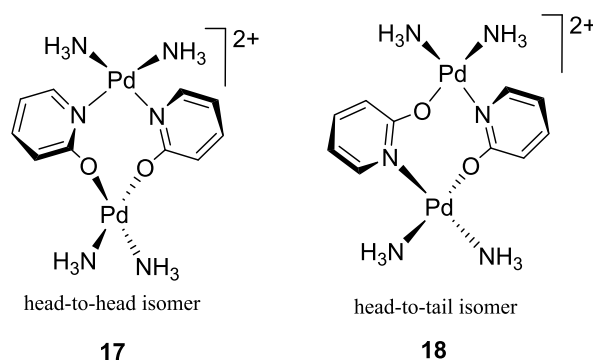
Figure 1.10: Dimeric Pd complexes, **17** and **18**, showing 'head-to-head' and 'head-to-tail' isomers.

Following this brief introduction to the interesting properties of an OH functionality in coordination chemistry and catalysis, we now focus deeply more on complexes bearing proton responsive ligands and their activity in catalytic reactions.

1.4 Complexes bearing proton responsive ligands in catalysis

The selective oxidation of alcohols to the corresponding aldehydes and ketones has received much attention due to the wide application of the products in organic chemistry and industrial chemistry.[46] Therefore, the use of transition metals has been well studied to promote these reactions with a view to using less toxic oxidants such as hydrogen peroxide, oxygen or acetone and increase its environmental applicability. However, the oxidation of an alcohol with a free oxidant will release hydrogen gas, which is superior from the viewpoint of atom economy.[19] Nevertheless, water is considered as a green solvent, hence, utilisation of aqueous medium for a transition-metal catalysed reactions is of great interest. Different research groups have applied various strategies to enhance the hydrophilic behaviour of complexes, such as by the introduction of an ionic or a strongly polar functionality such as carboxylate, polyether, sulfonate or ammonium to the desired ligand. Liu *et al.* reported a water soluble (η^6-arene)-Ru(II) complex **19a** and **19b** based on a pyrazolyl-naphthyridine ligand modified with a carboxylate group (Scheme 1.4).[47] This complex acted as an excellent catalyst for the reduction of aldehydes and ketones presumably due to their water solubility.
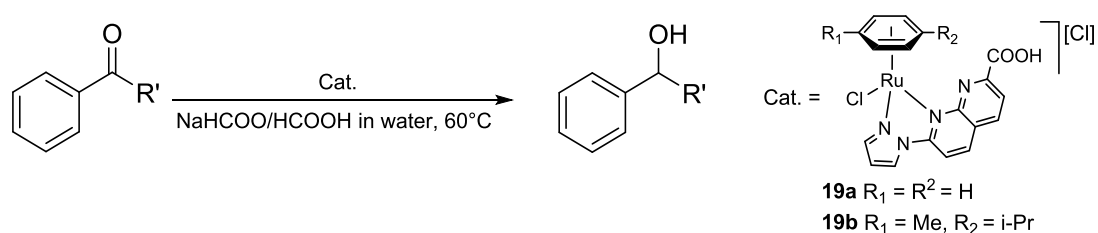
Scheme 1.4: Reduction of a carbonyl compound in aqueous medium using **19** as catalyst.

In 2015, Szymczak *et al.*[48] reported the Ru-based pincer complex **20** in which a bifunctional ligand framework bearing a pendant proton-responsive hydroxyl group is present. This complex was found to be an effective catalyst for the hydroboration of nitriles (Figure 1.11). It also showed high catalytic activity in the hydroboration of a variety of aromatic nitriles at room temperature with an initial TOF = 1.2 s^{-1}.
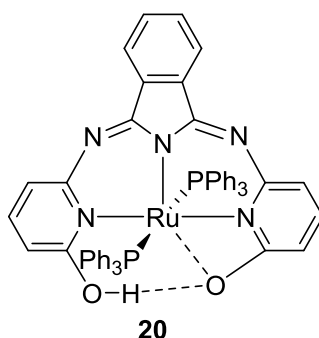
Figure 1.11: Ru-based NNN-pincer complex **20**

Hydroxyl-substituted bipyridine ligands have been the subject of many studies in this area using a number of different metals. For example, palladium complexes coordinated by bidentate bipyridine ligands bearing two hydroxyl groups at different positions on the heterocyclic rings have been reported by Cadierno *et al.*[49] The palladium(II) complex [PdCl$_2$(6,6'-(OH)$_2$-2,2'-bipy] (**21a**) was an excellent pre-catalyst for the selective conjugate addition of aryl-boronic acids to an α,β-unsaturated carbonyl compound under environmentally friendly aqueous media in air when compared to the other palladium complexes with an OH at the 3,4 and 5 positions (Scheme 1.5).
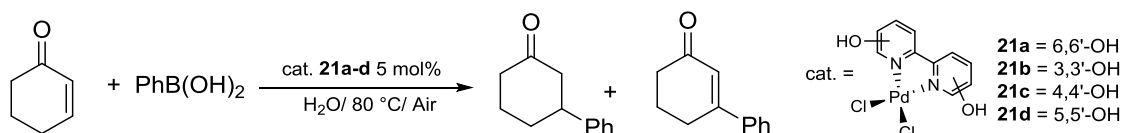
Scheme 1.5: Conjugate addition of arylboronic acids to an α,β-unsaturated carbonyl compound using **21** as catalyst

Fujita, Yamaguchi and co-workers developed a series of iridium complexes bearing bidentate 2-hydroxypyridyl derivatives for the dehydrogenative oxidation of an alcohol. In 2011 they reported a new iridium catalyst (**22**) coordinated by a C,N-chelate ligand for the dehydrogenation oxidation of primary and secondary alcohols which exhibited high catalytic activity and gave up to 90% of the ketone in the presence of NaOMe as base (Scheme 1.6).[19]
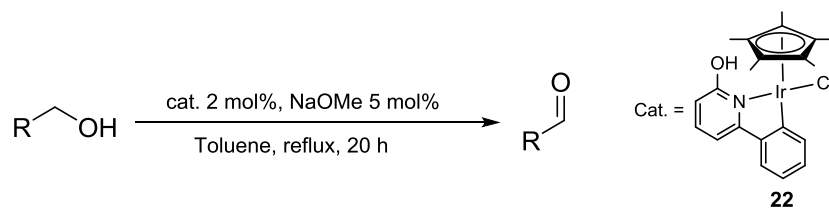
Scheme 1.6: Dehydrogenation oxidation of alcohol using C,N-chelated Ir complex **22**

Later the same group reported the dehydrogenative oxidation of an alcohol using the water soluble Cp*Ir complex **10** bearing a NN-bipyridine-based functional ligand. They found that the complex exhibited high catalytic activity with a high turnover number, which was the first example of the dehydrogenation of an alcohol in aqueous media (Scheme 1.7).[31] Furthermore, the re-use of the catalyst for the dehydrogenation oxidation of alcohol was also examined. They found that after the third run the catalyst was still active for the reaction affording up to 95%.
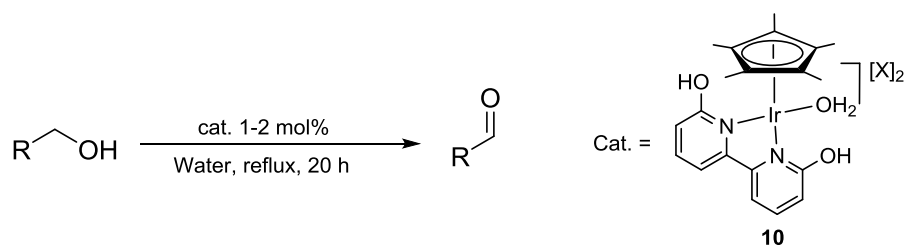
Scheme 1.7: Dehydrogenation oxidation of alcohol with water soluble Cp*Ir complex **10**

Rhodium-COD complex **23** bearing 6,6'-dihydroxy-2,2'-bipyridine was reported by Britovsek *et al.* (Figure 1.12).[50] This complex was used in the catalytic carbonylation of methyl acetate to acetic acid in water under an atmosphere of CO giving a TOF up to 180 h^{-1}.
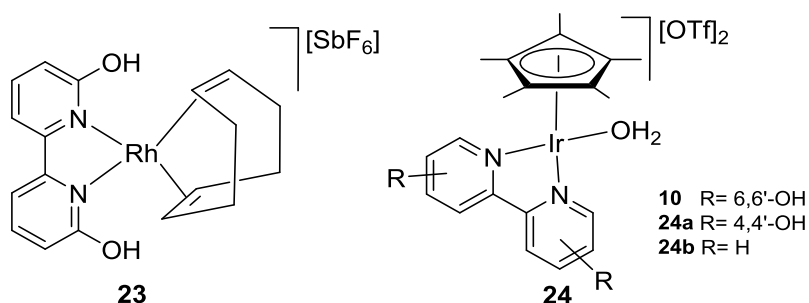
Figure 1.12: Rhodium and iridium complexes bearing dipyridinol ligands, **23** and **24**

In 2014, the Li group used the cationic Cp*Ir complex, **10**, bearing the 6,6'-dihydroxy-2,2'-bipyridine, developed by the Fujita and Yamaguchi group, in the N-alkylation of

sulphonamides with alcohol in water (Figure 1.12). They used 1 mol% of catalyst and 0.1 equivalent of Cs_2CO_3 as base in aqueous media. They found that the complex was highly efficient catalyst affording up to 92% of the product. By contrast, using the same complex without OH units gave no reaction. Therefore, the presence of the OH units in the bipyridine ligand is crucially important for N-alkylation of sulphonamides with an alcohol.[51]

Shortly afterwards, the same group reported the alpha-alkylation of ketone with primary alcohol using Cp*Ir-bipyridonate catalyst **10'** (Scheme 1.8). The reaction was carried out under mild conditions and in air with 1 mol% of catalyst. This complex was a highly effective and flexible catalyst under mild and environmentally friendly conditions. Additionally, this complex was found to be highly active in the alpha-methylation of ketones with methanol.[52]
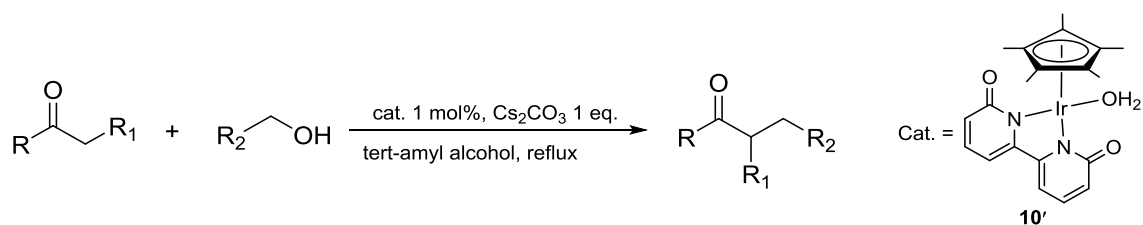
Scheme 1.8: Alpha-alkylation of ketones with a primary alcohol using **10'** as catalyst

Moreover, the cationic iridium complex **10** shown Figure 1.12, bearing a bidentate 6,6'-dihydroxy-2,2'-bipyridine, was used as well in the dehydrogenative lactonization of diols in aqueous media[53] and in the production of hydrogen from methanol-water solution.[54] With regard to the hydrogen production reaction, the group also tested iridium complexes bearing bidentate 4,4'-dihydroxy-2,2'-bipyridine **24a** and 2,2'-bipyridine **24b**. They found that the complex **24b** with 2,2'-bipyridine ligand without a hydroxyl moiety and complex **24a** with 4,4'-dihydroxy-2,2'-bipyridine did not show any catalytic activity. This indicated that the OH functionality at position six is important to be make the catalyst effective. Additionally, this catalyst was found to be highly active in water oxidation in combination with pH switching.[55] This framework offers insight into how hydrogen bonds and how this acid-base sensitive group can influence organometallic catalysis.

Recently, Szymczak *et al.* have been developed the tridentate ruthenium complex **25** bearing 6,6´-dihydroxy-terpyridine as a proton-responsive bifunctional ligand (dhtp)

(Figure 1.13).[56] This complex efficiently catalysed the transfer hydrogenation of a range of ketones in the presence of KO^{t}Bu in isopropanol and the TOF number was up to 82 h^{-1} to form 1-phenylethanol. However, the same group reported later some difference in selectivity and activity of ruthenium complexes, which have OH group at different positions (Figure 1.13). They studied the effect of the OH groups on the electronic environment of the metal centre upon deprotonation and hence providing a more electron rich ruthenium centre under basic conditions. They showed that the Ru complex with an OH group at the 2-position was superior when compared to the similar ruthenium complexes having 4,4´-dihydroxy-terpyridine or terpyridine as the ligand (Figure 1.13).[57] Therefore, deprotonation of the OH group controls the electronic properties of the metal centre, providing a more electron rich ruthenium centre under basic conditions.
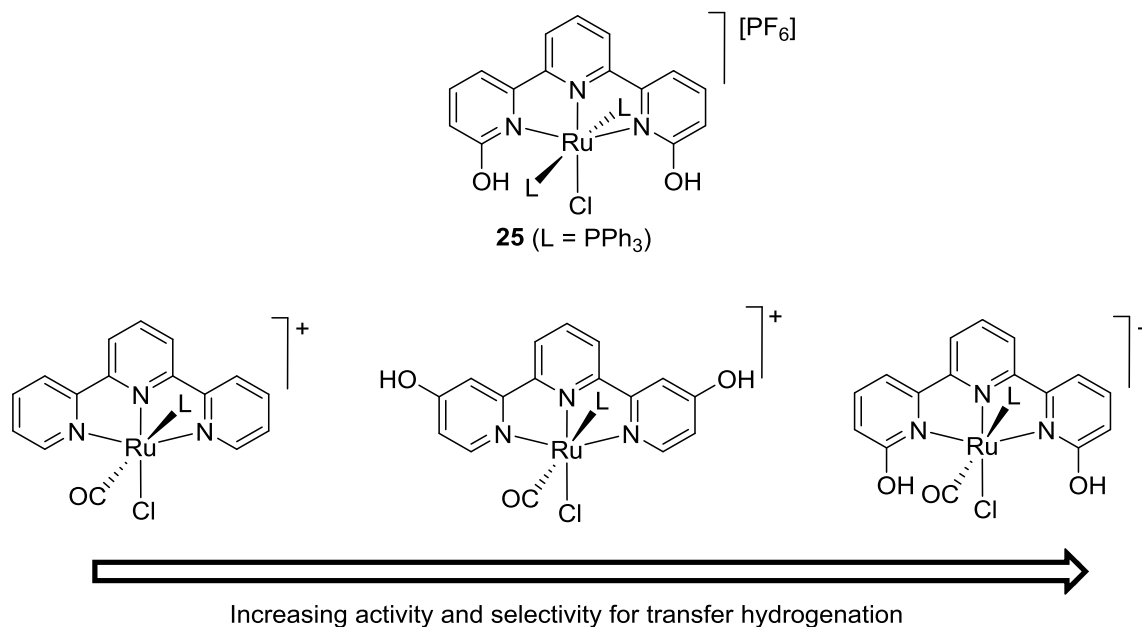
Figure 1.13: Influence of the OH group on the activity and selectivity of catalysis

Kundu's group synthesized another similar ruthenium complex, **26** (Figure 1.14) based on the ligand 2-(2-pyridyl-2-ol)-1,10-phenanthroline, which has been used as a catalyst in the transfer hydrogenation of ketones and nitriles with 0.1 mol% of catalyst in 30 minutes. The complex showed high catalytic activity with TOF up to 2.40 x 10^3 h^{-1} for the transfer hydrogenation of acetophenone. In addition, the complex displayed an interaction between the –OH group of the ligand with a metal bound chloride, which probably leads to strong metal-ligand cooperativity in the transfer hydrogenation reaction.[58]
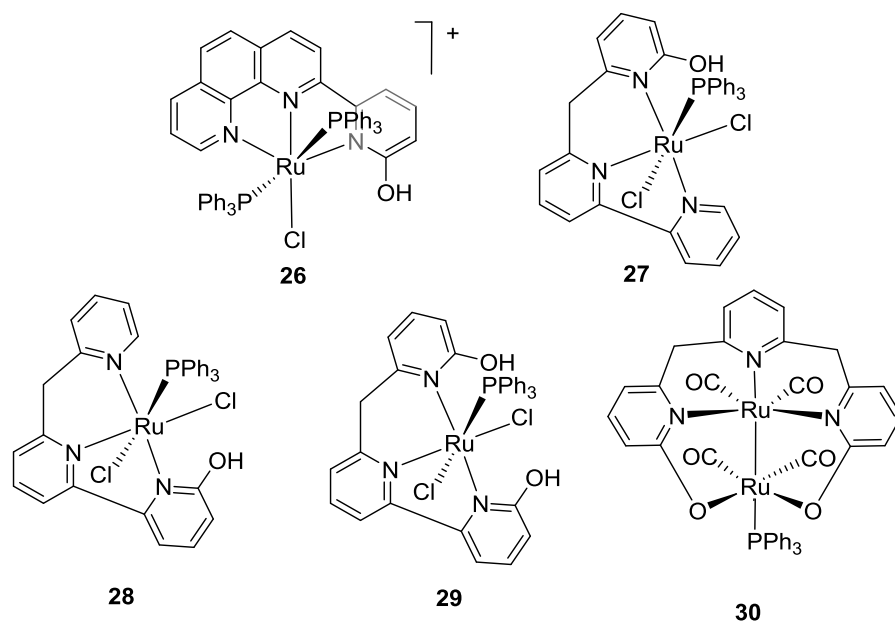
Figure 1.14: Some examples of functionalised NNN-Ru(II) complexes, **26**-**30**

The ruthenium(II) complex **27** bearing a NNN ligand with 2-hydroxypridylmethylene unit was reported by Chen *et al.* (Figure 1.14).[59] **27** has been used as an active catalyst in transfer hydrogenation of ketones to alcohols using 1 mol% of catalyst and 10 mol% of K^{t}OBu as base in 10 minutes. They found that this complex exhibits high catalytic activity in transfer hydrogenation with a TOF number up to 1.16 x 10^3 h^{-1}.

Then later in 2017, the same group developed some active catalysts, **28-30**, in the transfer hydrogenation of ketones (Figure 1.14). However, this time the position of the OH has been changed when compared to that in **27**. They found that **28** showed a better catalytic activity than either **29** or **30** but it is not as active as **27**, which means that for complexes **29-30** the position of hydroxyl group is also important for the catalytic activity. The absence of hydroxyl group in bimetallic **30** was used to explain its lower activity when compared to the **28** and **29**.[60]

1.5 Pyridylimines and dipyridylimines

Pyridylimines and dipyridylimines represent two other classes of NN and NNN ligands that have received considerable interest over the last decade or so. Pyridylimines contain a pyridine nitrogen donor along with an imine group attached to the 2-position of the pyridine, while for dipyridylimines the imine group is attached the 6-position of the 2,2'-bipyridine (Figure 1.15).
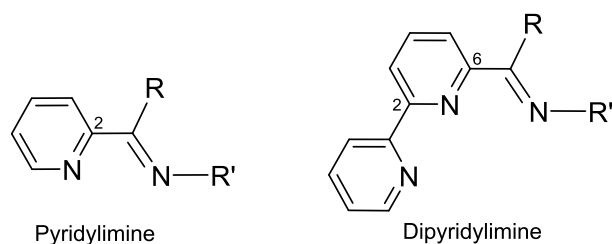
Figure 1.15: General structure of a pyridylimine and a dipyridylimine

Pyridylimines have the ability to bind strongly to metals such as Pd and Pt due to the chelate effect and the strong electron donating ability of the nitrogen atoms.[61,62] These types of ligands have been coordinated to a range of different metals and have showed broad applications as catalysts in a variety of different reactions including C-H bond activation,[63] polymerisation[64] and C-C bond forming reactions (cross coupling reactions).[65]

Laine *et al.*[66] developed pyridylimine-based palladium complexes (**31**), which on activation with MAO, were active for norbornene polymerisation under mild reactions (Figure 1.16). All the systems gave quantitative amounts of polymer in only two hours. Alt and Taubmann used a similar ligand in 2008, which facilitated CH activation (Figure 1.16). They found that the Ir complex bearing a pyridylimine ligand, **32**, was an active catalyst for the CH activation of cyclooctane (dehydrogenation of alkane).[63] In addition this class of ligand has been used for supporting catalysts that promote the formation of carbon-carbon bonds.[67]
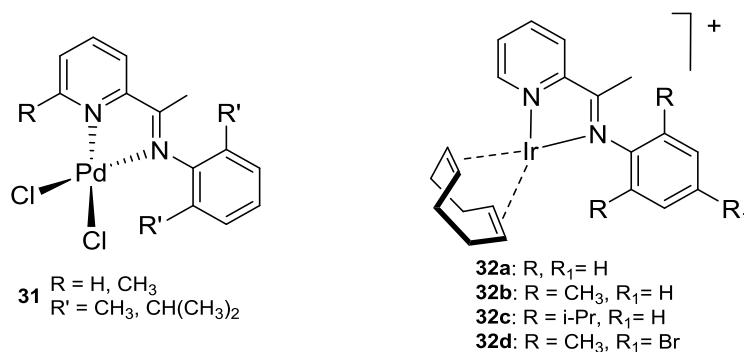
Figure 1.16: Pyridylimines as NN-ligands for palladium (**31**) and iridium (**32**) complexes

Some additional importance of pyridylimines was demonstrated by Nagesh *et al.* in the form of *in vitro* anticancer drugs.[68] The group developed a novel sugar-boronate ester scaffold tethered to a pyridylimine palladium(II) complex **33** (Figure 1.17). These complexes displayed significant cytotoxicity against the MDA-MB-231 and HT-29 cancer cell lines, which was superior to that observed for cisplatin.
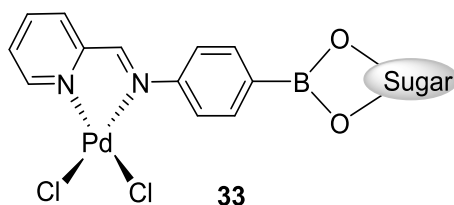
Figure 1.17: Sugar-boronate ester scaffold tethered pyridylimn palladium (II) complexes **33**

By contrast, dipyridylimines have received relatively less attention. Nevertheless, they have been coordinated to a range of different metals including Fe(II), Co(II) and Ni(II), with a view to applying these systems as catalysts in the polymerisation or oligomerisation of ethylene and in the hydrosilylation of olefins. Bianchini *et al.*[69] have been reported a dipyridylimine-Co(II) complex **34** which has been used as a pre-catalyst in the oligomerisation of ethylene with MAO as co-catalyst (Figure 1.18). Moreover, this ligand has been used by Gibson *et al.* to coordinate to iron(II) metal to generate a dipyridylimine-Fe(II) complex **35** (Figure 1.18).[70] This iron(II) complex, in the presence of MAO is highly active (up to 570 g mmol^{-1} h^{-1} bar^{-1}) for the oligomerisation of ethylene. The Solan *et al.* have reported the dipyridylimine-Ni(II) analogue **36** that on activation with MAO is modestly active for ethylene oligomerisation.[71]
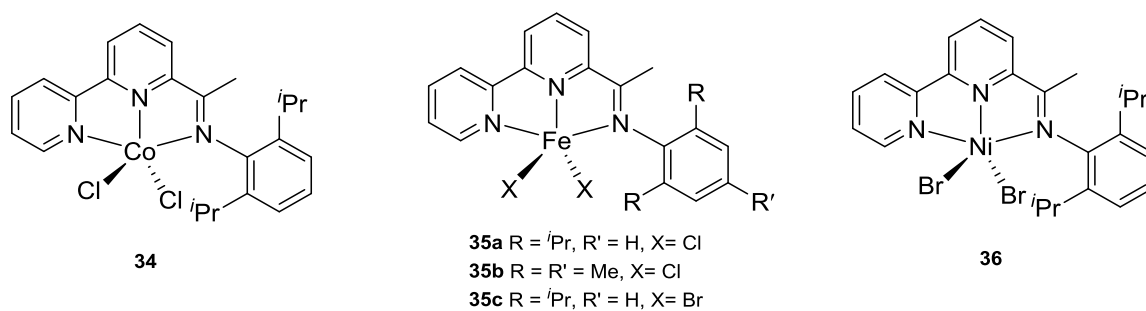
Figure 1.18: Co, Fe and Ni-based dipyridylimine pincer complexes, **34-36**

Recently in 2017, complex **35c** has been used by Nakazawa *et al.* in the hydrosilylation of olefins (Scheme 1.9).[72] Indeed **35c**, bearing a dipyridylimine exhibited high catalytic activity for hydrosilylation of terminal olefins with primary, secondary and tertiary silanes.
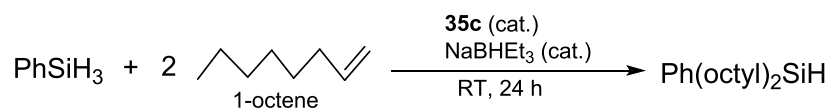
Scheme 1.9: Hydrosilylation of terminal olefins using **35c**

1.6 Aims and objectives of the thesis

It is clear from the introduction that the application of pyridone/pyridinol-containing ligands in platinum group chemistry and catalysis is an emerging area that has been the subject of a large number of reports in recent years. Furthermore, it is apparent that NN-pyridylimines, and to a lesser degree the NNN-dipyridylimines, represent two important classes of nitrogen donor ligands that have found importance in a wide range of applications. The presence of an N-aryl group makes these bi- and tridentate ligands attractive as the electronic and steric properties can be systematically varied as can the solubility properties of the resultant complexes.

In this thesis, we are aiming to introduce an OH-functionality to the periphery of an NNN-dipyridylimine and an NN-pyridylimine with a view to exploring the coordination chemistry of the resultant ligands and their proton responsiveness. Platinum group metals (*e.g.*, Pd, Pt, Ru) are the main focus of the study (the exception being nickel) and the application of their complexes as catalysts in transfer hydrogenation and ethylene oligo-/polymerisation will be explored. In particular, three main classes of ligand are being targeted namely the 6-(2-pyridone)-2-pyridylimines (H**L1**), 6-imino-2-pyridones (H**L2**) and 6-imino-4-pyridones (H**L3**) (Figure 1.19). To allow an investigation of steric and electronic properties, three examples are being sought for each class, H**L1**$_a$/H**L1**$_b$/H**L1**$_c$, H**L2**$_a$/H**L2**$_b$/H**L2**$_c$ and H**L3**$_a$/H**L3**$_b$/H**L3**$_c$, that differ in the substitution pattern of the N-aryl group (*e.g.*, Ar = 2,6-diisopropylphenyl, 2,4,6-triisopropylphenyl, 2,4,6-trimethylphenyl and 2,6-diisopropyl-4-bromophenyl).

In Chapter 2, the synthesis and reactivity of OH-functionalised H**L1**$_{a-c}$ towards the platinum group metals, Pd, Pt and Ru and in particular the divalent metal salts, $Pd(OAc)_2$, $(MeCN)_2PdCl_2$, $Na_2[PdCl_4]$, $(DMSO)_2PtCl_2$ and $RuCl_2(PPh_3)_3$ is explored. When coordinated, any proton responsiveness or reversible proton transfer processes within the ligand will be investigated. To complement this work, complexes will also be targeted bearing the structurally related NNN ligands **L1**$_{OMe}$ and **L1**$_H$ (Figure 1.19). Additionally, the reactivity of selected palladium complexes towards stoichiometric amounts of $AgPF_6$ will be explored with a view to introducing a range of two electron donor ligands (L) to the coordination sphere of the metal centre, including acetonitrile, 3,5-lutidine, 3,5-dichloropyridine and triphenylphosphine.

Chapter 3 describes the synthesis and reactions of two classes of OH-functionalised NN-bidentate ligand namely, H$L2_{a-c}$ and H$L3_{a-c}$, towards a range of group 10 metal salts of Pd(II), Pt(II) and Ni(II) including Pd(OAc)$_2$, (MeCN)$_2$PdCl$_2$ and (DME)NiBr$_2$. A thorough investigation is performed to ascertain the preferred coordination mode and charge on the heterocyclic unit of the NN-ligand. Furthermore, since the ligands are expected to be proton responsive, the reactions of a selection of the resulting compounds towards acids and bases will be investigated. In addition, the reactivity of a selection of the palladium complexes towards a range of two electron donor ligands (L), including acetonitrile, and triphenylphosphine is also studied.

In Chapter 4, the application of the NNN-Ru complexes developed in the thesis will be assessed as catalysts in transfer hydrogenation. Additionally, an investigation of the NN-nickel complexes will be evaluated as catalysts in ethylene oligo-/polymerisation.

Chapter 5 details the experimental work discussed in Chapters 2-4.
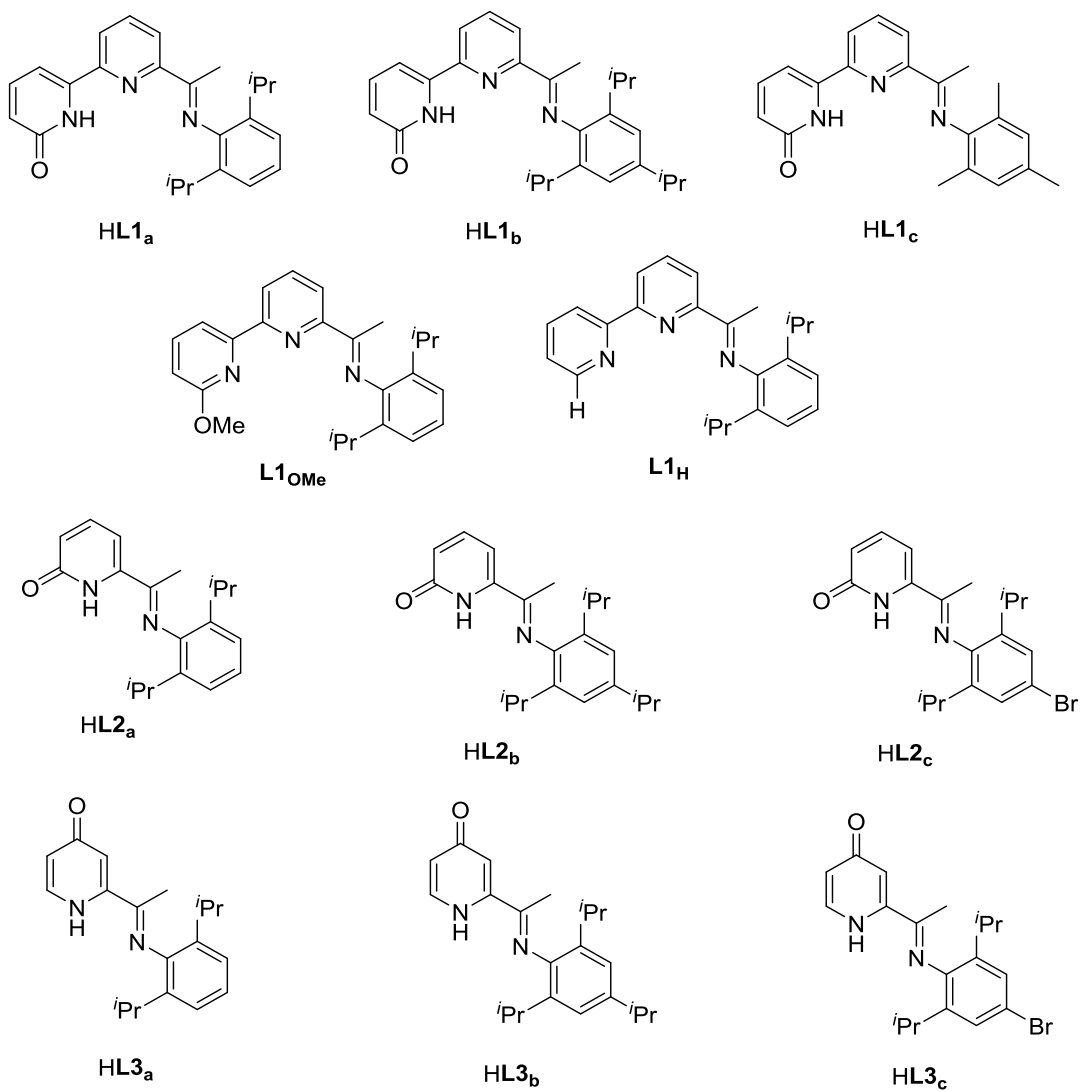
Figure 1.19: (Pro-)ligands to be targeted in the thesis

References

1. R. H. Crabtree, *New J. Chem.,* 2011, **35**, 18.

2. W-H. Wang, J. T. Muckerman, E. Fujita and Y. Himeda, *New J. Chem.,* 2013, **37**, 1860.

3. A. M. Allgeier, C. A. Mirkin, *Angew. Chem. Int. Ed*. 1998, **37**, 894.

4. R. A. Periana, D. J. Taube, S. Gamble, H.Taube, T. Satoh and H. Fujii, *Science*, 1998, **280**, 560.

5. B. G. Hashiguchi, K. J. H. Young, M. Yousufuddin, W. A. Goddard and R. A. Periana, *J. Am. Chem. Soc.*, 2010, **132**, 12542.

6. D. H. Lee, H. J. Kwon, P. P. Patel, L. M. Liable-Sands, A. L. Rheingold and R. H. Crabtree, *Organometallics,* 1999, **18**, 1615.

7. Y. Blum and Y. Shvo, *J. Organomet. Chem.*, 1985, **282**, C7.

8. Y. Shvo, D. Czarkie, Y. Rahamim and D. F. Chodosh, *J. Am. Chem. Soc.*, 1986, **108**, 7400.

9. H. J. Knolker, E. Baum, H. Goesmann and R. Klauss, *Angew. Chem.*, *Int. Ed.*, 1999, **38**, 2064.

10. C. P. Casey and H. Guan, *J. Am. Chem. Soc.*, 2007, **129**, 5816.

11. B. L. Conley, M. K. Pennington-Boggio, E. Boz and T. J. Williams, *Chem. Rev.*, 2010, **110**, 2294.

12. O. Eisentein and R. H. Crabtree, *New J. Chem.*, 2013, **37**, 21.

13. R. M. Bullock, *Angew. Chem., Int. Ed.,* 2007, **46**, 7360.

14. R. M. Bullock, *Chem-Eur. J.,* 2004, 10, 2366.

15. Y. Yuki, K. Takahashi, Y. Tanaka and K. Nozaki, *J. Am. Chem. Soc.*, 2013, **135**, 17393.

16. Y. Himeda, N. Onozawa-Komatsuzaki, H. Sugihara, H. Arakawa and K. Kasuga, *Organometallics,* 2004, **23**, 1480.

17. R. Yamaguchi, C. Ikeda, Y. Takahashi and K. Fujita, *J. Am. Chem. Soc.*, 2009, **131**, 8410.

18. K. Fujita, N. Tanino and R. Yamaguchi, *Org. Lett.*, 2007, **9**, 109.

19. K. Fujita, T. Yoshida, Y. Imori and R. Yamaguchi, *Org. Lett.*, 2011, **13**, 2278.

20. K. Fujita, Y. Tanaka, M. Kobayashi and R. Yamaguchi, *J. Am. Chem. Soc.*, 2014, **136**, 4829.

21. K. Fuijta, R. Tamura, Y. Tanaka, M. Yoshida, M. Onoda and R. Yamaguchi, *ACS Catal.,* 2017, **7**, 7226.

22. L. S. Hollis and S. J. Lippard, *J. Am. Chem. Soc.,* 1981, **103**, 1230.

23. L. S. Hollis, A. R. Amundsen and E. W. Stern, *J. Med. Chem.,* 1989, **32**, 128.

24. L. S. Hollis and S. J. Lippard, *J. Am. Chem. Soc.,* 1983, **105**, 3494.

25. B. Breit and W. Seiche, *J. Am. Chem. Soc.,* 2003, **125**, 6608.

26. R. B. Penfold, *Acta Cryst.,* 1953, **6**, 707.

27. A. Kvick and I. Olovsson, *Ark. Kemi.,* 1968, **30**,71.

28. J. Almlof, A. Kvick and I. Olovsson, *Acta Cryst.,* 1971, **B27**, 1201.

29. (a) P. Beak, *Acc. Chem. Res.,* 1977, **10**, 186. (b) H. W. Yang and B. M. Craven, *Acta Cryst.,* 1998, **B54**, 912.

30. Y. Himeda, *Eur. J. Inorg. Chem.,* 2007, **25**, 3927.

31. (a) R. Kawahara, K. Fujita and R. Yamaguchi, *J. Am. Chem. Soc.*, 2012, **134**, 3643. (b) R. Kawahara, K. Fujita and R. Yamaguchi, *Angew. Chem. In. Ed.,* 2012, **51**, 12790.

32. E. P. Kelson and P. P. Phengsy, *J. Chem. Soc., Dalton Trans.,*2000, 4023.

33. A. R. Sahoo, F. Jiang, C. Bruneau, G. V.M .Sharma, S. Suresh, T. Roisnel, V. Dorcet and M. Achard, *Catal. Sci. Technol.,* 2017, **7**, 3492.

34. A. R. Sahoo, G. Lalitha, V. Murugesh, C. Bruneau, G. V.M .Sharma, S. Suresh and M. Achard, *J. Org. Chem.,* 2017, **82**, 10727.

35. P. C. Kong and F. D. Rochan, *Can. J. Chem.,* 1981, **59**, 3293.

36. E. Watanabe, K. Murayama, K. Ida, K. Wada and Y. Kasori, *Japan Pat.*, EP532861A1, 1993.

37. H. Watanabe and K. Murayama, *Japan Pat.*, JP05255197A, 1993.

38. H. Watanabe, K. Murayama, K. Ida, K. Wada and Y. Kasori, *Japan Pat.*, JP04356446A, 1992**.**

39. N. Yamagata and T. Masunaga, *Japan Pat.*, JP08169863A, 1996.

40. J. Yasumaru, H. Watanabe, T. Masunaga and M. Higashijima, *Japan Pat.,* JP07138207A, 1995.

41. M. Higashijima, T. Masunaga, Y. Kojima, E. Watanabe and K. Wada, *Stud. Surf. Sci. Catal.,* 1995, **92**, 319.

42. F. Huq, H. Tayyem, A. Abdullah, P. Beale and K. Fisher, *Asian J. Chem.*, 2005, **18**, 65.

43. S. Chouzier, M. Gruber and L. Djakovitch, *J. Mol. Catal. A: Chem.*, 2004, **212**, 43.

44. H. Cheng, F. Huq, P. Beale and K. Fisher, *Eur. J. Med. Chem.,* 2006, **41**, 896.

45. K.Matsumoto, H. Moriyama and K. Suzuki, *Inorg. Chem.,* 1990, **29**, 2096.

46. (a) The Activation of Dioxygen and Homogeneous Catalytic Oxidation, ed. D. H. R. Barton, A. E. Martell, D. T. Sawyer, *Plenum Press, New York*, **1993**. (b) G. Tojo and M. Fernandez, Oxidation of Alcohols to Aldehyde and Ketones: A Guide to Current Common Practice, *Springer, New York*, **2006.**

47. C. Y. Huang, K. Y. Kuan, Y. H. Liu, S. M. Peng and S. T. Liu, *Organometallics*, 2014, **33**, 2831.

48. J. B. Geri and N. K. Szymczak, *J. Am. Chem. Soc.,* 2015, **137**, 12808.

49. E. T-Mendivil, J. Diez and V. Cadierno, *Catal. Sci. Technol.*, 2011, **1**, 1605.

50. C. M. Conifer, R. A. Taylor, D. J. Law, G. J. Sunley, A. J. White and G. J. Britovsek, *Dalton Trans.*, 2011, **40**, 1031.

51. P. Qu, C. Sun, J. Ma and F. Li, *Adv. Synth. Catal.,* 2014, **356**, 447.

52. N. Wang, J. Ma and F. Li, *J. Org. Chem.,* 2014, **79**, 10447.

53. K. Fujita, W. Ito and R. Yamaguchi, *ChemCatChem.,* 2014, **6**, 109.

54. K. Fujita, R. Kawahara, T. Aikawa and R. Yamaguchi, *Angew. Chem. Int. Ed.,* 2015, **54**, 9057.

55. (a) J. Depasquale, I. Nieto, L. E. Reuther, C. J. H-Gervasoni, J. J. Paul, V. Mochalin, M. Zeller, C. M. Thomas, A. W. Addison and E. T. Papish, *Inorg. Chem.,* 2013, **52**, 9175. (b) A.L-Andralojc, D. E. Polyansky, C. Wang, W. Wang, Y. Himeda and E. Fujita, *Phys. Chem. Chem. Phys.,* 2014, **16**, 11976.

56. C. M. Moore and N. K. Szymczak, *Chem. Commun.,* 2013, **49**, 400.

57. C. M. Moore, B. Bark and N. K. Szymczak, *ACS Catal.,* 2016, **6**, 1981.

58. B. Paul, K. Chahrabarti and S. Kundu, *Dalton Trans.,* 2016, **45**, 11162.

59. J. Shi, B. Hu, D. Gong, S. Shang, G. Hou and D. Chen, *Dalton Trans.,* 2016, **45**, 4828.

60. J. Shi, B. Hu, S. Shang, D. Deng, Y. Sun, W. Shi, X. Yang, X. Chen and D. Chen, *ACS Omega*, 2017, **2**, 3406.

61. W. M. Motswainyana, S. O. Ojwach, M. O. Onani, E. I. Iwuoha and J. Darkwa, *Polyhedron,* 2011, **30**, 2574.

62. W. B. Cross, E. G. Hope, G. Forrest, K. Singh and G. A. Solan, *Polyhedron,* 2013, **59**, 124

63. S. Taubmann and H. G. Alt, *J. Mol. Cat. A: Chem.,* 2008, **284**, 134.

64. J. M. Benito, E. D-Jesus, F. J. D-Mata, J. C. Flores and R. G-Sal, *Organometallics,* 2006, **25**, 3876.

65. (a) M. Carcelli, M. Costa, S. Ianelli, C. Pelizzi, D. Rogolino and P. Pelagatti, *J. Mol. Cat. A:Chem.,* 2005, **226**, 107. (b) J. Yorke, C. Dent, A. Decken and A. Xia, *Inorg. Chem. Commun.,* 2010, **13**, 54.

66. M. Leskela, E. Aitola, M. Klinga, K. Lappalainen, U. Piironen and T. V. Laine, *J. Organomet. Chem.,* 2000, **606**, 112.

67. W. B. Cross, E. G. Hope, Y. H. Lin, S. A. Macgregor, K. Singh, N. Yahya and G. A. Solan, *Chem. Commun.,* 2013, **49**, 1918.

68. E. R. Reddy, R. Trivedi, A. V. S. Sarma, B. Sridhar, H. S. Anantaraju, D. Sriram, P. Yogeeswari and N. Nagesh, *Dalton Trans.,* 2015, **44**, 17600.

69. F. Vizza, A. Toti, L. Sorace, A. Meli, C. Mealli, F. Laschi, I. G. Rios, G. Giambastiani, D. Gatteschi and C. Bianchini, *Organometallics*, 2007, **26**, 726.

70. G. J. P. Britovsek, S.P. D. Baugh, O. Hoarau, D. F. Wass, A. J. P. White, D. J. Williams and V. C. Gibson, *Inorg. Chim. Acta,* 2003, **345**, 279.

71. A. P. Armitage, Y. D. M. Champouret, H. Grigoli, J. D. A. Pelletier, K. Singh and G. A. Solan, *Eur. J. Inorg. Chem.,* 2008, 4597.

72. Y. Toya, K. Hayasaka and H. Nakazawa, *Organometallics,* 2017, **36**, 1727.

Chapter two

Synthesis of OH-functionalised NNN pincer ligands and
their reactivity towards platinum group metals

2.1 Introduction

2.1.1 Pincer complexes

Tridentate ligands containing a central donor and two exterior donors that bind to a metal center in a meridional conformation are commonly termed pincer ligands (Figure 2.1). In 1976, Shaw and co-workers[1] reported the first example of a pincer ligand which was of the PCP type and this pioneering work has been followed by a large number of reports of the synthesis and applications of a wide variety of pincer ligands. The most popular combination of donor atoms used is NCN, PNP and NNN.[2-5] Since then, NNN pincer ligands, and in particular where a pyridine defines the central unit, have gained a great deal of interest with regard to their synthesis and applications.[5-7] Indeed, the organometallic chemistry of these ligands has received considerable attention over the last decade due to the properties and catalytic reactivity of the resultant complexes in synthetic inorganic and organic chemistry.[8-12] Today, these complexes are designed and synthesized not just for structural interest, but also for their applications in various fields, such as their use as a robust catalysts, motifs in molecules that exhibit self-assembly arrangements, synthons for their employment in medicinal chemistry and as fundamental components in the synthesis of dendrimeric materials for their potential use in catalysis.

L = C or N donor
D = O, N, C, S or P donor
M = metal
X = monodentate ligand, *e.g.*, Cl, OAc
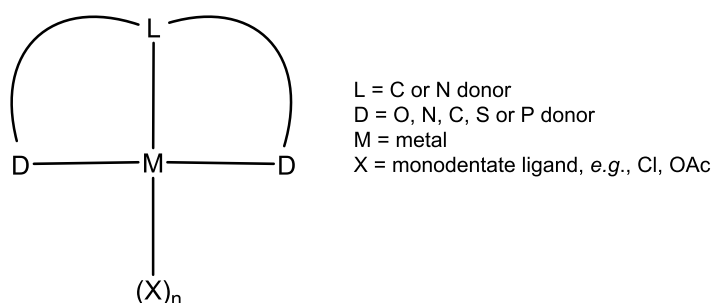
Figure 2.1: General structure of a DLD pincer ligand.

Over the last few decades a number of applications of pincer complexes as catalysts have been reported.[11,13,14] There are two significant features which make pincer complexes attractive species to be used in such applications.

1. Firstly, the tridentate ligand is strongly coordinated to the metal center preventing ligand exchange processes which ensures a high stability and durability of the catalyst. Consequently, these complexes are often stable at high temperatures (above 120 °C) even under harsh conditions.

2. Due to the strong tridentate coordination of the pincer ligand, there is only a single coordination site in a 4-coordinate square planar complex available for external ligands (*e.g.*, when n = 1 in Figure 2.1). Hence, the catalytic activities in pincer complexes are restricted to this single site on the metal center.

In 2011, Ozerov *et al.* reported the bis(imino)carbazolyl-palladium complex **37**.[15] The same tridentate NNN ligand was first reported by Gibson and co-workers who examined their Mn, Fe, Co as well as Rh complexes.[16-18] NNN pincer complexes can be easily prepared and are usually stable complexes during preparation, storage and are more reactive than their analogues bearing a phosphine ligand.[19]

37
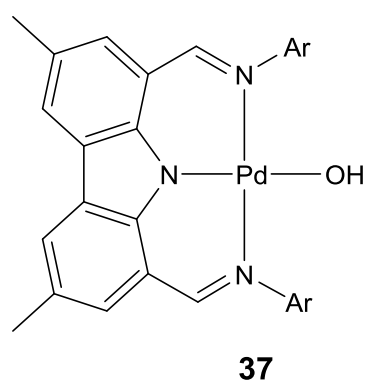
Figure 2.2: An example of an NNN-type palladium(II) pincer complex

In addition, Gibson and co-workers reported a dipyridylimine ligand bound to Fe(II) to form complex **35** (Figure 2.3). Complex **35** has been used as a pre-catalyst in oligomerisation of ethylene.[20] Also this pincer ligand have been exporled with other transition metals.[21]

R = alkyl or aryl
X= Cl

35
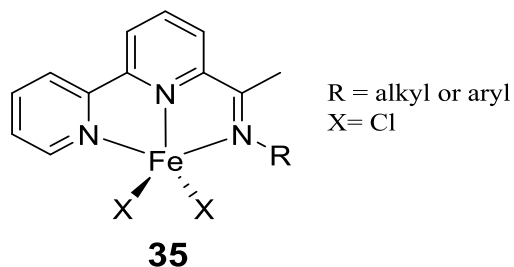
Figure 2.3: NNN-Pyridylimine-iron complexes **35**

Since then, a range of NNN-pincer complexes of various transition metals have been reported and their applications thoroughly investigated. Another example is the unsymmetrical ruthenium (II) pyrazolyl-pyridyl-pyrazole species **38** reported by Yu *et al.*

(Figure 2.4).[19a] Complex **38** at a loading of 0.05 mol% exhibited exceptionally high catalytic activity in the transfer hydrogenation of ketones at 82 °C with K^{t}OBu as base and isopropanol as the solvent. Indeed, this complex gave a TOF number up to 1144000 h^{-1}. The authors ascribe this high catalytic activity to the β-NH functionality on the imidazole arm of the ligand leading to a remarkable acceleration effect on the reaction rate.

In 2016, the same group developed a similar ruthenium complex **39** in which the imidazole arm of the pincer ligand is fused by a phenyl ring (Figure 2.4). Complex **39** has been used as a catalyst in the β-alkylation of secondary alcohols with primary alcohols. Notably this complex exhibits very high catalytic activity affording up to 90% yield of the product in 6 hours.[19b]

38   **39**
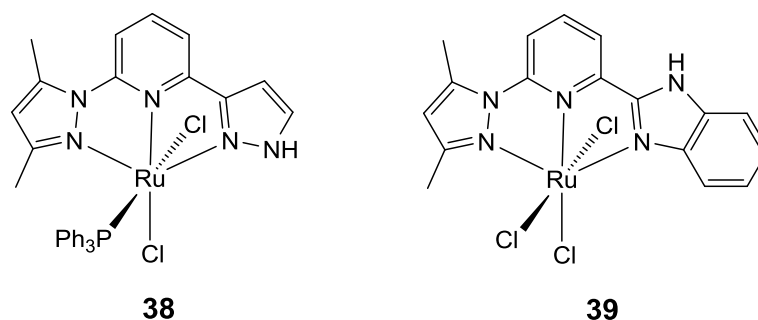
Figure 2.4: Unsymmetrical pyridine-based ruthenium (II) pincer complexes

Elsewhere, developments of the NNN class of pincer complex have seen the introduction of functional groups to the periphery of the ligand. The hydroxyl group is one key example of such a functional group and its presence imparts some intriguing properties to the ligand. It can undergo acid-base reaction to switch the pH of the complex and it can form hydrogen bonds to stabilise the structure.[22] Notably, these NNN^{OH}-type of pincer complexes have been found to be active catalysts in hydrogenation/dehydrogenation and other reactions, including hydrogen storage.[22-25] One such example is the 6,6′-dihydroxyterpyridine-ruthenium complex **25** (Figure 2.5) reported by Szymczak et al.[25] The tautomerism of the bifunctional ligand provides accessible proton donors and acceptors in the secondary coordination sphere of the metal center. As we discussed in Chapter 1 this feature of proton responsiveness when combined with a metal catalyst can be hugely beneficial in a catalytic reaction. Indeed, the ruthenium(II) complex **25** was found to efficiently catalyse the transfer hydrogenation of a variety of ketones in the

presence of KO^{t}Bu as base and isopropanol as solvent giving acetophenone with a TOF of up to 82 h^{-1}.
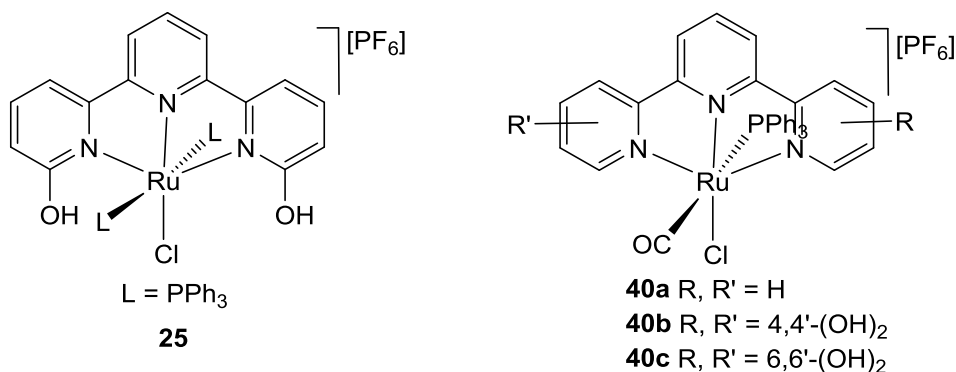
Figure 2.5: Two examples of a cationic NNN^{OH} pincer complexes.

Later, Szymczak *et al.*[24] reported differences in selectivity and activity of the ruthenium(II) complexes **40a-40c** in transfer hydrogenation. They found that complex **40a** gave a TON of 17 while complex **40b** gave a TON of 83. However, **6c** was the best of the three giving a 163 TON in same time. This implies that the complex bearing the OH-functional groups at the 6-position results in dramatic improvements in the catalytic performance. The capacity of the electron rich ruthenium centre to modulate the deprotonation of the OH groups under basic conditions may be influential.

2.1.2 Aims and objectives

This chapter describes the synthesis and reactivity of three novel pyridone-substituted pyridyl-imine NNN-ligands H**L1**$_a$, H**L1**$_b$ and H**L1**$_c$ (Figure 2.6) towards the platinum group metals, Pd, Pt and Ru and in particular the divalent metal salts, Pd(OAc)$_2$, (MeCN)$_2$PdCl$_2$, Na$_2$[PdCl$_4$], (DMSO)$_2$PtCl$_2$ and RuCl$_2$(PPh$_3$)$_3$. It is envisaged that these ligands can remain protonated or undergo deprotonation reactions on coordination to such metals. When coordinated, any proton responsiveness or reversible proton transfer processes will be investigated. In addition, three types of N-aryl group will be prepared (Ar = 2,6-i-Pr$_2$C$_6$H$_3$, 2,4,6-i-Pr$_3$C$_6$H$_2$, 2,4,6-Me$_3$C$_6$H$_2$) so as to allow a means of influencing the steric, electronic as well as solubility properties of the complex. To complement this work, complexes will also be targeted bearing the structurally related N,N,N ligands **L1**$_{OMe}$ and **L1**$_H$ (Figure 2.6). Additionally, the reactivity of selected palladium complexes towards stoichiometric amounts of AgPF$_6$ will be explored with a view to introducing a range of two electron donor ligands (L) to the coordination sphere

of the metal centre, including acetonitrile, 3,5-lutidine, 3,5-dichloropyridine and triphenylphosphine.

All the products will be characterized, where possible, by mass spectrometry, IR and ^{1}H/^{13}C NMR spectroscopy and by elemental analysis. In addition, crystals suitable for single crystal X-ray diffraction will be grown for selected complexes and ligands.
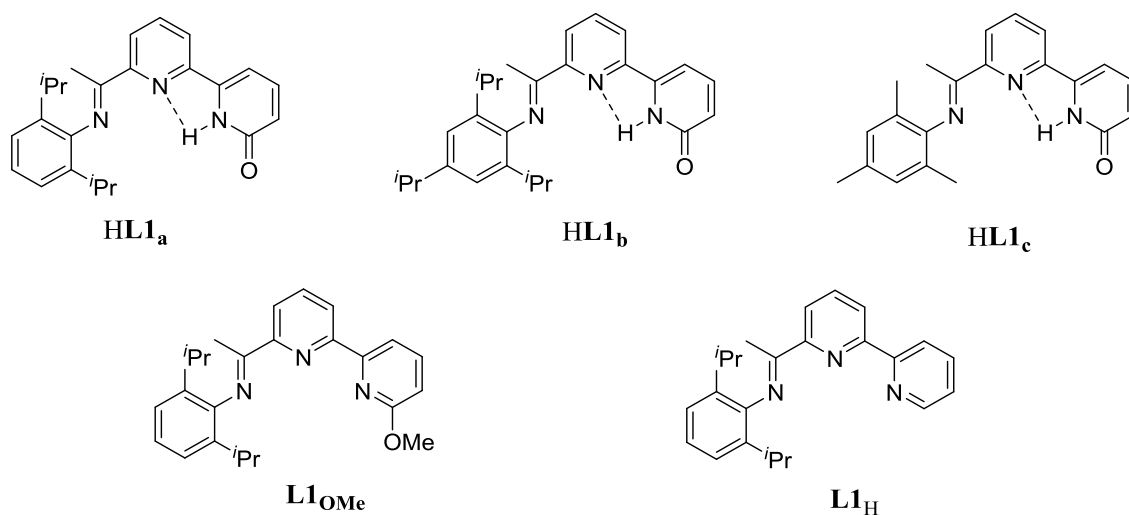
Figure 2.6: The target NNN-ligands

2.2 Results and discussion

2.2.1 Ligand synthesis

This section is concerned with the synthesis of the novel compounds, 2-{C_5H_3NH-2-O)-6-(CMe=NAr)C_5H_3N (Ar = 2,6-i-$Pr_2C_6H_3$ H**L1**$_a$, 2,4,6-i-$Pr_3C_6H_2$ H**L1**$_b$, 2,4,6-$Me_3C_6H_2$ H**L1**$_c$) and 2-{C_5H_4N-2-OMe)-6-(CMe=NAr)C_5H_3N (**L1**$_{OMe}$) from the commercially available starting material 2,6-dibromopyridine (**I**) (Scheme 2.1).
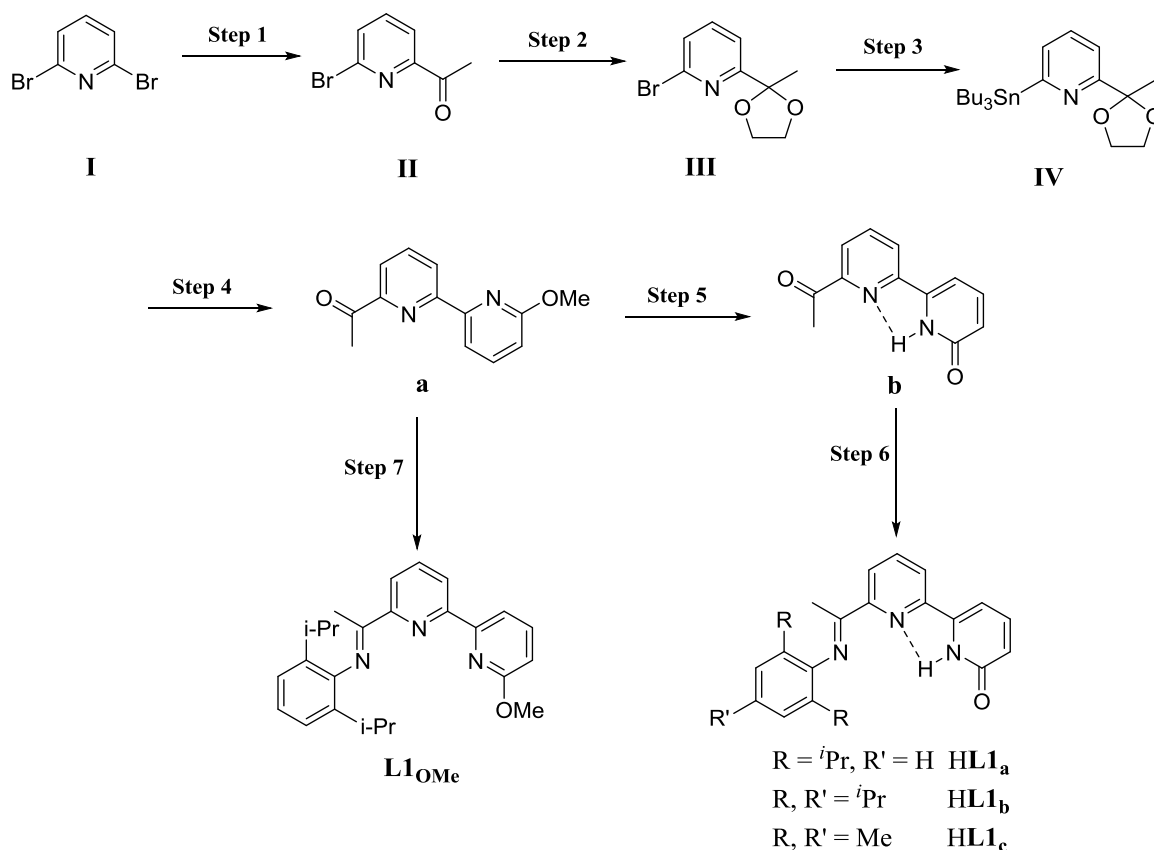
Scheme 2.1: The overall synthetic routes to H**L1**$_a$, H**L1**$_b$, H**L1**$_c$ and **L1**$_{OMe}$

2.2.1.1 Synthesis of tin reagent IV

Acetal-protected 2-(tributylstannyl)-6-(2-methyl-1,3-dioxolan-2-yl)-pyridine (**IV**) was synthesised in good yield (77%) in three consecutive steps, following the literature method described by Solan *et al.* (Scheme 2.1).[26] In the first step, 2,6-dibromopyridine was reacted with *n*-butyllithium followed by treatment with *N,N*-dimethylacetamide, affording 2-bromo-6-acetylpyridine (**II**) in high yield (up to 88%).[27] Protection of the carbonyl group in **II** to give 2-Br-6-{C(Me)OCH_2CH_2O}C_5H_3N (**III**) was achieved by reacting it with 1,2-ethanediol in benzene at reflux for 48 hours to generate **III** in high

34

yield (95%).[27] The third step involved the reaction of **III** with firstly *n*-butyllithium and then tributyltin chloride at -100 °C to afford the tin compound **IV** in a good yield (77%).

2.2.1.2 Synthesis of 1-(6'-methoxy-2,2'-bipyridin-6-yl)ethanone

The dipyridyl compound, 1-(6'-methoxy-2,2'-bipyridin-6-yl)ethanone] (**a**), was prepared using a Stille cross-coupling approach. 2-Bromo-6-methoxypyridine was reacted with **IV** in the presence of the palladium(0) catalyst, Pd(PPh$_3$)$_4$ (4 mol%), affording the acetal derivative which could be readily deprotected by the addition of acid to give **a** in good yield (83%) (Scheme 2.2).

(i) 2-bromo-6-methoxypyridine (1 eq.) Pd(PPh$_3$)$_4$, (0.04 eq.), toluene, 100 °C, 72 h
(ii) 4 M HCl, 60 °C, overnight
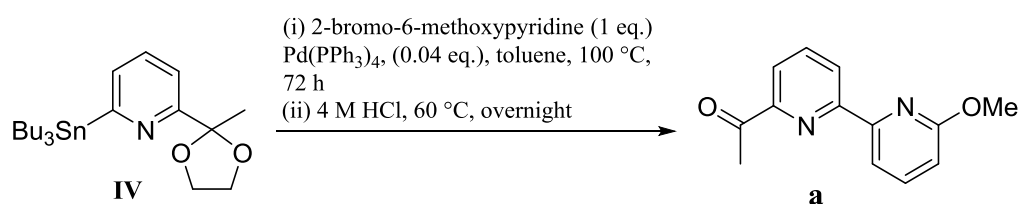
Scheme 2.2: Synthesis of **a** using Stille cross coupling and subsequent acetal deprotection

A conventional Stille cross coupling mechanism is presumed to account for the formation of **a**. In the first step ligand dissociation of triphenylphosphine from Pd(PPh$_3$)$_4$ provides the active Pd(0) species [Pd(PPh$_3$)$_2$].[28] The second step is the oxidative addition of 2-bromo-6-methoxypyridine. Thirdly, transmetallation takes place followed by reductive elimination to give **a** (Scheme 2.3).
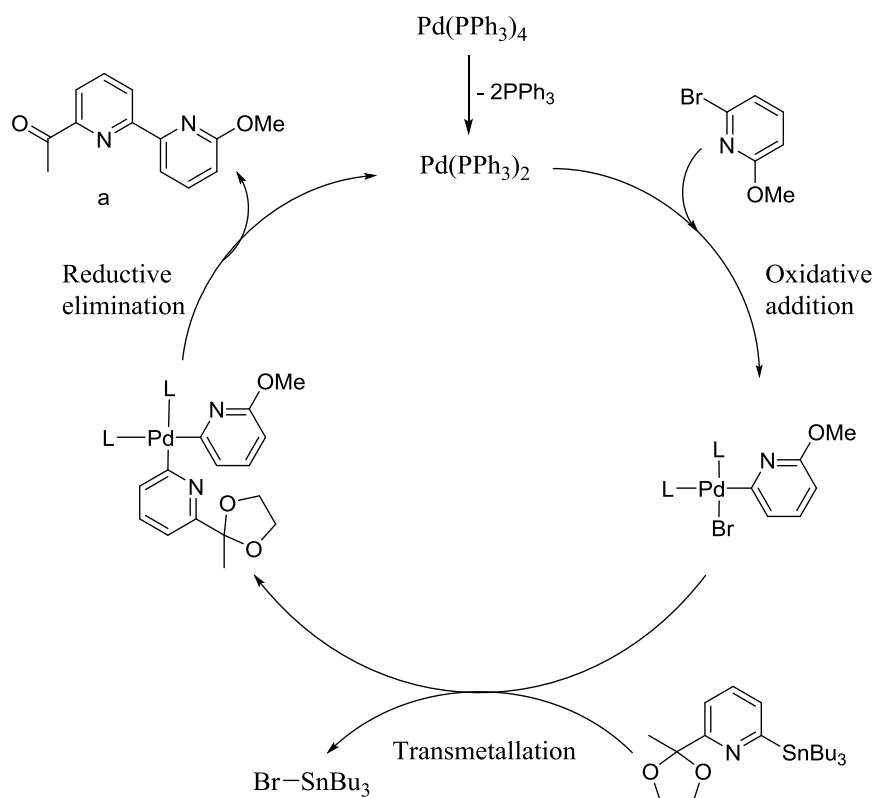
Scheme 2.3: Proposed Stille coupling mechanism for the formation of **a**.

Compound **a** has been fully characterised by ^{1}H NMR, ^{13}C NMR, IR spectroscopy and by HR mass spectrometry. The ^{1}H NMR spectrum shows a singlet peak for the ketone COCH$_3$ methyl at 2.82 ppm while the methoxy methyl (OCH$_3$) was shifted to 4.06 ppm due to the de-shielding influence of the neighboring oxygen and pyridine ring. Non-coordinated bipyridine compounds in general show the lowest energy conformation with the nitrogen atoms in the trans position in both solid and solution state. However, in acidic solution bipyridine adopts a *cis* conformation.[29] Hence, neutral **a** is considered to adopt the *trans* conformation. The ^{13}C NMR spectrum of this compound showed a peak at 199.3 ppm which is assigned to the C=O carbon. The ESI mass spectrum shows two peaks at 229 (M+H) and 227 (M-H) which agree with the calculated molecular mass of the desired product. The IR spectrum shows a peak at 1701 cm^{-1} which corresponds to the absorption for the (C=O)$_{ketone}$ unit.

2.2.1.3 Synthesis of 1-(6'-hydroxy-2,2'-bipyridin-6-yl)ethanone

The methoxy deprotection reaction is performed by heating compound **a** under reflux with aqueous HBr solution (48%) for 4 hours to generate **b** in high yield (98%) (Scheme 2.4).
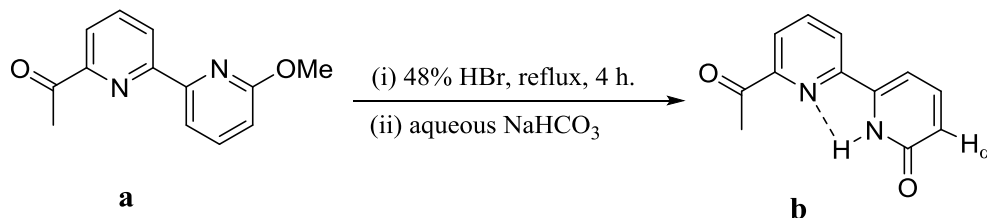
Scheme 2.4: Deprotection of **a** to give **b**

As discussed in Chapter 1 (Introduction), 2-hydroxypyridine (2-pyridinol) exhibits lactam-lactim tautomerism between 2-hydroxypyridine (the hydroxyl or lactim form) and 2-pyridone (2-oxopyridone, the oxo or lactam form). Similar to 2-pyridone, the acidic hydrogen can, in principle, occupy different places in compound **b** *i.e.*, either at the nitrogen or at the oxygen, as both have similar electron densities and electronegativities; therefore, the two forms of **b** could exist in equilibrium (Scheme 2.5).
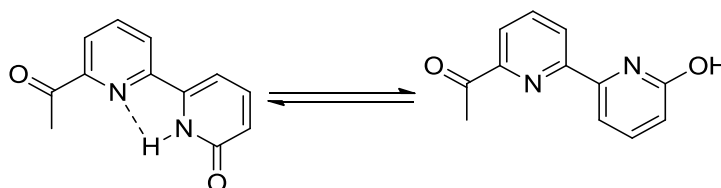
Scheme 2.5: Proposed lactam-lactim tautomerism for **b**.

To identify the tautomer exhibited in the solid state, a crystal of **b** was the subject of a crystal X-ray diffraction study. Suitable crystals were grown by slow cooling of a hot methanol solution containing **b**. A view of **b** is shown in Figure 2.7; Table 2.1 lists selected bond lengths and angles. The bond length of the ketone O(1)-C(1) [1.213(4) Å] is similar to the O(2)-C(11) [1.254(6) Å] distance suggesting double bond character in the latter. The pyridine and exterior heterocycle units are mutually *cis*, which is likely to be due to a N-H proton undergoing a hydrogen bonding interaction with the pyridine nitrogen [N(2)-H(2)···N(1) 2.151 Å]. Therefore, on the basis of this data the pyridone form is adopted by **b** in the solid state.
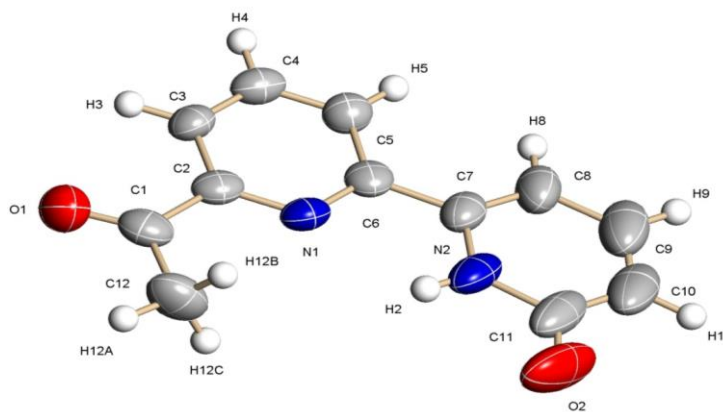
Figure 2.7: Molecular structure of **b**; the thermal ellipsoids are set at the 30% probability level

Table 2.1: Selected bond lengths (Å) and angles (°) for **b**.

Bond lengths (Å)		Bond Angles (°)	
O(1)-C(1)	1.213(4)	O(1)-C(1)-C(2)	121.0(4)
O(2)-C(11)	1.254(6)	C(2)-C(1)-C(12)	117.6(4)
N(1)-C(6)	1.331(4)	O(2)-C(11)-N(2)	117.8(6)
N(1)-C(2)	1.335(4)		
N(2)-C(11)	1.390(5)		

Compound **b** has been fully characterised by $^1H/^{13}C$ NMR and IR spectroscopies. The ^1H NMR spectrum showed a peak at 10.79 ppm corresponding to an NH proton. A peak at 6.71 ppm is assigned to the proton on the pyridone ring α to the C(O) group (see H_α in Scheme 2.4). The upfield nature of this signal suggests that the product is in the lactam form and hence in the de-aromatized form. The ^{13}C NMR spectrum revealed a peak at 162.9 ppm corresponding to the C=O carbon in the pyridone ring and a peak at 198.8 ppm for the C=O carbon of the ketone. The high resolution mass spectrum revealed a peak at 215.0822 while the calculated molecular mass for $C_{12}H_{11}N_2O_2$ (M+H) is 215.0821. In the IR spectrum the ketone C=O peak was seen at 1698 cm^{-1} and C=O pyridone came at 1474 cm^{-1}. In addition, the C=N stretch for pyridine appeared at 1595 cm^{-1} which compares with 1574 cm^{-1} in precursor **a**.

2.2.1.4 Synthesis of H$L1_a$, H$L1_b$ and H$L1_c$

Ligands H$L1_{a-c}$ were obtained from **b** in good yield (52-80%) by Schiff base condensation reactions. The reactions were carried out by heating **b** with the corresponding aniline under reflux in toluene for 3 days using formic acid as catalyst (Scheme 2.6). Each ligand could be readily crystallised from hot methanol.
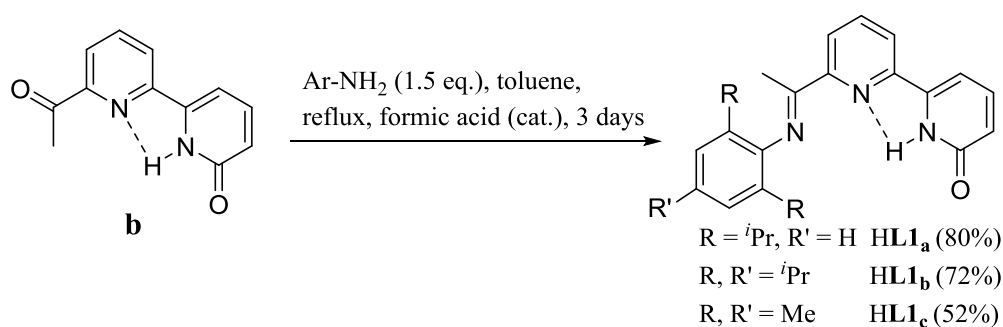
Scheme 2.6: Synthesis of H$L1_a$, H$L1_b$ and H$L1_c$

H$L1_a$ was characterised by both ^{1}H and ^{13}C NMR spectroscopy. There were no signs of any contamination or impurities in either spectra. It was also characterised by HRMS, ESMS spectrometry and IR spectroscopy. In the IR spectrum the N-H peak was observed at 3332 cm^{-1} as a medium intensity sharp band. Hence, ligand H$L1_a$ is considered to be in the lactam form consistent with that observed in most 2-pyridones.[30] In the ^{1}H NMR spectrum in CDCl$_3$ the NH peak was observed at 10.52 ppm and the imine methyl peak was found at 2.29 ppm. Moreover, H$L1_a$ showed a 2H septet at 2.71 ppm (C2, 2′) and 12H doublet at 1.16 ppm (C3,3′, C4,4′). The ^{13}C NMR spectrum revealed two signals at 21.8 ppm and 22.2 ppm for the methyl carbons of the [i]Pr groups, indicating that the methyl groups (C3,4) were inequivalent (Figure 2.8). The methyl of [i]Pr groups doublet is actually two overlapping doublets rather than one doublet. This was confirmed by 1D, 2D spectra as well as from the ^{13}C{^{1}H} NMR spectra. Furthermore, the H$_\alpha$ proton was observed at 6.66 ppm, consistent with the molecule adopting the de-aromatised lactam form. The imine C=N absorption appeared as a sharp peak at 1644 cm^{-1} in the IR spectrum. In addition, the ^{13}C NMR spectrum showed a peak at 161.8 ppm and 165.1 ppm corresponding to the C=O carbon in the pyridone ring and C=N$_{imine}$, respectively.
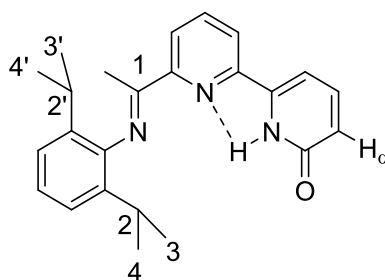
Figure 2.8: Key environments in H**L1**$_a$ are labelled

Single crystals of H**L1**$_a$ suitable for an X-ray diffraction study were obtained by slow cooling of a hot methanol solution of the compound. A view of the structure is shown in Figure 2.9; selected bond lengths and angles are collected in Table 2. The crystal structure reveals the molecule to exhibit the lactam/pyridone form. The O(1)-C(1) bond length of 1.232(2) Å is short and consistent with double bond character.[31] As with compound **b**, atoms N1 and N2 adopt a *cis*-arrangement,[32] which can be ascribed to an intra-molecular hydrogen bonding between H1 and N2 [N(1)-H(1)···N(2) 2.02 Å].
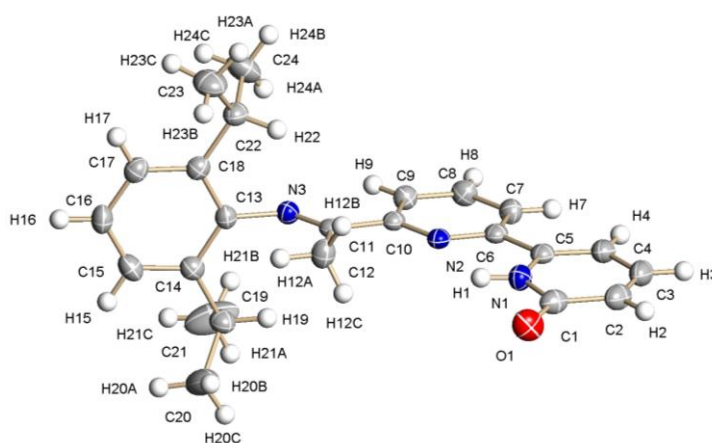
Figure 2.9: Molecular structure of H**L1**$_a$; the thermal ellipsoids are set at the 30% probability level

Table 2.2: Selected bond lengths (Å) and angles (°) for H**L1**$_a$

Bond Lengths (Å)		Bond Angles (°)	
O(1)-C(1)	1.232(2)	O(1)-C(1)-N(1)	119.82(19)
N(1)-C(5)	1.363(2)	C(15)-N(1)-C(1)	126.31(18)
N(1)-C(1)	1.377(2)	N(1)-C(1)-C(2)	113.56(19)
N(3)-C(13)	1.428(2)	N(3)-C(11)-C(12)	125.41(18)

The ^{1}H NMR spectrum of **HLl$_b$** showed a singlet peak for the NH proton at 10.52 ppm and a septet peak at 2.68 ppm for the two protons of the equivalent isopropyl group in the ortho-position. Another septet for the proton of the isopropyl moiety in the para-position was also evident. The ESI mass spectrum showed a peak corresponding to the ligand at m/z 416 [M+H]. The IR spectrum showed a medium peak for C=N$_{imine}$ at 1644 cm^{-1} and a NH peak at 3332 cm^{-1}. As with **HL1$_a$**, **HL1$_b$** adopts the pyridone form as indicated by the proton NMR data which reveals an upfield signal at 6.68 ppm corresponding to the H$_\alpha$ proton.

Compared to **HL1$_a$** and **HL1$_b$**, mesityl-containing **HL1$_c$** was found to be less soluble, a factor that affected the progress of the reaction and moreover the yield (Scheme 2.6). The ^{1}H NMR spectrum of **HL1$_c$** showed a singlet peak for the NH proton at 10.44 ppm, and a singlet peak at 1.93 ppm for the six protons of the equivalent methyl groups in the ortho-position. The ^{13}C NMR spectrum showed a peak at 161.7 ppm and 165.4 ppm assigned to C=O and C=N$_{imine}$ carbons, respectively. As discussed previously the upfield nature of the H$_\alpha$ proton at 6.61 ppm suggests the de-aromatised pyridone form to be adopted. The ESI mass spectrum showed a peak corresponding to the protonated molecular ion at 332 [M+H].

2.2.1.5 Synthesis of L1$_{OMe}$

The methoxy ligand, 2-{C$_5$H$_3$N-2-OMe)-6-(CMe=NAr)C$_5$H$_3$N (Ar = 2,6-i-Pr$_2$C$_6$H$_3$ **L1$_{OMe}$**), was targeted to allow a comparison with OH-functionalised **HL1$_a$**. The reaction conditions are outlined in Scheme 2.7. **L1$_{OMe}$** was formed by reacting compound **a** with 2,6-diisopropylaniline under reflux in toluene for 3 days using formic acid as catalyst.
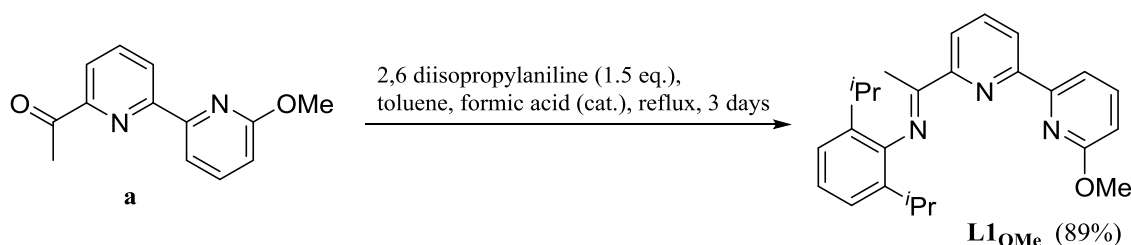
Scheme 2.7: Synthesis of **L1$_{OMe}$**

L1$_{OMe}$ was fully characterised by ^{1}H, ^{13}C and IR spectroscopy as well as by HR mass spectrometry. The ^{1}H NMR spectrum showed a singlet peak for OMe at 4.00 ppm and a

41

peak at 2.25 ppm due to the imine methyl. The ESI mass spectrum revealed a peak at m/z 387 corresponding to the protonated molecular ion.

2.2.1.6 Synthesis of L1$_H$

Ligand 2-{C$_5$H$_4$N)-6-(CMe=NAr)C$_5$H$_3$N (Ar = 2,6-i-Pr$_2$C$_6$H$_3$ **L1$_H$**), was obtained in a good yield (89%) in three straightforward steps following the literature method described by Bianchini *et al.* (Scheme 2.8).[21]
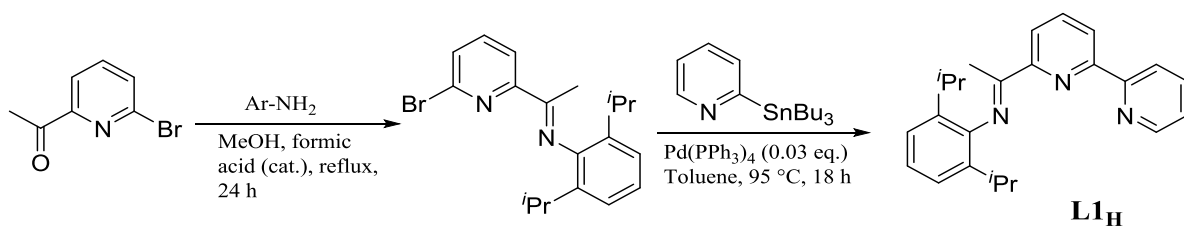
Scheme 2.8: Synthesis of **L1$_H$**

2.2.2 Reaction chemistry of HL1$_a$, HL1$_b$ and HL1$_c$

2.2.2.1 Reactions of HL1$_a$, HL1$_b$ and HL1$_c$ with Pd(OAc)$_2$

Reaction of HL1$_{a-c}$ with Pd(OAc)$_2$ at room temperature in toluene for 18 hours results in deprotonation and formation of **L1$_a$PdOAc**, **L1$_b$PdOAc** and **L1$_c$PdOAc**, respectively, in good to excellent yields (68 – 94%) (Scheme 2.9). The lower yield of mesityl-containing **L1$_c$PdOAc** (68%) can be attributed to the poorer solubilty of HL1$_c$ in the reaction solvent. Complexes **L1$_a$PdOAc**, **L1$_b$PdOAc** and **L1$_c$PdOAc** have been characterised by ^{1}H/^{13}C, IR spectroscopy and mass spectrometry. **L1$_a$PdOAc** has additionally been the subject of a single crystal X-ray diffraction study.

R = ^{i}Pr, R' = H   HL1$_a$
R = R' = ^{i}Pr   HL1$_b$
R = R' = Me   HL1$_c$

R = ^{i}Pr, R' = H   **L1$_a$PdOAc** (94%)
R = R' = ^{i}Pr   **L1$_b$PdOAc** (96%)
R = R' = Me   **L1$_c$PdOAc** (68%)
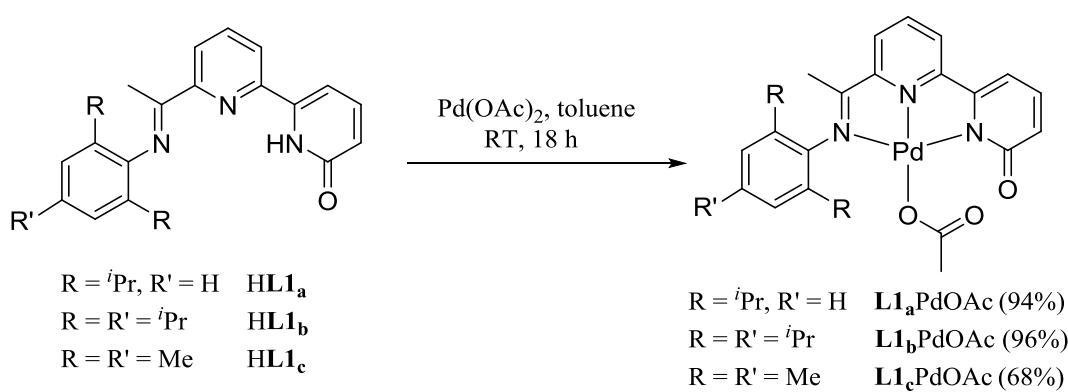
Scheme 2.9: Syntheses of **L1$_a$PdOAc**, **L1$_b$PdOAc** and **L1$_c$PdOAc**

The ^{1}H NMR spectrum of **L1$_a$PdOAc** showed two separate 6H doublets at 1.36 ppm and 1.17 ppm corresponding to the inequivalent CH*Me*$_a$*Me*$_b$ protons belonging to the two isopropyl groups, while in the free ligand, these hydrogen signals appear as one doublet. A singlet has been detected at 1.86 ppm which corresponds to the acetate. Additionally, the IR spectrum showed a peak at 1620 cm^{-1} which corresponds to C=N$_{imine}$ absorption, which compares with 1644 cm^{-1} in the free ligand. The FAB mass spectrum revealed a peak at *m/z* 478 for the molecular fragment [M-OAc].

Single crystals of **L1$_a$PdOAc** were grown by layering a dichloromethane solution of the complex with hexane. A view of **L1$_a$PdOAc** is shown in Figure 2.10; selected bond distances and angles are collected in Table 2.3. The structure consists of palladium centre bound by three nitrogen atoms belonging to **L1$_a$** and an O-bound acetate to complete a geometry that can be best described as square planar geometry. Within the **L1$_a$Pd** unit there are two five-membered chelate rings with N(2)-Pd(1)-N(1) and N(2)-Pd(1)-N(3)

angles of 80.82(14)° and 80.15(14)°, respectively, highlighting the role played by the pincer ligand on the distortion to the geometry. The C(1)-O(1) bond length at 1.266(6) Å is loger for double bond which could be delocalised bond. However, the C(25)-O(3) bond length at 1.222(6) Å is consistent with a double bond and implies the exterior heterocycle is in the monoanionic pyridonate form.
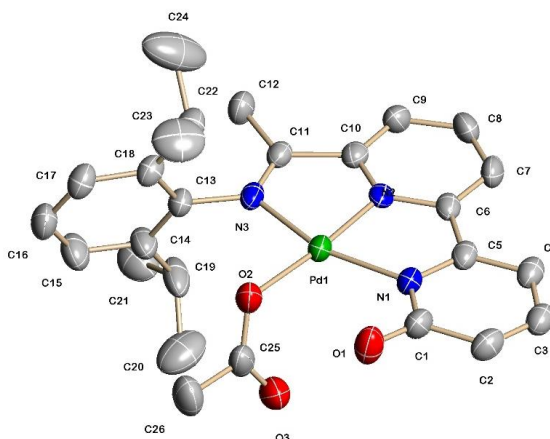
Figure 2.10: Molecular structure of **L1$_a$PdOAc**; the thermal ellipsoids are set at the 30% probability level (all hydrogen atoms have been removed for clarity)

Table 2.3: Selected bond lengths (Å) and angles (°) for **L1$_a$PdOAc**

Bond Length (Å)		Bond Angle (°)	
O(1)-C(1)	1.266(6)	N(2)-Pd(1)-N(3)	80.15(14)
N(1)-Pd(1)	2.043(3)	N(2)-Pd(1)-N(1)	80.82(14)
N(2)-Pd(1)	1.927(3)	O(2)-Pd(1)-N(3)	94.59(14)
N(3)-Pd(1)	2.038(4)	O(2)-Pd(1)-N(1)	104.42(14)
C(25)-O(3)	1.222(6)		

Analysis of the ^{1}H NMR spectrum of **L1$_b$PdOAc** revealed features in agreement with the *N*-(2,4,6-triisopropylphenyl) substituted imine compounds coordinated to palladium. To be precise, the presence of two different 6H doublet peaks at 1.16 ppm and 1.49 ppm coupling to the same 2H septet peak at 3.12 ppm. Further indications of the structure include the presence of 3H singlet peaks at 1.60 ppm and 2.29 ppm, which correspond to acetate- and imine-methyl groups, respectively. Moreover, the ^{13}C NMR spectrum showed a peak at 168.9 ppm corresponding to the C=N carbon, which compares to 166.0 ppm in the free ligand. The ESI mass spectrum rendered a peak at m/z 520 which can be assigned to the (M-OAc) fragment.

For **L1cPdOAc**, the spectroscopic data suggested that coordination of the ligand to palladium had also been achieved. One indication is the C=N absorption in the infrared spectrum shifted to 1618 cm^{-1} as compared to 1651cm^{-1} in the free ligand. The ^{1}H NMR spectrum revealed 3H singlet peaks at 2.13 ppm and 2.23 ppm which correspond to the methyl protons of the acetate and imine, respectively. The mass spectrum (FAB) showed a fragmentation peak at m/z 436 (M-OAc).

2.2.2.2 Reactions of L1PdOAc with aqueous NaCl

L1a PdOAc and **L1b**PdOAc can be readily converted to their chloride derivatives **L1a**PdCl and **L1b**PdCl by reacting them with a biphasic mixture of chloroform and a saturated aqueous sodium chloride solution at room temperature (Scheme 2.10). By contrast, **L1c**PdOAc could not be converted to its chloride derivative due its poor solubility in chloroform. Complexes **L1a**PdCl and **L1b**PdCl have been characterised by ^{1}H/^{13}C, IR spectroscopy and mass spectrometry; a single crystal X-ray determination was also performed on **L1a**PdCl.

R = ^{i}Pr, R' = H **L1a**PdOAc
R = R' = ^{i}Pr   **L1b**PdOAc

NaCl/H$_2$O, CHCl$_3$
RT, 16 h

R = ^{i}Pr, R' = H **L1a**PdCl (100%)
R = R' = ^{i}Pr   **L1b**PdCl (100%)
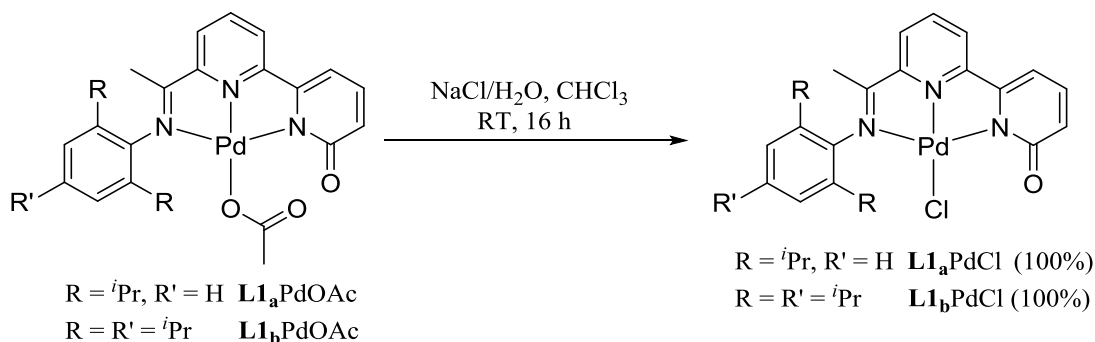
Scheme 2.10: Synthesis of **L1a**PdCl and **L1b**PdCl

The absence of an acetate carbon group in the ^{13}C NMR spectrum of **L1a**PdCl or **L1b**PdCl is supportive of the complexes having been formed. Moreover, the protons of the acetate group were not found in the ^{1}H NMR spectrum. The accurate ESI mass spectrum revealed a strong molecular ion peaks for each complex, which confirmed the formation of the desired product. The IR spectra showed a peak at 1620 cm^{-1} and 1619 cm^{-1} for the C=N$_{imine}$ bond in both complexes.

Single crystals of **L1a**PdCl suitable for the X-ray determination were grown by slow evaporation of methanol solution containing the complex. A view of **L1a**PdCl is shown

in Figure 2.11; selected bond lengths and angles are given in Table 2.4. The molecular structure of **L1ₐ**PdCl revealed a distorted square planar geometry about Pd and an almost perfectly planar N^N^N conjugated neutral system. The Pd–N bond length to the central atom of the N^N^N ligand is the shortest and significantly shorter than the Pd–Cl bond distance. The 2,6-diisopropylphenyl ring orientates itself in a perpendicular fashion relative to the plane of the coordination plane, which probably reduces any steric clash between itself and the NNN-Pd plane. The C=O bond in the **L1ₐ**PdCl is 1.236(10) Å which is consistent with exterior heterocycle remaining in the pyridonate form.
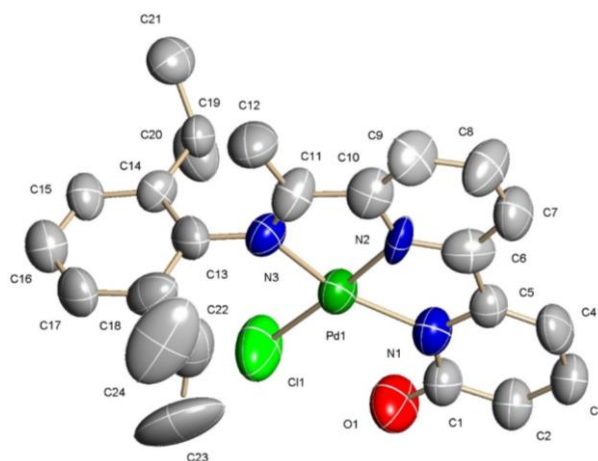
Figure 2.11: Molecular structure of **L1ₐ**PdCl; the thermal ellipsoids are set at the 30% probability level (all hydrogen atoms have been removed for clarity)

Table 2.4: Selected bond lengths (Å) and angles (°) of **L1ₐ**PdCl

Bond Length (Å)		Bond Angle (°)	
Pd(1)-N(2)	1.912(8)	N(2)-Pd(1)-N(1)	80.8(3)
Pd(1)-N(3)	2.060(7)	N(2)-Pd(1)-N(3)	79.2(3)
Pd(1)-N(1)	2.051(8)	N(1)-Pd(1)-N(3)	160.0(3)
Pd(1)-Cl(1)	2.250(3)	N(1)-Pd(1)-Cl(1)	103.4(2)
O(1)-C(1)	1.236(10)	N(3)-Pd(1)-Cl(1)	96.5(2)

2.2.2.3 Synthesis of [HL1PdCl][Cl]

A potential alternative and more direct way to make neutral **L1**PdCl involves treating the free ligands, H**L1**, with bis(acetonitrile)dichloropalladium(II). Unexpectedly, on reacting H**L1**ₐ₋c with Cl₂Pd(NCMe)₂ in toluene at room temperature, the ligands remain protonated, and afford the poorly soluble cationic complexes [H**L1ₐ**PdCl][Cl], [H**L1_b**PdCl][Cl] and [H**L1_c**PdCl][Cl] in good yield (70-98%), (Scheme 2.11). All

complexes have been characterised by ^{1}H/^{13}C, IR spectroscopy and mass spectrometry; a single crystal X-ray determination was also performed on [HL1$_c$PdCl][Cl].

R = ^{i}Pr, R' = H   HL1$_a$
R = R' = ^{i}Pr   HL1$_b$
R = R' = Me   HL1$_c$

R = ^{i}Pr, R' = H   [HL1$_a$PdCl][Cl] (81%)
R = R' = ^{i}Pr   [HL1$_b$PdCl][Cl] (98%)
R = R' = Me   [HL1$_c$PdCl][Cl] (70%)
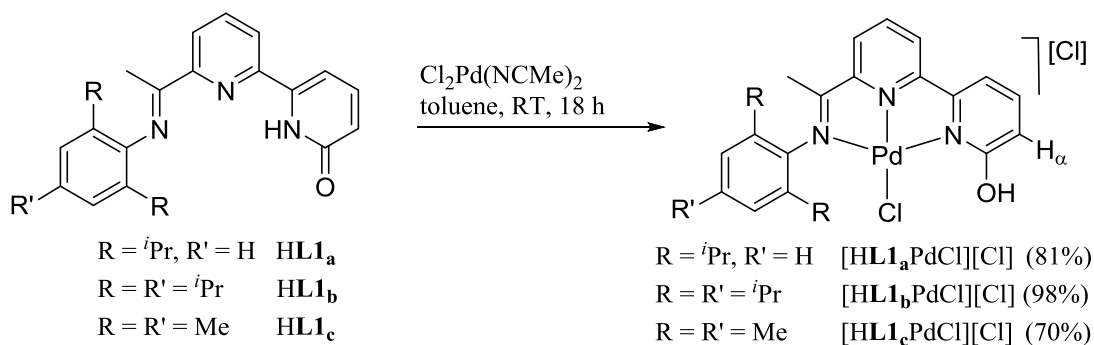
Scheme 2.11: Synthesis of [HL1$_a$PdCl][Cl], [HL1$_b$PdCl][Cl] and [HL1$_c$PdCl][Cl]

The structure of [HL1$_a$PdCl][Cl] was consistent with the data in the ^{1}H NMR spectrum revealing two 6H doublet peaks at 1.31 ppm and 1.12 ppm for the inequivalent CH$Me_a Me_b$ methyl groups belonging to the two isopropyl groups; the observation compares to one doublet in the free ligand. Additionally, the IR spectrum showed a strong C=N$_{imine}$ stretching frequency at 1613 cm^{-1} confirming the formation of an imine-containing metal complex and a peak at 3644 cm^{-1} due to the OH vibrations. The FAB mass spectrum showed a fragmentation peak at m/z 478 [M$^+$- 2Cl]. Unfortunately, the ^{1}H NMR spectra could only be performed in deuterated methanol meaning that the OH peak could not be observed. Nevertheless, the more downfield nature of the H$_\alpha$ proton at 7.09 ppm (see Scheme 2.11) indicates the exterior heterocyclic unit to be in the neutral pyridinol form.

The ^{1}H NMR spectrum of [HL1$_b$PdCl][Cl] revealed the formation of the desired product, showing two different 6H doublets peaks at 1.29 ppm and 1.13 ppm for the ortho-CH$Me_a Me_b$ methyls which were coupling to the same 2H (CH) septet peak at 3.11 ppm. The IR spectrum revealed a characteristic OH peak at 3510 cm^{-1}. Further indication of the desired product was provided by the high resolution mass spectrum which revealed a peak at 560.1872 which compares to 560.1862 for the calculated molecular mass for C$_{27}$H$_{33}$N$_3$OPdCl$_2$ (M-Cl).

The ^{1}H NMR spectrum of [H**L1**$_c$PdCl][Cl] indicated a peak at 2.31 ppm attributable to the imine-methyl group which compares to 2.17 ppm in the free ligand. Furthermore, the IR spectrum showed peaks at 1623 cm^{-1} and 3605 cm^{-1} corresponding to C=N$_{imine}$ and OH bands, respectively.

Single crystals of [H**L1**$_c$PdCl][Cl] suitable for an X-ray determination were grown by
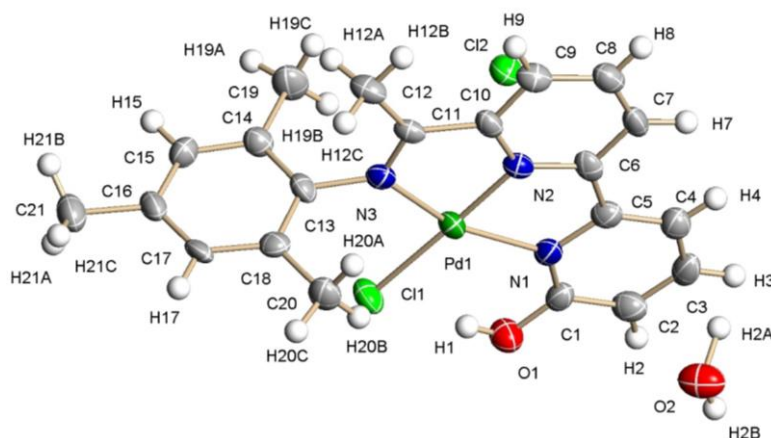
slow evaporation of methanol solution containing the complex. A view of the structure is shown in Figure 2.12; selected bond lengths and angles are given in Table 2.5. The structure reveals a distorted square planar environment about Pd and an almost perfectly planar N^N^N conjugated cationic unit with a Cl acting as the counter-ion. The Pd–N bond length to the central atom of N^N^N ligand is the shortest and significantly shorter than Pd–Cl bond distance. The C(1)-O(1) bond distance is 1.331(8) Å, which is consistent with a single bond. The O(1)H(1) functionality undergoes an   intramolecular hydrogen bonding interaction with O(1)-H(1)···Cl(1) 2.134 Å. Also hydrogen bonding between water molecular with Cl(2) has been noted.

Figure 2.12: Molecular structure of [H**L1**$_c$PdCl][Cl]; the thermal ellipsoids are set at the 30% probability level

Table 2.5: Selected bond lengths (Å) and bond angles (°) for [H**L1**$_c$PdCl][Cl]

Bond Lengths (Å)		Bond Angles (°)	
Pd(1)-N(1)	2.059(5)	N(2)-Pd(1)-N(3)	79.7(2)
Pd(1)-N(2)	1.937(5)	N(2)-Pd(1)-N(1)	80.9(2)
Pd(1)-N(3)	2.034(5)	N(3)-Pd(1)-N(1)	160.6(2)
Pd(1)-Cl(1)	2.3119(18)		
C(1)- O(1)	1.331(8)		

2.2.2.4 Counter-ion exchange reactions of [HL1PdCl][Cl]

To improve the solubility of [HL1PdCl][Cl] (HL1 = HL1$_a$, HL1$_b$), counter-ion metathesis was performed with KPF$_6$. Hence, reactions of [HL1$_a$PdCl][Cl] and [HL1$_b$PdCl][Cl] in a dichloromethane with an aqueous solution of potassium hexafluorophosphate gave [HL1$_a$PdCl][PF$_6$] and [HL1$_b$PdCl][PF$_6$] respectively in high yields (Scheme 2.12). Both complexes were characterized by ^{1}H, ^{13}C and ^{19}F NMR spectroscopy. The appearance of the 6F doublet at -70 ppm in the ^{19}F NMR spectra revealed the presence of PF$_6$.
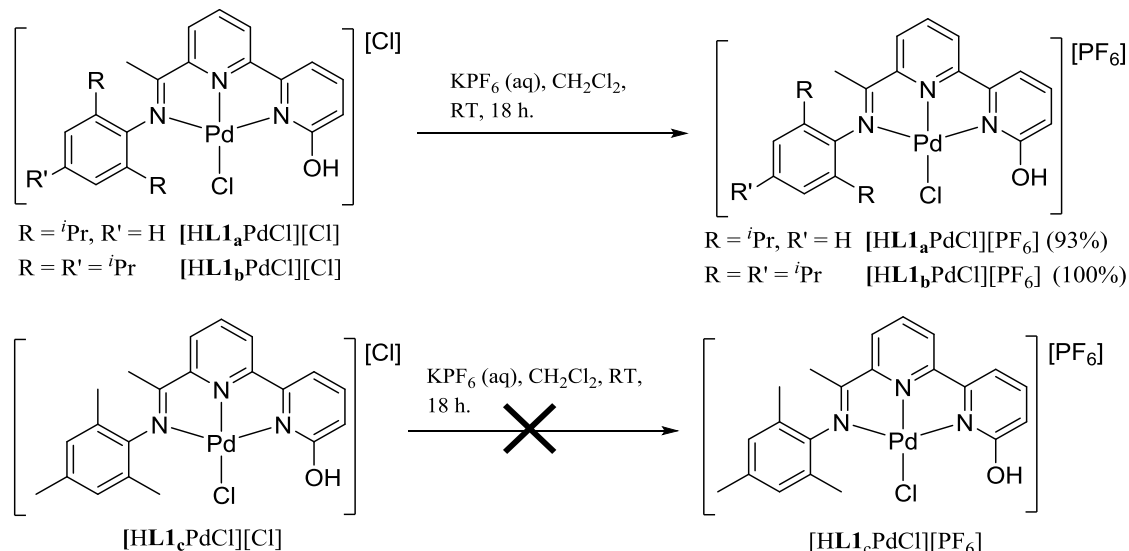
Scheme 2.12: Chloride anion exchange the for PF$_6$ anion

The analysis of [HL1$_a$PdCl][PF$_6$] in the ^{1}H NMR spectra showed signals associated with the isopropyl methyl groups at 1.28 ppm and 1.11 ppm whereas in [HL1$_a$PdCl][Cl] they were observed at 1.31 ppm and 1.12 ppm, respectively. The ^{31}P NMR spectrum displayed peak at -144.6 ppm was assigned to PF$_6$ anion. The ESI spectrum showed a peak at 516 corresponding to the [M-PF$_6$] fragment.

For [HL1$_b$PdCl][PF$_6$], the spectroscopic data showed a septet peak for the P in the ^{31}P NMR spectra, confirming the presence of PF$_6$. The high resolution mass spectrum revealed a mass for the compound of 522.1592 which compares with 522.1584 calculated for C$_{27}$H$_{33}$N$_3$OPdClPF$_6$ [M$^+$- (Cl+PF$_6$)].

Another confirmation of both complexes comes from the X-ray diffraction analysis. Crystals of [HL1$_a$PdCl][PF$_6$] and [HL1$_b$PdCl][PF$_6$], suitable for X-ray determination

were grown by slow diffusion of hexane in to dichloromethane solutions of the complexes. A view of the PF$_6$ salts are shown in Figure 2.13; selected bond distances and angles are compiled in Table 2.6a and 2.6b. The X-ray results revealed a distorted square planar geometry around Pd and an almost perfectly planar N^N^N conjugated cationic system and a PF$_6$ anion.
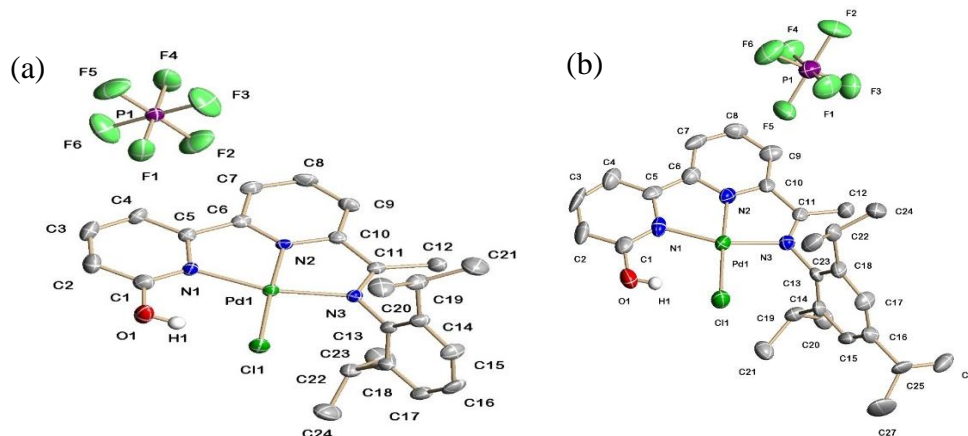
Figure 2.13: Molecular structure of [H**L1**$_a$PdCl][PF$_6$] (a) and [H**L1**$_b$PdCl][PF$_6$] (b); the thermal ellipsoids are set at the 30% probability level (all hydrogen atoms removed except OH on O(1))

Table 2.6a: Selected bond lengths (Å) and angles (°) for [H**L1**$_a$PdCl][PF$_6$]

Bond Length (Å)		Bond Angle (°)	
Pd(1)-N(2)	1.929(3)	N(2)-Pd(1)-N(3)	80.50(14)
Pd(1)-N(3)	2.032(3)	N(2)-Pd(1)-N(1)	80.53(14)
Pd(1)-N(1)	2.063(3)	N(3)-Pd(1)-N1	161.02(13)
Pd(1)-Cl(1)	2.3624(11)	N(2)-Pd(1)-Cl(1)	177.30(10)
O(1)-C(1)	1.324(5)	N(1)-Pd(1)-Cl(1)	102.02(10)

Table 2.6b: Selected bond lengths (Å) and angles (°) of [H**L1**$_b$PdCl][PF$_6$]

Bond lengths (Å)		Bond angles (°)	
Pd(1)-N(2)	1.922(7)	N(2)-Pd(1)-N(3)	79.3 (3)
Pd(1)-N(3)	2.021(6)	N(2)-Pd(1)-N(1)	80.1 (3)
Pd(1)-N(1)	2.065(7)	N(3)-Pd(1)-N1	159.3 (3)
Pd(1)-Cl(1)	2.302(2)	N(2)-Pd(1)-Cl(1)	177.5 (2)
O(1)-C(1)	1.359(10)	N(1)-Pd(1)-Cl(1)	102.3(2)

The synthesis of [H**L1**$_c$PdCl][PF$_6$] was also investigated using the conditions established for the successful preparation of [H**L1**$_a$PdCl][PF$_6$] and [H**L1**$_b$PdCl][PF$_6$]. However, only 20% of [H**L1**$_c$PdCl][PF$_6$] could be observed by proton NMR spectroscopy, the remaining

portion being unreacted starting material and some unknown impurity (Scheme 2.12). Attempts to purify the product were unsuccessful.

2.2.2.5 Reactions of [HL1ₐPdCl][PF₆] and [HL1ₐPdCl][Cl] with base

To explore the proton responsiveness of [H**L1**ₐPdCl][PF₆] and [H**L1**ₐPdCl][Cl], both salts were treated with the base NEt₃ with a view to eliminating HNEt₃X (X = Cl, PF₆) (Scheme 2.13).
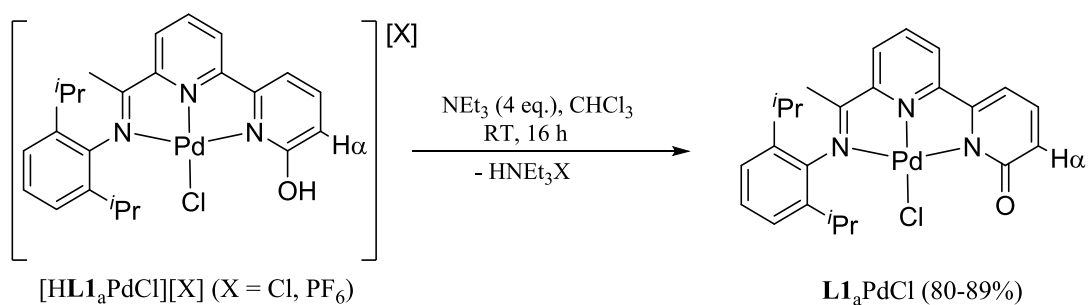
Scheme 2.13: Deprotonation of [H**L1**ₐPdCl][X] with NEt₃ to give **L1**ₐPdCl

Both reactions worked efficiently generating **L1**PdCl with good yields and high purity. Notably, comparison of the ^{1}H NMR spectra [H**L1**ₐPdCl][Cl] and **L1**ₐPdCl reveals the H$_\alpha$ proton to shift downfield from 7.09 ppm to 6.52 ppm, respectively, consistent with the aromatic pyridinol being converted to a de-aromatised pyridonate (Figure 2.14). Moreover, the data for the product formed by this route is consistent with that previously obtained for **L1**ₐPdCl prepared by OAc/Cl exchange. The ESI mass spectrum revealed a peak of *m/z* 516 [M+H].
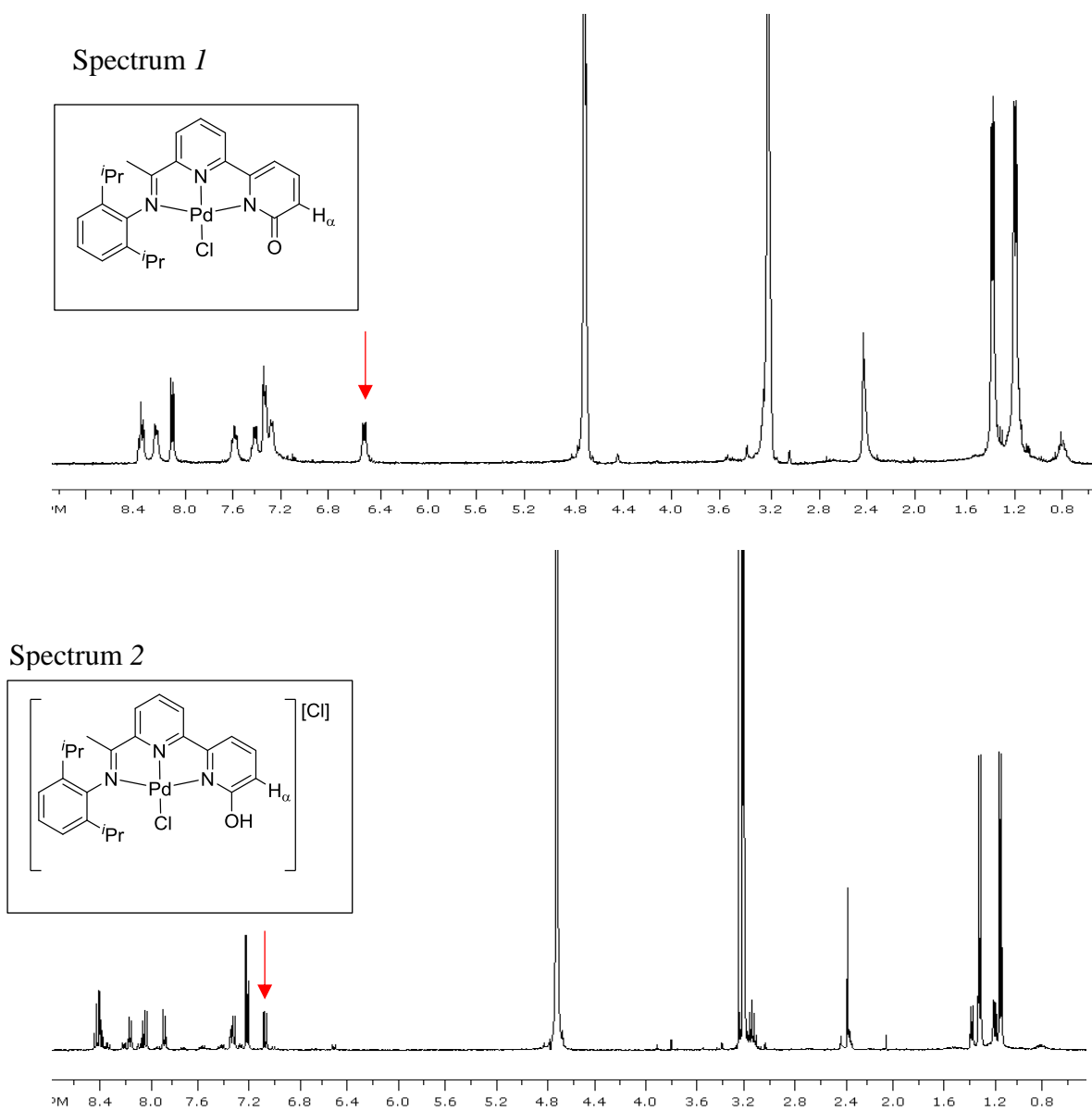
Figure 2.14: ^{1}H NMR spectra of **L1**$_a$PdCl (1) and [H**L1**$_a$PdCl][Cl] (2); recorded in CD$_3$OD at room temperature. The red arrows show the signal for the H$_\alpha$ proton. In spectrum *1* the signal appears at 6.52 ppm (pyridonate form) while in spectrum *2* it is seen at 7.09 ppm (pyridinol form).

2.2.2.6 Reactions of HL1$_a$ with other palladium sources

After observing different reactivity of H**L1** with Pd(OAc)$_2$ and (MeCN)$_2$PdCl$_2$, we decided to explore their reactivity towards other common palladium(II) reagents such as Na$_2$[PdCl$_4$]. Since Na$_2$[PdCl$_4$] is not soluble in routine organic solvents, the reactions were carried out in acetic acid. Hence, reaction of this metal salt with H**L1**$_a$ gave after 24 hours at 100°C a 50:50 mixture of [H**L1**$_a$PdCl][Cl] and [**L1**$_a$PdCl] as a red powder in high yield (Scheme 2.14). Both compounds have already been independently prepared so their ^{1}H NMR spectra could be used to support the assignment. To further confirm the structural assignment, a concentrated HCl solution was added to the mixture of [H**L1**$_a$PdCl][Cl] and [**L1**$_a$PdCl] in dichloromethane at room temperature. The ^{1}H NMR spectrum of the resulting product showed 100% pyridinol-containing [H**L1**$_a$PdCl][Cl].
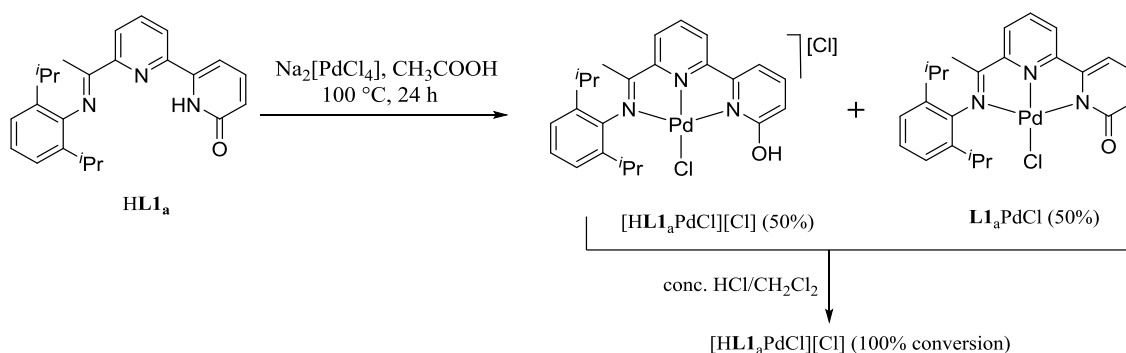
Scheme 2.14: Synthesis of a 50:50 mixture of [H**L1**$_a$PdCl][Cl] and **L1**$_a$PdCl and complete conversion to [H**L1**$_a$PdCl][Cl].

2.2.2.7 Synthesis of cationic [L1PdL][PF$_6$] (L = MeCN, H$_2$O)

To examine the capacity of the chloride ligands in **L1**PdCl to undergo substitution reactions with neutral two electron donor ligands such as water or acetonitrile, selected examples were reacted with silver salts (*e.g.*, AgPF$_6$ or AgOTf) in the presence of acetonitrile as solvent. Hence, treatment of **L1**$_a$PdCl and **L1**$_b$PdCl with a slight excess of AgPF$_6$ in acetonitrile gave [**L1**$_a$Pd(NCCH$_3$)][PF$_6$] and [**L1**$_b$Pd(NCCH$_3$)][PF$_6$], respectively (Scheme 2.15). Similarly, reaction of **L1**$_a$PdCl with AgOTf in acetonitrile afforded [**L1**$_a$Pd(NCCH$_3$)][OTf] in good yield.
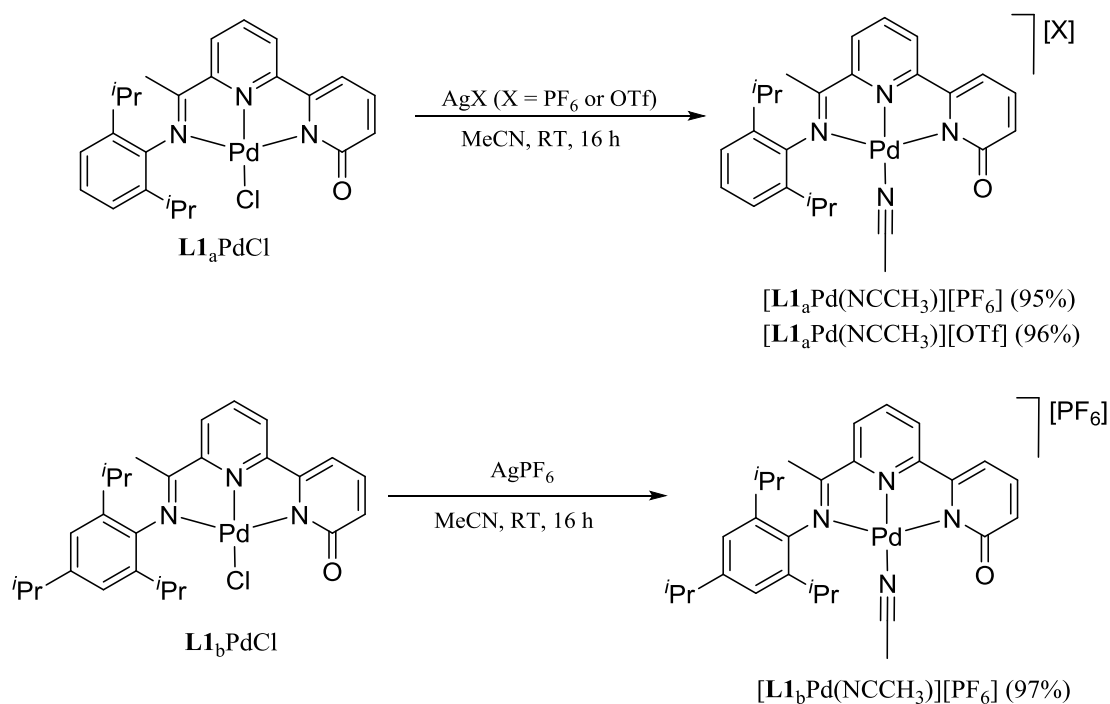
Scheme 2.15: Synthesis of [**L1**Pd(NCCH$_3$)][X] (X = PF$_6$ or OTf)

The ^{1}H NMR spectrum (recorded in CD$_3$CN at room temperature) of [**L1**$_a$Pd(NCCH$_3$)][PF$_6$] revealed a singlet at 1.88 ppm which corresponds to the coordinated acetonitrile protons. Another indication that the product was successfully formed was provided by the ^{19}F NMR spectrum which showed a doublet peak at -71.9 ppm for the PF$_6$ anion in the structure as well a peak at -144.6 ppm as a septet for PF$_6$ in the ^{31}P NMR spectrum. In the IR spectrum a peak at 2336 cm^{-1} confirmed the coordinated acetonitrile ligand. The HR mass spectrum revealed peaks for the cation at 519.1393 which compares with calculated mass for C$_{29}$H$_{29}$N$_4$OPdPF$_6$ of 519.1376 [M$^+$- PF$_6$].

In attempt to grow crystals of [**L1**$_a$Pd(NCCH$_3$)][PF$_6$] suitable for an X-ray diffraction study a sample was dissolved in bench dichloromethane and layered with hexane. After several days of standing at room temperature yellow blocks formed that were subject to the crystallographic study. A view of the structure is shown in Figure 2.15; selected bond lengths and angles are given in Table 2.7. Unexpectedly, the structure reveals that the NCMe ligand in [**L1**$_a$Pd(NCCH$_3$)][PF$_6$] had been substituted by a water molecule to give [**L1**$_a$Pd(OH$_2$)][PF$_6$]. The structure of [**L1**$_a$Pd(OH$_2$)][PF$_6$] consists of a distorted square planar geometry at Pd and an almost perfectly planar N^N^N conjugated cationic system and a PF$_6$ couter-ion. The Pd–N(2) bond length of 1.917(5) Å to the central atom of the N^N^N ligand is noticeably shorter when compared to the exterior Pd-N(1,3) distances

54

of 2.022(6)-2.026(6) Å and significantly shorter than the Pd–O bond distance [2.035(5)Å]. The exterior heterocyclic unit adopts the deprotonated pyridonate form which is evidenced by the C(1)-O(1) distance of 1.290(8) Å which is a bit long for the double bond. This could be the affect of the intramolecular hydrogen bonding between O(2)-H(2A)···O(1).
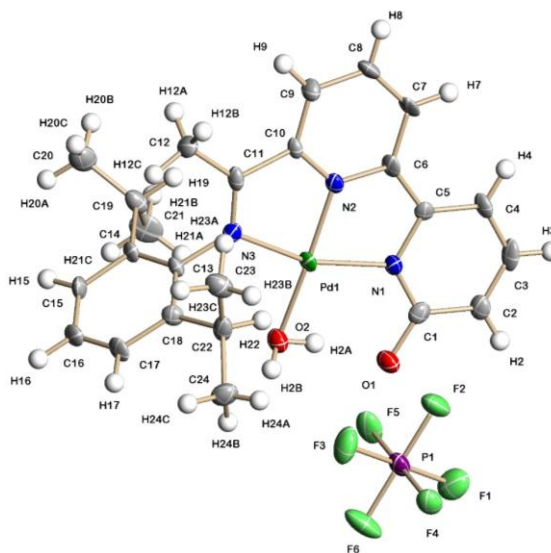
Figure 2.15: Molecular structure of [**L1**$_a$Pd(OH$_2$)][[PF$_6$]; the thermal ellipsoids are set at the 30% probability level

Table 2.7: Selected bond lengths (Å) and angles (°) of [**L1**$_a$Pd(OH$_2$)][PF$_6$]

Bond lengths (Å)		Bond angles (°)	
Pd(1)-N(2)	1.917(5)	N(2)-Pd(1)-N(1)	81.7(2)
Pd(1)-N(3)	2.022(6)	N(2)-Pd(1)-N(3)	80.2(2)
Pd(1)-N(1)	2.026(6)	N(1)-Pd(1)-N(3)	161.9(2)
Pd(1)-O(2)	2.034(5)	N(1)-Pd(1)-O(2)	97.7(2)
O(1)-C(1)	1.290(8)	N(3)-Pd(1)-O(2)	100.4(2)

It is likely that the water molecule in [**L1**$_a$Pd(OH$_2$)][PF$_6$] originates from small amounts of water present in bench dichloromethane. Several attempts were made to grow the crystals from acetonitrile and on one occasion a data set was collected which unfortunately again showed [**L1**$_a$Pd(OH$_2$)][PF$_6$]. Clearly, the acetonitrile ligand in [**L1**$_a$Pd(NCCH$_3$)][PF$_6$] is labile and reacts with any moisture present. Interestingly, [**L1**$_a$Pd(OH$_2$)][PF$_6$] undergoes self-dimerisation as shown in a Mercury® generated image (Figure 2.15.1) in a manner similar to some related complexes.[33] Both inter- and intramolecular hydrogen bonding are a feature of the resulting assembly.
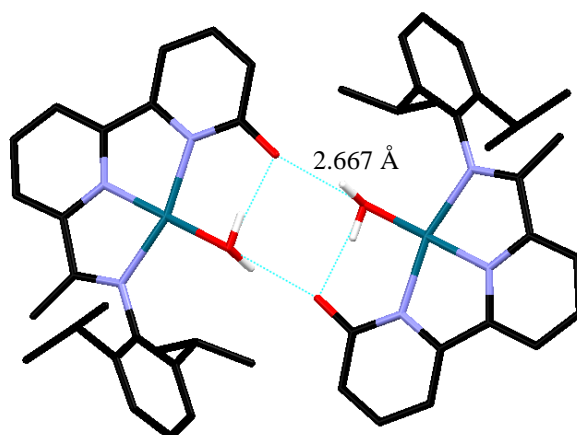
Figure 2.15.1: Self dimerization of the cationic units in $[(\mathbf{L1_a})Pd(OH_2)][PF_6]$ through inter- and intramolecular hydrogen bonding

The spectroscopic data for $[\mathbf{L1_a}Pd(NCMe)][OTf]$ and $[\mathbf{L1_b}Pd(NCMe)][PF_6]$ resemble those for $[\mathbf{L1_a}Pd(NCMe)][PF_6]$ with a signal for the bound acetonitrile appearing at 1.88 ppm in their ^{1}H NMR spectra. Additionally, their IR spectra reveal an absorption band at 2332 cm^{-1} for the bound acetonitrile. Support for the presence of the counter-ion is provided by a peak at -80.2 ppm corresponding to the anion in OTf and at -73.9 ppm for PF_6 in the ^{19}F NMR spectra. In their ESI mass spectra peaks corresponding to [M-OTf] and [M-PF$_6$] are evident. As with $[\mathbf{L1_a}Pd(NCMe)][PF_6]$ hydrolysis occurs on crystallisation from dichloromethane/hexane affording $[\mathbf{L1_a}Pd(OH_2)][OTf]$ and $[\mathbf{L1_b}Pd(OH_2)][PF_6]$. Views of $[\mathbf{L1_a}Pd(OH_2)][OTf]$ and $[\mathbf{L1_b}Pd(OH_2)][PF_6]$ are shown in Figure 2.16; selected bond distances and angles are presented in Tables 2.8a and 2.8b.
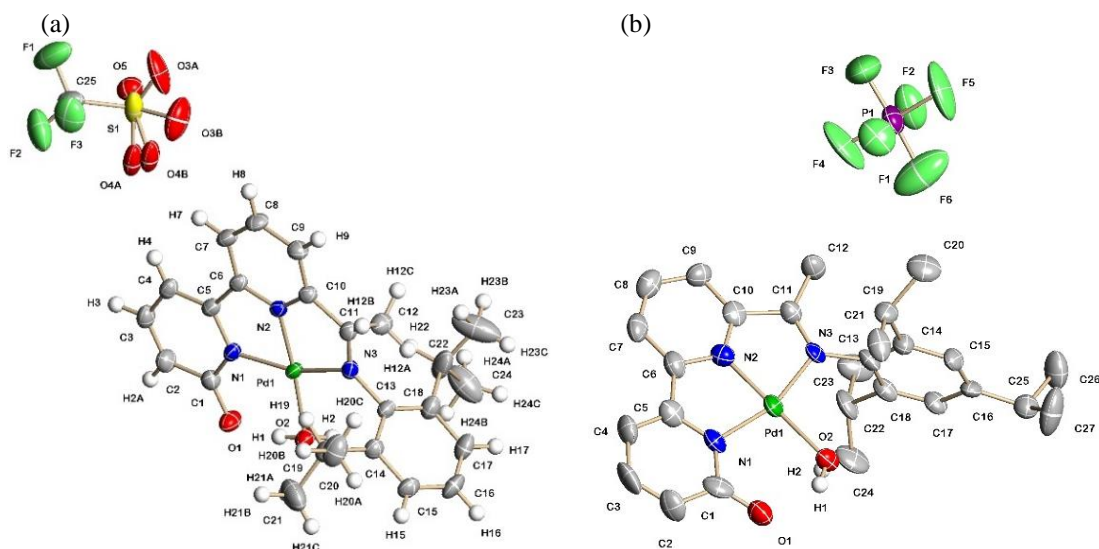
Figure 2.16: Molecular structures of (a) $[\mathbf{L1_a}Pd(OH_2)][OTf]$ and (b) $[\mathbf{L1_b}Pd(OH_2)][PF_6]$; the thermal ellipsoids are set at the 30% probability level

Table 2.8a: Selected bond lengths (Å) and angles (°) of [$\mathbf{L1}_a$Pd(OH$_2$)][PF$_6$]

Bond lengths (Å)		Bond angles (°)	
Pd(1)-N(2)	1.919(3)	N(2)-Pd(1)-N(1)	81.57 (14)
Pd(1)-N(3)	2.037(3)	N(2)-Pd(1)-N(3)	80.20 (14)
Pd(1)-N(1)	2.016(3)	N(1)-Pd(1)-N(3)	161.7 (14)
O(1)-C(1)	1.266(5)		

Table 2.8b: Selected bond lengths (Å) and angles (°) of [$\mathbf{L1}_b$Pd(OH$_2$)][PF$_6$]

Bond lengths (Å)		Bond angles (°)	
Pd(1)-N(2)	1.903(9)	N(2)-Pd(1)-N(1)	82.4 (4)
Pd(1)-N(3)	2.039(8)	N(2)-Pd(1)-N(3)	79.6 (4)
Pd(1)-N(1)	2.017(9)	N(1)-Pd(1)-N(3)	161.9 (4)
O(1)-C(1)	1.284(15)		

2.2.2.8 Exchange of acetonitrile in [L1Pd(NCMe)][X] for pyridines

Following the successful synthesis of cationic, [**L1**Pd(NCMe)][X], in which acetonitrile ligand has proved highly labile, it was of interest to substitute the acetonitrile for other nitrogen-based two electron donors. Firstly, we explored the exchange reaction of [**L1**Pd(NCMe)][PF$_6$] (**L1** = **L1**$_a$, **L1**$_b$) with 3,5-lutidine and found that [**L1**Pd(3,5-Me$_2$Py)][PF$_6$] (**L1** = **L1**$_a$, **L1**$_b$) could be isolated in good yield (Scheme 2.16). Moreover, [**L1**Pd(3,5-Me$_2$Py)][PF$_6$] (**L1** = **L1**$_a$, **L1**$_b$) can be prepared more directly from the one-pot reaction of **L1**PdCl with AgPF$_6$ and 3,5-lutidine in methanol. Both methods (1 and 2 in Scheme 2.16) gave spectroscopic and analytical data that were identical. Given the directness of route 2 we decided to focus on this approach to prepare other cationic complexes with the other pyridine ligands.
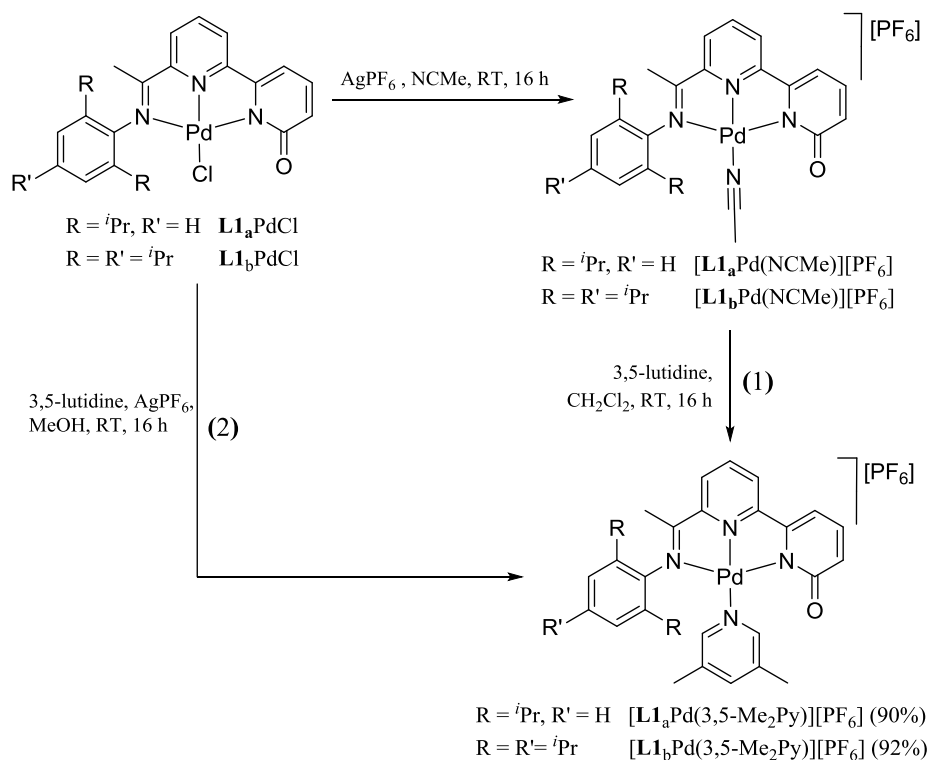
Scheme 2.16: Two approaches to [**L1**_aPd(3,5-Me₂Py)][PF₆] and [**L1**_bPd(3,5-Me₂Py)][PF₆]

The appearance of the three pyridine protons of the (3,5-Me₂*Py*) as two singlets in the aromatic region indicates the formation of [**L1**$_a$Pd(3,5-Me₂Py)][PF₆]. Also a singlet at 2.02 ppm for methyl of (3,5-*Me*₂Py). The FAB mass spectrum revealed a peak at m/z 585 corresponding to the cationic unit [M-PF₆]. The IR showed a peak at 1616 cm^{-1} for C=N$_{imine}$. A doublet peak at -72.1 ppm in the ^{19}F NMR spectra indicated the presence of PF₆ anion. Similar results were observed for [**L1**$_b$Pd(3,5-Me₂Py)][PF₆] and the proton NMR spectrum revealed singlet peaks at 7.90 ppm and 7.33 ppm corresponding to the pyridine protons of (3,5-Me₂*Py*). The FAB mass spectrum revealed a peak at m/z 627 corresponding to the cationic unit [M-PF₆].

In addition, crystals of [**L1**$_a$Pd(3,5-Me₂Py)][PF₆] suitable for an X-ray diffraction study were grown by slow evaporation of a methanol solution containing the complex. A view of the structure is shown in Figure 2.17; selected bond distances and angles are collected in Table 2.9. Surprisingly, the structure reveals a 1:1 mixture of [H**L1**$_a$Pd(3,5-Me₂Py)][PF₆]₂ and [**L1**$_a$Pd(3,5-Me₂Py)][PF₆]. Consequently, there are 1.5 PF₆ counter ions per Pd(+2) species in the unit cell (space group C2/c).
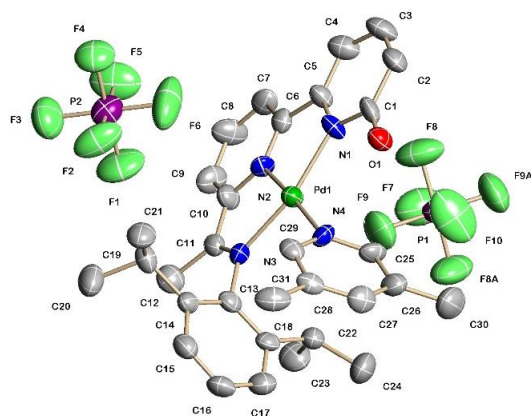
Figure 2.17: Molecular structure of a superimposed mixture of [H**L1**$_a$Pd(3,5-Me$_2$Py)][PF$_6$]$_2$ and [**L1**$_a$Pd(3,5-Me$_2$Py)][PF$_6$]. Note: solved in C2/c space group.

Table 2.9: Selected bond lengths (Å) and angles (°) for superimposed [H**L1**$_a$Pd(3,5-Me$_2$Py)][PF$_6$]$_2$ and [**L1**$_a$Pd(3,5-Me$_2$Py)][PF$_6$].

Bond Lengths (Å)		Bond Angles (°)	
Pd(1)-N(2)	1.947(6)	N(2)-Pd(1)-N(1)	80.6(3)
Pd(1)-N(3)	2.021(6)	N(2)-Pd(1)-N(3)	80.4(3)
Pd(1)-N(1)	2.046(6)	N(1)-Pd(1)-N(3)	160.9(3)
Pd(1)-N(4)	1.041(7)	N(2)-Pd(1)-N(4)	174.3(3)
O(1)-C(1)	1.277(9)		

To lend more support to the assignment of a mixture of [H**L1**$_a$Pd(3,5-Me$_2$Py)][PF$_6$]$_2$ and [**L1**$_a$Pd(3,5-Me$_2$Py)][PF$_6$], the structure was solved in the lower symmetry space group Cc. Pleasingly, the gross structures of the two separate complexes could be distinguished. While the data are not completely reliable, as this is the incorrect space group, it does clearly reveal distinct C-O distances for pyridinol [H**L1**$_a$Pd(3,5-Me$_2$Py)][PF$_6$]$_2$ and pyridonate [**L1**$_a$Pd(3,5-Me$_2$Py)][PF$_6$], *i.e.*, 1.37(3) vs. 1.18(4) Å for single and double bonds, respectively.
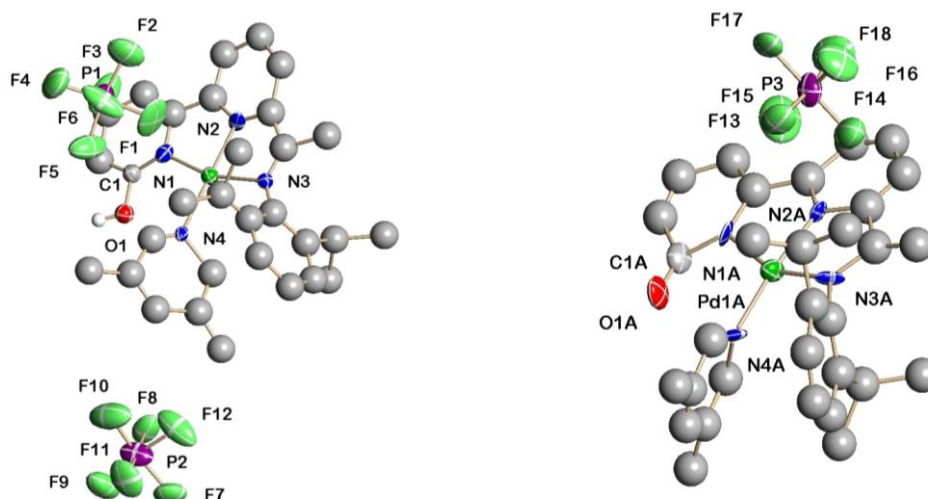
Figure 2.18: Molecular structure of co-crystallised [H**L1**$_a$Pd(3,5-Me$_2$Py))][PF$_6$]$_2$ and [**L1**$_a$Pd(3,5-Me$_2$Py))][PF$_6$]. Note: solved in the incorrect Cc space group.

Notably, a similar superposition of structures was observed for a crystal grown of [**L1**$_b$Pd(3,5-Me$_2$Py)][PF$_6$] (Figure 2.19). Again the two forms namely, [H**L1**$_b$Pd(3,5-Me$_2$Py)][PF$_6$]$_2$ and [**L1**$_b$Pd(3,5-Me$_2$Py)][PF$_6$], could be identified in the lower symmetry space group Cc. In this case the C-O distance for the pyridinol and pyridonate units are 1.330(15) and 1.274(14) Å, respectively.
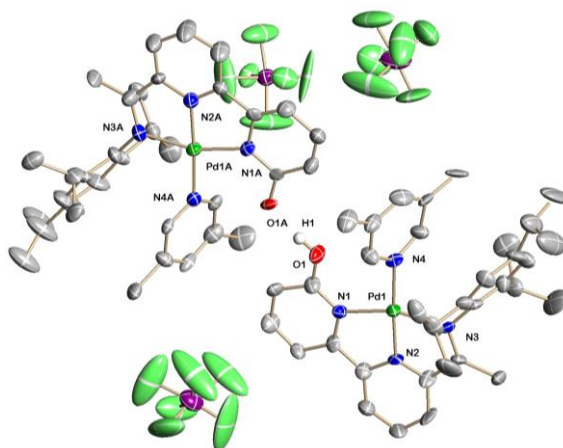
Figure 2.19: Molecular structure of co-crystallised [H**L1**$_b$Pd(3,5-Me$_2$Py))][PF$_6$]$_2$ and [**L1**$_b$Pd(3,5-Me$_2$Py))][PF$_6$]. Note: solved in the incorrect Cc space group.

It is uncertain as to how [H**L1**$_a$Pd(3,5-Me$_2$Py)][PF$_6$]$_2$ and [H**L1**$_b$Pd(3,5-Me$_2$Py)][PF$_6$]$_2$ were formed from their respective monocationic precursors [**L1**$_a$Pd(3,5-Me$_2$Py)][PF$_6$] and [**L1**$_b$Pd(3,5-Me$_2$Py)][PF$_6$] during crystallisation. It may be due to the acidity of methanol used for crystallisation.

Unfortunately, the one-pot reactions of **L1**PdCl with AgPF$_6$/PPh$_3$ or AgPF$_6$/3,5-dichloropyridine were unsuccessful (Scheme 2.17). It is likely the steric bulk of the

triphenylphosphine prevented its coordination while poor donor properties of 3,5-dichloropyridine inhibited its coordination.
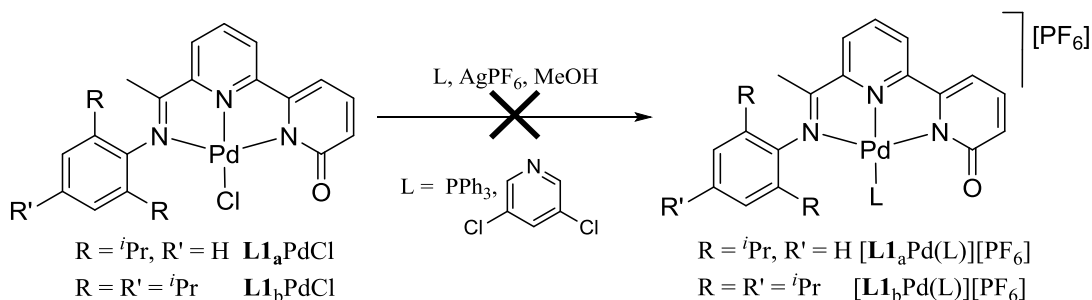
Scheme 2.17: Attempted chloride exchange with PPh$_3$ and 3,5-Cl$_2$C$_5$H$_3$N

2.2.2.9 Synthesis of dicationic [HL1Pd(NCMe)][PF$_6$]$_2$

Given the inadvertent dication formation during the crystallisation of both [**L1**$_a$Pd(3,5-Me$_2$Py)][PF$_6$] and [**L1**$_b$Pd(3,5-Me$_2$Py)][PF$_6$], we set about trying to prepare well-defined dications bearing H**L1**. Hence, reaction of H**L1**$_{a-c}$ with [Pd(NCMe)$_4$][PF$_6$]$_2$ (prepared *in-situ*) in acetonitrile at room temperature gave [H**L1**$_{a-c}$Pd(NCMe)][PF$_6$]$_2$ in high yield (90-98%) (Scheme 2.18).
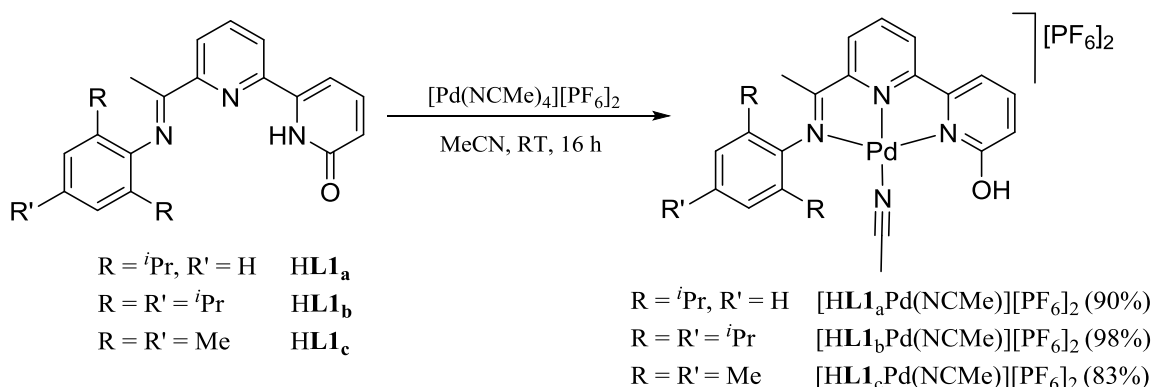
Scheme 2.18: Synthesis of [H**L1**$_a$Pd(NCMe)][PF$_6$]$_2$, [H**L1**$_b$Pd(NCMe)][PF$_6$]$_2$

and [H**L1**$_c$Pd(NCMe)][PF$_6$]$_2$

Analysis of the ^{1}H NMR spectrum for [H**L1**$_a$Pd(NCMe)][PF$_6$]$_2$ revealed two 6H doublets for the isopropyl methyl groups at 1.18 ppm and 1.00 ppm. In addition, a 3H singlet peak at 1.75 ppm corresponding to the coordinated acetonitrile ligand was detected. A 1H singlet at 10.77 pm was assigned to the OH proton indicating that the exterior heterocyclic unit adopts the pyridinol form. In addition, the Hα proton is seen in the aromatic region at 7.09 ppm further supporting the preference for the aromatic pyridinol form. The HR mass spectrum revealed peaks for the dicationic unit at 521.01389 which compares with

61

521.1380 calculated for $C_{26}H_{30}N_4OPd$ [M -PF_6(-HPF_6)]. In the IR spectrum an absorption band at 2339 cm^{-1} confirmed the presence of a bound acetonitrile ligand and at 3415 cm^{-1} for the OH vibrations.

The analytical data for [H**L1**$_b$Pd(NCMe)][PF$_6$]$_2$ and [H**L1**$_c$Pd(NCMe)][PF$_6$]$_2$ were similarly consistent with their formulations. Their ^{19}F NMR spectra revealed strong peaks at -72.4 ppm, indicating the presence of PF$_6$ units as the counter-ions. In addition, their ESI positive mass spectra gave strong [M -PF$_6$(-HPF$_6$)] peaks, while the PF$_6$ ions could be seen in their ESI negative mass spectra at m/z 145. Their IR spectra revealed absorption bands at 2336 cm^{-1} and 2333 cm^{-1} for the bound acetonitrile ligands in [H**L1**$_b$Pd(NCMe)][PF$_6$]$_2$ and [H**L1**$_c$Pd(NCMe)][PF$_6$]$_2$, respectively.

It is noteworthy that dicationic [H**L1**$_a$Pd(NCMe)][PF$_6$]$_2$ and [H**L1**$_b$Pd(NCMe)][PF$_6$]$_2$ can also be prepared by treating **L1**PdOAc with HPF$_6$ in acetonitrile (Scheme 2.19).

| R = ^{i}Pr, R' = H | **L1**$_a$PdOAc |
| R = R' = ^{i}Pr | **L1**$_b$PdOAc |

| R = ^{i}Pr, R' = H | [H**L1**$_a$Pd(NCMe)][PF$_6$]$_2$ |
| R = R' = ^{i}Pr | [H**L1**$_b$Pd(NCMe)][PF$_6$]$_2$ |
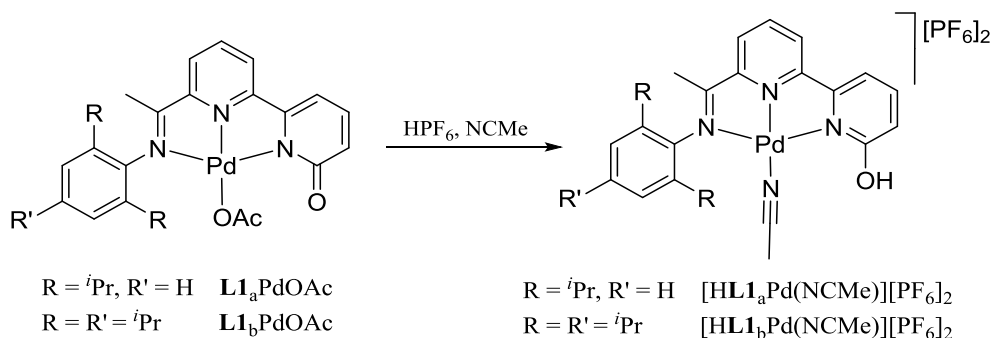
Scheme 2.19: Protonation of acetate-containing **L1**PdOAc as a route [H**L1**Pd(NCMe)][PF$_6$]$_2$

2.2.2.9 Probing the acid-base chemistry of the NNN-Pd complexes

As discussed in Chapter 1, complexes displaying proton responsiveness can be of importance in catalytic reactions. That is, the ligand structure of a metal complex can support deprotonation/re-protonation reversibly without undergoing undesirable side-reactions. Herein, we explore the reactivity of the NNN pincer complexes under different conditions to show that the ligand can change its bonding character to a metal during the introduction or removal of a proton.

From Scheme 2.20, [**L1**ₐPd(NCMe)][PF₆] can undergo reactions under acidic conditions to form the pyridinol form which is confirmed by proton NMR spectroscopy. Moreover, treating [H**L1**ₐPd(NCMe)][PF₆]₂ with Ag₂O regenerated the pyridonate form under these basic conditions. Based on these results it is apparent that these palladium(II) complexes can be readily protonated and deprotonated under mild conditions.
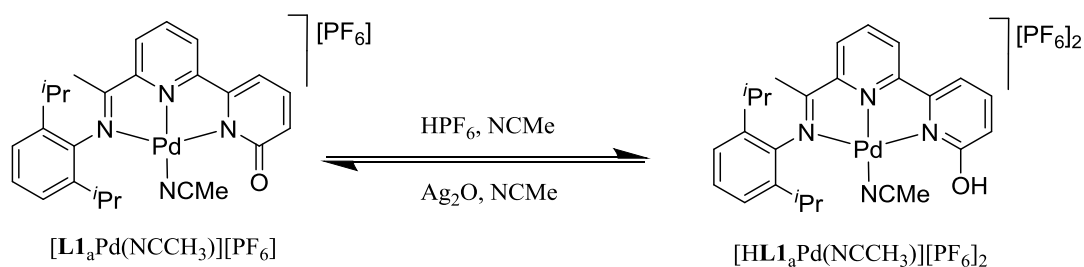
Scheme 2.20: Acid – base reactions between [**L1**ₐPd(NCMe)][PF₆] and [H**L1**ₐPd(NCMe)][PF₆]₂

Another example of the acid-base chemistry displayed by these palladium(II) complexes, is provided by the reactions of **L1**ₐPdCl with concentrated HCl to give cationic [H**L1**ₐPdCl][Cl]. This reaction can be readily reversed by treating [H**L1**ₐPdCl][Cl] with base (Scheme 2.20.1).
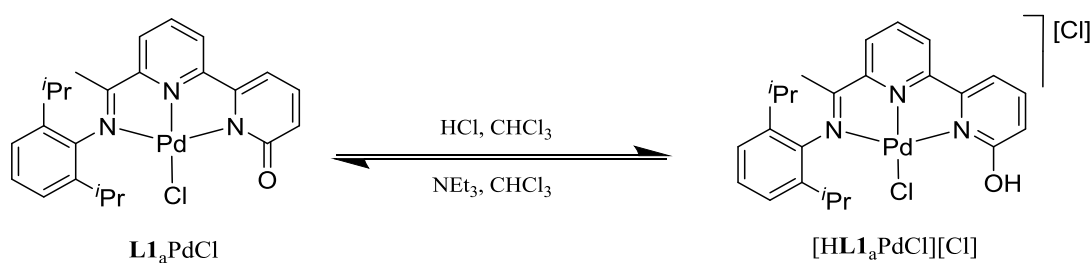
Scheme 2.20.1: Acid – base reactions

2.2.3 Reactions of HL1ₐ, HL1_b and HL1_c with Cl₂Pt(DMSO)₂

After noting the different reactivity patterns for these NNN pincer ligands with different palladium sources, we were interested to look at the reactivity of these ligands with other metals. Hence, reactions of H**L1**ₐ₋c with Cl₂Pt(DMSO)₂ (DMSO = dimethylsulfoxide) at elevated temperature in chloroform gave [H**L1**ₐPtCl][PtCl₃(DMSO)], [H**L1**_bPtCl][PtCl₃(DMSO)] and [H**L1**_cPtCl][PtCl₃(DMSO)] in good to excellent yield (Scheme 2.21). However, the reaction of H**L1**_c with Pt source takes 48h instead of 18h, this is likely due to solubility issues of the ligand. The three complexes have been

63

characterised by ^{1}H/^{13}C NMR, IR spectroscopy and mass spectrometry. In addition, [H**L1**$_a$PtCl][PtCl$_3$(DMSO)] and [H**L1**$_b$PtCl][PtCl$_3$(DMSO)] have been the subject of single crystal X-ray diffraction studies.

R = ^{i}Pr, R' = H	H**L1**$_a$	
R = R' = ^{i}Pr	H**L1**$_b$	
R = R' = Me	H**L1**$_c$	

R = ^{i}Pr, R' = H	[H**L1**$_a$PtCl][PtCl$_3$(DMSO)] (92%)
R = R' = ^{i}Pr	[H**L1**$_b$PtCl][PtCl$_3$(DMSO)] (96%)
R = R' = Me	[H**L1**$_c$PtCl][PtCl$_3$(DMSO)] (60%)
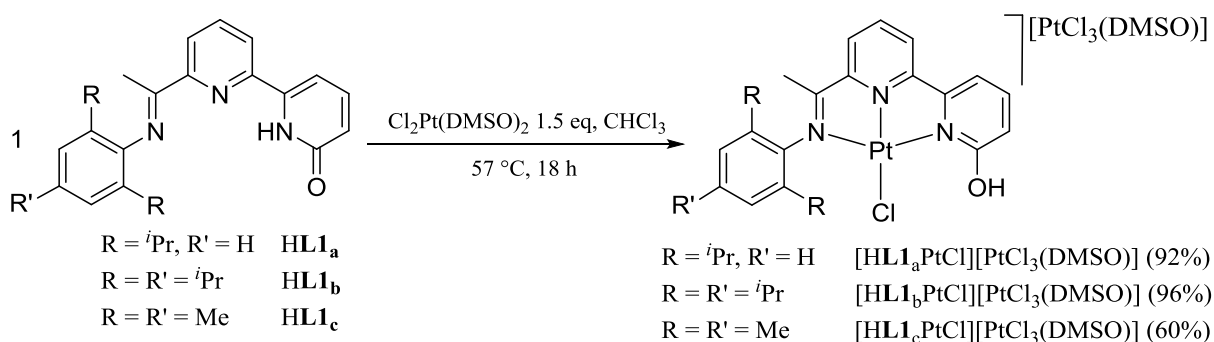
Scheme 2.21: Synthesis of [H**L1**$_a$PtCl][PtCl$_3$(DMSO)], [H**L1**$_b$PtCl][PtCl$_3$(DMSO)] and [H**L1**$_c$PtCl][PtCl$_3$(DMSO)]

In the ^{1}H NMR spectrum of [H**L1**$_a$PtCl][PtCl$_3$(DMSO)], a singlet peak corresponding to the OH proton was observed at 11.05 ppm. Two 6H doublets were observed for the isopropyl CH*Me*$_a$*Me*$_b$ methyl groups at 1.35 ppm and 1.21 ppm. The IR data showed bands at 1630 cm^{-1} and 3663 cm^{-1} which indicated the C=N$_{imine}$ and OH functional groups, respectively. The high resolution mass spectrum revealed a peak at 604.1478 corresponding to the cationic unit which compared with 604.1492 for the calculated mass for M-(DMSOPtCl$_3$).

The ^{1}H NMR spctrum of [H**L1**$_b$PtCl][PtCl$_3$(DMSO)] and [H**L1**$_c$PtCl][PtCl$_3$(DMSO)] showed similar features to the [H**L1**$_a$PtCl][PtCl$_3$(DMSO)], with the OH peak detected at 10.99 ppm and 11.01 ppm in their proton NMR, respectively. The IR spectra showed a peak at 1631 cm^{-1} and 1629 cm^{-1} corresponding to the C=N$_{imine}$ bond coordinating to the metal. The high resolution mass spectrum revealed a peak for [M-(PtCl3(DMSO))]in both complexes.

Single crystals of [H**L1**$_a$PtCl][PtCl$_3$(DMSO)] and [H**L1**$_b$PtCl][PtCl$_3$(DMSO)] suitable for the X-ray determinations were grown by slow diffusion of hexane in chloroform solution of the complexes. The views structure are shown in Figures 2.20 and 2.21; selected bond distances and angles are given in Tables 2.10 and 2.11. The structures of [H**L1**$_a$PtCl][PtCl$_3$(DMSO)] and [H**L1**$_b$PtCl][PtCl$_3$(DMSO)] are similar and will be

discussed together. The X-ray structures consist of a complex cation and a complex anion. Within the cation a distorted square planar geometry is exhibited by the Pt centre and is bound by an almost planar N^N^N ligand and a chloride while in the anion the Pt centre is surrounded by three chloride ligands and sulphur bound DMSO. As with previous structures Pt–N bond length to the central atom of N^N^N ligand is the shortest of the three NNN-Pt contacts. The C(1)-O(1) bond lengths for[H**L1**$_a$PtCl][PtCl$_3$(DMSO)] and [H**L1**$_b$PtCl][PtCl$_3$(DMSO)] are 1.329(17) and 1.309(10) Å which is consistent with as a single bond and hence the exterior heterocyclic unit is adopting the pyridinol form. An intramolecular hydrogen bond has been seen in both structure between O(1)-H(1)···Cl(1) 2.11 Å and 2.116 Å.
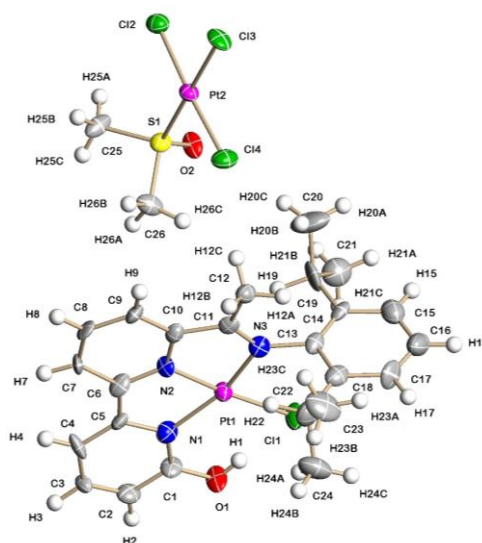
Figure 2.20: Molecular structure of [H**L1**$_a$PtCl][PtCl$_3$(DMSO)]; the thermal ellipsoids are set at the 30% probability level

Table 2.10: Selected bond lengths (Å) and angles (°) of [H**L1**$_a$PtCl][PtCl$_3$(DMSO)]

Bond Lengths (Å)		Bond Angles (°)	
Pt(1)-N(2)	1.927(11)	N(2)-Pt(1)-N(3)	79.8(5)
Pt(1)-N(3)	2.039(12)	N(2)-Pt(1)-N(1)	81.8(5)
Pt(1)-N(1)	2.076(13)	N(3)-Pt(1)-N(1)	161.3 (5)
Pt(1)-Cl(1)	2.306(4)	N(1)-Pt(1)-Cl(1)	101.7 (4)
O(1)-C(1)	1.329(17)	N(3)-Pt(1)-Cl(1)	96.8 (4)
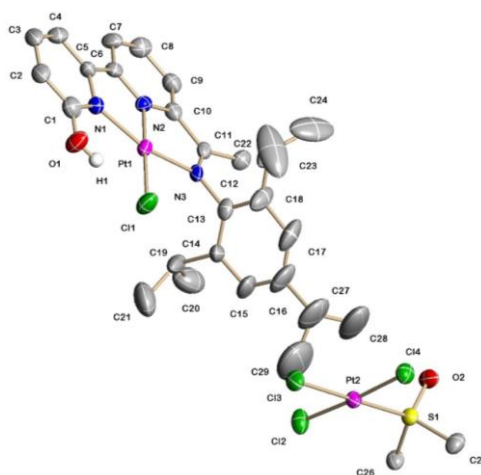
Figure 2.21: Molecular structure of [H**L1**_bPtCl][PtCl₃(DMSO)]; the thermal ellipsoids are set at the 30% probability level (all hydrogen atoms have been removed for clarity)

Table 2.11: Selected bond lengths (Å) and angles (°) for [H**L1**ₐPtCl][PtCl₃(DMSO)]

Bond Length (Å)		Bond Angle (°)	
Pt(1)-N(2)	1.936(6)	N(2)-Pt(1)-N(3)	81.2 (3)
Pt(1)-N(3)	2.034(6)	N(2)-Pt(1)-N(1)	80.1 (2)
Pt(1)-N(1)	2.037(6)	N(3)-Pt(1)-N(1)	161.0 (3)
Pt(1)-Cl(1)	2.309(2)	N(1)-Pt(1)-Cl(1)	102.64 (18)
O(1)-C(1)	1.309(10)	N(3)-Pt(1)-Cl(1)	96.18 (19)

2.2.4 Reactions of HL1ₐ, HL1_b, HL1_c, L1_OMe and L1_H with RuCl₂(PPh₃)₃

Complexation of H**L1**$_{a-c}$ with ruthenium(II) has been achieved using RuCl₂(PPh₃)₃ as the source of ruthenium. Typically, the reactions were carried out in toluene at reflux resulting in the products, H**L1**ₐRuCl₂(PPh₃), H**L1**_bRuCl₂(PPh₃) and H**L1**_cRuCl₂(PPh₃), precipitating in the reaction pot (Scheme 2.22). Very high yields were reported with the exception of H**L1**_cRuCl₂(PPh₃). The three complexes have been characterised by ¹H/¹³C NMR, IR spectroscopy and mass spectrometry.

Scheme 2.22: Synthesis of $HL1_aRuCl_2(PPh_3)$, $HL1_bRuCl_2(PPh_3)$ and $HL1_cRuCl_2(PPh_3)$

In the ^1H NMR spectrum of the $HL1_aRuCl_2(PPh_3)$ a few interesting features have been observed. There were two septets corresponding to $CH(Me_2)$ protons of the isopropyl moiety and four 3H doublets for the $CH(Me_2)$ methyl groups. This indicated that the coordination has been achieved, the two ^iPr groups now inequivalent due to lack of symmetry of carbon atoms C5/5´ and C6/6´ (Figure 2.21). Moreover, one of the ^iPr methyl peaks came at -0.44 ppm in the proton NMR spectrum; this could be caused by the PPh_3 group on the ligand. Additionally, the ^{31}P NMR showed a peak at 40.8 ppm supportive of PPh_3 coordination to the metal. The high resolution mass spectrum revealed a fragmentation peak at 738.2064 which compares with 738.2041 calculated for $C_{42}H_{42}N_3ORuP$ [M-Cl(-HCl)]. The IR spectrum showed the imine absorption to have shifted from 1644 cm^{-1} (in the ligand) to 1630 cm^{-1} in the complex. In addition, a peak at 3694 cm^{-1} corresponded to the OH functionality.

Figure 2.21: C5, C6 in $HL1_aRuCl_2(PPh_3)$

The analysis of $HL1_bRuCl_2(PPh_3)$ and $HL1_cRuCl_2(PPh_3)$ in the proton NMR spectrum showed similar features to $HL1_aRuCl_2(PPh_3)$. To be precise, three septet peaks corresponding to the proton on the ^iPr moiety, six 3H doublets of triisopropyl methyl

group and three singlets for the methyl group were observed in their proton NMR respectively. A fragment peak of [M-Cl] at m/z 778 and m/z 694 in the mass spectrum for **HL1$_b$RuCl$_2$(PPh$_3$)** and **HL1$_c$RuCl$_2$(PPh$_3$)**, respectively. The ^{31}P NMR spectrum revealed a peak at 40.9 ppm in both complexes.

In addition, complex **L1$_H$RuCl$_2$(PPh$_3$)** was obtained in 69% yield by treating **L1$_H$** with RuCl$_2$(PPh$_3$) in toluene at reflux (Scheme 2.23) The ^{1}H NMR spectrum revealed two septet peaks at 4.82 ppm and 2.04 ppm which were assigned to the inequivalent C*H*Me$_2$ protons of the isopropyl groups, as well as four 3H isopropyl methyl groups at 1.54 ppm, 0.93 ppm, 0.76 ppm and - 0.55 ppm. The high resolution mass spectrum showed a peak at 756.1879 corresponding to M-Cl, which compared to the calculated value of 756.1848 for C$_{42}$H$_{42}$N$_3$ORuClP [M$^+$- Cl].
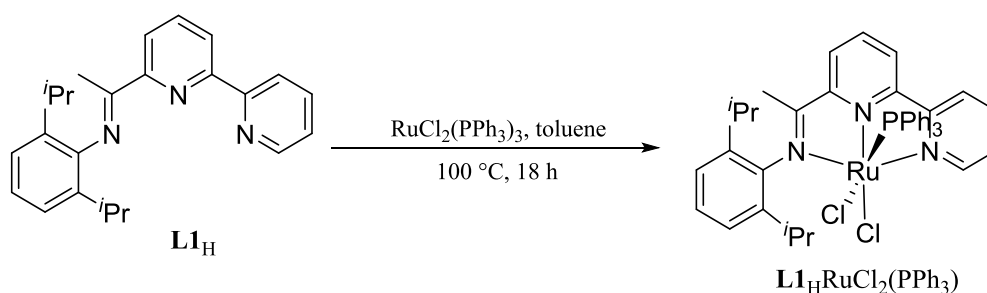
Scheme 2.23: Synthesis of **L1$_H$RuCl$_2$(PPh$_3$)**

On the other hand, the synthesis of **L1$_{OMe}$RuCl$_2$(PPh$_3$)** was not achieved under the same reaction conditions to the other ligands discussed above (Scheme 2.24); with starting material still present after 18 hours at reflux. In addition, changing the reaction solvent or time gave no evidence of the target complex. It is uncertain as to the origin of this difference in reactivity but it may due to the steric properties of methoxy group at the 2-position of the pyridine.
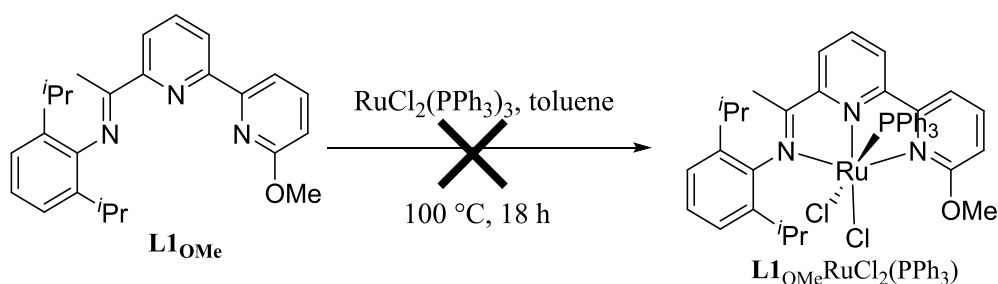
Scheme 2.24: Attempted synthesis of **L1$_{OMe}$RuCl$_2$(PPh$_3$)**

2.3 Conclusions

The synthesis of three novel OH-functionalised NNN-pincer ligands, H**L1**$_a$, H**L1**$_b$ and H**L1**$_c$ and their reactivity has been described in this Chapter. The ligands have been prepared by Stille cross coupling followed by Schiff base condensation reactions with three types of sterically and electronically different anilines. All the ligands were obtained in good to excellent yields. Furthermore, the reaction of these ligands with various transition metals including palladium, platinum and ruthenium are discussed. The palladium(II) complexes have been prepared and fully characterised by ^{1}H/^{13}C NMR, IR spectroscopy and by mass spectrometry; in many cases single crystal X-ray diffraction studies have been performed. The reaction of the H**L1** with Pd(OAc)$_2$ has been shown to give the neutral pyridonate complexes **L1**Pd(OAc). On the other hand, reacting H**L1** with Cl$_2$Pd(NCMe)$_2$ has been shown to form the cationic pyridinol complexes, [H**L1**PdCl][Cl], which can be used in counterion metathesis or be deprotonated with base under mild conditions to form neutral **L1**PdCl. Moreover, the reactivity of **L1**PdCl has been explored and it has been shown that on treatment with a silver salt in acetonitrile the cationic species, [**L1**Pd(NCMe)][X], are afforded in good yield. Exchange of the MeCN ligand with 3,5-lutidine gave monocationic [**L1**Pd(3,5-Me$_2$Py)][X], which on crystalliation from methanol gave an unexpected mixture of both monocation and dicationic [H**L1**Pd(3,5-Me$_2$Py)][X]$_2$. The palladium complexes were also shown to be susceptible to reactivity under basic and acidic conditions leading to some unusual acid-base chemistry and hence highlighting the proton responsiveness of this ligand set. In addition, complexes of the type [H**L1**PtCl][PtCl$_3$(DMSO)], H**L1**RuCl$_2$(PPh$_3$) and **L1**$_H$RuCl$_2$(PPh$_3$) were isolated and fully characterised.

References

1. C. J. Moulton and B. L. Shaw, *J. Chem. Soc. Dalton Trans*., 1976, 1020.

2. E. Kinoshita, K. Arashiba, S. Kuriyama, Y. Miyake, R. Shimazaki, H. Nakanishi and Y. Nishibayashi, *Organometallics*, 2012, **31**, 8437.

3. D. Benito-Garagorri, L. G. Alves, M. Puchberger, K. Mereiter, L. F. Veiros, M. J. Calhorda, M. D. Carvalho, L. P. Ferreira, M. Godinho and K. Kirchner, *Organometallics,* 2009, **28**, 6902

4. M. A. Halcrow, *Coord. Chem. Rev*., 2005, **249**, 2880.

5. F. Zeng and Z. Yu, *Organometallics*, 2008, **27**, 2898

6. (a) W. Jin, L. Wang and Z. Yu, *Organometallics*, 2012, **31**, 5664; (b) M. Zhao, Z. Yu, S. Yan and Y. Li, J. *Organomet. Chem*., 2009, **694**, 3068.

7. W. Ye, M. Zhao, W. Du, Q. Jiang, K. Wu, P. Wu and Z. Yu, *Chem. – Eur. J.,* 2011, **17**, 4737.

8. M. Albrecht, G. V. Koten, *Angew. Chem. Int. Ed*. 2001, 3750.

9. M. E. V. D. Boom and D. Milstein, *Chem. Rev*., 2003, **103**, 1759.

10. J. T. Singleton, *Tetrahedron*, 2003, **59**, 1837.

11. I. P. Beletskaya and A. V. J. Cheprakov, *J. Organomet. Chem.,* 2004, **689**, 4055.

12. J. Dupont, M. Pfeffer and J. Spencer, *Eur. J. Inorg. Chem*., 2001, 1917.

13. B. L. Shaw, S. D. Perera and E. A. Staley, *Chem. Comm.,* 1998, 1361.

14. M. R. Eberhard, *Org. Lett.* 2004, **6**, 2125.

15. M. H. Aaron, Gu. Weixing, B. Nattamai, andV. O. Oleg, *Inorg. Chem*., 2011, **50**, 3673.

16. J. A. Gaunt, V. C. Gibson, A. Haynes, S. K. Spitzmesser, A. J. P. White and D. J. Williams, *Organometallics,* 2004, **23**, 1015.

17. V. C. Gibson, S. K. Spitzmesser, A. J. P. White and D. J. Williams, *Dalton Trans*., 2003, 2718.

18. G. J. P. Britovsek, V. C. Gibson, O. D. Hoarau, S. K. Spitzmesser, A. J. P. White and D. J. Williams, *Inorg. Chem*., 2003, **42**, 3454.

19. (a) W. Jin, L. Wang and Z. Yu, *Organometallics*, 2012, **31**, 5664. (b) Q. Wang, K. Wu and Z. Yu, *Organometallics*, 2016, **35**, 1251.

20. G. J. P. Britovsek, S.P. D. Baugh, O. Hoarau, D. F. Wass, A. J. P. White, D. J. Williams and V. C. Gibson, *Inorg. Chim. Acta.,* 2003, **345**, 279.

21. F. Vizza, A. Toti, L. Sorace, A. Meli, C. Mealli, F. Laschi, I. G. Rios, G. Giambastiani, D. Gatteschi and C. Bianchini, *Organometallics*, 2007, **26**, 726.

22. W-H. Wang, J. T. Muckerman, E. Fujita and Y. Himeda, *New J. Chem.*, 2013, **37**, 1860.

23. J. B. Geri, N. K. Szymczak, *J. Am. Chem. Soc.,* 2015, **137**, 12808.

24. C. M. Moore, B. Bark, N. K. Szymczak, *ACS Catal*., 2016, **6**, 1981.

25. C. M. Moore and N. K. Szymczak, *Chem. Commun.,* 2013, **49**, 400.

26. Y. D. M. Champouret, R. K. Chaggar, I. Dadhiwala, J. Fawcett and G. A. Solan, *Tetrahedron,* 2006, **62**, 79.

27. B. E. Wagner, R. H. Holm and J. E. Parks, *J. Organoment. Chem.,* 1974, **56**, 53.

28. D. Milsten and J. K. Stille, *J. Am. Chem. Soc.,* 1978, **100**, 3636.

29. A. Goller and U. W. Grummt, *Chem. Phys. Lett*., 2000, **321**, 399.

30. P. Beak, *Acc. Chem. Res.,* 1977, **10**, 186.

31. Handbook of chemistry and physics, 55th edition, O. Kennard, 1974-1975, F 201.

32. B. Crociani, M. Sala, A. Polo and G. Bombieri, *Organometallics,* 1986, **5**, 1369.

33. A. Kvick, *Acta Crystallogr*., 1953, **6**, 591.

Chapter Three

Synthesis of OH-functionalised NN ligands and their

reactivity towards group 10 metals

3.1 Introduction

Over the years transition metal complexes containing bidentate ligands have received considerable attention due to their unusual properties and catalytic reactivity in synthetic inorganic and organic chemistry.[1-3] There are many types of bidentate ligand that on coordination to a metal form chelates that can have applications as catalysts or as stoichiometric reagents in chemical synthesis. N,N-chelating ligands are among the most common examples of bidentate ligands and one well-known class is the pyridylimines (Figure 3.1), which contain a pyridine and an imine as the nitrogen donors with the N_{imine}-substituent typically an aryl group; alkyl substituents are also known. Significantly, the nature of the substitution pattern on the N-aryl group can affect the electronic and steric properties of the resultant complex as well as its solubility.[4,5] These ligands have been explored with different metals and used as catalysts in a wide range of reactions.[4-7]

R_1 = H, alkyl or aryl
R_2 = alkyl or aryl
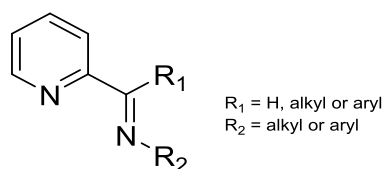
Figure 3.1: N,N-Pyridylimines

Elsewhere, 2,2'-bipyridine represents another important class of chelating ligand in coordination and organometallic chemistry (Figure 3.2).[8-13]Among this class, 6,6'- and 4,4'-dihydroxy derivatives of 2,2'-bipyridine have been of great interest in recent years due to their functional properties which include their ability to mediate hydrogen bonds and their capacity to act as sources of protons. These ligands which are called proton responsive ligands have been studied with different metals such as Ir, Rh, Ru and their resultant complexes have been reported to be highly active catalysts in C-C bond forming reactions[10] and in transfer hydrogenation reactions.[14-20] Given the rapid advances in proton responsive catalysis, the development of new functional ligand systems represents a key target in homogeneous catalysis.
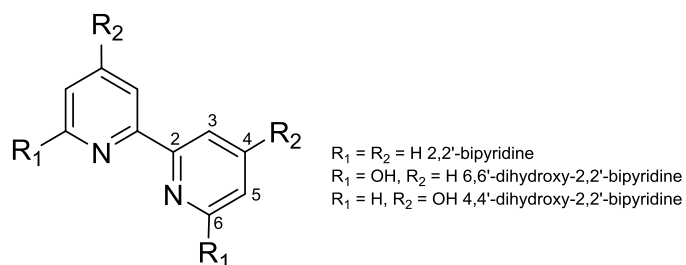
Figure 3.2: 2,2'-Bipyridine and its hydroxy derivatives

One example of a complex bearing the proton responsive, 6,6'-dihydroxy-2,2'-bipyridine, has been reported by Fujita *et al.* (Figure 3.3).[19a] This iridium complex has been used in the dehydrogenation of alcohols under mild conditions and it is found that the catalyst efficiently converted alcohols to aldehydes and ketones with high turnover numbers.
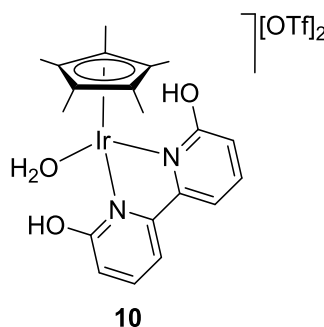
Figure 3.3: Iridium complex bearing a proton responsive ligand

Later Li and co-workers reported that the same iridium complex can be used as a catalyst in the formation of α-alkylated ketones via the tandem dehydrogenation/α-alkylation of secondary and primary alcohols.[19b] They found that the complex was a highly active catalyst in this reaction and gave up to 90% yield of the product.

From the literature review in Chapter 1 and above, it is notable that the incorporation of a hydroxypyridine (*i.e.*, a pyridinol/pyridone) group within a multidentate ligand has emerged as an important topic and especially in the context of platinum group metals. This is due to the fascinating properties that this unit can impart on the complex (*e.g.*, de-protonation/re-protonation chemistry, hydrogen bonding etc) and in particular with regard to its function as a catalyst for a variety of processes. Elsewhere, pyridylimine complexes have also been studied and used as catalysts in many different types of transformation including alkene polymerisation, C-C bond formation and C-H activation. However, from examination of the literature no reports, to the knowledge of the author, have emerged of

74

group 10 complexes containing pyridone-imine (or pyridinol-imine) as the N,N-ligand manifold.

3.1.2 Aims and objectives

In this Chapter we target two classes of N,N-bidentate ligand namely, H**L2** and H**L3**, in which an OH functional group is located at either the 2- or 4-position, respectively (Figure 3.4). In addition, three types of sterically bulky N-aryl groups, 2,6-diisopropylphenyl, 2,4,6-triisopropylphenyl and 2,6-diisopropyl-4-bromophenyl, will be prepared in which the electronic properties of the 4-position are systematically varied; some impact on ligand/complex solubility is also anticipated. The reactivity of H**L2** and H**L3** towards a range of Pd(II), Pt(II) and Ni(II) salts will be thoroughly investigated in order to ascertain the preferred coordination mode and charge on the heterocyclic unit of the N,N-ligand. Furthermore, since the ligands are expected to be proton responsive, the reactions of a selection of the resulting compounds towards acids and bases will be investigated. All ligands and complexes will be fully characterised by ^{1}H/^{13}C, NMR and IR spectroscopies as well as by mass spectrometry and elemental analysis. Where possible single crystal X-ray diffraction will be used to fully elucidate the structural features.

R = H   H**L2**$_a$
R = ^{i}Pr H**L2**$_b$
R = Br H**L2**$_c$

R = H   H**L3**$_a$
R = ^{i}Pr H**L3**$_b$
R = Br H**L3**$_c$
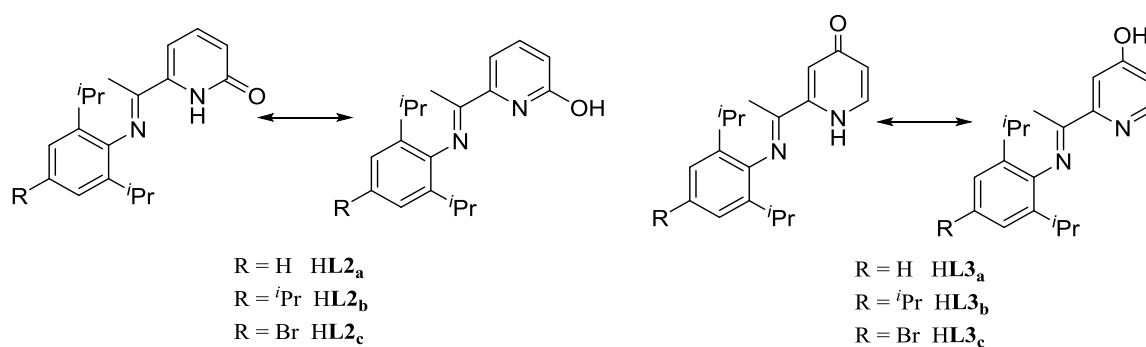
Figure 3.4: Target N,N-ligands, H**L2** and H**L3**, to be developed in this Chapter; their tautomeric forms are also shown.

3.2 Results and discussion

3.2.1 Ligand synthesis

This section focuses on the synthesis of the 6-imino-2-pyridones, **HL2ₐ HL2ᵦ, HL2ᵧ** and the 6-imino-4-pyridones, **HL3ₐ, HL3ᵦ** and **HL3ᵧ**. The overall multi-step synthetic routes adopted for each class are shown in Schemes 3.1a and 3.1b.
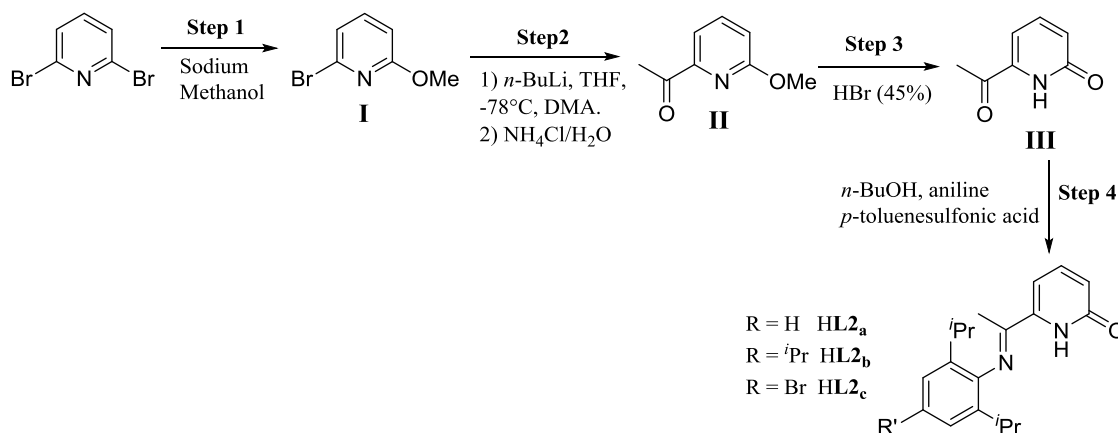
Scheme 3.1a: Four step synthesis of **HL2**
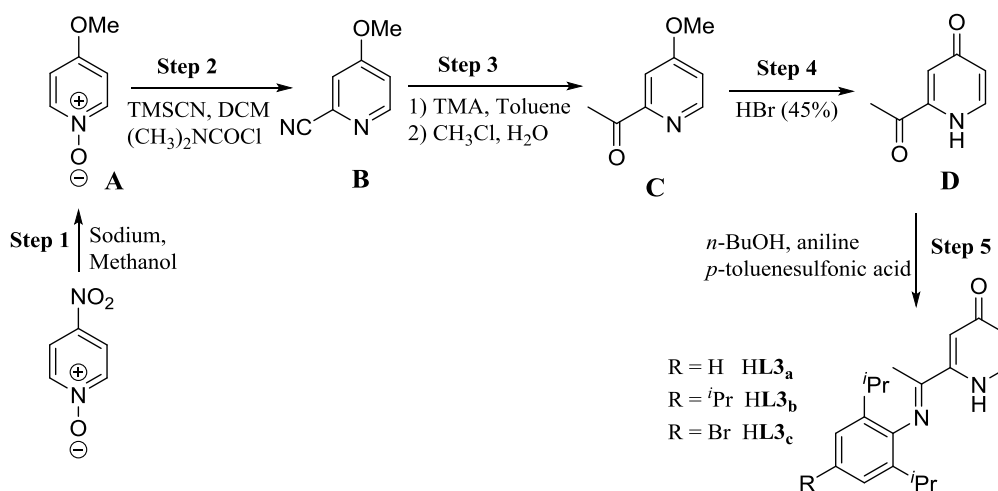
Scheme 3.1b: Five step synthesis of **HL3**

3.2.1a Synthesis of HL2

2-Bromo-6-methoxypyridine (**I**) was obtained in 99% from 2,6-dibromopyridine using the method described by Snieckus *et al* (Scheme 3.1a).[21] Conversion of **I** to 1-(6-methoxypyridine-2-yl)ethanone (**II**) was achieved by treatment firstly with *n*-BuLi and then dimethylacetamide (DMA) affording **II** in 92% yield.[22,23] The next step was the

deprotection of the methoxy group in **II**, which was carried out by heating it in HBr in glacial acetic acid (45%) to form the 6-acetylpyridine-2-(IH)-one (**III**) in 92% yield.[22] All the synthetic intermediates were characterized by proton NMR spectroscopy and the data are consistent with those reported in the literature.

The 6-imino-2-pyridones, 6-(4-R-2,6-i-Pr$_2$C$_6$H$_2$)N=CMe)C$_5$H$_3$NH-2-O (R = H H**L2**$_a$, i-Pr H**L2**$_b$, Br H**L2**$_c$), were then formed via the condensation reaction of the ketone precursor, **III**, with the corresponding aniline (Scheme 3.2). In each case the reactions were carried out under reflux in n-BuOH for 3 days in the present of *p*-toluene sulfonic acid as catalyst affording **L2**$_a$ – **L2**$_c$ in yields between 82 and 89%.[22,24]

R = H   H**L2**$_a$ (82%)
R = ^{i}Pr H**L2**$_b$ (89%)
R = Br   H**L2**$_c$ (85%)
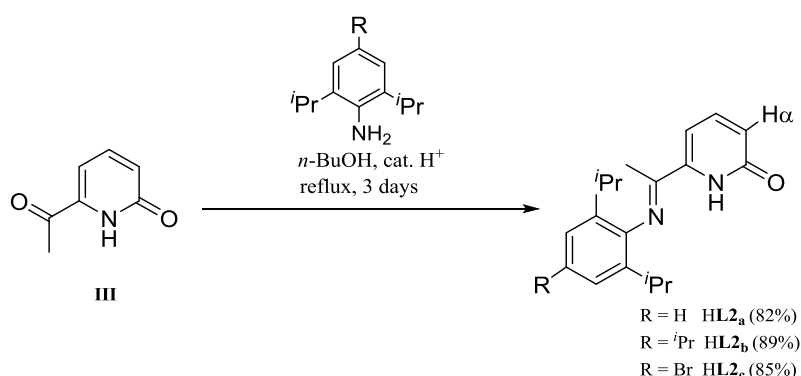
Scheme 3.2: Synthesis of H**L2**$_a$, H**L2**$_b$ and H**L2**$_c$

The ^{1}H NMR spectrum of H**L2**$_a$, showed a 12H doublet at 1.11 ppm and 2H septet at 2.56 ppm, signals assigned to the isopropyl group. The NH proton of the pyridone was seen at 10.33 ppm. The IR spectrum showed an absorption band at 1651 cm^{-1} which is typical of a C=N$_{imine}$ functionality.

A crystal of H**L2**$_a$ suitable for a single crystal X-ray diffraction study was grown by slow diffusion of hexane into a dichloromethane solution of the compound. A view of H**L2**$_a$ is shown in Figure 3.5; selected bond distances and angles are given in Table 3.1. The structure consists of a 2-pyridone heterocycle linked at its 6-position by a CMe=N(2,6-i-Pr$_2$C$_6$H$_3$) unit. Both the imine and the pyridone nitrogens, N1 and N2, are found in a *cis*-arrangement to one another.[25] This is due to intra-molecular hydrogen-bonding associated with N2 and H1 allowing for this conformation to exist (N(1)-H(1)···N(2) 2.010 Å). The C(1)-O(1) bond distance is 1.251(4) Å which is consistent with a double bond, supporting the presence of the pyridone tautomer in the solid state. As previously observed for 2-

pyridones,[26] H**L2**$_a$ undergoes self-dimerisation as shown be in a Mercury® generated image (Figure 3.6).
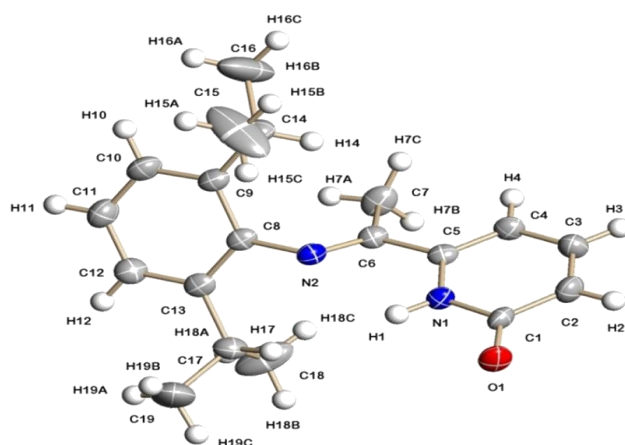
Figure 3.5: Molecular structure of H**L2**$_a$; the thermal ellipsoids are set at the 30% probability level

Table 3.1: Selected bond lengths (Å) and angles (°) for H**L2**$_a$

Bond lengths (Å)		Bond angles (°)	
O(1)-C(1)	1.251(4)	O(1)-C(1)-N(1)	121.4(3)
N(2)-C(5)	1.288(4)	C(5)-N(1)-C(1)	124.4(3)
N(1)-C(1)	1.369(4)	C(6)-N(2)-C(8)	120.9(3)
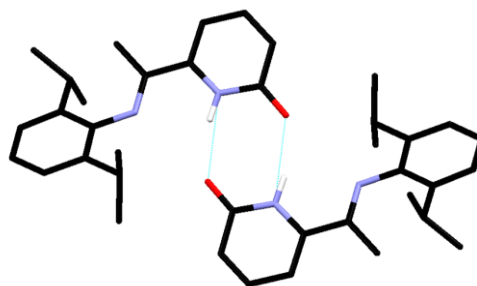
Figure 3.6: Self-dimerisation through intermolecular NH···O hydrogen bonding in H**L2**$_a$

As with H**L2**$_a$, the ^{1}H NMR spectrum of H**L2**$_b$ showed peaks at 6.64 ppm and at 10.33 ppm corresponding to the Hα and NH proton respectively, suggesting the ligand adopts the pyridone form. There were two septets in the proton NMR spectrum one at 2.89 ppm (1H) which belongs to the para-C*H*Me$_2$ proton, while the other 2H septet at 2.54 ppm is due to the two ortho-C*H*Me$_2$ protons. The ESI mass spectral data revealed a peak at m/z 339 corresponding to the protonated molecular ion [M+H]. The HR mass spectrum result

confirmed the product by giving a peak at m/z 339.2436 [M+H] for $C_{22}H_{31}N_2O$ which compares to the calculated value of m/z 339.2435.

A peak present at 10.17 ppm in the proton NMR spectrum of H$L2_c$ corresponds to the NH proton of the pyridone while a 2H septet at 2.46 ppm to the equivalent CHMe$_2$ protons. The H$_\alpha$ proton on the heterocycle (see Scheme 3.2) appeared at 6.59 ppm with its relatively upfield chemical shift a clear indication of the de-aromatised form (i.e., the 2-pyridone). The HR mass spectrum showed a protonated molecular ion peak at m/z 375.1066 [M+H] for $C_{19}H_{23}N_3OBr$ which compares to the calculated value of m/z 375.1072.

Compound H$L2_a$ has been published by Huang *et al.*[24] and indeed their data is consistent with what we disclose. However, the X-ray structure has not been previously published.

3.2.1b Synthesis of HL3

Following the successful synthesis of three examples of H$L2$ in high yield, we decided to explore the synthesis of their 4-pyridone counterparts H$L3$. Since the area is still under-developed and relatively little is known about this class of compound, the synthetic pathway to H$L3$ has been devised and is shown in Scheme 3.1b involving five steps.

4-Methoxypyridine N-oxide (**A**) was obtained in 98% yield by reacting 4-nitropyridine N-oxide with sodium methoxide (Scheme 3.1b).[27] Conversion to 2-cyano-4-methoxypyridine (**B**) was achieved by treatment of **A** with trimethylsilyl cyanide (TMSCN) in the presence of dimethylcarbamoyl chloride in dichloromethane at room temperature.[28] 2-Acetyl-4-methoxypyridine (**C**) was then obtained by the reaction of **B** with trimethylaluminium followed by hydrolysis of the aluminium intermediate. The deprotection of the methoxy group in **C** was achieved by reacting it with 45% HBr in acetic acid at 115 °C for 18 hours to afford the 2-acetyl-4-pyridone (**D**) in 79% yield. It was found that this deprotection step required more forcing conditions when compared to that used to prepare **III** (Scheme 3.1a). The new intermediate compounds, **C** and **D**, were fully characterized.
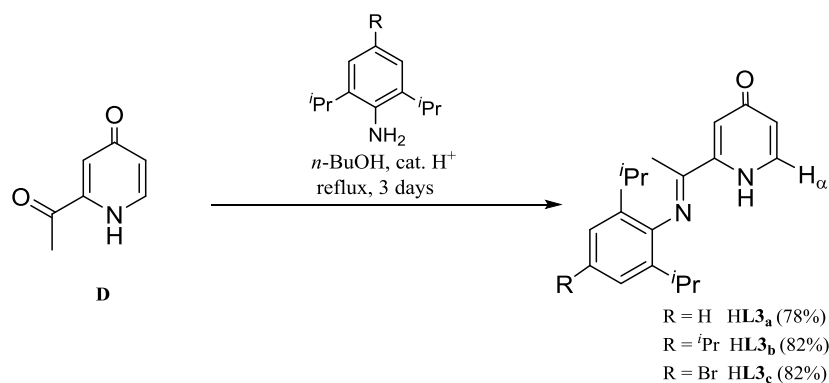
Scheme 3.3: Synthesis of H**L3**$_a$, H**L3**$_b$ and H**L3**$_c$

The 6-imino-4-pyridones, 6-(4-R-2,6-i-Pr$_2$C$_6$H$_2$)N=CMe)C$_5$H$_3$NH-4-O (R = H H**L3**$_a$, i-Pr H**L3**$_b$, Br H**L3**$_c$), were then formed via the condensation reaction of **D** with the corresponding aniline (Scheme 3.3). In each case the reactions were carried out under reflux in n-BuOH for three days in the present of *p*-toluene sulfonic acid as catalyst affording H**L3**$_a$ – H**L3**$_c$ in yields between 78 and 82%.

The ^{1}H NMR spectrum of H**L3**$_a$ showed a doublet at 1.06 ppm corresponding to the methyl in the isopropyl moiety while the NH peak came at 9.95 ppm. The proton H$_\alpha$ (Scheme 3.3) came at 6.42 ppm, which is supporting the pyridone structure in the ligand. The IR spectra showed an absorption band at 1648 cm^{-1} for the C=N$_{imine}$ functionality. High resolution mass spectrum revealed an ion at m/z 297.1977 [M+H] for C$_{19}$H$_{24}$N$_2$O which compares with the calculated value of 297.1967.

Single crystals of H**L3**$_a$ suitable for an X-ray determination were grown by slow diffusion of hexane into a dichloromethane solution of the compound. A view of H**L3**$_a$ is given in Figure 3.7; selected bond distances are collected in Table 3.2. The structure of H**L3**$_a$ revealed a mutually cis arrangement between the imine nitrogen and the pyridone nitrogen, which is held in place by an intramolecular hydrogen bonding interaction between H1A and N2 (N(1)-H(1A)···N(2) 2.285 Å). The C(6)-N(2) bond length of 1.286(5) Å is indicative of a C=N$_{imine}$ bond. Moreover, the C=O double bond length is 1.258(4) Å which supports the 4-pyridone form of the ligand. Furthermore, intermolecular NH···O hydrogen bonding (N(1)-H(1A)···O(1) 2.002 Å) is a feature of the crystal structure which results in a 2D network of linked molecules (Figure 3.8).
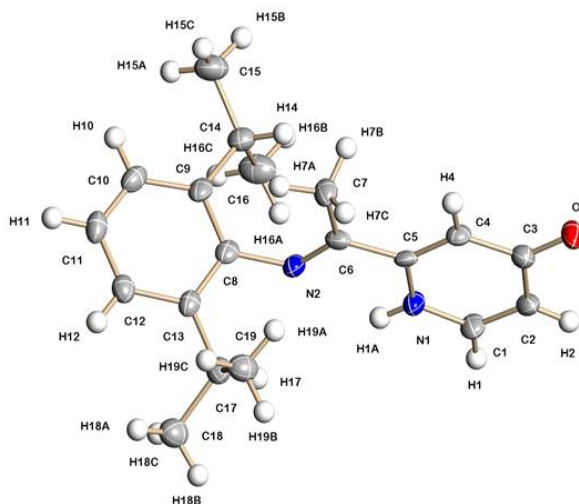
Figure 3.7: Molecular structure of H**L3ₐ**; the thermal ellipsoids are set at the 30% probability level

Table 3.2: Selected bond lengths (Å) and angles (°) for H**L3ₐ**

Bond lengths (Å)		Bond angles (°)	
O(1)-C(3)	1.258(4)	C(1)-N(1)-C(5)	121.4(3)
N(2)-C(6)	1.286(5)	C(6)-N(2)-C(8)	121.0(3)
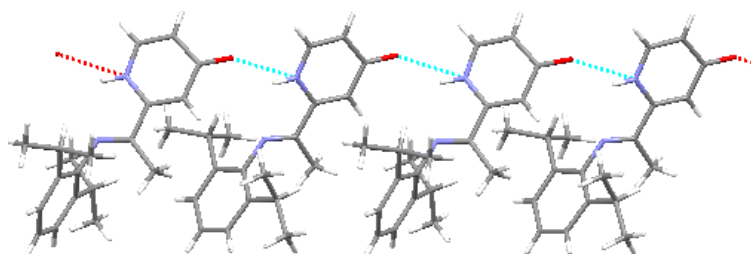
Figure 3.8: Network formation through intermolecular NH···O hydrogen bonding in H**L3ₐ**

The ^{1}H NMR spectrum of H**L3b** revealed a characteristic 12H doublet peak at 1.05 ppm corresponding to the four equivalent CH*Me*$_2$ methyls belonging to the two isopropyl groups along with a 2H septet at 2.47 ppm for the C*H*Me$_2$ protons. In a similar manner to the 2-pyridone ligands, the NH appeared at 10.05 ppm. In addition, the IR spectrum showed an absorption at 1650 cm^{-1} which is assigned to C=N$_{imine}$ functionality. Further evidence for the formation of the ligand was provided by the HR mass spectrum which revealed a 339.2449 [M+H] for $C_{19}H_{24}N_2O$ which compares with the calculated value of 339.2436. The X-ray structure of H**L3b** was also determined and again the 4-pyridone form was evident (see Appendix).

In the ^{1}H NMR spectrum of H**L3**$_c$, signals for the isopropyl methyl proton were seen at 1.05 ppm as a 12H doublet. A doublet and singlet at 7.52 ppm and 6.79 ppm corresponding to the protons on the pyridone ring were also evident. Moreover, a doublet detected at 6.42 ppm was assigned to the H$_\alpha$ proton confirming the structure as the pyridone form. The IR spectrum showed a peak at 1647 cm^{-1} characteristic of an imine group. Further confirmation of the structure was provided by an X-ray diffraction study.
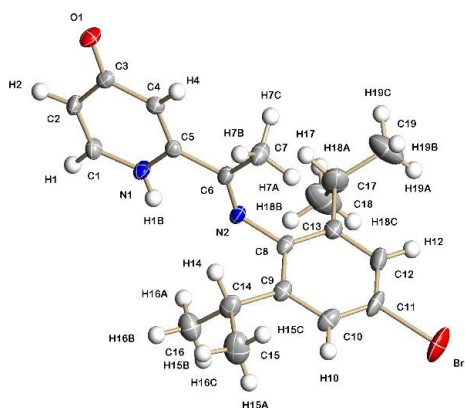
Figure 3.9: Molecular structure of H**L3**$_c$; the thermal ellipsoids are set at the 30% probability level

Table 3.3: Selected bond lengths (Å) and angles (°) for H**L3**$_c$

Bond lengths (Å)		Bond angles (°)	
O(1)-C(3)	1.263(3)	C(1)-N(1)-C(6)	120.9(3)
N(2)-C(6)	1.269(3)	C(6)-N(2)-C(5)	114.4(3)

Single crystals of H**L3**$_c$ were grown by slow evaporating of dichloromethane solution containing the compound. A view of the structure is shown in Figure 3.9; selected bond distances and angles are given in Table 3.3. The structure of H**L3**$_c$ reveals a *cis* arrangement between the pyridone nitrogen and imine nitrogen, due to the hydrogen interaction between N2 and H1B (N(1)-H(1B)···N(2) 2.049 Å). Moreover, the C=N$_{imine}$ and C(3)=O(1) bonds were 1.269(3) and 1.263(3) (Å), respectively, both indicative of double bonds. The N(2)-C(6)-C(5) bond angle of 114.4(3)° is consistent with an sp^2 hybridised imine unit.[29]

3.2.2 Reactions of HL2 and HL3 with palladium(II)

3.2.2.1a HL2PdOAc

The reaction of H**L2**_{a-c} with palladium(II) acetate in toluene at room temperature afforded the bimetallic complexes (**L2**_aPd)₂(OH)(OAc), (**L2**_bPd)₂(OH)(OAc) and (**L2**_cPd)₂(OH)(OAc), respectively, in yields between 70 and 98% (Scheme 3.4). The complexes have been characterised by ^{1}H/^{13}C NMR, IR spectroscopy and mass spectrometry. In addition, (**L2**_aPd)₂(OH)(OAc) and (**L2**_bPd)₂(OH)(OAc) have been the subject of single crystal X-ray diffraction studies.
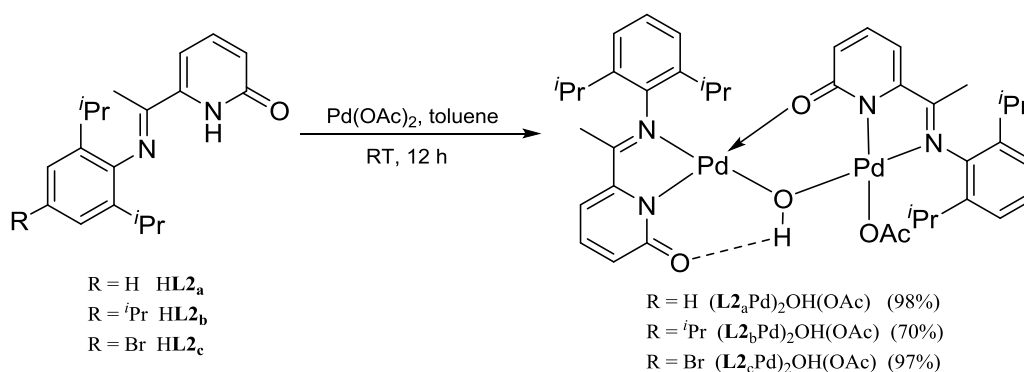
Scheme 3.4: Synthesis of (**L2**Pd)₂OH(OAc)

Analysis of the ^{1}H NMR spectrum of (**L2**_aPd)₂OH(OAc) revealed a peak at 7.44 ppm for the OH proton and four 6H doublets between 1.37-1.07 ppm corresponding to the twenty-four CH*Me*₂ methyl protons. The presence of four doublets can be explained by considering the two pyridonate-imines to be in inequivalent environments resulting in two types of CH*Me*_a*Me*_b methyl for one N-aryl group and two for the other, CH*Me*_{a'}*Me*_{b'}. A 3H singlet appeared at 1.87 ppm which was assigned to the acetate methyl group while the imine methyl groups appeared at 1.94 ppm and 1.93 ppm. In the ^{13}C NMR spectrum two downfield quaternary carbon signals at 176.5 ppm and 175.9 ppm showed the presence of the acetate C=O and imine C=N carbons, respectively. Additionally, the IR spectrum showed a C=N_{imine} stretch at 1614 cm^{-1} which is 30 cm^{-1} lower in wavenumber when compared to that observed in the free ligand and hence supportive of coordination. The HR mass spectrum revealed an accurate mass for the compound of m/z 878.2786 [M^{+}] which compares with the calculated value for C₄₀H₅₀N₄O₅Pd₂ of 878.2656.
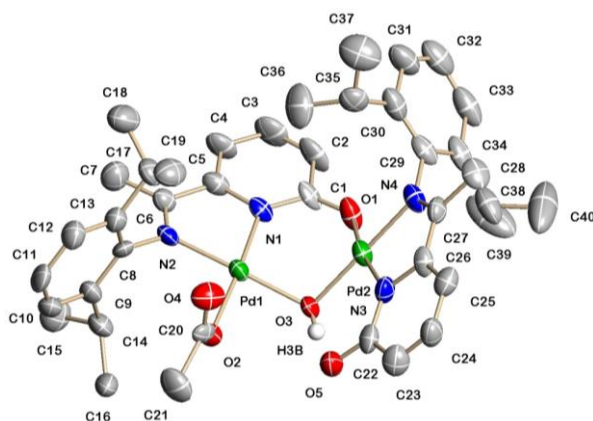
Figure 3.10: Molecular structure of (**L2**$_a$Pd)$_2$OH(OAc); the thermal ellipsoids are set at the 30% probability level (all hydrogen atoms have been removed for clarity except on O(3))

Table 3.4: Selected bond lengths (Å) and angles (°) for (**L2**$_a$Pd)$_2$OH(OAc)

Bond lengths (Å)		Bond angles (°)	
Pd(1)-O(2)	1.992(5)	N(1)-Pd(1)-N(2)	79.6(2)
Pd(1)-O(3)	2.003(5)	N(3)-Pd(2)-N(4)	80.0(2)
O(1)-C(1)	1.268(8)	N(1)-Pd(1)-O(3)	96.3(2)
Pd(2)-O(1)	2.054(4)	O(3)-Pd(2)-N(3)	98.42(19)
Pd(2)-O(3)	1.987(4)		
O(5)-C(22)	1.259(9)		

Single crystals of (**L2**$_a$Pd)$_2$OH(OAc) suitable for the X-ray determination were grown by slow diffusion of hexane onto chloroform solution of the complex. A perspective view of the structure is given Figure 3.10; selected bond distances and angles are compiled in Table 3.4. The molecular structure is based on a bimetallic species, in which one pyridonate-imine acts as a bidentate N,N ligand while the other N,N-chelates and uses the oxygen atom to coordinate to the second palladium centre. Additionally, a bridging hydroxide links the two metal centres and also undergoes an intramolecular hydrogen bonding interaction with the pendant pyridonate oxygen atom (O(3)-H(3B)···O(5) 1.793 Å). More interestingly, the unit cell contains a pair of independent molecules connected by π-stacking (separation = 3.460 Å) (Figure 3.11).
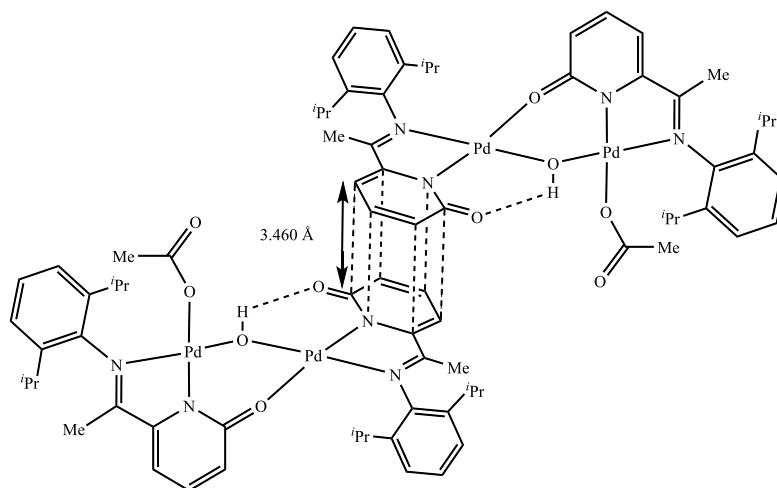
Figure 3.11: π-Stacking between adjacent molecules of (**L2**$_a$Pd)$_2$OH(OAc)

The proton NMR spectrum of (**L2**$_b$Pd)$_2$OH(OAc) showed a peak at 7.22 ppm corresponding to the bridging OH proton. In addition, four 6H doublets for the ortho-CH*Me*$_a$*Me*$_b$ and CH*Me*$_{a'}$*Me*$_{b'}$ methyl protons along with a 4H septet for the ortho C*H*Me$_2$ protons at 3.17 ppm. The para-C*H*Me$_2$'s are seen as two septets at 2.78 ppm and 2.83 ppm. Furthermore, two singlets for the inequivalent imine-methyl protons at 1.95 ppm and 1.87 ppm were clearly visible. The ESI mass spectrum displayed a strong fragmentation peak at m/z 905 [M$^+$-OAc].

A crystal of (**L2**$_b$Pd)$_2$OH(OAc) suitable for X-ray diffraction studies were grown by slow diffusion of hexane onto a dichloromethane solution of the complex. A view of the structure is shown in Figure 3.12; selected bond lengths and angles are given in Table 3.5. As with (**L2**$_a$Pd)$_2$OH(OAc), (**L2**$_b$Pd)$_2$OH(OAc) adopts a bimetallic structure with the heterocyclic unit in the pyridonate form. The bond length of C(1)-O(1) and C(22)-O(5) are 1.287(5) and 1.248(5) Å respectively, which is supportive of a double bond. Additionally, there is intramolecular hydrogen bonding interaction between the pendant pyridonate oxygen atom and the OH bridging (O(3)-H(3A)···O(5) 1.957 Å). Moreover, the unit cell contains a pair of independent molecules connected by π-stacking similar to which have been seen in (**L2**$_a$Pd)$_2$OH(OAc) (separation = 3.466 Å) (see Appendix).
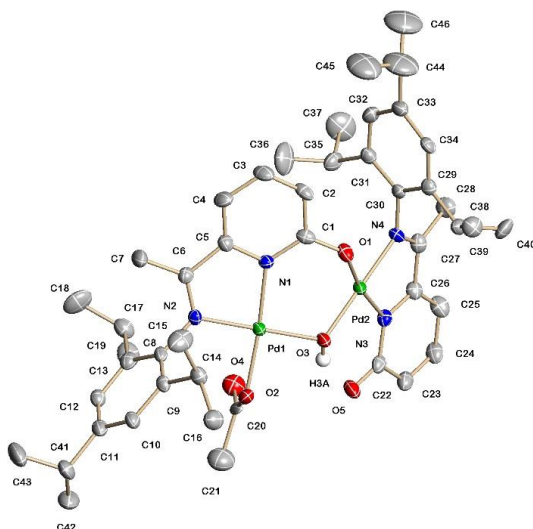
Figure 3.12: Molecular structure of (**L2**_bPd)₂OH(OAc); the thermal ellipsoids are set at the 30% probability level (all hydrogen atoms have been removed for clarity except on O(3))

Table 3.5: Selected bond lengths (Å) and angles (°) for (**L2**_bPd)₂OH(OAc)

Bond lengths (Å)		Bond angles (°)	
Pd(2)-O(3)	1.984(3)	N(1)-Pd(1)-N(2)	80.84(15)
Pd(1)-O(3)	2.000(3)	N(3)-Pd(2)-N(4)	80.40(15)
O(1)-C(1)	1.287(5)	N(1)-Pd(1)-O(3)	98.78(13)
Pd(2)-O(1)	2.005(3)	O(3)-Pd(2)-N(3)	99.39(14)
O(5)-C(22)	1.248(5)		

In the ^{1}H NMR spectrum of (**L2**$_c$Pd)$_2$OH(OAc), four 6H doublets were assigned to the ortho-CH*Me*$_a$*Me*$_b$ and CH*Me*$_{a'}$*Me*$_{b'}$ methyl protons while the C*H*Me$_2$ protons appeared as a 4H septet at 3.30 ppm; the bridging OH proton is seen at 8.12 ppm. The inequivalent imine-methyl protons came at 2.02 ppm and 1.97 ppm. The high resolution mass spectrum showed a fragmentation peak at m/z 977 [M-OAc], while the IR spectrum revealed a C=N$_{imine}$ absorption at 1614 cm^{-1}, a stretching frequency supportive of coordination.

The origin of the bridging hydroxide functionality in (**L2**$_a$Pd)$_2$OH(OAc), (**L2**$_b$Pd)$_2$(OH)(OAc) and (**L2**$_c$Pd)$_2$(OH)(OAc), is unclear but could be due to moisture in the reaction rather than during crystallisation; monitoring of the reaction by ^{1}H NMR spectroscopy reveals its formation following the reaction. Attempts at carrying out the reactions in dry solvent still surprisingly gave the same products.

3.2.2.1b (HL3)₂Pd

In an attempt to form a complex of composition (**L3**$_a$PdOAc)$_2$, H**L3**$_a$ was treated with one molar equivalent of Pd(OAc)$_2$ in toluene at room temperature. However, on work-up, the only complex that could be isolated was (**L3**$_a$)$_2$Pd, albeit in low yield. To increase the yield the reaction was repeated in a 2:1 molar ratio of ligand to metal salt affording (**L3**$_a$)$_2$Pd in 89% yield (Scheme 3.5). Extension of this approach to reactions of H**L3**$_b$ and H**L3**$_c$ with Pd(OAc)$_2$ gave (**L3**$_b$)$_2$Pd and (**L3**$_c$)$_2$Pd, respectively, in high yield. All three complexes have been characterised by ^{1}H/^{13}C NMR, IR spectroscopy and mass spectrometry. In addition, (**L3**$_a$)$_2$Pd has been characterised by single crystal X-ray diffraction.
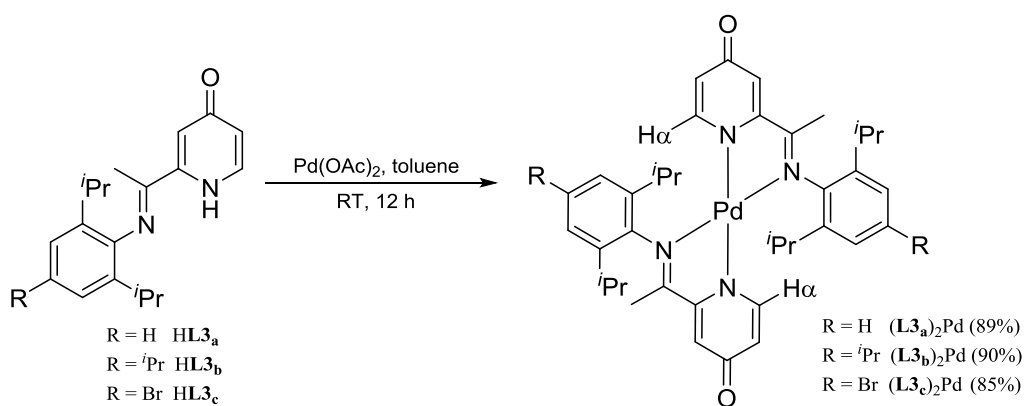
Scheme 3.5: Synthesis of (**L3**)₂Pd

Analysis of (**L3**$_a$)$_2$Pd by ^{1}H NMR spectroscopy revealed a 4H septet at 3.10 ppm and two 12H doublets at 1.15 ppm and 1.08 ppm which are assigned to the isopropyl moiety. The imine methyl came at 2.15 ppm whereas in the free ligand it came at 1.95 ppm. Moreover, the proton NMR data reveals an upfield signal at 5.29 ppm corresponding to the Hα proton, which is indictive of the pyridonate form of the complex. The high resolution mass spectrum revealed the molecular weight of the compound as m/z 696.2750 which compares with the calculated value of 696.2767 [M]. In addition, the presence of a strong C=N$_{imine}$ stretching frequency at 1614 cm^{-1} is evidence for the formation of a coordinated imine.

Single crystals of (**L3**$_a$)$_2$Pd suitable for the X-ray determination were obtained by slow diffusion of hexane into dichloromethane solution of the complex. A perspective view of the structure is shown in Figure 3.13; selected bond distances and angles are given in Table 3.6). The N(4)-Pd(1)-N(3) and N(1)-Pd(1)-N(2) angles of 78.53(15)° and

78.40(14)° (**L3**$_a$)$_2$Pd are indicative of a distorted square planar geometry. The C(3)-O(1) and C(22)-O(2) bond distances of 1.260(6) and 1.263(5) Å are typical of double bonds hence supporting the heterocycles to be in the pyridonate form.
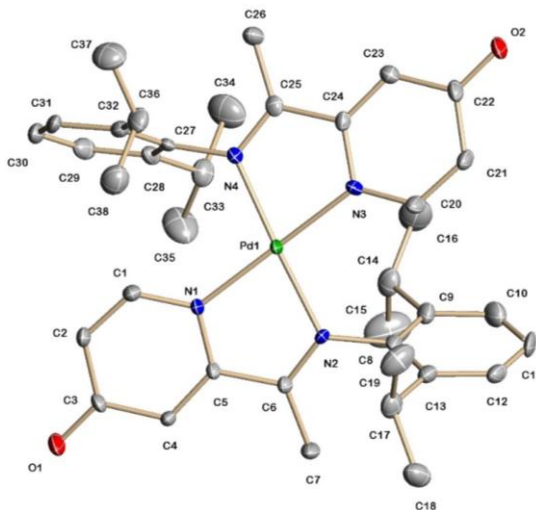
Figure 3.13: Molecular structure of (**L3**$_a$)$_2$Pd; the thermal ellipsoids are set at the 30% probability level (all hydrogen atoms have been removed for clarity)

Table 3.6: Selected bond lengths (Å) and angles (°) for (**L3**$_a$)$_2$Pd

Bond lengths (Å)		Bond angles (°)	
Pd(1)-N(4)	2.045(4)	N(4)-Pd(1)-N(3)	78.53(15)
Pd(1)-N(3)	2.042(3)	N(1)-Pd(1)-N(2)	78.40(14)
Pd(1)-N(2)	2.056(4)	N(3)-Pd(1)-N(2)	101.84(14)
Pd(1)-N(1)	2.049(4)	N(4)-Pd(1)-N(1)	101.82(15)
C(3)-O(1)	1.260(6)		
C(22)-O(2)	1.263(5)		

The ^{1}H NMR spectra of (**L3**$_b$)$_2$Pd and (**L3**$_c$)$_2$Pd were difficult to analyse due to the broad nature of the signals. The explanation for this broadness is uncertain. Nonetheless, in the ESI mass spectra strong peaks for the molecular ions of each of these complexes were evident at m/z 738 [M] and m/z 775 [M], respectively. Furthermore, the IR spectra of (**L3**$_b$)$_2$Pd and (**L3**$_c$)$_2$Pd showed bands at 1616 cm^{-1} and 1615 cm^{-1}, respectively, characteristic of a bound imine.

It is unclear why a 1:1 **L3**PdOAc complex could not be formed for any of the H**L3** ligand variations. This finding is quite different to that observed with H**L2** where bimetallic

acetate complexes were the preferred product type. Nevertheless, the position of the C=O unit within the pyridonate ring clearly influences the reaction pathway.

3.2.2.2a Reaction of HL2 with (MeCN)₂PdCl₂

After observing unexpected reactivity of $HL2_{a-c}$ with palladium(II) acetate (in the form of OH-bridged bimetallic acetate complexes), we were interested to look at the reactions of these ligands with other palladium sources, *e.g.*, $(MeCN)_2PdCl_2$. Hence, the reaction of $HL2_{a-c}$ with bis(acetonitrile)palladium(II) chloride was carried out in toluene at room temperature affording the pyridinol complexes $HL2_aPdCl_2$, $HL2_bPdCl_2$ and $HL2_cPdCl_2$, respectively, in almost quantitative yields (Scheme 3.6). All three complexes were fully characterised by $^1H/^{13}C$ NMR, IR spectroscopies and mass spectrometry. In addition, $HL2_aPdCl_2$ and $HL2_bPdCl_2$ were the subject of single crystal X-ray diffraction studies.

$$R = H \quad HL2_a$$
$$R = {}^iPr \quad HL2_b$$
$$R = Br \quad HL2_c$$

$$R = H \quad HL2_aPdCl_2 \ (100\%)$$
$$R = {}^iPr \quad HL2_bPdCl_2 \ (99\%)$$
$$R = Br \quad HL2_cPdCl_2 \ (98\%)$$
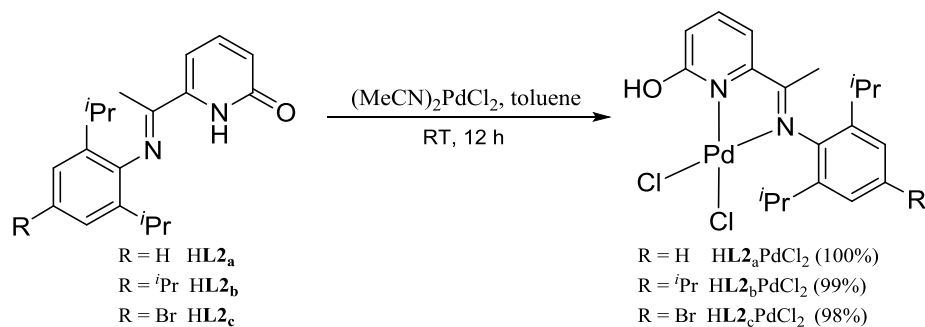
Scheme 3.6: Synthesis of $HL2PdCl_2$

The ^1H NMR spectrum of $HL2_aPdCl_2$ revealed a peak at 12.49 ppm corresponding to the OH proton. The appearance of two 6H doublets at 1.40 ppm and 1.12 ppm can be assigned to the CHMe_aMe_b methyl protons, this being a clear indication of complex formation. The methyl-imine peak shifted to 2.15 ppm as compared to 2.00 ppm in free $HL2_a$. In addition, the Py-H and Ar-H signals fall in the 7.0 – 8.0 ppm range which is consistent with the heterocycle adopting the aromatic pyridinol form in solution (see the ^1H NMR spectrum of $HL2_aPdCl_2$ in Figure 3.15). The IR spectrum displayed a strong absorption at 1625 cm^{-1} which is assigned to the υ(C=N) band which has shifted from 1651 cm^{-1} in the free ligand. The HR FAB mass spectrum revealed a fragmentation peak at 439.3709 which compares with the calculated value for $C_{19}H_{24}N_2OPdCl_2$ of 439.3720 $[M-Cl]^+$. Similar features were observed for $HL2_bPdCl_2$ and $HL2_cPdCl_2$ in their proton NMR spectra. In addition, the ES mass spectra of these complexes showed $[M-Cl]^+$ fragmentation peak.
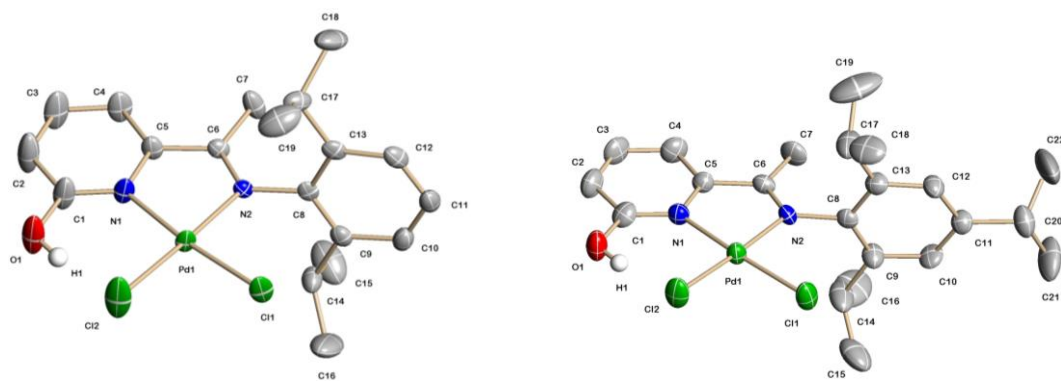
Figure 3.14: Molecular structures of H$L2_a$PdCl$_2$ and H$L2_b$PdCl$_2$; the thermal ellipsoids are set at the 30% probability level (Only the hydrogen on O(1) is shown for clarity in both molecular structures)

Table 3.7a: Selected bond lengths (Å) and angles (°) for H$L2_a$PdCl$_2$

Bond lengths (Å)		Bond angles (°)	
Pd(1)-N(1)	2.070(5)	N(1)-Pd(1)-N(2)	79.97(19)
Pd(1)-N(2)	2.010(5)	Cl(1)-Pd(1)-Cl(2)	87.09(7)
O(1)-C(1)	1.339(8)		

Table 3.7b: Selected bond lengths (Å) and angles (°) for H$L2_b$PdCl$_2$

Bond lengths (Å)		Bond angles (°)	
Pd(1)-N(1)	2.056(5)	N(1)-Pd(1)-N(2)	80.79(18)
Pd(1)-N(2)	2.016(4)	Cl(1)-Pd(1)-Cl(2)	87.83(6)
O(1)-C(1)	1.325(7)		

Single crystals of H$L2_a$PdCl$_2$ and H$L2_b$PdCl$_2$ suitable for the X-ray determinations were grown by slow diffusion of hexane into dichloromethane solution of complexes. Views of both are shown side-by-side in Figure 3.14; selected bond distances and angles are given in Tables 3.7a and 3.7b. The structures of H$L2_a$PdCl$_2$ and H$L2_b$PdCl$_2$ reveal distorted square planar geometries about the central palladium. The Pd–N bond lengths are inequivalent with the Pd-N$_{imine}$ distance shorter than the Pd-M$_{pyridine}$ distance. The 2,6-diisopropylphenyl and 2,4,6-triisopropylphenyl aryl groups are inclined almost perpendicularly to the coordination plane, which probably reduces any steric clash between itself and the adjacent chlorine atom. The C-O bond distance is 1.339(8) Å in H$L2_a$PdCl$_2$ and 1.325(7) Å in H$L2_b$PdCl$_2$ which is typical of a single bond and hence the heterocyclic unit is in the pyridinol form in each complex. In addition, intra-molecular

90

hydrogen-bonding involving O(1)-H1···Cl(2) is apparent with bond lengths of H1···Cl(2) 2.030 Å in **HL2$_a$PdCl$_2$** and 2.060 Å in **HL2$_b$PdCl$_2$**. No intermolecular contacts of note were apparent.
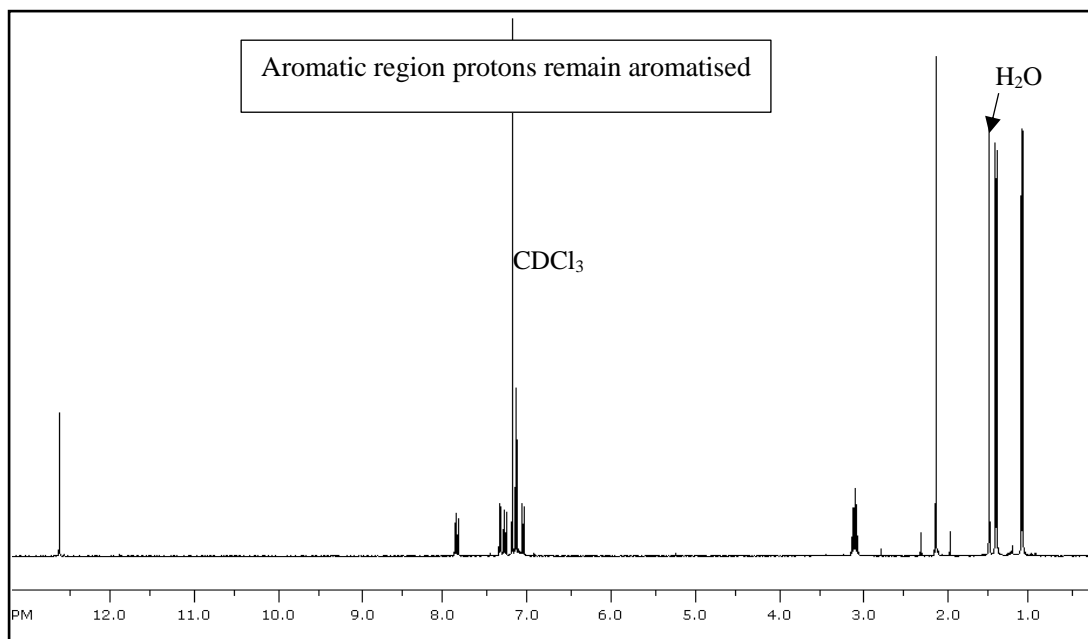
Figure 3.15: ^{1}H NMR spectrum of **HL2$_a$PdCl$_2$** (recorded in CDCl$_3$ at room temperature)

3.2.2.2b Reaction of HL3 with (MeCN)$_2$PdCl$_2$

HL3$_{a-c}$ were each treated with an equimolar ratio of bis(acetonitrile)palladium(II) chloride in toluene at room temperature affording, on work-up, **HL3$_a$PdCl$_2$**, **HL3$_b$PdCl$_2$** and **HL3$_c$PdCl$_2$**, respectively, in 89 to 91% yield (Scheme 3.7). All three complexes have been characterised by ^{1}H/^{13}C NMR, IR spectroscopy and mass spectrometry. In addition, **HL3$_a$PdCl$_2$**, **HL3$_b$PdCl$_2$** and **HL3$_c$PdCl$_2$** have been the subject of a single crystal X-ray diffraction studies.
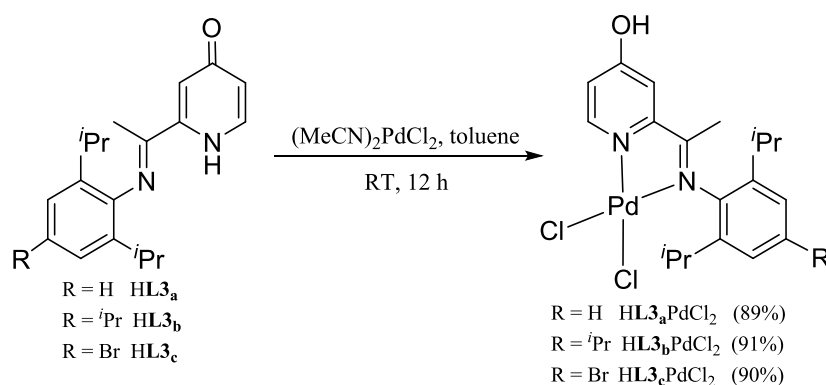
Scheme 3.7: Synthesis of HL3PdCl$_2$

The ^{1}H NMR spectrum of H**L3**$_a$PdCl$_2$ showed the typical features for the CH*Me*$_a$*Me*$_b$ protons with two 6H doublets at 1.36 ppm and 1.11 ppm. Unlike with H**L2**PdCl$_2$, the OH peak was not detected in the proton NMR spectrum, which is likely attributed to the spectrum being run in CD$_3$OD. However, similar to H**L2**PdCl$_2$ the heterocyclic protons appear in the region 7.05 – 8.78 ppm, which is evidence for the pyridinol form. The C=N absorption at 1617 cm^{-1} in the IR spectrum is supportive of a bound imine. The ESI mass spectrum revealed a fragmentation peak at m/z 437 corresponding to the loss of a chloride from the molecular ion.

Single crystals of H**L3$_a$**PdCl$_2$ suitable for the X-ray determination were grown by slow evaporation of methanol solution of the complex. A view of the complex is seen in Figure 3.16; selected bond distances and angles are listed in Table 3.8. The structure of H**L3**$_a$PdCl$_2$ shows a distorted square planar geometry about palladium. The Pd–N bond lengths are similar unlike that seen in H**L2**$_a$PdCl$_2$. The N-aryl substituents are orientated virtually perpendicularly to the coordination plane, a confirmation that is likely preferred due to the lowering in any steric clash between the bulky ring and the adjacent chlorine atom. The C-O bond length is 1.348(6) Å, which is typical of a single bond hence indicating the heterocyclic unit adopts the 4-pyridinol form. Furthermore, the OH proton in H**L3**$_a$PdCl$_2$ can act as hydrogen bond donor resulting in a 2D polymer involving O-H···Cl interactions (Figure 3.17); the H···Cl bond length was determined as 2.146 Å which is consistent with a hydrogen bond.[30]
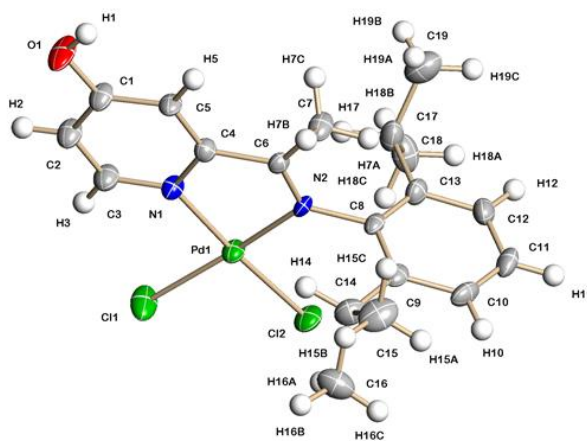
Figure 3.16: Molecular structure of H**L3**$_a$PdCl$_2$; the thermal ellipsoids are set at the 30% probability level

Table 3.8: Selected bond lengths (Å) and angles (°) for HL3$_a$PdCl$_2$

Bond lengths (Å)		Bond angles (°)	
Pd(1)-N(1)	2.006(4)	N(1)-Pd(1)-N(2)	80.44(17)
Pd(1)-N(2)	2.015(4)	Cl(1)-Pd(1)-Cl(2)	90.26(6)
O(1)-C(1)	1.348(6)	C(6)-N(2)-C(8)	115.6(3)
Pd(1)-Cl(1)	2.296(17)		
Pd(1)-Cl(2)	2.294(16)		
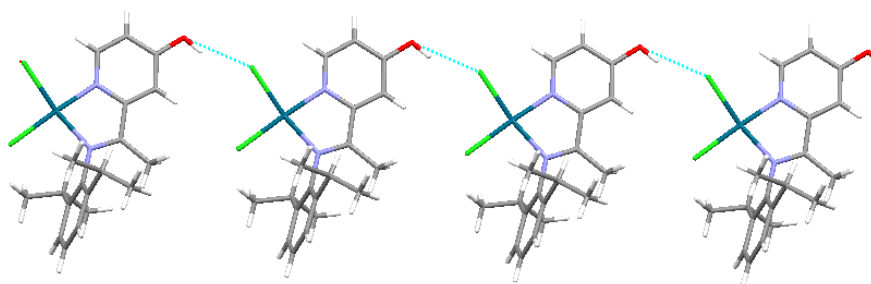
Figure 3.17: Intermolecular OH···Cl hydrogen bonding between neighbouring HL3$_a$PdCl$_2$ molecules

The proton NMR spectra of both HL3$_b$PdCl$_2$ and HL3$_c$PdCl$_2$ showed similar features to that seen in HL3$_a$PdCl$_2$ with separate resonances for the CH*Me*$_a$*Me*$_b$ methyl protons, which is a clear indication of coordination. The IR spectra revealed strong peaks at *ca.* 3450 cm^{-1} and *ca.* 1624 cm^{-1} corresponding to the OH and C=N functionalities. Further confirmation of the structure comes from the ESI mass spectrum which shows a M-Cl fragmentation peak for both complexes.

Single crystals of HL3$_b$PdCl$_2$ and HL3$_c$PdCl$_2$ suitable for the X-ray determinations were grown by slow evaporation of a dichloromethane solutions of the complexes. Views of each structure are shown side-by-side in Figure 3.18; selected bond distances and angles are given in Tables 3.9a and 3.9b. The structure of both complexes are similar to that for HL3$_a$PdCl$_2$ and are consistent with the spectroscopic data.

Figure 3.18: Molecular structures of H**L3**ₐPdCl₂ and H**L3**cPdCl₂; the thermal ellipsoids are set at the 30% probability level

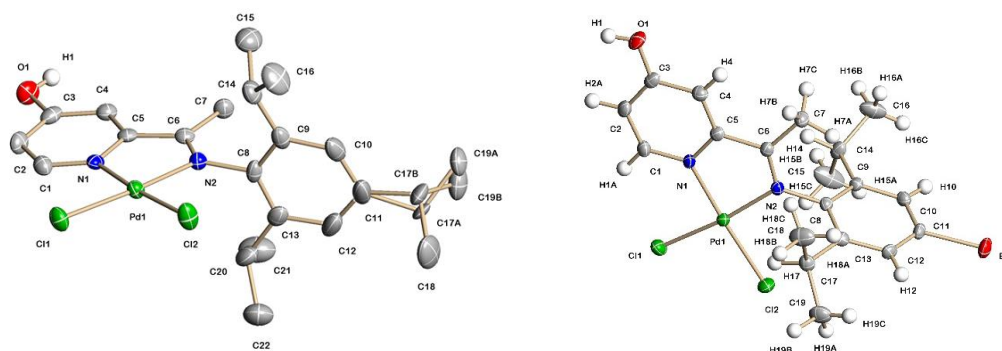**Table 3.9a**: Selected bond lengths (Å) and angles (°) for H**L3**ₐPdCl₂

Bond lengths (Å)		Bond angles (°)	
Pd(1)-N(1)	2.018(3)	N(1)-Pd(1)-N(2)	80.35(13)
Pd(1)-N(2)	2.023(3)	Cl(1)-Pd(1)-Cl(2)	91.10(5)
O(1)-C(3)	1.349(4)	C(6)-N(2)-C(8)	120.6(3)

Table 3.9b: Selected bond lengths (Å) and angles (°) for H**L3**cPdCl₂

Bond lengths (Å)		Bond angles (°)	
Pd(1)-N(1)	2.031(3)	N(1)-Pd(1)-N(2)	79.73(11)
Pd(1)-N(2)	2.031(3)	Cl(1)-Pd(1)-Cl(2)	90.32(4)
O(1)-C(3)	1.334(4)	C(6)-N(2)-C(8)	119.7(3)

It is clear that pyridone-imines H**L2** and H**L3** react quite differently with palladium(II) acetate and palladium(II) chloride. With palladium(II) chloride the ligands remain intact and do not undergo deprotonation reactions. This could be due to the Cl being a weak conjugate base (pKa -7). On the other hand with palladium(II) acetate deprotonation of H**L2** and H**L3** readily occurs because the basicity of the OAc is higher (pKa 4.87) resulting in proton abstraction and the formation of pyridonate complexes.

3.2.2.3 Reaction chemistry of HL2PdCl₂ and HL3PdCl₂

The palladium(II) chloride complexes, H**L2**PdCl₂ and H**L3**PdCl₂, were further investigated to explore the ability of the pyridinol functionality to donate a proton. In particular, we explored their reactivity towards the base Ag₂O as it was envisaged that this reagent could also abstract a chloride eliminating AgCl.

94

Firstly, the reaction of **HL2$_\mathbf{a\text{-}c}$PdCl$_2$** was carried out using Ag$_2$O in dichloromethane at room temperature (Scheme 3.8). On work-up, **(L2$_\mathbf{a}$Pd)$_2$OH(Cl)**, **(L2$_\mathbf{b}$Pd)$_2$OH(Cl)** and **(L2$_\mathbf{c}$Pd)$_2$OH(Cl)** were isolated in yields of 82 – 88% yield. All three complexes have been characterised by ^{1}H/^{13}C NMR, IR spectroscopy and mass spectrometry. The single crystal X-ray structures have been additionally determined for **(L2$_\mathbf{a}$Pd)$_2$OH(Cl)** and **(L2$_\mathbf{c}$Pd)$_2$OH(Cl)**.

R = H **HL2$_\mathbf{a}$PdCl$_2$**
R = ^{i}Pr **HL2$_\mathbf{b}$PdCl$_2$**
R = Br **HL2$_\mathbf{c}$PdCl$_2$**

R = H **(L2$_\mathbf{a}$Pd)$_2$OH(Cl)** (82%)
R = ^{i}Pr **(L2$_\mathbf{b}$Pd)$_2$OH(Cl)** (88%)
R = Br **(L2$_\mathbf{c}$Pd)$_2$OH(Cl)** (87%)
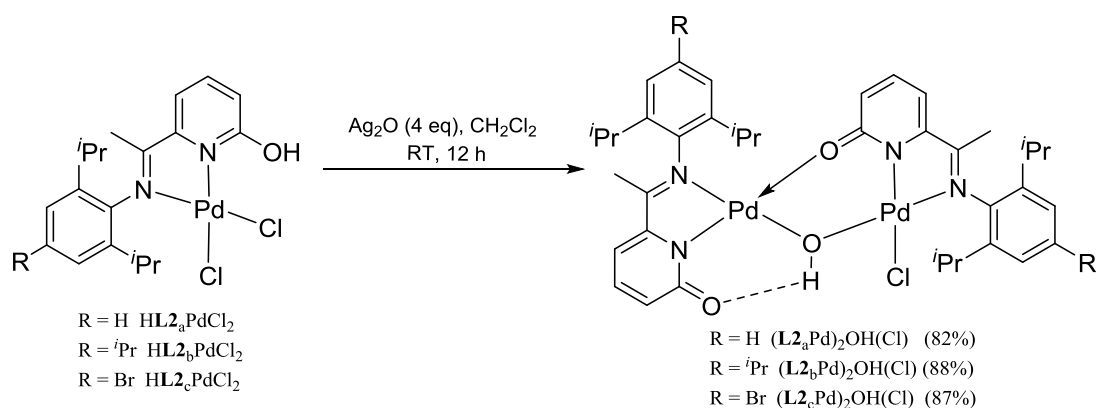
Scheme 3.8: Synthesis of **(L2Pd)$_2$OH(Cl)**

From the ^{1}H NMR data of **(L2$_\mathbf{a}$Pd)$_2$OH(Cl)** the reaction was hypothesised to undergo deprotonation followed by dimerisation through OH bridging in a manner similar to that seen for **(L2$_\mathbf{a}$Pd)$_2$OH(OAc)**. In this case the origin of the OH group could be more easily understood due to water being eliminated in the reaction. The OH peak in the new complex came at 7.38 ppm in the proton NMR spectrum. The H$_\alpha$ and H$_{\alpha'}$ proton on the heterocyclic ring could be seen at 6.54 and 6.56 ppm, which is evidence for the dearomatized pyridonate form. Four 6H doublets detected at 1.44 ppm, 1.29 ppm, 1.16 ppm and 1.08 ppm can be assigned to the CH*Me*$_\mathrm{a}$*Me*$_\mathrm{b}$ and CH*Me*$_\mathrm{a'}$*Me*$_\mathrm{b'}$ methyl protons. The HR mass spectrum showed a M-Cl fragmentation peak at 803.1844 which compares with calculated value for C$_{38}$H$_{47}$N$_4$O$_3$Pd$_2$Cl of 803.1769 [M-Cl]$^+$.

Single crystals of **(L2$_\mathbf{a}$Pd)$_2$OH(Cl)** suitable for the X-ray determination were grown by slow diffusion of hexane into a dichloromethane solution of the complex. A view of the structure is shown in Figure 3.19; selected bond distances and angles are collected in Table 3.10. The structure is based on bimetallic species that resembles **(L2$_\mathbf{a}$Pd)$_2$OH(OAc)** in which a OH ligand bridges the two metal centres. The geometry at each palladium can be best described as distorted square planar with the N(1)-Pd(1)-N(2) bite angle being 80.1(2)° while the N(3)-Pd(2)-N(4) angle is 80.6(2)° highlighting the origin of the

distortion. The C(1)-O(1) bond distance is 1.261(8) Å while the C(20)-O(3) distance is 1.272(8) Å which are both consistent with double bonds. The latter bond lengths are clear evidence that the deprotonated pyridonate form is adopted by both heterocyclic units. An intermolecular hydrogen bond can be seen between the water molecule and O(3), and Cl(1), the distances are O(5)-H(5A)···O(3) 2.168 Å, O(5)-H(5B)···Cl(1) 2.436 Å. Another intra-molecular hydrogen bonding seen in O(2)-H(2)···O(3) 1.655 Å. More interestingly, the unit cell contains a pair of independent molecules connected by π-stacking (separation = 3.547 Å) (see Appendix).
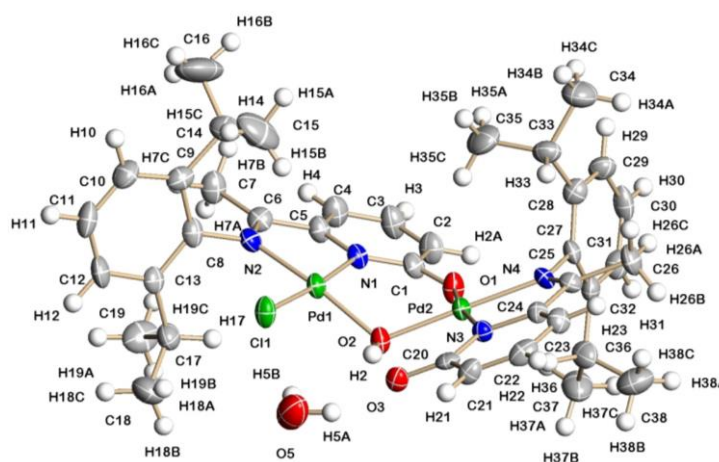
Figure 3.19: Molecular structure of ($\mathbf{L2_a}$Pd)$_2$OH(Cl)·OH$_2$ the thermal ellipsoids are set at the 30% probability level

Table 3.10: Selected bond lengths (Å) and angles (°) for ($\mathbf{L2_a}$Pd)$_2$OH(Cl)

Bond lengths (Å)		Bond angles (°)	
Pd(2)-O(2)	1.977(4)	N(1)-Pd(1)-N(2)	80.1(2)
Pd(1)-O(2)	2.001(5)	N(3)-Pd(2)-N(4)	80.6(2)
O(1)-C(1)	1.261(8)	N(1)-Pd(1)-O(2)	96.6(2)
Pd(2)-O(1)	2.015(5)	O(2)-Pd(2)-N(3)	98.2(2)

The ^{1}H NMR spectrum of ($\mathbf{L2_b}$Pd)$_2$OH(Cl) showed a peak at 7.49 ppm corresponding to the bridging OH a well as four 6H doublets at 1.38 ppm, 1.15 ppm, 1.08 ppm and 0.99 ppm for the ortho-CH*Me*$_a$*Me*$_b$ and CH*Me*$_{a'}$*Me*$_{b'}$ methyl protons. A two doublets at 1.21 ppm and 1.22 ppm for the para-CH*Me*$_{a2}$ and CH*Me*$_{a'2}$. In addition, the H$_\alpha$ and H$_{\alpha'}$ proton can be seen at 5.52 ppm and 6.49 ppm which supports the presence of pyridonate forms of the heterocycle. The IR spectrum revealed an adsorption band at 1618 cm^{-1} for the

C=N$_{imine}$ functionality. The complex exhibited a strong M-Cl fragmentation peak by ESI and FAB mass spectrometry at m/z 904.

Similar features were observed in the proton NMR spectrum of (**L2**$_c$Pd)$_2$OH(Cl), with four 6H doublets at 1.34 ppm, 1.22 ppm, 1.08 ppm and 0.98 ppm corresponding to the methyl proton on the isopropyl moiety. A new resonance was detected at 7.77 ppm which is assigned to the bridging OH ligand. The H$_\alpha$ and H$_{\alpha'}$ protons of the heterocyclic rings were shifted upfield at 5.69 and 6.53 ppm when compared with that in H**L1**$_c$PdCl$_2$, suggesting the pyridonate form. The ESI and FAB mass spectra show fragmentation peaks corresponding to the loss of a chloride.

Further confirmation of the structure of (**L2**$_c$Pd)$_2$OH(Cl) was provided by the X-ray structure. Single crystals were grown by slow diffusion of hexane into a dichloromethane solution of the complex. A view of the structure is given in Figure 3.20. The structure reveals similar features to that seen for (**L2**$_a$Pd)$_2$OH(Cl) the structure of (**L2**$_c$Pd)$_2$OH(Cl) based on an OH-bridged dipalladium complex. In addition, there is an intramolecular hydrogen bonding interaction between O2-H2···O(3) of 2.670 Å. Intermolecular π-π stacking of the pyridonate rings resembling that seen (**L2**$_c$Pd)$_2$OH(Cl) is also feature (separation = 3.398 Å).
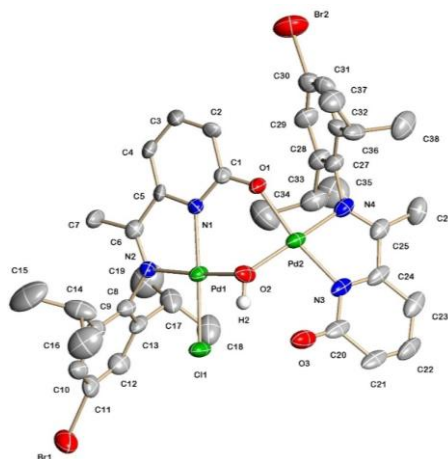
Figure 3.20: Molecular structure of (**L2**$_c$Pd)$_2$OH(Cl); the thermal ellipsoids are set at the 30% probability level (all hydrogen atoms have been removed for clarity)

Secondly, the reactivity of H**L3**$_{a-c}$PdCl$_2$ towards Ag$_2$O was carried using similar conditions to that applied with H**L2**$_{a-c}$PdCl$_2$. Hence, H**L3**$_{a-c}$PdCl$_2$ were treated with Ag$_2$O in dichloromethane at room temperature (Scheme 3.9). However, attempts at trying to

characterise the resultant complexes were unsuccessful. Indeed, the proton NMR spectra of the products showed particularly broad peaks which made it difficult to precisely determine the structure of the products. Nevertheless, the ^{1}H NMR spectra suggested that a reaction occurred and moreover based on the chemical shift of the heterocyclic protons (range: 5.5-8.0 ppm) the de-aromatised 4-pyridonate forms were present *e.g.* '**L3**$_a$PdCl', **L3**$_b$PdCl' and **L3**$_c$PdCl'. Unfortunately, single crystals suitable for X-ray diffraction studies could not be obtained.
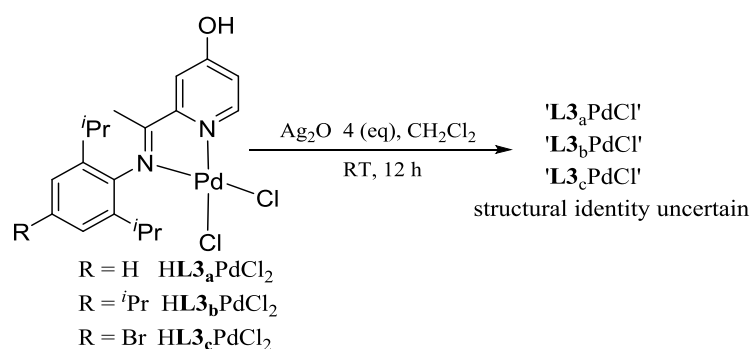
Scheme 3.9: Attempted deprotonation of H**L3**PdCl$_2$

3.2.2.4 Reaction of (L2Pd)$_2$OH(Cl) with triphenylphosphine

To explore the amenability of bimetallic (**L2**Pd)$_2$OH(Cl) to undergo cleavage of the bridging hydroxide and pyridonate, each complex was treated with triphenylphosphine. Hence, the reactions of (**L2**$_a$Pd)$_2$OH(Cl) and (**L2**$_c$Pd)$_2$OH(Cl) with PPh$_3$ in dichloromethane at temperatures of up to 40 °C for 7 days gave, following crystallisation from a mixture of dichloromethane and hexane, **L2**$_a$PdCl(PPh$_3$) and **L2**$_c$PdCl(PPh$_3$) in yields between 26 and 48% yield, respectively (*route 1* in Scheme 3.10); only poor conversion could be observed using (**L2**$_b$Pd)$_2$OH(Cl). The reason for the low yield could due to the formation of **L2**$_c$PdOH(PPh$_3$) as side product. In an attempt to prevent the formation of the bridging hydroxide, we also examined the more direct reaction of H**L2**$_a$PdCl$_2$ with Ag$_2$O in the presence of PPh$_3$ leading a higher yield of 75% for **L2**$_a$PdCl(PPh$_3$) (*route 2* in Scheme 3.10). Complexes **L2**$_a$PdCl(PPh$_3$) and **L2**$_c$PdCl(PPh$_3$) were characterised by ^{1}H/^{13}C NMR, IR spectroscopy and by mass spectrometry. In addition, **L2**$_a$PdCl(PPh$_3$) was the subject of a single crystal X-ray diffraction study.
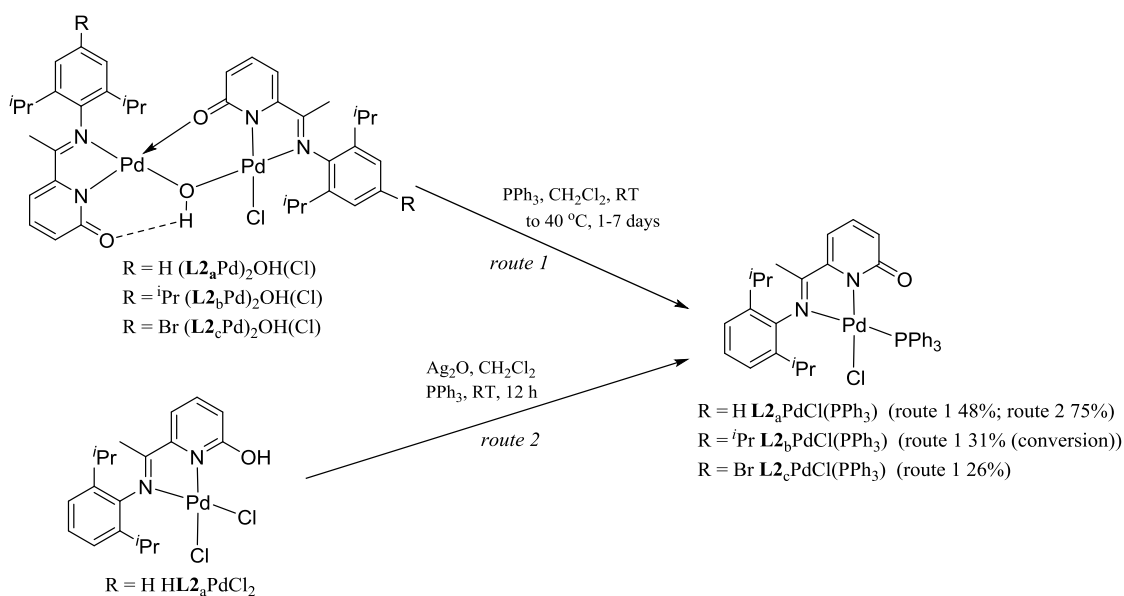
Scheme 3.10: Two routes to $\mathbf{L2}_{\text{a-c}}\text{PdCl(PPh}_3)$

The ^{1}H NMR spectrum of $\mathbf{L2}_a\text{PdCl(PPh}_3)$ showed new peaks between 7.67 ppm − 7.22 ppm corresponding the phenyl protons. The H_α proton of the heterocycle can be seen at 6.15 ppm which is clear evidence for the pyridonate form. In addition, a peak appeared at 25.30 ppm in the ^{31}P NMR spectrum which was clear confirmation of triphenylphosphine coordination. The high resolution mass spectrum revealed a molecular ion peak at m/z 699.1274 which compares with a calculated value of m/z 699.1330 for $C_{37}H_{38}N_2OPdClP$ [M]. The IR spectrum shows a peak at 1623 cm^{-1} which can be assigned to the coordinated imine.

Further confirmation of the identity of $\mathbf{L2}_a\text{PdCl(PPh}_3)$ was provided by the X-ray structure. Single crystals were grown by slow diffusion of hexane into a dichloromethane solution of the complex. A view of the structure is given in Figure 3.21; selected bond distance and angles are collected in Table 3.10. The structure reveals a square planar palladium centre surrounded by an NN-chelating pyridonate-imine, a chloride and a P-bound triphenylphosphine. The PPh$_3$ ligand adopts a position trans to the imine presumably due to the steric properties of the N-aryl group. The C(1)-O(1) bond length is 1.247(5) Å which is a typical of a double bond and hence confirming the heterocyclic unit adopts the pyridonate form. There are no intermolecular contacts of note.
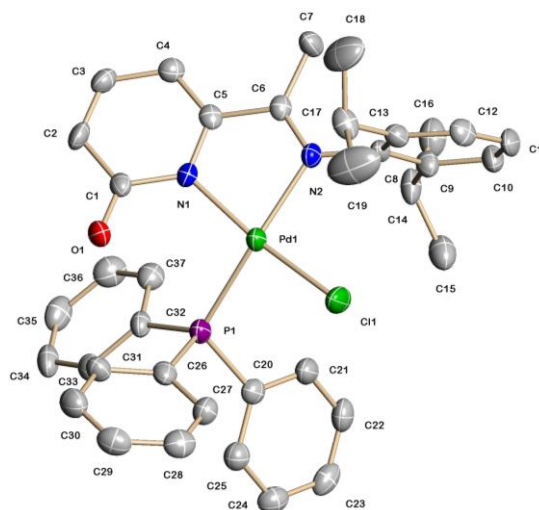
Figure 3.21: Molecular structure of **L2**$_a$PdCl(PPh$_3$); the thermal ellipsoids are set at the 30% probability level (all hydrogen atoms have been removed for clarity)

Table 3.10: Selected bond lengths (Å) and angles (°) for **L2**$_a$PdCl(PPh$_3$)

Bond lengths (Å)		Bond angles (°)	
Pd(1)-N(1)	2.013(3)	N(1)-Pd(1)-N(2)	79.14(13)
Pd(1)-N(2)	2.082(3)	N(1)-Pd(1)-P(1)	98.82(10)
O(1)-C(1)	1.247(5)	N(2)-Pd(1)-Cl(1)	94.83(10)

The ^{1}H NMR spectrum of **L2**$_c$PdCl(PPh$_3$) showed multiple peaks between 7.55-7.39 ppm corresponding to the PPh$_3$ protons. Two 6H doublets at 1.23 ppm and 1.08 ppm were assigned to the methyl protons of the isopropyl moieties. The ESI mass spectrum revealed a fragmentation peak at m/z 742 [M-Cl]. Further confirmation of the structure was provided by the IR spectrum which showed an absorption band at 1618 cm^{-1} corresponding to the C=N$_{imine}$ functional group. The ^{31}P NMR spectrum showed a peak at 25.6 ppm which can be assigned to the coordinated triphenylphosphine. Unfortunately, single crystals of **L2**$_c$PdCl(PPh$_3$) suitable for X-ray diffraction studies could not be obtained.

Given the variable yields of **L2**$_a$PdCl(PPh$_3$), we also explored a salt elimination approach in which the sodium salt of H**L2**$_a$ [prepared by reacting it with NaH in THF at 40 °C] was reacted with (MeCN)$_2$PdCl$_2$ in the presence of triphenylphosphine (Scheme 3.11). Pleasingly, this method gave a higher yield of **L2**$_a$PdCl(PPh$_3$) compared to those shown in Scheme 3.10.
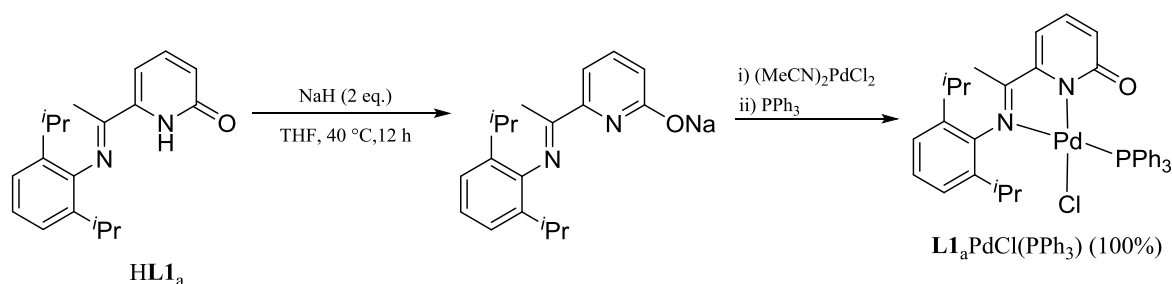
Scheme 3.11: Alternative salt elimination route to **L2**$_a$PdCl(PPh$_3$)

It is noteworthy that other different 2-electron donor ligands (including 3,5-lutidine and 3,5-dichloropyridine) were also explored in their reactions with (**L2**$_{a-c}$Pd)$_2$OH(Cl). However, no reaction occurred even after heating at 40 °C for 7 days. It is uncertain as the lack of reactivity but could be due to the relative donor properties of triphenylphosphine versus these pyridines.

3.2.2.5 Synthesis of [HL2Pd(NCMe)$_2$][PF$_6$]$_2$ and [HL3Pd(NCMe)$_2$][PF$_6$]$_2$

With a view to developing **HL2**- or **HL3**-containing palladium(II) complexes incorporating labile ligands that may be displaced in a potential catalytic process, bis-acetonitrile complexes of the type [**HL2**Pd(NCMe)$_2$][PF$_6$]$_2$ and [**HL3**Pd(NCMe)$_2$][PF$_6$]$_2$ were targeted. Firstly, the synthesis of dicationic [**HL2**$_{a-c}$Pd(NCMe)$_2$][PF$_6$]$_2$ was carried out by reacting **HL2**$_{a-c}$ with one molar equivalent [Pd(NCMe)$_4$][PF$_6$]$_2$ [made *in situ* by reacting (MeCN)$_2$PdCl$_2$ with AgPF$_6$ in acetonitrile] in acetonitrile at room temperature forming the products in yields between 97 and 99% (Scheme 3.12). Complexes [**HL2**$_a$Pd(NCMe)$_2$][PF$_6$]$_2$, [**HL2**$_b$Pd(NCMe)$_2$][PF$_6$]$_2$ and [**HL2**$_c$Pd(NCMe)$_2$][PF$_6$]$_2$ have been characterised by ^{1}H/^{13}C NMR, IR spectroscopy and mass spectrometry.
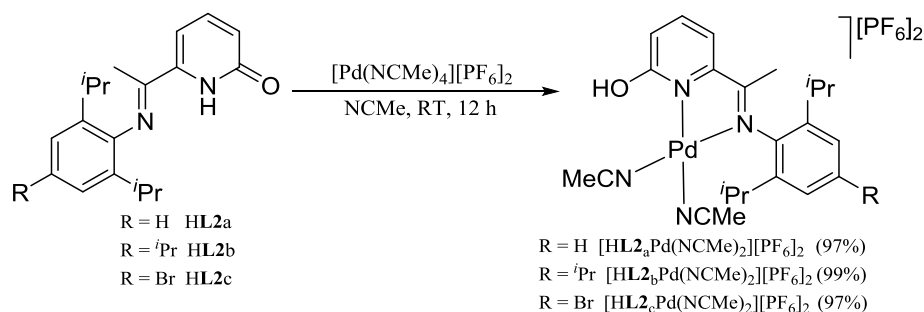
Scheme 3.12: Synthesis of [HL2Pd(NCMe)$_2$][PF$_6$]$_2$

The appearance of a new 6H singlet at 1.87 ppm in the ^{1}H NMR spectrum (recorded in CD$_3$CN at room temperature) of [H**L2**$_a$Pd(NCMe)$_2$][PF$_6$]$_2$ can be assigned to the methyl groups belonging to the two coordinated acetonitrile ligands. Two 6H doublets at 1.37 ppm and 1.19 p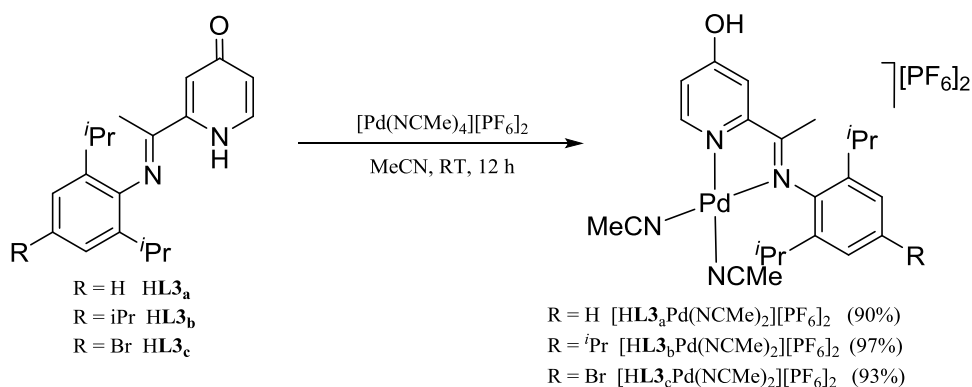pm correspond to the methyl protons of the ortho CH*Me*$_a$*Me*$_b$ protons. The H$_\alpha$ proton of heterocyclic unit came at 7.40 ppm which is in agreement with the aromatized pyridinol form. Moreover, the OH appeared appears at 10.15 ppm which further confirms the pyridinol form of the heterocyclic unit. The ^{19}F NMR spectrum showed a doublet peak at -72.9 ppm indicating the presence of the PF$_6$ anion.

Similar features were observed in the proton NMR spectra of [H**L2**$_b$Pd(NCMe)$_2$][PF$_6$]$_2$ and [H**L2**$_c$Pd(NCMe)$_2$][PF$_6$]$_2$. The presence of a new 6H singlet at 1.97 ppm can be assigned to the two coordinated acetonitrile ligands. Their IR spectra revealed characteristic C=N$_{imine}$ absorption bands at 1620 cm^{-1} and 1621 cm^{-1}; the OH bands are seen at 3311 cm^{-1} and 3306 cm^{-1}. In addition, the FAB mass spectra of [**L2**$_b$Pd(NCMe)$_2$][PF$_6$]$_2$ and [H**L2**$_c$Pd(NCMe)$_2$][PF$_6$]$_2$ showed peaks for [M-PF$_6$] at m/z 526 and m/z 522, respectively. Unfortunately, these PF$_6$ salts were not conducive to crystal growth hence ruling out X-ray determinations.

Secondly, the synthesis of [H**L3**$_{a-c}$Pd(NCMe)$_2$][PF$_6$]$_2$ was conducted in a similar manner to that described using H**L2** (Scheme 3.12). Hence, H**L3**$_{a-c}$ were treated with one molar equivalent of [Pd(NCMe)$_4$][PF$_6$]$_2$ in acetonitrile at room temperature overnight (Scheme 3.13). The resultant complexes, [H**L3**$_a$Pd(NCMe)$_2$][PF$_6$]$_2$, [H**L3**$_b$Pd(NCMe)$_2$][PF$_6$]$_2$ and [H**L3**$_c$Pd(NCMe)$_2$][PF$_6$]$_2$ were obtained in high yields and were characterised by ^{1}H/^{13}C NMR, IR spectroscopy and mass spectrometry.

R = H   H**L3**$_a$
R = iPr H**L3**$_b$
R = Br H**L3**$_c$

R = H   [H**L3**$_a$Pd(NCMe)$_2$][PF$_6$]$_2$ (90%)
R = ^{i}Pr [H**L3**$_b$Pd(NCMe)$_2$][PF$_6$]$_2$ (97%)
R = Br [H**L3**$_c$Pd(NCMe)$_2$][PF$_6$]$_2$ (93%)

Scheme 3.13: Synthesis of [H**L3**Pd(NCMe)$_2$][PF$_6$]$_2$

Analysis of [H**L3**_aPd(NCMe)₂][PF₆]₂ by ¹H NMR spectroscopy (recorded in CD₃CN at room temperature) revealed a 3H singlet for the imine methyl which had been shifted from 1.95 ppm in the free ligand to 2.30 ppm. In addition, a 6H singlet at 1.89 ppm can be assigned to the two coordinated acetonitrile ligands. The resonance at 10.51 ppm and 7.16 ppm corresponds to an OH and H_α protons, respectively, which are indicative of the heterocyclic unit adopting the pyridinol form. The IR spectrum revealed a C=N$_{imine}$ stretch at 1620 cm⁻¹, which is shifted to lower wavenumber when compared with the free ligand indicating imine coordination. Moreover, the presence of the OH stretch at 3310 cm⁻¹ further confirms the pyridinol form. In the FAB mass spectrum a strong [M-PF₆] peak is seen at m\z 443.

The ¹H NMR spectrum of [H**L3**_bPd(NCMe)₂][PF₆]₂ showed three 6H doublets at 1.33 ppm, 1.18 ppm and 1.11 ppm corresponding to the methyl protons of the isopropyl group, two doublets for the ortho CH*Me₂*'s and one doublet for the para CH*Me₂*. The septets for ortho C*H*Me₂ and para C*H*Me₂ protons are observed at 3.10 ppm and 2.88 ppm, respectively. In addition, a new 6H peak appeared at 1.89 ppm which can be assigned to methyl protons of the two coordinated acetonitrile ligands. Further confirmation of the structure came from the ¹⁹F NMR spectrum which revealed a doublet peak at -72.6 ppm which can be attributed to the PF₆ anion. The ESI mass spectrum showed a strong fragmentation peak at m\z 527 which corresponds to the loss of a PF₆ anion.

Likewise, analysis of the ¹H NMR spectrum of [H**L3**_cPd(NCMe)₂][PF₆]₂ revealed similar features to that observed for [H**L3**_aPd(NCMe)₂][PF₆]₂ and [H**L3**_bPd(NCMe)₂][PF₆]₂. A 6H singlet peak detected at 1.89 ppm corresponds to the two coordinated acetonitrile ligands. Additionally, an OH appeared at 10.95 ppm supports the heterocyclic unit adopting the pyridinol form. A strong peak at 1626 cm⁻¹ in the IR spectrum is visible for the coordinated imine. Unfortunately single crystals of [H**L3**_aPd(NCMe)₂][PF₆]₂, [H**L3**_bPd(NCMe)₂][PF₆]₂ or [H**L3**_cPd(NCMe)₂][PF₆]₂, suitable for X-ray diffraction, could not be grown.

It is noticeable in the ¹H NMR spectra of all examples of [H**L2**Pd(NCMe)₂][PF₆]₂ and [H**L3**Pd(NCMe)₂][PF₆]₂, the acetonitrile ligands were observed as one singlet despite being in inequivalent environments. While the reason for the singlet is uncertain, Abu

Omar *et al.* reported a similar observation for the ^{1}H NMR spectrum of $6(C_6H_5)N=CMeC_5H_4NPd(NCCH_3)_2][BAr^{F4}]_2$.[31]
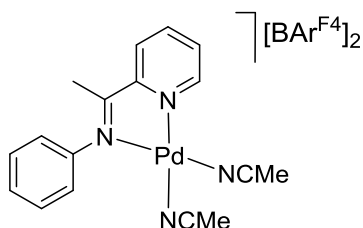
Figure 3.22: Structure of $6(C_6H_5)N=CMeC_5H_4NPd(NCCH_3)_2][BAr^{F4}]_2$

3.2.2.6 Reactivity of [HL2Pd(NCMe)$_2$][PF$_6$]$_2$ and [HL3Pd(NCMe)$_2$][PF$_6$]$_2$

With the aim to investigate the acidic behaviour of pyridinol-containing dications, [H**L2**Pd(NCMe)$_2$][PF$_6$]$_2$ and [H**L3**Pd(NCMe)$_2$][PF$_6$]$_2$, we explored their reactivity towards base and in particular Ag$_2$O. Firstly, the reaction [H**L2$_{a-c}$**Pd(NCMe)$_2$][PF$_6$]$_2$ with Ag$_2$O in acetonitrile at room temperature gave [(**L2$_a$**Pd)$_2$OH(NCMe)][PF$_6$], [(**L2$_b$**Pd)$_2$OH(NCMe)][PF$_6$] and [(**L2$_c$**Pd)$_2$OH(NCMe)][PF$_6$] in high yield (Scheme 3.14). All three complexes have been characterised by ^{1}H/^{13}C NMR, IR spectroscopy and mass spectrometry. In addition, [(**L2$_b$**Pd)$_2$OH(NCMe)][PF$_6$] has been the subject of a single crystal X-ray diffraction study.
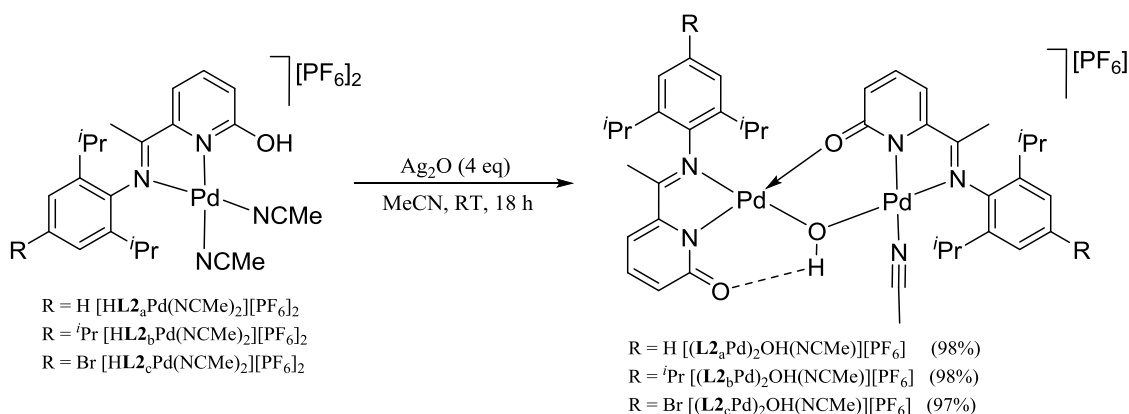
Scheme 3.14: Synthesis of [(**L2**Pd)$_2$OH(NCMe)][PF$_6$]

The ^{1}H NMR spectrum of [(**L2$_a$**Pd)$_2$OH(NCMe)][PF$_6$] displayed four 6H doublets between 1.38-1.08 ppm which can be assigned to the CH*Me$_a$Me$_b$* and CH*Me$_a$'Me$_b$'* protons belonging to the inequivalent pyridonate ligands. Peaks at 9.06 ppm and 1.99 pm correspond to the bridging OH and the coordinated acetonitrile ligands, respectively. Further indication of the structure was afforded by the high resolution mass spectrum

which revealed a [M-PF$_6$] peak at 860.1994 which compares with the calculated value of 860.1983 for C$_{40}$H$_{50}$N$_5$O$_3$Pd$_2$. Moreover, the ^{19}F NMR spectrum showed a peak at -73.2 ppm which indicates the presence of the PF$_6$ counterion.

In the ^{1}H NMR spectrum of [(**L2**$_b$Pd)$_2$OH(NCMe)][PF$_6$] the presence of two 3H singlets at 2.09 ppm and 2.00 ppm for the inequivalent imine methyls support the proposed bimetallic structure; the bridging OH is clearly visible at 8.86 ppm. In addition, a septet peak in the ^{31}P NMR spectrum at -144.6 ppm can be attributed to the phosphorus atom in the PF$_6$ counterion. The FAB mass spectrum revealed a strong peak at m/z 944 for cationic unit [M-PF$_6$].

Single crystals of [(**L2**$_b$Pd)$_2$OH(NCMe)][PF$_6$] suitable for an X-ray diffraction study were grown by slow evaporation of acetonitrile solution of the complex. A view of [(**L2**$_b$Pd)$_2$OH(NCMe)][PF$_6$] is shown in Figure 3.23; selected bond lengths and angles are given in Table 3.11. The structure consists of a cation-anion pair in which the cationic unit is based on a **L2**$_b$Pd(NCMe) fragment that is connected to another **L2**$_b$Pd fragment by an OH bridge and by an oxygen atom (O1) of one of the pyridonate ligands. The coordination geometry at each metal centre can be described as distorted square planar. The O(1)-C(1) bond distance is 1.278(5) Å, while the O(3)-C(22) distance is 1.262(6) Å which are both consistent with double bond and supporting the pyridonate form. An intramolecular hydrogen bond is seen between O(2)-H(2A)$\cdots$O(3) at 1.987 Å. In addition, intermolecular π-π stacking of the pyridonate rings resembling that seen in (**L2**Pd)$_2$OH(Cl) is also featured (separation = 3.364 Å) (Figure 3.24).
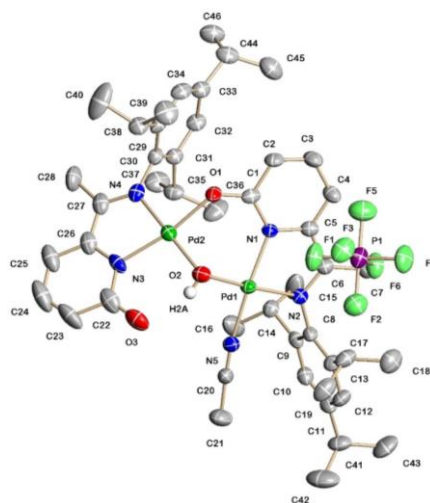
Figure 3.23: Molecular structure of [(**L2**$_b$Pd)$_2$OH(NCMe)][PF$_6$]; the thermal ellipsoids are set at the 30% probability level (all hydrogen atoms have been removed for clarity)

Bond lengths (Å)		Bond angles (°)	
Pd(2)-O(2)	1.980(3)	N(1)-Pd(1)-N(2)	80.42(14)
Pd(1)-O(2)	1.999(3)	N(3)-Pd(2)-N(4)	80.01(17)
O(1)-C(1)	1.278(5)	N(1)-Pd(1)-O(2)	95.45(13)
Pd(2)-O(1)	2.007(3)	O(2)-Pd(2)-N(3)	99.93(15)
O(3)-C(22)	1.262(6)		
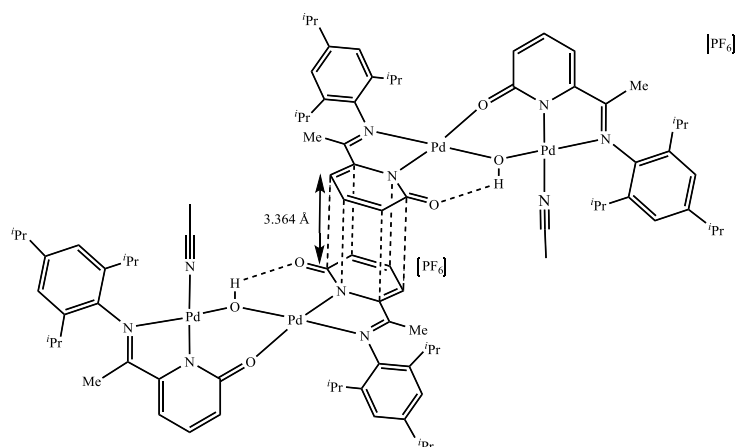
Figure 3.24: π-Stacking between adjacent molecules of [(**L2**$_b$Pd)$_2$OH(NCMe)][PF$_6$]

The ^{1}H NMR spectrum of [(**L2**$_c$Pd)$_2$OH(NCMe)][PF$_6$] revealed four different 6H doublets peaks at 1.37 ppm, 1.18 ppm, 1.09 ppm and 1.07 ppm for the isopropyl methyl protons while the CHMe$_2$ protons appear as two distinct 2H septets at 3.15 ppm and 3.05 ppm; the inequivalency of the septets highlights than the two pyridonate ligands are in different environments. Furthermore, the bridging OH proton is evident at 9.20 ppm. The IR spectrum revealed a characteristic C=N$_{imine}$ peak at 1619 cm^{-1} consistent with a bound imine nitrogen. In the ^{31}P NMR spectrum the peak at -144.6 ppm was assigned to PF$_6$ counterion. A strong peak at 1018 in the ESI mass spectrum can be assigned to the [M-PF$_6$] fragment.

The incorporation of a bridging hydroxide in [(**L2**Pd)$_2$OH(NCMe)][PF$_6$] following the deprotonation of [H**L2**Pd(NCMe)$_2$][PF$_6$] with Ag$_2$O can be attributed to the water eliminated during the reaction:

$$Ag_2O + 2\ [HL2Pd(NCMe)_2][PF_6] \rightarrow 2\ AgPF_6 + H_2O + [L2Pd(NCMe)_2]^+$$
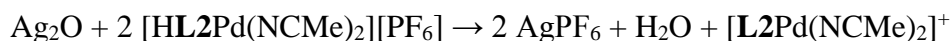
It is considered that the resulting palladium(II) cation $[\mathbf{L2}Pd(NCMe)_2]^+$ then undergoes *in-situ* reaction with water. Notably, $[H\mathbf{L2_a}Pd(NCMe)_2][PF_6]$ can also be formed by reacting $(\mathbf{L2_a}Pd)_2OH(Cl)$ with $AgPF_6$ in acetonitrile at room temperature for 18 hours.

Secondly, the reaction of $[H\mathbf{L3_{a-c}}Pd(NCMe)_2][PF_6]_2$ with Ag_2O in acetonitrile at room temperature was attempted (Scheme 3.15). Unfortunately, the ^1H NMR spectra of the products in each case were very broad and not conducive to full characterisation. Nevertheless, there was evidence of deprotonation of the starting material with silver oxide, the proton NMR spectra present a chemical shift of the heterocyclic proton de-aromatized 4-pyridonate form. Unfortunately, the single crystals for X-ray diffraction, could not be grown.

R = H $[H\mathbf{L3_a}Pd(NCMe)_2][PF_6]_2$
R = i-Pr $[H\mathbf{L3_b}Pd(NCMe)_2][PF_6]_2$
R = Br $[H\mathbf{L3_c}Pd(NCMe)_2][PF_6]_2$
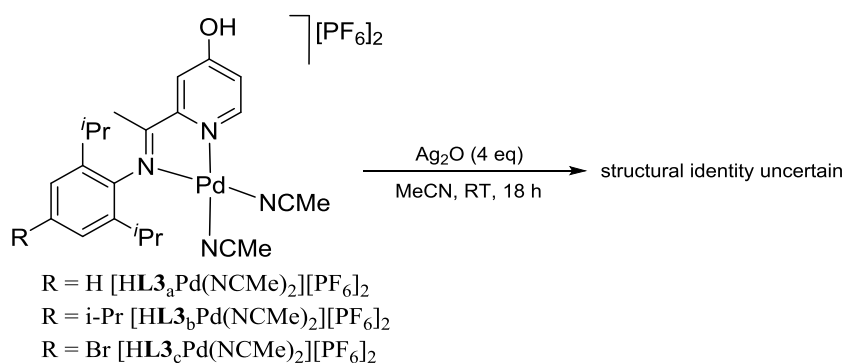
Scheme 3.15: Attempted deprotonation reactions of $[H\mathbf{L3}Pd(NCMe)_2][PF_6]_2$

3.2.2.7 Acid-base switchability of HL2PdCl₂ and HL3PdCl₂

Given the ready reactivity of $H\mathbf{L2}PdCl_2$ with base affording bimetallic $(\mathbf{L2}Pd)_2OH(Cl)$, we were interested in exploring the proton acceptor ability of these bimetallic pyridonate complexes. On an NMR scale, one drop of concentrated hydrochloric acid (37 M) was added to CD_2Cl_2 solutions of $(\mathbf{L2_a}Pd)_2OH(Cl)$, $(\mathbf{L2_b}Pd)_2OH(Cl)$ and $(\mathbf{L2_c}Pd)_2OH(Cl)$ and shaken vigorously (Scheme 3.16). After one hour their ^1H NMR spectra showed that $H\mathbf{L2_a}PdCl_2$, $H\mathbf{L2_b}PdCl_2$ and $H\mathbf{L2_c}PdCl_2$, respectively, had been formed in quantitative yield (see Figure 3.25 for a representative set of NMR spectra).
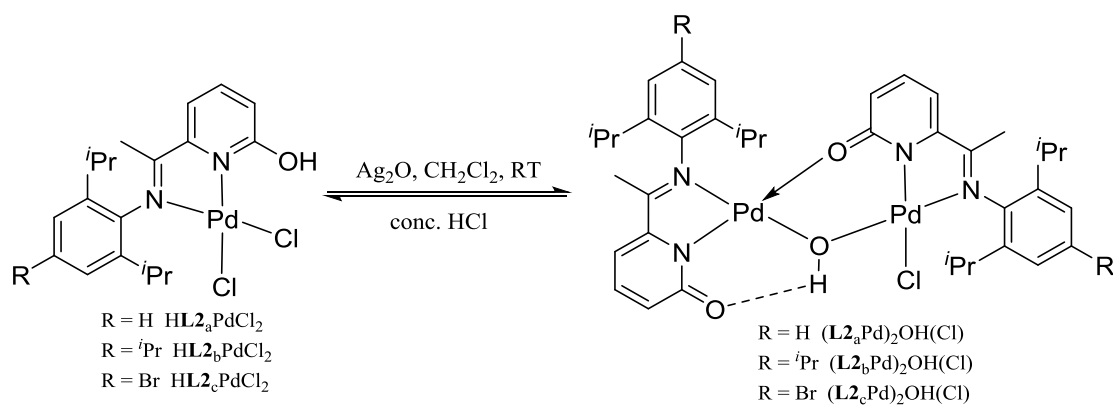
Scheme 3.16: Acid-base switchability
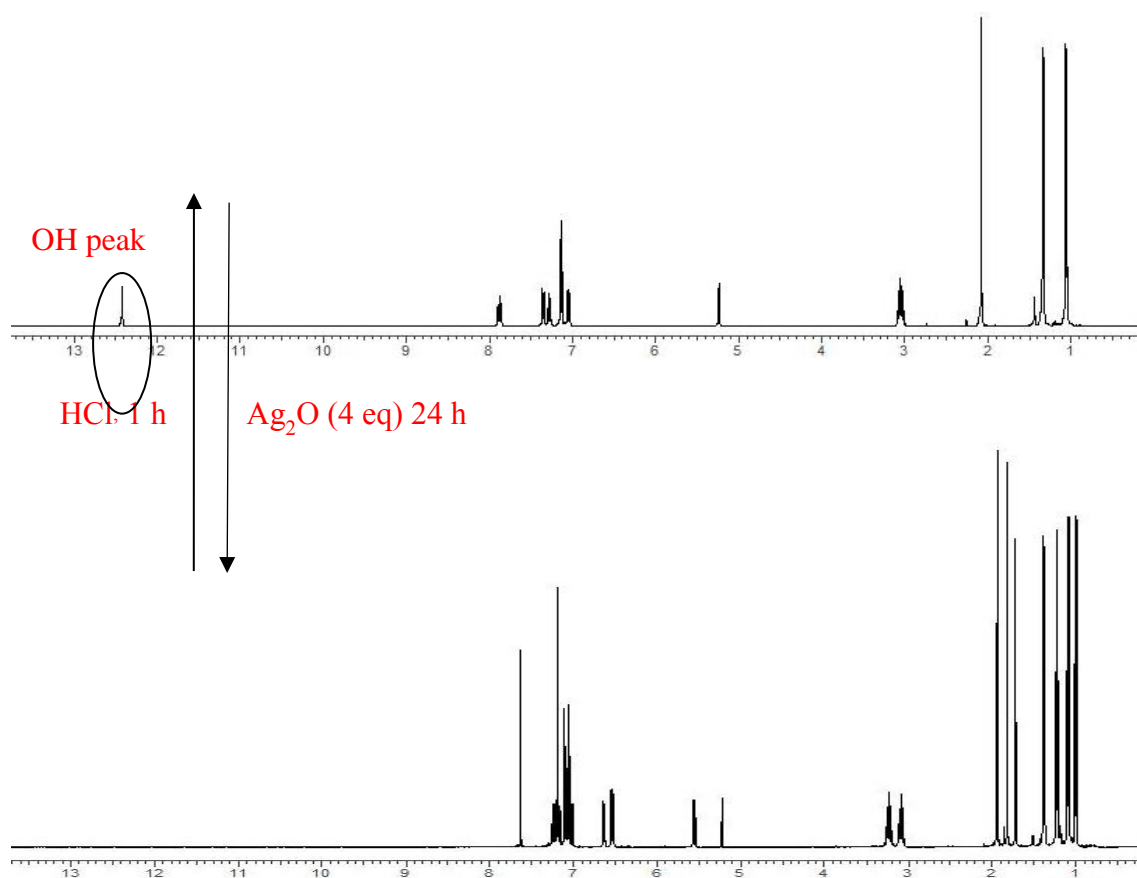
Figure 3.25: ^{1}H NMR spectra of $HL2_aPdCl_2$ (top) and $(L2_aPd)_2OH(Cl)$ (bottom); the spectra were recorded in CD_2Cl_2 at room temperature.

As discussed previously the reaction of H**L3**PdCl$_2$ with base (silver oxide) was found to form a deprotonated pyridonate complex of uncertain composition, '**L3**PdCl' (Scheme 3.9). We were interested to examine whether these deprotonated species would undergo clean protonation reactions. On an NMR scale, one drop of concentrated hydrochloric acid (37 M) was added to CD$_2$Cl$_2$ solutions of '**L3$_a$**PdCl', '**L3$_b$**PdCl', and '**L3$_c$**PdCl', and shaken vigorously (Scheme 3.17). After one hour, H**L3$_a$**PdCl$_2$, H**L3$_b$**PdCl$_2$ and H**L3$_c$**PdCl$_2$, respectively, were identified as the only product.

$$R = H \quad H\mathbf{L3_a}PdCl_2$$
$$R = {}^iPr \quad H\mathbf{L3_b}PdCl_2$$
$$R = Br \quad H\mathbf{L3_c}PdCl_2$$
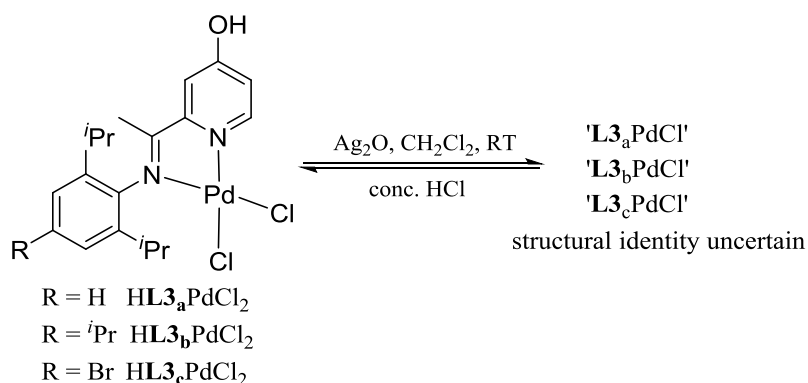
Scheme 3.17: Acid-base switchability

We also explored the reaction of dimeric (**L2$_a$**Pd)$_2$OH(OAc) towards the non- hypohalous acid HPF$_6$ (60% in water) (Scheme 3.18). Unfortunately, the ^{1}H NMR spectrum of the crude product was unclear although the ^{19}F and ^{31}P NMR spectra supported the presence of a PF$_6$ counterion. Nevertheless, on one occasion a few crystals suitable for a single crystal X-ray diffraction study could be grown. A view of [(**L2$_a$**Pd)$_2$OH(HOAc)][PF$_6$] is shown in Figure 3.26.
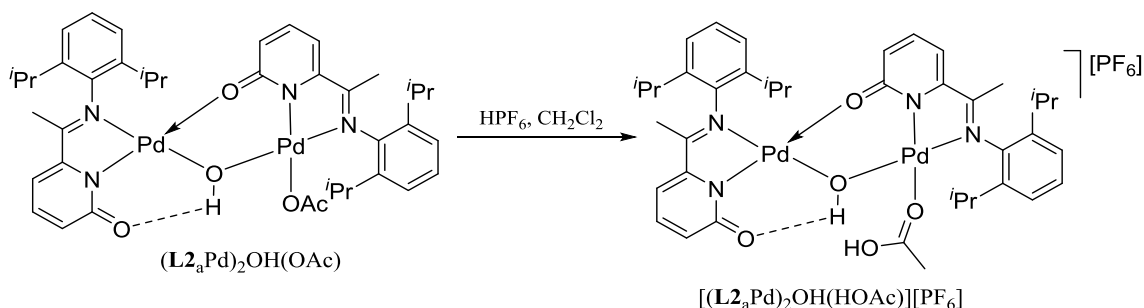
Scheme 3.18: Protonation of (**L2$_a$**Pd)$_2$OH(OAc)

The structure of [(**L2$_a$**Pd)$_2$OH(HOAc)][PF$_6$] consists of a cation-anion pair. The coordination geometry at each metal centre can be described as distorted square planar.

109

The O(4)-C(20) bond distance is 1.322(15) Å which is consistent with a single bond and supporting the presence of an O-bound acetic acid. Furthermore, the Pd(1)-O(2)$_{HOAc}$ bond distance of 2.031(9) Å which is also longer than the Pd-O$_{OAc}$ distance of 1.992(5) Å in neutral (**L2**$_a$Pd)$_2$OH(OAc) in agreement with the presence of a dative bond. With regard to the pyridonate units, the double bond character is maintained as is revealed by the O(5)-C(22) and O(1)-C(1) distances of 1.263(15) and 1.294(15) Å, respectively. Otherwise, the features of the structure are similar to that described for (**L2**$_a$Pd)$_2$OH(OAc) (see before).
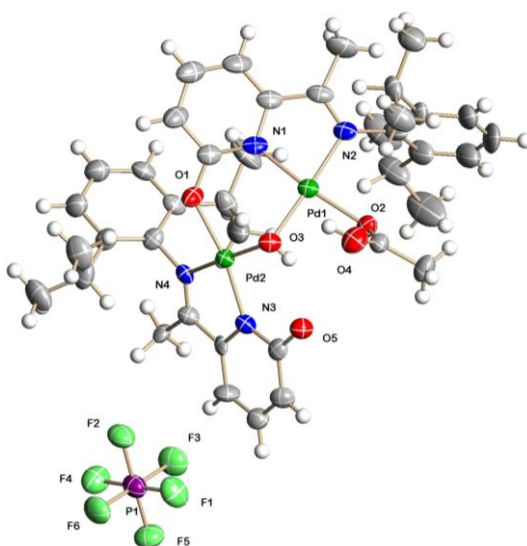
Figure 3.26: Molecular structure of [(**L2**$_a$Pd)$_2$OH(HOAc)][PF$_6$]; the thermal ellipsoids are set at the 50% probability level

3.2.3 Complexation of HL2 and HL3 with Pt(II)

Following a thorough investigation of the chemistry of H**L2** and H**L3** with various sources of palladium(II), we decided to widen the scope of the ligands by reacting them with different metals. As previously described in Chapter 1 there have been many applications of Pt(II) complexes containing pyridine-like ligands. To explore the capability of H**L2** and H**L3** to form platinum(II) chloride complexes we undertook a study of their chemistry with platinum dichloride.

Firstly, the reactions of H**L2**$_{a-c}$ with (DMSO)$_2$PtCl$_2$ (DMSO = dimethylsulphoxide) were carried out in chloroform at 57 °C affording H**L2**$_a$PtCl$_2$, H**L2**$_b$PtCl$_2$ and H**L2**$_c$PtCl$_2$ in close to quantitative yield in 24 hours (Scheme 3.19). All three complexes have been characterised by ^{1}H/^{13}C NMR, IR spectroscopy and mass spectrometry. In addition,

HL2$_a$PtCl$_2$ and HL2$_c$PtCl$_2$ have been the subject of single crystal X-ray diffraction studies.
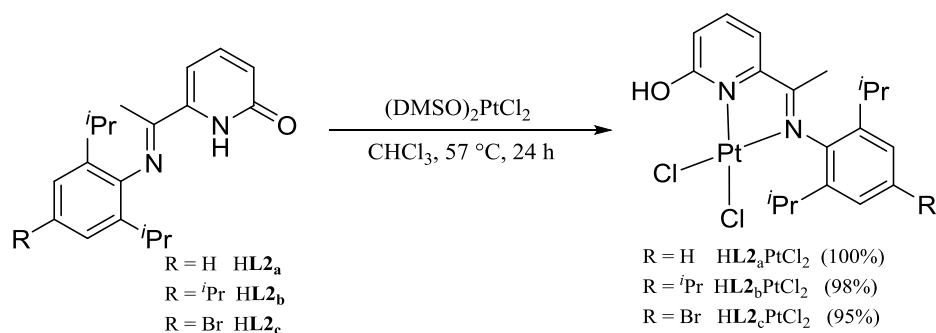
Scheme 3.19: Synthesis of HL2PtCl$_2$

In the ^{1}H NMR spectrum of HL2$_a$PtCl$_2$, a singlet peak corresponding to the OH proton was observed at 12.55 ppm and two 6H doublets were observed for the isopropyl CH*Me$_a$Me$_b$* protons at 1.36 ppm and 1.11 ppm. The IR spectrum showed peaks at 1625 cm^{-1} and 3665 cm^{-1} which are assigned to the C=N$_{imine}$ and OH functionalities, respectively. The ESI mass spectrum revealed a strong [M-Cl] fragmentation peak at m/z 491.

Single crystals of HL2$_a$PtCl$_2$ suitable for the X-ray determination were grown by slow evaporation of a chloroform solution of the complex. A view of the structure is shown in Figure 3.27; selected bond lengths and angles are presented in Table 3.12. The structure is based on a distorted square planar platinum centre bound by two nitrogen atoms belonging to HL2$_a$ and two chloride ligands. The chelating bidentate ligand enforces the chloride ligands into a *cis* arrangement. With regard to the heterocyclic unit, inspection of C(1)-O(1) bond length of 1.322(6) Å confirms that that it adopts the pyridinol form as was observed with HL2$_a$PdCl$_2$. Moreover, the 2,6-diisopropylphenyl ring is inclined close to perpendicular with respect to the coordination plane. Intra-molecular hydrogen-bonding is a feature of the structure with an O(1)-H(1)⋯Cl(2) contact of 2.046 Å.[32]
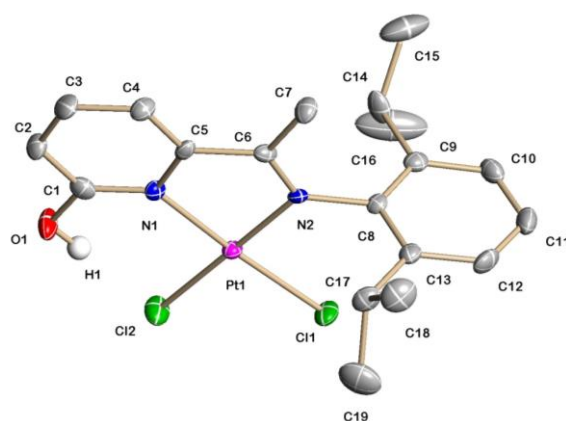
Figure 3.27: Molecular structure of H**L2**$_a$PtCl$_2$; the thermal ellipsoids are set at the 30% probability level (Only the hydrogen on O(1) is shown for clarity)

Table 3.12: Selected bond lengths (Å) and angles (°) for H**L2**$_a$PtCl$_2$

Bond lengths (Å)		Bond angles (°)	
Pt(1)-N(2)	2.014(4)	N(1)-Pt(1)-N(2)	94.83(12)
Pt(1)-N(1)	2.045(4)	Cl(1)-Pt(1)-Cl(2)	85.36(5)
O(1)-C(1)	1.322(6)	N(1)-Pt(1)-Cl(2)	100.11(12)
C(6)-N(2)	1.292(6)	N(2)-Pt(1)-Cl(1)	94.83(12)

The characterisation data for H**L2**$_b$PtCl$_2$ were in agreement with the proposed structure and consistent with a square planar platinum(II) complex supported by the bidentate ligand. A peak appeared at 12.50 ppm corresponding to the OH proton in the ^{1}H NMR spectrum, which is a clear indication of the pyridinol form. Additionally, the ortho and para isopropyl methyl groups give rise to three doublets at 1.37 ppm, 1.27 ppm and 1.12 ppm; two septets of integration 2:1 are also seen for the ortho and para C*H*Me$_2$ protons. As was seen with H**L2**$_b$PdCl$_2$ there are two types of methyl groups for the ortho position, CH*Me*$_a$*Me*$_b$, and one type for the para position. More downfield the protons all fall in the aromatic region further supporting the pyridinol form for the heterocyclic unit. Further confirmation of the structure came from the IR spectrum which revealed a strong absorption peaks at 1624 cm^{-1} and 3660 cm^{-1} which can be assigned to the imine and OH functionalities, respectively. The high resolution mass spectrum revealed a [M-Cl] fragmentation peak at m/z 568.1652 which compares to the calculated value of m/z 568.1697 for C$_{24}$H$_{33}$ON$_2$PtCl.

The analysis of H**L2**$_c$PtCl$_2$ showed similar features to that seen for H**L2**$_a$PtCl$_2$ and H**L2**$_b$PtCl$_2$. In the ^{1}H NMR spectrum a peak at 12.62 ppm could be assigned to the OH

proton. Moreover, the IR spectrum showed strong absorption peaks at 1623 cm^{-1} and 3500 cm^{-1} which correspond to the bound imine and OH groups, respectively. The ESI and FAB mass spectra both revealed the presence of a strong [M-Cl] peak at m/z 606.

Single crystals of H$L2_c$PtCl$_2$ suitable for the X-ray determination were grown by slow evaporation of chloroform solution containing the complex. A perspective view is shown in Figure 3.28; selected bond distances and angles are listed in Table 3.13. The structural features confirm the pyridinol form for the heterocyclic unit and indeed the structures resembles that seen for H$L2_a$PtCl$_2$. Intramolecular hydrogen bond has been seen with an O(1)-H(1)···Cl(1) of 2.040 Å.

Figure 3.28: Molecular structure of H$L2_c$PtCl$_2$; the thermal ellipsoids are set at the 30% probability level (Only the hydrogen on O(1) is shown for clarity)

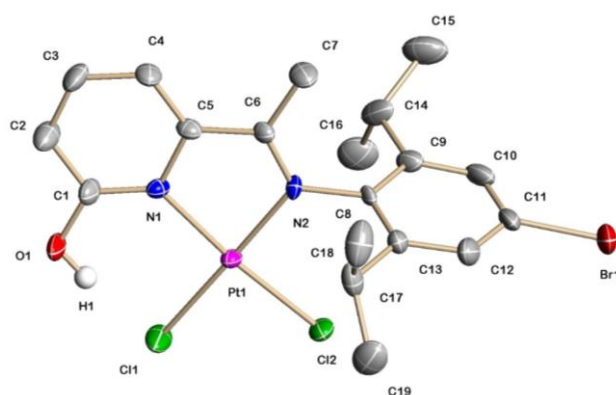**Table 3.13**: Selected bond lengths (Å) and angles (°) for H$L2_c$PtCl$_2$

Bond lengths (Å)		Bond angles (°)	
Pt(1)-N(2)	2.008(6)	N(1)-Pt(1)-N(2)	79.7(2)
Pt(1)-N(1)	2.056(5)	Cl(1)-Pt(1)-Cl(2)	86.16(7)
O(1)-C(1)	1.322(9)	N(1)-Pt(1)-Cl(2)	174.35(17)
C(6)-N(2)	1.293(8)	N(2)-Pt(1)-Cl(1)	178.91(16)
C(11)-Br(1)	1.898(8)		

Secondly, the reactions of H$L3_{a-c}$ with (DMSO)$_2$PtCl$_2$ were carried out in chloroform at 57 °C affording H$L3_a$PtCl$_2$, H$L3_b$PtCl$_2$ and H$L3_c$PtCl$_2$ in 87 to 90% yield after 72 hours (Scheme 3.20). All three complexes have been characterised by ^{1}H/^{13}C NMR, IR spectroscopy and mass spectrometry. In addition, H$L3_a$PtCl$_2$ has been the subject of a single crystal X-ray diffraction study.
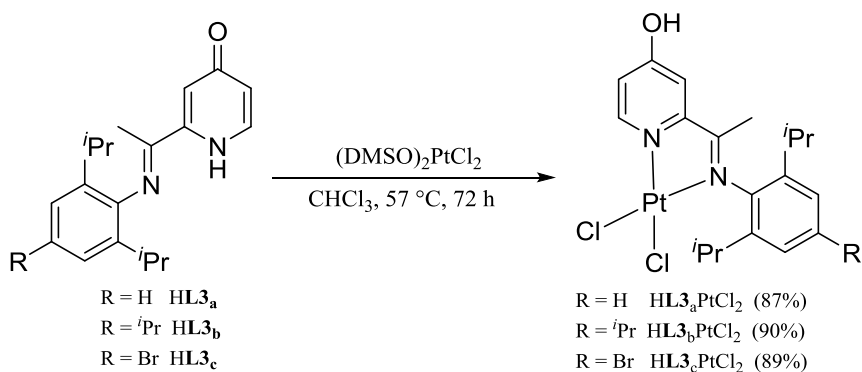
Scheme 3.20: Synthesis of H**L3**PtCl$_2$

The ^{1}H NMR spectrum of H**L3**$_a$PtCl$_2$ confirmed that the heterocyclic unit to adopt the pyridinol form by revealing a singlet at 11.39 ppm for the OH proton. Likewise, the downfield region of the spectrum reveals all signals to fall in the aromatic region supporting the aromatic pyridinol form of the heterocycle. The CH*Me*$_a$*Me*$_b$ methyl protons appeared as doublets at 1.33 ppm and 1.10 ppm. In the IR spectrum a strong absorption peak at 1617 cm^{-1} was assigned to the coordinated imine.

Single crystals of H**L3**$_a$PtCl$_2$, suitable for an X-ray diffraction study, were grown by slow evaporation of chloroform solution containing the complex. A view of the structure is give in Figure 3.29; selected bond distances and angles are compiled in Table 3.14. The structure reveals a distorted square planar geometry about the central platinum. The Pt-N bond lengths show a modest variation [2.023(8) vs. 2.003(8) Å] with distance to the pyridine the longer of the two. The 2,6-diisopropylphenyl is inclined almost perpendicularly to the coordination plane, which might be to reduce any steric clash between itself and the chloride ligand. The C(3)-O(1) bond distance is 1.351(11) Å which is consistent with a single bond and hence the heterocyclic unit is in the pyridinol form. Furthermore, the OH proton can act as hydrogen bond donor resulting in 2D polymer involving O-H···Cl interactions; the OH···Cl bond length was determined as 2.176 Å which resemblies that seen in H**L3**$_a$PdCl$_2$.

114
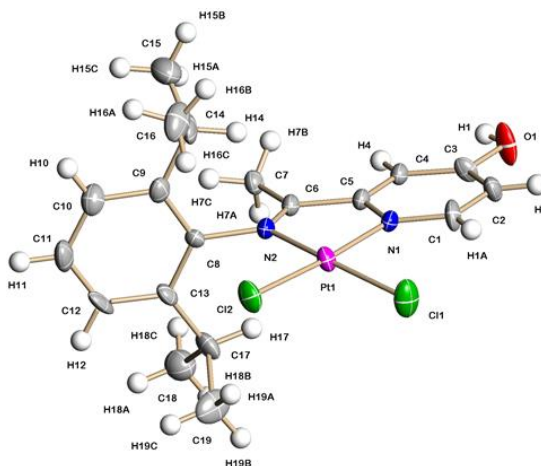
Figure 3.29: Molecular structure of HL3$_a$PtCl$_2$; the thermal ellipsoids are set at the 30% probability level

Table 3.14: Selected bond lengths (Å) and angles (°) for HL3$_a$PtCl$_2$

Bond lengths (Å)		Bond angles (°)	
Pt(1)-N(2)	2.003(8)	N(1)-Pt(1)-N(2)	79.0(3)
Pt(1)-N(1)	2.023(8)	Cl(1)-Pt(1)-Cl(2)	89.45(10)
O(1)-C(3)	1.351(11)	N(1)-Pt(1)-Cl(2)	176.1(2)
C(6)-N(2)	1.275(12)	N(2)-Pt(1)-Cl(1)	179.12(5)

In the ^{1}H NMR spectrum of **HL3$_b$PtCl$_2$**, the signal for the OH proton could been detected at 11.37 ppm while the imine methyl group came at 1.90 ppm, upfield shifted when compared with that observed in the free ligand (at 2.00 ppm). The ESI mass spectrum revealed a peak at 608 m/z which corresponds to the protonated molecular ion.

Similarly, for **HL3$_c$PtCl$_2$** the presence of the OH signal in the proton NMR spectrum suggested that the complex has been formed in the pyridinol form. The splitting of the methyl isopropyl groups at 1.32 ppm and 1.09 ppm providing another indication that the ligand had coordinated. Moreover, the IR spectrum showed a peak at 1617 cm^{-1} and 3633 cm^{-1} for the bound imine and OH, respectively. The ESI mass spectrum revealed a strong protonated molecular peak at m/z 644 [M+H].

Interestingly, on comparison of the reactions of **HL2** and **HL3** with (DMSO)$_2$PtCl$_2$, it was clear that the reactions with **HL3** took a significantly longer time to form the products when compared to that seen with **HL2**. It would seem the position of pyridone oxygen in the free ligand is responsible for the differences in rates of reaction, but it is unclear why.

115

3.2.4 Reactions of HL2 and HL3 with Ni(II)

To complete the survey of the reactivity of H**L2** and H**L3** towards group 10 divalent metal halides, in this section, we explore their reactions with (DME)NiBr$_2$ (DME = 1,2-dimethoxyethane). Firstly, the reactions of H**L2$_{a-c}$** with (DME)NiBr$_2$ were carried out with an equimolar ratio in dichloromethane at room temperature. However, the reactions were not clean affording multiple products including (H**L2**)$_2$Ni-type species (using ESI mass spectrometry). In order to drive the reactions to form mainly the (H**L2**)$_2$Ni-type complexes we adjusted the stoichiometry to 2:1 and were delighted to form paramagnetic (H**L2$_a$**)$_2$NiBr$_2$, (H**L2$_b$**)$_2$NiBr$_2$ and (H**L2$_c$**)$_2$NiBr$_2$ as yellow powders in yields of between 95 and 98% (Scheme 3.21). All three complexes have been characterised by IR spectroscopy, magnetic measurements and mass spectrometry, while (H**L2$_{a-c}$**)NiBr$_2$ have also been the subject of a single crystal X-ray diffraction study.

R = H   (H**L2$_a$**)$_2$NiBr$_2$ (98%)
R = ^{i}Pr (H**L2$_b$**)$_2$NiBr$_2$ (97%)
R = Br   (H**L2$_c$**)$_2$NiBr$_2$ (95%)

R = H   H**L2$_a$**
R = ^{i}Pr H**L2$_b$**
R = Br   H**L2$_c$**
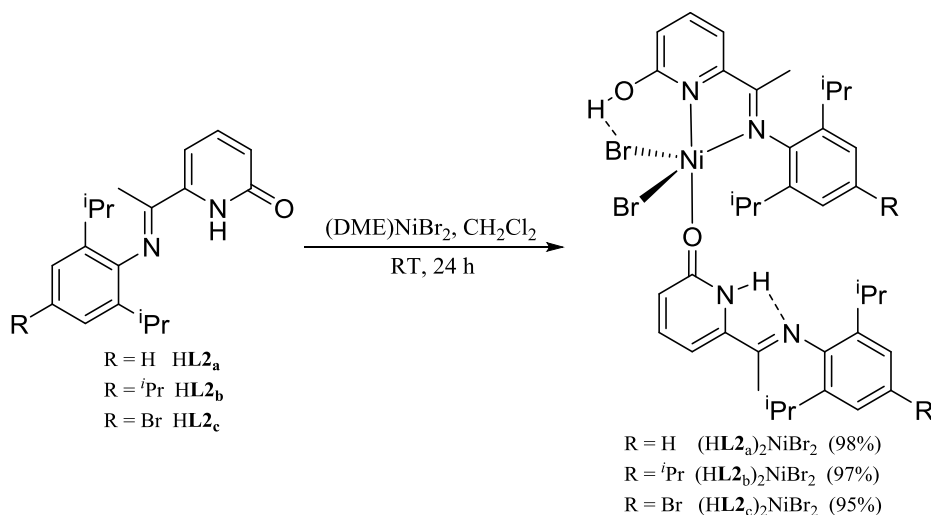
Scheme 3.21: Synthesis of (H**L2**)$_2$NiBr$_2$

The analysis of (H**L2$_a$**)NiBr$_2$ confirmed the proposed structure. The ESI mass spectrum displayed a strong [M-Br] fragmentation peak at m/z 652. The magnetic moment was found to be 2.82 BM (Evans Balance at ambient temperature) which is consistent with two unpaired electrons, typical of a high spin Ni(II) d^8 species.[33] In the infrared spectrum a peak at 1632 cm^{-1} and 3329 cm^{-1} correspond to a bound C=N$_{imine}$ and an OH functionality, respectively. The ^{1}H NMR spectrum was recorded but the peaks were too broad and shifted to allow characterisation which can be attributed to the paramagnetic nature of the complex.

Single crystals of (H**L2ₐ**)NiBr₂ suitable for the X-ray determination were grown by slow diffusion of petroleum ether into a dichloromethane solution of the complex. A view of the structure is shown in Figure 3.30; selected bond distances and angles are given in Table 3.15. The structure consists of nickel(II) centre surrounded by an NN-chelating H**L2**ₐ, an O-bound H**L2**ₐ and two bromide ligands to complete a geometry best described as trigonal bipyramidal geometry. Remarkably, the structure was found to contain coordinated H**L2**ₐ in both the neutral pyridinol and pyridone forms. This unusual binding pattern might be the influenced by the steric properties of the bulky N-aryl group. Additionally, there is a O(1)-H(1)···Br(2) hydrogen bonding interaction of 2.305 Å which likely stabilizes the structure. Intramolecular hydrogen bond can be seen in N(3)-H(3A)···N(4) of 2.223 Å.
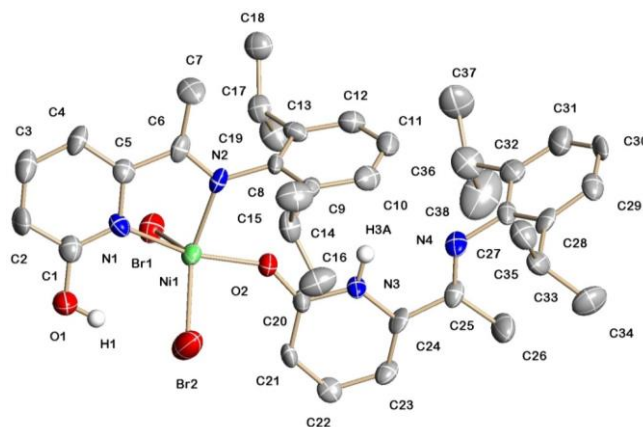
Figure 3.30: Molecular structure of (H**L2**ₐ)₂NiBr₂; the thermal ellipsoids are set at the 30% probability level (all hydrogen atoms have been removed for clarity)

Table 3.15: Selected bond lengths (Å) and angles (°) for (H**L2**ₐ)₂NiBr₂

Bond lengths (Å)		Bond angles (°)	
Ni(1)-N(2)	2.031(8)	N(1)-Ni(1)-N(2)	79.5(3)
Ni(1)-N(1)	2.067(8)	O(2)-Ni(1)-N(2)	87.1(3)
O(1)-C(1)	1.341(11)	O(2)-Ni(1)-Br(2)	94.61 (19)
Ni(1)-O(2)	2.000(6)		

In the ESI and FAB mass spectra of (H**L2**ᵦ)₂NiBr₂ and (H**L2**ᵧ)₂NiBr₂, strong [M-Br] fragmentation peaks at m/z 735 and m/z at 810 were visible, respectively. In addition, a strong absorption bands at 1635 cm⁻¹ and 1634 cm⁻¹ detected in their IR spectra could be assigned for the bound C=N_imine functionalities in (H**L2**ᵦ)₂NiBr₂ and (H**L2**ᵧ)₂NiBr₂, respectively.

Single crystals of $(HL2_b)_2NiBr_2$ and $(HL2_c)_2NiBr_2$ suitable for X-ray determinations were grown by slow diffusion of petroleum ether into a dichloromethane solution of the complex. Views of both are shown side-by-side in Figure 3.31; selected bond distances and angles are given in Table 3.16a and 3.16b. The structures are isostructural to that found for $(HL2_a)_2NiBr_2$ revealing a trigonal bipyramidal geometry for nickel with the two neutral HL2 ligands adopting both pyridone and pyridinol forms. Additionally, there is intramolecular hydrogen bonding between the pyridinol OH and a neighbouring bromide ligand and between a pyridone NH and an imine nitrogen.

Figure 3.31: Molecular structures of $(HL2_b)_2NiBr_2$ and $(HL2_c)_2NiBr_2$; the thermal ellipsoids are set at the 30% probability level (all hydrogen atoms have been removed for clarity)

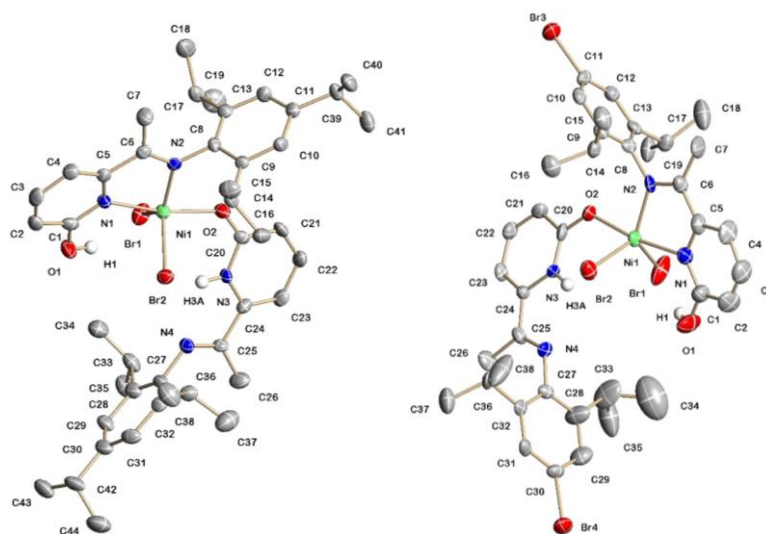**Table 3.16a**: Selected bond lengths (Å) and angles (°) for $(HL2_b)_2NiBr_2$

Bond lengths (Å)		Bond angles (°)	
Ni(1)-N(2)	2.035(3)	N(1)-Ni(1)-N(2)	79.21(12)
Ni(1)-N(1)	2.067(3)	O(2)-Ni(1)-N(2)	90.16(11)
O(1)-C(1)	1.330(4)	O(2)-Ni(1)-Br(2)	97.19(8)
Ni(1)-O(2)	2.005(2)		

Table 3.16b: Selected bond lengths (Å) and angles (°) for $(HL2_c)_2NiBr_2$

Bond lengths (Å)		Bond angles (°)	
Ni(1)-N(2)	2.023(7)	N(1)-Ni(1)-N(2)	79.9(3)
Ni(1)-N(1)	2.073(7)	O(2)-Ni(1)-N(2)	92.1(2)
O(1)-C(1)	1.319(19)	O(2)-Ni(1)-Br(2)	93.68 (16)
Ni(1)-O(2)	2.020(5)		

Secondly, we explored the reaction of H**L3$_{a-c}$** with (DME)NiBr$_2$ initially in a 1:1 molar ratio in dichloromethane at 0 °C temperature, in a manner similar to that with H**L2** (Scheme 3.22). The analytical data for the isolated complexes suggested compositions of the type, H**L3**$_a$NiBr$_2$, H**L3**$_b$NiBr$_2$ and H**L3**$_c$NiBr$_2$.

R = H H**L3**$_a$
R = ^{i}Pr H**L3**$_b$
R = Br H**L3**$_c$

R = H H**L3**$_a$NiBr$_2$
R = ^{i}Pr H**L3**$_b$NiBr$_2$
R = Br H**L3**$_c$NiBr$_2$
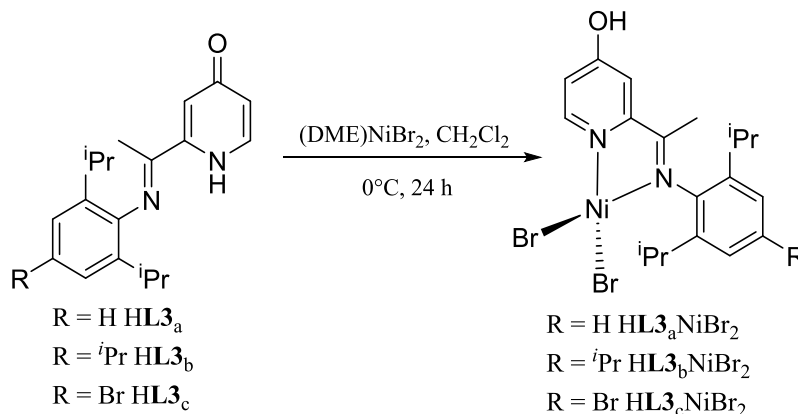
Scheme 3.22: Synthesis of **L3**NiBr$_2$

In the FAB mass spectrum of H**L3**$_a$NiBr$_2$ a [M-Br] fragmentation peak at m/z 434 was clearly evident. A peak at 1605 cm^{-1} in the IR spectrum corresponds to the bound imine. All the complexes gave magnetic moments consistent with two unpaired electrons. The ^{1}H NMR data gave no useful information.

The FAB mass spectrum of H**L3**$_b$NiBr$_2$ showed a [M-Br] fragmentation peak at m/z 477. In the IR spectrum a band at 1606 cm^{-1} was clearly visible corresponding to the bound imine. In addition, a crystal of '**L3**$_b$NiBr$_2$' was grown by prolonged standing (*ca.* 7 days) in bench acetonitrile. A view of the structure is given in Figure 3.32; selected bond distances and angles are collected in Table 3.17. Examination of the structure reveals the formation of **L3**$_{b+Br}$NiBr(OH$_2$)$_2$NCMe, in which a bromide atom has unexpectedly attached to the 3-position of the monoanionic NN-chelating pyridonate ligand. The coordination sphere of this six-coordinate neutral complex is completed by a bromide, an acetonitrile and two water molecules. The heterocyclic unit adopts the pyridonate from which is evidenced by the relatively short C(3)-O(1) bond distance of 1.274(10) Å. The origin of the brominated pyridonate is uncertain but could be due to the excess of NiBr$_2$ present leading to oxidation of the ring during the recrystallization process. However, it is viewed that **L3**$_{b+Br}$NiBr(OH$_2$)$_2$NCMe is not representative of the product and indeed there is no evidence for this species in the mass spectrum. There is intermolecular

hydrogen bonding, O(2)-H(2A)···O(1) 1.930 Å, O(2)-H(2B)···Br(1) 2.672 Å, O(3)-H(3A)···O(1) 1.806 Å and O(3)-H(3B)···O(1) 1.965 Å.
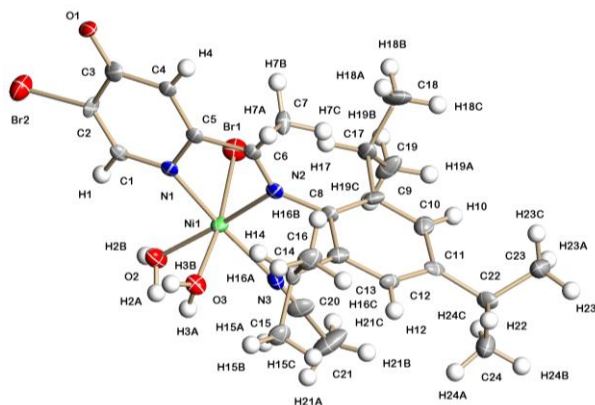

Figure 3.32: Molecular structure of **L3**$_{b+Br}$NiBr(OH$_2$)$_2$NCMe; the thermal ellipsoids are set at the 30% probability level

Table 3.17: Selected bond lengths (Å) and angles (°) for **L3**$_{b+Br}$NiBr(OH$_2$)$_2$NCMe

Bond lengths (Å)		Bond angles (°)	
Ni(1)-N(2)	2.114(8)	N(1)-Ni(1)-N(2)	79.2(3)
Ni(1)-N(1)	1.998(7)	O(2)-Ni(1)-N(3)	88.6(3)
Ni(1)-N(3)	2.064(8)	N(2)-Ni(1)-N(3)	97.6(3)
Ni(1)-O(2)	2.105(6)	N(1)-Ni(1)-O(2)	94.7(3)
O(1)-C(3)	1.274(10)		
C(2)-Br(2)	1.893(9)		

Analysis of the FAB mass spectrum of **L3**$_c$NiBr$_2$ showed a strong [(M+NCMe)-Br] fragmentation peak at m/z 477. Additionally, the IR spectrum detected an absorption band at 1606 cm^{-1} which can be assigned to a bound imine. The magnetic moment was found to be 2.87 BM (Evans Balance at ambient temperature) which is consistent with two unpaired electrons.

To explore the potential to form (H**L3**)$_2$Ni-type complexes, the relative stoichiometry of H**L3** to (DME)NiBr$_2$ was changed to 2:1. In this case, the reaction was performed solely with H**L3**$_a$ in dichloromethane at 0 ^{o}C leading to the formation of the salt [(H**L3**)$_2$NiBr][Br] in high yield (Scheme 3.23). The complex has been characterised by IR spectroscopy, magnetic measurements, mass spectrometry and additionally has been the subject of a single crystal X-ray diffraction study.
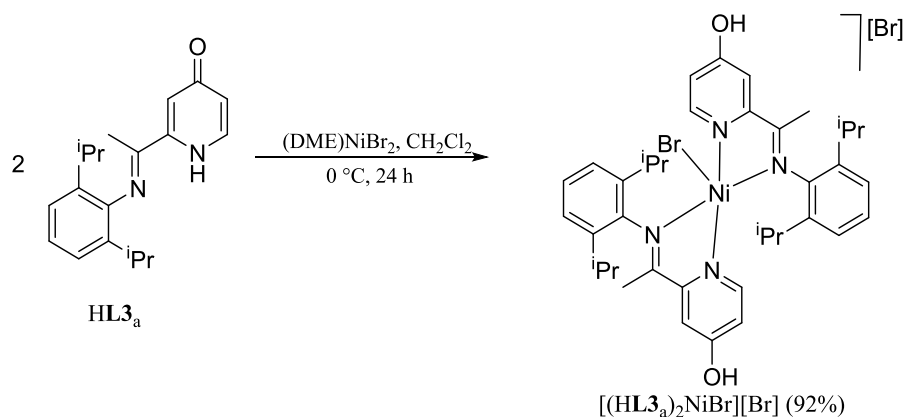
Scheme 3.23: Synthesis of [(HL3$_a$)$_2$NiBr][Br]

In the IR spectrum of [(HL3$_a$)$_2$NiBr][Br] a peak at 1604 cm^{-1} could be assigned to a bound imine while a peak at 3368 cm^{-1} to the OH group. The FAB mass spectrum revealed a strong [M$^+$-Br] peak at m/z 652. Magnetic measurements (Evans balance at room temperature) gave a value of 2.64 BM which is consistent with two unpaired electrons. Single crystals of the complex suitable for the X-ray determination could be grown by slow evaporation of an acetonitrile solution containing the complex. A view of [(HL3$_a$)$_2$NiBr][Br] is shown in Figure 3.33; selected bond distances and angles are given in Table 3.18. The structure comprises a cation-anion pair in which the cation consists of a nickel centre surrounded by two chelating HL3$_a$ ligands and a bromide to complete a geometry best described trigonal bipyramidal geometry. Examination of each heterocyclic unit reveals relatively long C-O bonds of 1.300(12) Å (O(1)-C(3)) which is a characteristic of single bond and hence the pyridinol form is adopted. The 2,6-diisopropylphenyl rings adopt a perpendicular conformation with respect to each Ni-N-C-C-N chelate ring presumably to reduce any steric hindrance. There is intermolecular hydrogen bonding between the water molecule O(1)-H(1)···O(2) 1.773 Å and in O(2)-H(2A)···Br(1) 2.448 Å.
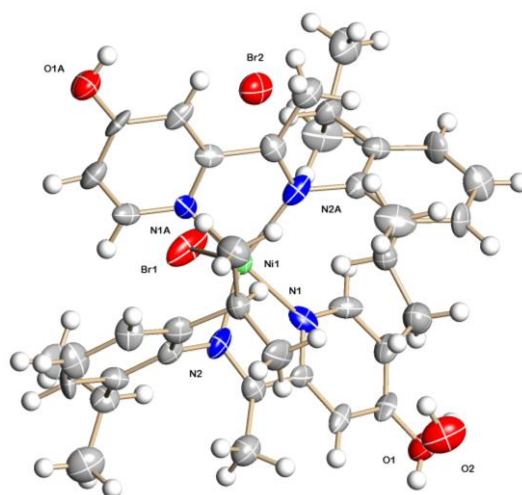
Figure 3.33: Molecular structure of [(H**L3**$_a$)$_2$NiBr][Br]; the thermal ellipsoids are set at the 30% probability level

Table 3.18: Selected bond lengths (Å) and angles (°) for **L3**$_{b+Br}$NiBr(OH$_2$)$_2$NCMe

Bond lengths (Å)		Bond angles (°)	
Ni(1)-N(2)	2.062(10)	N(1)-Ni(1)-N(2)	77.7(4)
Ni(1)-N(1)	2.044(10)	N(2)-Ni(1)-Br(1)	111.6(2)
Ni(1)-Br(1)	2.4303)	N(1)-Ni(1)-Br(1)	94.4(3)
O(1)-C(3)	1.300(12)		

3.3 Conclusions

In this chapter, the preparation of a range of group 10 (Pd, Ni, Pt) transition metal complexes bearing OH-functionalised N,N-pyridylimine ligands has been discussed. Two classes of pyridylimine ligand, H**L2** and H**L3**, differing in the position of the OH group on the pyridine unit (*i.e.*, 6-position H**L2** and 4-position H**L3**) have been synthesised in a sequence of steps from commercially available starting materials. Imine condensation forms the final step in the synthesis of both classes of ligand and allows three types of electronically different N-2,6-i-Pr$_2$C$_6$H$_2$-4-R groups (R = H, i-Pr, Br) to be introduced. The reactivity of H**L2** and H**L3** towards a variety of Pd(II) sources has been thoroughly investigated. Interaction of H**L2** with Pd(OAc)$_2$ results in deprotonation of the ligand and the formation of bimetallic complexes of the type (**L2**Pd)$_2$OH(OAc), while with H**L3** deprotonation also results forming in this case the bis-chelates (**L3**)$_2$Pd. With (MeCN)$_2$PdCl$_2$, the complexes, H**L2**PdCl$_2$ and H**L3**PdCl$_2$, can be isolated in which the corresponding ligand remains intact. In the case of H**L2**PdCl$_2$ deprotonation with Ag$_2$O presents an alternative route to (**L2**Pd)$_2$OH(Cl). Complexes of the type **L2**Pd(Cl)(PPh$_3$) have been prepared on reaction of (**L2**Pd)$_2$OH(Cl) with PPh$_3$ or in higher yield by the reactions of Na**L2** with a mixture of (MeCN)$_2$PdCl$_2$ and PPh$_3$. The dicationic complexes, [H**L2**Pd(NCMe)$_2$][PF$_6$]$_2$ and [H**L3**Pd(NCMe)$_2$][PF$_6$]$_2$ have been obtained in high yield by the reaction of [Pd(NCMe)$_4$][PF$_6$]$_2$ with either H**L2** or H**L3**, respectively. Bimetallic (**L2**Pd)$_2$OH(Cl), could be readily protonated by addition of HCl regenerating H**L2**PdCl$_2$, demonstrating the pH switchability of the complexes. In addition, the platinum complexes H**L2**PtCl$_2$ and H**L3**PtCl$_2$ were obtained under more forcing conditions. In addition, the reactivity of H**L2** and H**L3** towards (DME)NiBr$_2$ has been examined affording complexes of the type (H**L2**)$_2$NiBr$_2$ and [(H**L3**)$_2$NiBr][Br].

References

1. J. Kamatani, R. Ooishi, S. Okada and T. Takiguchi, **2007**, *U.S. Patent* No. 20070231600. New York.

2. F. Mao and A. Heller, **2003**, *U.S. Patent* No. 20030096997. San Francisco.

3. T. Fujita, M. Mitani, Y. Yoshida, T. Matsugi, Y. Suzuki, S. I shii, Y. Tohi, H. Makio, Y. Inoue and J. Saito, *PMSE Preprints*, 2002, **86**, 299.

4. W. M. Motswainyana, S. O. Ojwach, M. O. Onani, E. I. Iwuoha and J. Darkwa, *Polyhedron,* 2011, **30**, 2574.

5. W. B. Cross, E. G. Hope, G. Forrest, K. Singh and G. A. Solan, *Polyhedron,* 2013, **59**, 124.

6. V. C. Gibson and S. Spitzmesser, *Chem. Rev.*, 2003, **103**, 283.

7. S. Taubmann and H. G. Alt, *J. Mol. Cat. A: Chem.*, 2008, **284**, 134.

8. E. T. Mendivil, J. Diez and V. Cadierno, *Polyhedron*, 2013, **59**, 69.

9. E.D. Mckenzie, *Coord. Chem. Rev.,* 1971, **6**, 187.

10. E.C. Constable and P. J. Steel, *Coord. Chem. Rev.,* 1989, **93**, 205.

11. G. Chelucci and R. P. Thummel, *Chem. Rev.,* 2002, **102**, 3129.

12. N. C. Fletcher, *J. Chem. Soc.,* 2002, **1**, 1831.

13. G. R. Newkome, A. K. Patri, E. Holder and U. S. Schubert, *Eur. J. Org. Chem.,* 2004, **235**.

14. E. T. Mendivil, J. Diez and V. Cadierno, *Catal. Sci. Technol.,* 2011, **1**, 1605.

15. Y. Himeda, N. O. K, H. Sugihara, H. Arakawa and K. Kasuga, *Organometallics,* 2004, **23**, 1480.

16. Y. Himeda, N. O. Komatsuzaki, H. Sugihara and K. Kasuga, *Organometallics,* 2007, **26**, 702.

17. I. Nieto, M. S. Livings, J. B. Sacci, L. E. Reuther, M. Zeller and E. T. Papish, *Organometallics,* 2011, **30**, 6339.

18. C. M. Conifer, R. A. Taylor, D. J. Law, G. J. Sunley, A. J. P. White and G. J. P. Britovsek, *Dalton Trans.,* 2011, **40**, 1031.

19. (a) R. Kawahara, K. -I. Fujita and R. Yamaguchi, *J. Am. Chem. Soc.,* 2012, **134**, 3643. (b) R. Wang, J. Ma and F. Li, *J. Org. Chem.,* 2015, **80**, 10769.

20. D. Hoong, M. Murakami, Y. Yamada and S. Fukuzumi, *Energy Environ. Sci.,* 2012, **5**, 5708.

21. T. Nguyen, M. A. Wicki and V. Snieckus, *J. Org. Chem.*, 2004, **69**, 7816-7821.

22. O. K. and and G. Wassilios, *World Pat.*, WO9730032 (A1), **1996**.

23. B. M. L.and B. M. M., *USA Pat.*, WO2007017754 (A2), **2007**.

24. D. Peng, Y. Zhang, X. Du, L. Zhang, X. Leng, M.D.Walter and Z. Huang, *J. Am. Chem. Soc*, 2013, **135**, 19154.

25. B. Crociani, M. Sala, A. Polo and G. Bombieri, *Organometallics*, 1986, **5**, 1369.

26. A. Kvick, *Acta Crystallogr. Sect. B.*, 1976, **32**, 220.

27. S. J. Connon and A. F. Hegarty, *Eur. J. Org. Chem.,* 2004*,* **16**, 3477.

28. A. K. Ghosh, N. Kumaragurnbaran, C. Liu, T. Devasamudram, H. Lei, L. Swanson, S. Ankala, J. Tang and G. Bilcer, *World Pat*, WO2006110668 A1, **2006**.

29. B. G. Hashiguchi, K. J. H. Young, M. Yousufuddin, W. A. Goddard and R. A. Periana, *J. Am. Chem. Soc.,* 2010**, 132**, 12542.

30. T. Steiner, *Angew. Chem. Int. Ed.,* 2002, **41**, 48.

31. K. J. Miller, T. T. Kitagawa and M. M. Abu-Omar, *Organometallics,* 2001, **20**, 4403.

32. E. Tomás-Mendivil, J. Díez and V. Cadierno, *Polyhedron*, 2013, **59**, 69.

33. (a) J. Cho, Y-M. Lee, S. Y. Kim and W. Nam, *Polyhedron*, 2010, **29**, 446. (b) F. A. Cotton, G. Wilkinson, C. A. Murillo, M. Bochmann, Advanced Inorganic Chemistry, sixth ed., *Wiley*, New York, 1999.

Chapter Four

Exploring ligand functionalisation in metal-catalysed

transfer hydrogenation and ethylene oligomerisation

4.1 Introduction

This Chapter will explore the use of a selection of the OH-functionalised metal complexes developed in this thesis as catalysts in either transfer hydrogenation or as pre-catalysts in oligo-/polymerisation of ethylene. A brief introduction to these areas will be presented in separate sections, 4.2.1 and 4.3.1, before discussion of the results and conclusions.

4.2.1 Hydrogenation

Direct hydrogenation is the addition of molecular hydrogen to an unsaturated organic compound and represents a transformation that is used in a variety of applications. Moreover, the use of this process is of major significance and relevance to the chemical industry. Some of the most important commercial uses of hydrogenation relate to the upgrading of crude oil, production of bulk commodity materials, as well as fine chemicals used in the agricultural and pharmaceutical industries.[1,2]

Catalytic hydrogenation of unsaturated compounds was discovered by Wilkinson and others in the 1960s in which transition metal-based catalysts could mediate the transformation. In particular, olefin hydrogenation in the presence of hydrogen gas using a homogeneous rhodium catalyst represents a milestone in the area (Scheme 4.1).[3-5]
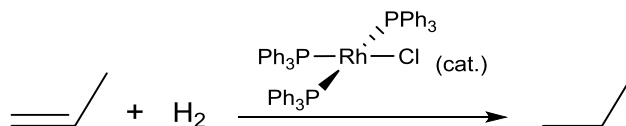

Scheme 4.1: Wilkinson's catalyst for the hydrogenation of alkenes
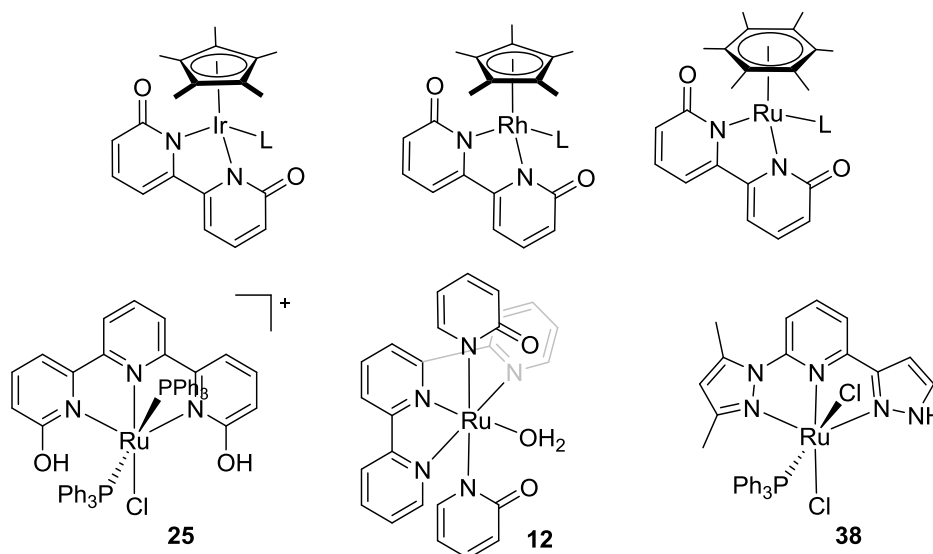
4.2.2 Transfer Hydrogenation

Catalytic hydrogenation of an unsaturated molecule by using a compound that can act as a source of hydrogen in place of molecular hydrogen is known as transfer hydrogenation. It has become an important catalytic reaction in a wide variety of chemical transformations and can be performed without the use of potentially explosive hydrogen gas or any hazardous hydride reagent.[1,2,6] Transfer hydrogenation can be used to hydrogenate a wide range of functional groups such as ketones, aldehydes and imines. The most typical source of hydrogen is an alcohol solvent such as isopropanol. Isopropanol is desirable since it is non-toxic, inexpensive, easy to handle, stable and environmentally friendly.[1,2,7] Furthermore, the by-product of the transformation is

acetone. To allow the promotion of transfer hydrogenation an inorganic base such as NaOH, K_2CO_3, KOH and K^tOBu is commonly used. The hydrogenation of acetophenone has become the general starting point for initial screens in catalytic transfer hydrogenation and results in the conversion to 1-phenylethanol (Scheme 4.2).
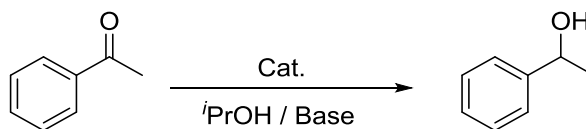
**Scheme 4.2:** Transfer hydrogenation of acetophenone to give 1-phenylethanol in the presence of a catalyst

Since the 1960s, a considerable amount of research and development has been focused on transition metal-mediated transfer hydrogenation. The most common types of transition metal to be used include ruthenium, rhodium and iridium. In addition, the nature of the auxiliary ligand has been shown to exert an effect on the catalytic reaction with a range of nitrogen-based bidentate and tridentate ligands emerging as ligand frames that actively participate and enhance the catalysis (Figure 4.1).[6,8,9]

**Figure 4.1:** Some examples of functionalised complexes which promote catalytic transfer hydrogenation

In 2013 Cameron and Szymczak reported the bifunctional complex, [(6,6'-dihydroxy-terpyridine)Ru(PPh_3)_3][PF_6]_2, that could undergo processes involving aromatization-dearomatization and more importantly showed that these processes could be beneficial in a variety of hydrogenation reactions. The general mechanism involves the

tautomerization of the 6,6'-dihydroxy-terpyridine and provides accessible proton acceptors and donors in the coordination sphere of the metal centre (Figure 4.2).[10] Moreover, they demonstrated the proton responsiveness of the 6,6'-dihydroxy-terpyridine ligand framework in this type of catalytic application leading to TOF's of up to 82 h^{-1} for the hydrogenation of acetophenone.
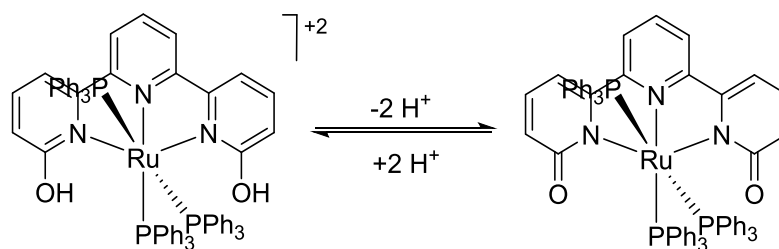
Figure 4.2: 6,6'-Dihydroxyterpyridine as a proton-responsive ligand on ruthenium

The same group later reported differences in the catalytic activity between the OH-substituted terpyridine-ruthenium complex, [(6,6'-dihydroxy-terpyridine)RuCl(CO)(PPh$_3$)]$^+$ and its unsubstituted counterpart, [(terpyridine)RuCl(CO)(PPh$_3$)]$^+$. In particular, they found that [(6,6'-dihydroxy-terpyridine)RuCl(CO)(PPh$_3$)]$^+$ significantly increased the catalytic activity for transfer hydrogenation with TON's up to 163 as compared 17 for the non-functionalised terpyridine derivative (Figure 4.3).[11] This result further highlights the importance of the OH group in this type of catalysis, likely due to its ability to modulate the electronic properties of the metal catalyst through proton dissociation and association.

Increasing activity and selectivity for transfer hydrogenation
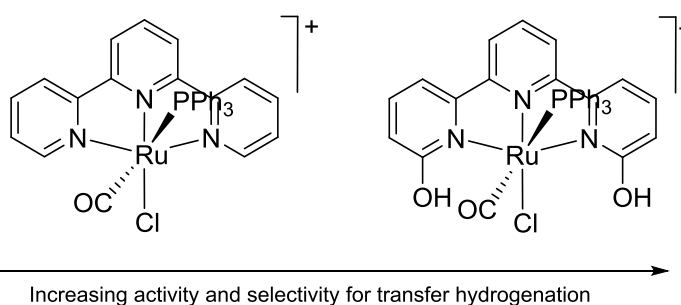
Figure 4.3: Relative transfer hydrogenation capacity of a terpyridine-ruthenium complex and its OH-substituted counterpart

Recently, Hou and Chen developed the ruthenium pincer complex, [6-([2,2'-bipyridin]-6-ylmethyl)pyridine-2-ol]RuCl$_2$(PPh$_3$), containing an OH-functionalised tri-pyridine

ligand (Figure 4.4).[12] This complex in comparison to [(6,6'-dihydroxy-terpyridine)Ru(PPh$_3$)$_2$Cl][PF$_6$] has a higher catalytic activity in transfer hydrogenation of ketones with TOFs up to 1.16×10^3 reported.

27
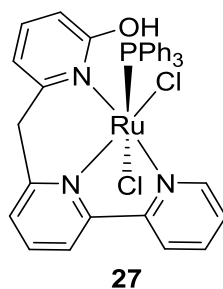
Figure 4.4: [6-([2,2'-bipyridin]-6-ylmethyl)pyridine-2-ol]RuCl$_2$(PPh$_3$)

In addition, Himeda and co-workers examined a series of iridium complexes bearing hydroxyl-substituted pyridylimidazoles in CO$_2$ hydrogenation and compared these with their unsubstituted pyridylimidaze counterpart (Figure 4.5). They found that the 6-OH-, 4-OH- and the 4,6-(OH)$_2$-substituted complexes showed higher activity (TOF up to 2600 h^{-1}) than the unsubstituted derivative (TOF 4 h^{-1}).[13]

R = 6-OH
R = 4-OH
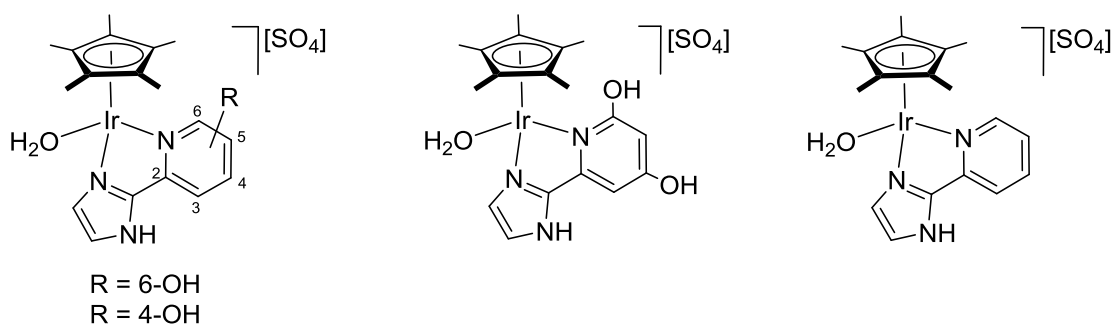
Figure 4.5: OH-substituted pyridylimidazoline-iridium complexes and their unsubstituted analogue

4.2.3 Aims and objectives

The NNN-ruthenium(II) complexes, **HL1**$_a$RuCl$_2$(PPh$_3$) (**41**), **HL1**$_b$RuCl$_2$(PPh$_3$) (**42**) and **HL1**$_c$RuCl$_2$(PPh$_3$) (**43**) bearing pyridone-substituted pyridyl-imine ligands described in Chapter 2 will be tested as catalysts for the transfer hydrogenation of various ketones and aldehydes incorporating different electronic and steric properties (Figure 4.6). The complexes themselves differ in the electronic or steric properties of the N-aryl group which may impact on the catalytic performance. In addition, these systems have different solubility characteristics which may be an important factor when considering the solvent used to conduct the reactions. To explore the effect of the pendant OH group on the transfer hydrogenation, unsubstituted **L1**$_H$RuCl$_2$(PPh$_3$) (**44**) will also be evaluated (Figure 4.6). It is envisaged that the complexes containing pendant OH groups (**41-43**) will be beneficial to the transfer hydrogenation as they will provide a means to accept and donate protons during the transformation. Moreover to explore the importance of the metal centre, palladium complexes, [**HL1**$_a$PdNCMe][PF$_6$]$_2$ (**45**) and [**HL2**$_a$Pd(NCMe)$_2$][PF$_6$]$_2$ (**46**), will be additionally tested as catalysts for the transfer hydrogenation.
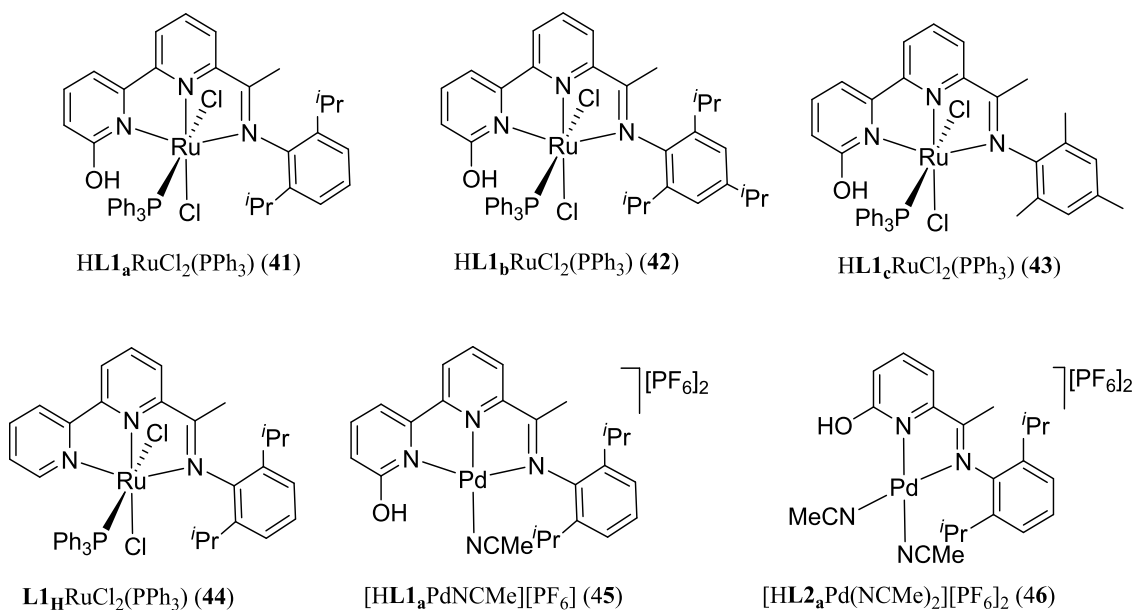
Figure 4.6: Complexes, **41-46**, to be tested as catalysts for transfer hydrogenation
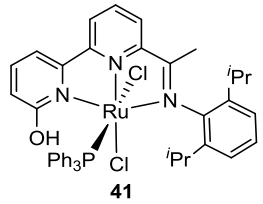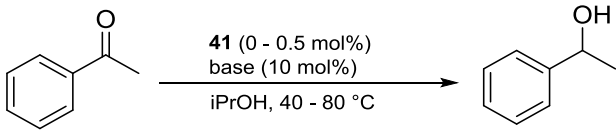
4.2.4 Results and discussion

To investigate the performance of ruthenium complexes **41 – 44** (Figure 4.6) as catalysts in transfer hydrogenation, the transformation of acetophenone to 1-phenylethanol was used as the test reaction. Typically, the reactions were performed under nitrogen in an alcohol in the presence of base at elevated temperature over reaction times up to 18 hours. To allow an optimisation of the reaction conditions, **41** was selected as the test catalyst and variations in loading, type of base, reaction duration, reaction temperature and type of solvent were all explored (entries 1-16, Table 4.1).

Firstly, the effect of catalyst loading of **41** on conversion was studied with KO^{t}Bu as the base (10 mol%), the temperature set at 80 ^{o}C, isopropanol as the solvent and the run time at 18 hours (entries 1-5, Table 4.1). It was shown that on increasing the amount of catalyst from 0.05 to 0.5 mol%, quantitative conversion could only be achieved with 0.5 mol% of **41** (entry 5, Table 4.1). With the conditions otherwise the same, but with methanol as the solvent and 0.5 mol% loading of **41**, only 3% conversion could be obtained (entry 6, Table 4.1).

Secondly, with the loading of **41** fixed at 0.5 mol%, three additional types of base, namely KOH, NaOH and K$_2$CO$_3$ (all at 10 mol%), were explored with isopropanol as solvent and the temperature at 80 ^{o}C (entries 7-9, Table 4.1). While KOH and NaOH resulted in 99% conversion, K$_2$CO$_3$ gave a lower conversion of 71% (entry 9, Table 4.1).

Thirdly, the effect of temperature was probed using **41** (0.5 mol%), base (KO^{t}Bu, KOH, NaOH: 10 mol%), isopropanol as solvent and the run time at 18 hours (entries 10-12, Table 4.1). At 40 ^{o}C, KO^{t}Bu proved the superior base with a conversion of 34% compared with 9 and 17% for KOH and NaOH, respectively. Moreover, at 80 ^{o}C, 100% conversion was achieved with KO^{t}Bu (entry 5, Table 4.1).

Fourthly, with the conditions fixed with **41** in 0.5 mol%, KO^{t}Bu (10 mol%) as base, isopropanol as solvent and the temperature at 80 ^{o}C, the effect of reaction time on the conversion was examined (entries 13 and 14, Table 4.1). After 4 hours 97% conversion could be obtained while after 6 hours 100% conversion was noted. It is worth highlighting that there was no reaction in the absence of the ruthenium catalyst (entry 15, Table 4.1) and also no reaction in the absence of base (entry 16, Table 4.1).

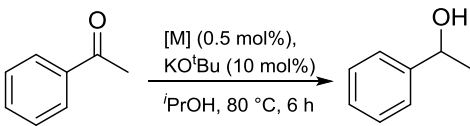**Table 4.1:** Optimizing the conditions for the transfer hydrogenation of acetophenone using **41**[a]

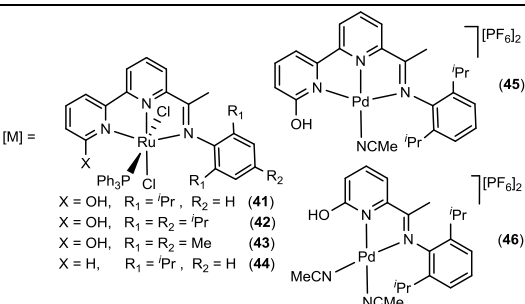| Entry	**41** (mol%)	Base (10 mol%)	Time (h)	Temp. (°C)	Solvent	Conv. (%)[b]
1	0.05	KO^{t}Bu	18	80	^{i}PrOH	17
2	0.1	KO^{t}Bu	18	80	^{i}PrOH	37
3	0.2	KO^{t}Bu	18	80	^{i}PrOH	60
4	0.3	KO^{t}Bu	18	80	^{i}PrOH	95
5	0.5	KO^{t}Bu	18	80	^{i}PrOH	100
6	0.5	KO^{t}Bu	18	80	MeOH	3
7	0.5	KOH	18	80	^{i}PrOH	99
8	0.5	NaOH	18	80	^{i}PrOH	99
9	0.5	K$_2$CO$_3$	18	80	^{i}PrOH	71
10	0.5	KO^{t}Bu	18	40	^{i}PrOH	34
11	0.5	KOH	18	40	^{i}PrOH	9
12	0.5	NaOH	18	40	^{i}PrOH	17
13	0.5	KO^{t}Bu	4	80	^{i}PrOH	97
14	0.5	KO^{t}Bu	6	80	^{i}PrOH	100
15	0	KO^{t}Bu	18	80	^{i}PrOH	0
16	0.5	no base	18	80	^{i}PrOH	0

[a] **General conditions: acetophenone (0.42 mmol), 41 (0-0.5 mol%), base (0-10 mol%), temperature (40 – 80 °C).**
[b] **The % conversion was calculated by integrating the CH$_3$ signal in acetophenone against the CH$_3$ signal in 1-phenylethanol in the ^{1}H NMR spectrum.**

On the basis of the results outlined above, the optimal conditions for the transfer hydrogenation for **41** were established as [Ru] (0.5 mol%), KO^{t}Bu (10 mol%), 80 °C, 6 hours with isopropanol as solvent. Hence, these conditions were employed to screen the other three ruthenium catalysts in the study, **41**, **43** and **44**, and in-turn to determine how the catalysts ranked in the terms of their catalytic activity (Table 4.2). For the sake of comparison, the palladium complexes **45** and **46** are also investigated under the optimised conditions

Table 4.2: Transfer hydrogenation of acetophenone using **1 – 6** as the catalysts[a]

Entry	Catalyst	Conversion (%)[b]
1	**41**	100%
2	**42**	98%
3	**43**	91%
4	**44**	83%
5	**45**	21%
6	**46**	19%

[a] **General conditions: acetophenone (0.42 mmol), catalyst (0.5 mol%), 80 ºC, KOᵗBu (10 mol%), 80 ºC**
[b] **The % conversion was calculated by integrating CH₃ signal in acetophenone against the CH₃ signal in 1-phenylethanol in the ¹H NMR spectrum**

According to the results in Table 4.2, the order of catalytic activity (in terms of percentage conversion) falls in the order: **41** (100%) > **42** (98%) > **43** (91%) > **44** (83%) > **45** (21%) ~ **46** (19%). Several points emerge form inspection of the results. Firstly the ruthenium catalysts (**41-44**) are superior to the palladium catalysts (**45**, **46**) for the transfer hydrogenation of acetophenone. Secondly, the ruthenium catalysts show some differences in performance with **41** proving the most active catalyst while dipyridylimine-containing **44** the least active. It would seem the absence of an OH group in **44** is impeding its performance in the transfer hydrogenation. On the other hand, the presence of an OH group in **41 – 43** is having an enhancing effect on the catalysis. One explanation behind these observations may be due to the capacity of **41** - **43** to undergo aromatization/dearomatization processes. To be precise, the hydroxyl group of the exterior pyridine donor will be deprotonated under basic conditions to form an anionic pyridonate. This dearomatised heterocycle can then act as an intramolecular base to abstract protons from the substrate. To explain the differences in performance between **41**, **42** and **43**, it would seem steric, electronic and solubility variations are important. In terms of electronic properties, the more electron donating para-substituents in **42** and **43** (ᶦPr, Me) could lead to an increase in the electron density on the metal centre and hence slow down substrate coordination (see later for a proposed mechanism).

Based on the superior performance of **41** in the transfer hydrogenation of acetophenone, we then explored its activity for the transfer hydrogenation of a variety of aryl ketones and aldehydes differing in their steric and electronic properties (entries 1 - 6, Table 4.3). All the substrates could be hydrogenated with the highest conversions being obtained with acetophenone, 4-bromoacetophenone and benzaldehyde (entries 1, 3 and 5, Table 4.3). With substrates containing electron donating groups such as 4-methoxyacetophenone and 4-methylacetophenone lower conversions were achieved (entries 2 and 4, Table 4.3); similar trends have been noted in the literature.[10,12] On the other hand, use of the more sterically hindered benzophenone gave the lowest conversion of 50% with a TOF of 15.9 h^{-1}.

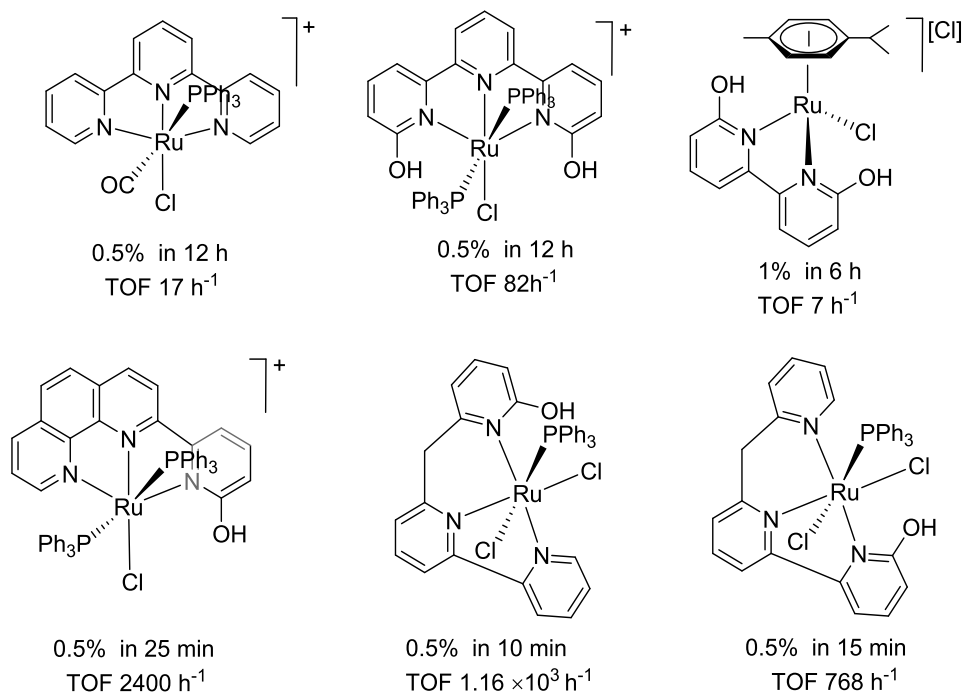**Table 4.3:** Transfer hydrogenation of ketones and aldehydes catalysed by 41[a]

41 (0.5 mol%), KO^{t}Bu (10 mol%), ^{i}PrOH, 80 °C, 6 h

Entry	Substrate (ketone/ aldehyde)	Product (alcohol)	Conv. (%)[b]	TON	TOF (h^{-1})	Yield (%)[c]
1			100%	200	33.3	98%
2			90%	175.6	29.3	87%
3			100%	198	33	98%
4			93%	165.9	26.7	82%
5			99%	192.7	32.1	95%
6			50%	95.1	15.9	48%

[a] General conditions: aldehyde/ketone (0.83 mmol), 1 (0.5 mol%), KO^{t}Bu (10 mol%), 80 °C, isopropanol (10 ml).
[b] The % conversion was calculated by integrating the ratio of keton to alcohol product in the ^{1}H NMR spectrum.
**[c]** Isolated yield.

From the literature review presented in Chapters 1 and 4, a number of NNN-pincer ruthenium complexes have showed high catalytic activity in transfer hydrogenation of acetophenone with TOF's in the range 7 to 2.4×10^4 h^{-1} (Figure 4.7).[10,11,12,14] It would appear the catalytic performance of **41** falls in the middle of this range.

0.5% in 12 h
TOF 17 h^{-1}

0.5% in 12 h
TOF 82h^{-1}

1% in 6 h
TOF 7 h^{-1}

0.5% in 25 min
TOF 2400 h^{-1}

0.5% in 10 min
TOF 1.16×10^3 h^{-1}

0.5% in 15 min
TOF 768 h^{-1}

Figure 4.7: Comparison of TOFs for a selection of NNN and NN symmetrical and unsymmetrical ruthenium complexes

With regard to the reaction mechanism, we propose a catalytic cycle which is related to that described by Fujita and Yamaguchi *et al.* (Scheme 4.3).[15] In the first step, reaction of **41** with KO^{t}Bu results in deprotonation, salt elimination and the formation of intermediate **A** containing a vacant coordination site. Dearomatized **A** then reacts with the solvent (^{i}PrOH) to form re-aromatized **B** bearing an isopropoxide ligand. β-H elimination can then occur to give hydride containing **C** (Ru-H) and acetone. Coordination/insertion of the carbonyl substrate (R$_1$C(O)R$_2$) affords R$_1$CH(O)R$_2$-containing **D** which then undergoes elimination of the alcohol R$_1$CH(OH)R$_2$ and re-generation of **A**.
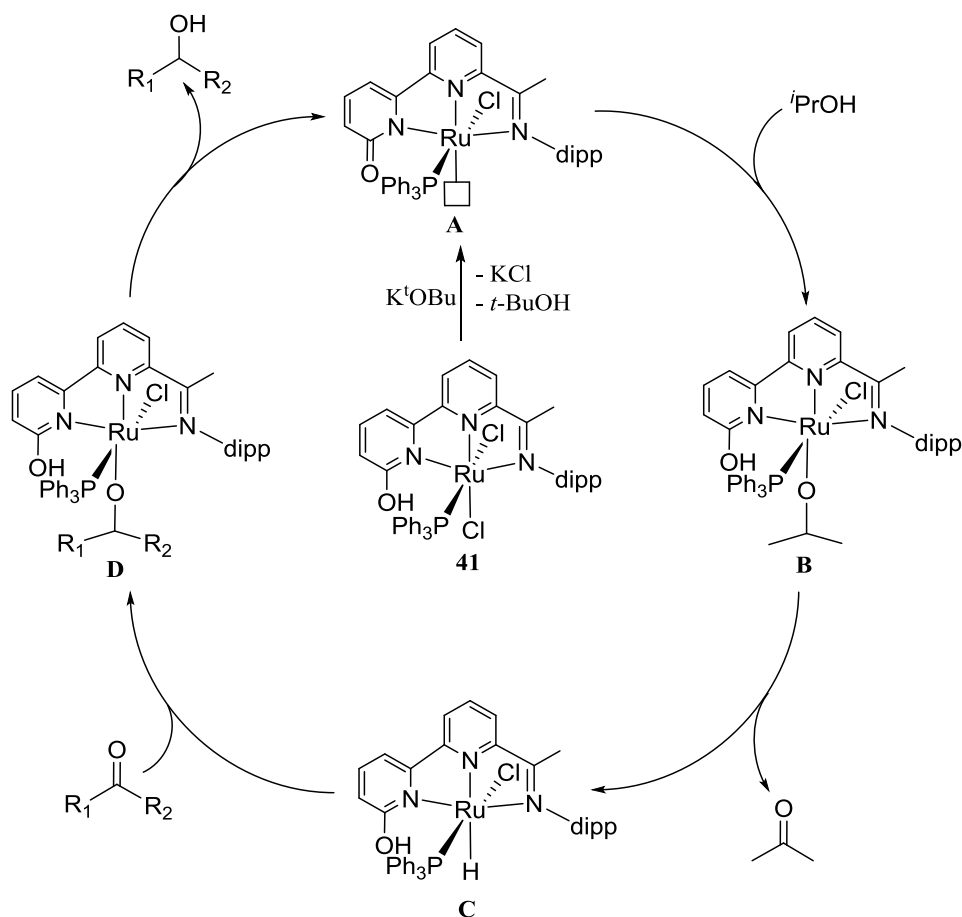
Scheme 4.3: Proposed catalytic cycle for the transfer hydrogenation of $R_1C(O)R_2$;

dipp = 2,6- diisopropylphenyl

4.2.5 Conclusions

The catalytic activity of the ruthenium(II) complexes, **41-44**, bearing either pyridone-substituted pyridyl-imines (**41-43**) or dipyridylimine (**44**) have been explored in transfer hydrogenation of carbonyl compounds (*e.g.*, ketones and aldehydes) using isopropanol as the solvent. A selection of bases have been evaluated and K^{t}OBu proved the most compatible. Similarly, the temperature of the reaction has been examined and 80 ^{o}C shown to be the most suitable. Using the optimised conditions established, the order of activity for the OH-functionalised complexes for the transfer hydrogenation of acetophenone was found to be **41** > **42** > **43**. By contrast, **44** showed lower catalytic activity which can be attributed to the absence of a functional OH group in the catalyst. Consequently, a mechanism for the transfer hydrogenation has been proposed involving aromatization-dearomatization via protonation/deprotonation of the pendant OH group. Moreover, **41** exhibits moderate catalyst efficiently for the transfer hydrogenation of a

variety of ketones and aldehydes in the presence of K^{t}OBu and isopropanol as the solvent. Their conversions have been correlated with the electronic and steric properties of the substrates and indicate electron withdrawing groups gave higher conversions while more sterically hindered ones gave lower conversions. By contrast, the palladium catalysts [H**L1**$_a$PdNCMe][PF$_6$]$_2$ (**45**) and [H**L2**$_a$Pd(NCMe)$_2$][PF$_6$]$_2$ (**46**) showed poor activity with no more than 20% conversion. In future, we would like to explore the ability of **41-43** as catalysts for the transfer hydrogenation of other types of unsaturated compound.

4.3.1 Ethylene oligomerisation and polymerisation

The oligo-/polymerisation of ethylene is one of the most important industrial processes. With particular regard to oligomerisation, the materials so-formed have considerable value as they have applications in various fields, such as feedstocks for detergents, lubricants, plasticizers, and oil field chemicals as well as monomers for copolymers of ethylene and α-olefins.
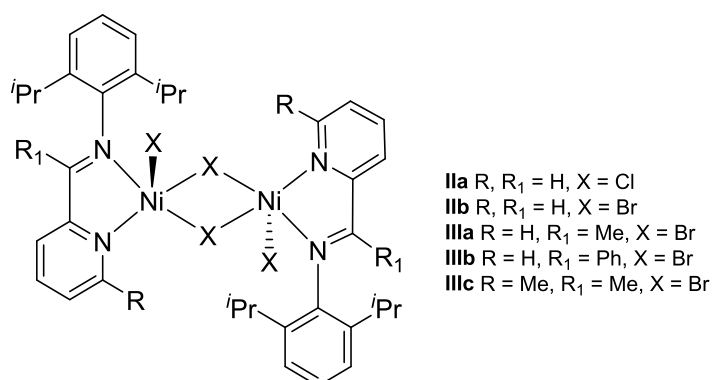
In the past decade, nickel complexes have received widespread attention as catalysts in both ethylene oligomerisation and polymerisation.[16] A wide variety of nickel complexes bearing an assortment of bidentate ligands such as NP,[17] NO,[18] PO,[19] NN[20] have been reported. In general, the NN-bidentate nickel(II) complexes are the most attractive due to their straightforward synthesis and better catalytic performances.[16,20h] Indeed NN α-diimine-M (Ni, Pd) catalysts, first disclosed by Brookhart *et al.* in the mid-1990s,[21,22] have inspired numerous reports with a view to developing more active and temperature stable systems. A number of important reviews have been published in the area.[23] Complexes **Ia** - **Ic** represent some of the early α-diimine examples of nickel pre-catalysts for ethylene polymerisation that, in the presence of methylaluminoxane (MAO), show activities as high as 1.1×10^7 g(PE) mol^{-1}(Ni) h^{-1} and TOF numbers up to 3.9×10^5 h^{-1} (Figure 4.8).
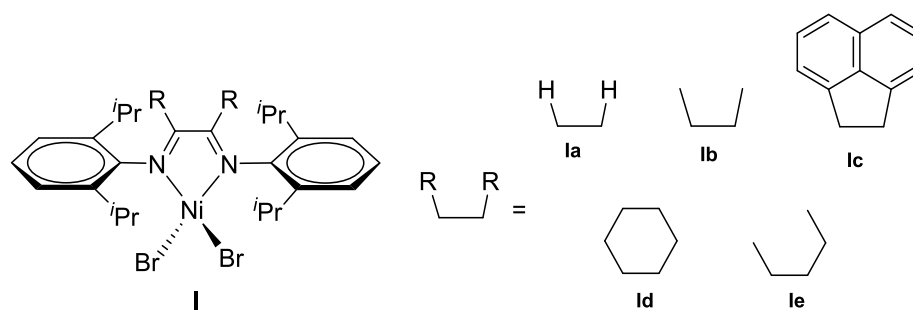
Figure 4.8: α-Diimine nickel(II) complexes **Ia** - **Ie**

More recent variations to the backbone of the α-diimine have seen the development of nickel complexes of the type **Id** and **Ie** (Figure 4.8), which have also shown high activities for ethylene polymerisation. In general, as the steric bulk of the ortho-substituents on the N-aryl groups increase, the molecular weights of the resultant polyethylene increase.[24,25]

Elsewhere, pyridylimine-nickel(II) complexes represent another class of α-diimine-nickel catalyst that have proved active for ethylene oligomerisation and in some cases polymerisation. The first examples of nickel pre-catalysts of this type, **IIa** and **IIb**, were reported by Laine *et al.* in 1999 which on treatment with MAO were found to be highly active for ethylene oligomerisation displaying activities up to 6.8×10^3 g mol^{-1} h^{-1} (Figure 4.9).[26a] The same group later reported catalysts **III** that were found to be active in oligomerisation and polymerisation of ethylene at 40 °C with activities up to 3.1×10^3 g mol^{-1} h^{-1} (Figure 4.9).[26b]

IIa R, R$_1$ = H, X = Cl
IIb R, R$_1$ = H, X = Br
IIIa R = H, R$_1$ = Me, X = Br
IIIb R = H, R$_1$ = Ph, X = Br
IIIc R = Me, R$_1$ = Me, X = Br

Figure 4.9: Pyridylimine-Ni(II) complexes **II** and **III**

Jing and Yi reported two pyridylimine-nickel complexes **IV** (Figure 4.10),[27] that in the presence of MAO or Et$_2$AlCl, are catalysts for ethylene oligomerisation with activities as high as 41×10^3 g mol^{-1} h^{-1}. However, **IVb** and **IVd** containing methyl substituents on the

carbon neighbouring the N atom of the pyridine ring showed lower activity than observed with **IVa** and **IVc**.
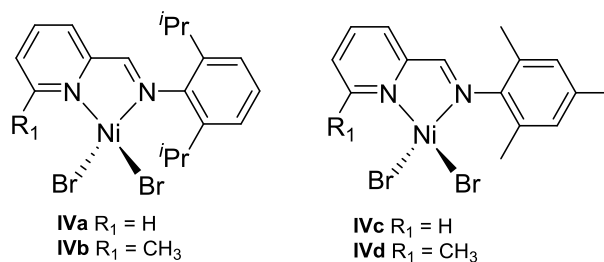
Figure 4.10: Pyridylimine-Ni(II) complexes **IV**

Complex **V** based on sterically hindered benzhydryl-containing pyridylimine ligands was reported by Sun *et al.* (Figure 4.11).[28] In the presence of either MAO or ethylaluminum sesquichloride (EASC) this complex has proved exceptionally productive in ethylene polymerisation with an activity of the order 10^7 g mol^{-1} h^{-1}. In 2012, pyridylimine-nickel(II) complex **VI** has been reported by the same group and when used with Et$_2$AlCl as co-catalyst showed high activity in ethylene oligomerisation at 80 °C (Figure 4.11).[29] In addition, Zhang *et al.* reported that **VII**,[30] on activation with (EASC), is a highly active catalyst for 1,3-butadiene polymerisation with selectivities up to 92% (Figure 4.11).
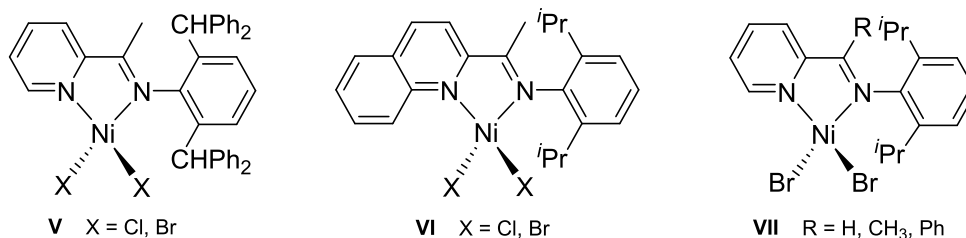
Figure 4.11: Pyridylimine-Ni(II) complexes **V**, **VI** and **VII**

More recently in 2016, Bryliakov and co-workers synthesised and tested iminopyridine-nickel(II) complexes **VIII** and **IX** bearing electron-withdrawing groups on the N-aryl unit (Figure 4.12).[31] They found that **VIII** and **IX** are highly active in the oligomerisation of ethylene (up to 9.6 $\times 10^6$ g mol^{-1}h^{-1}bar^{-1}) and in the polymerisation of ethylene (up to 6.6 $\times 10^6$ g mol^{-1}h^{-1}bar^{-1}).
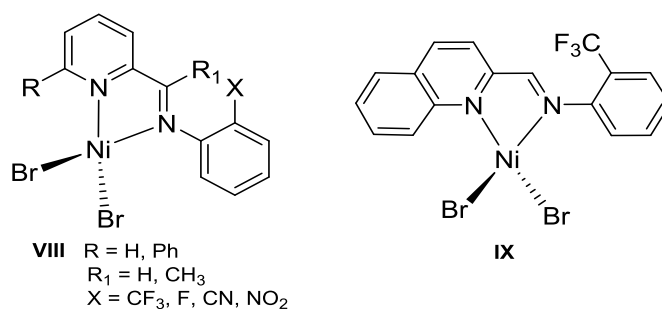
Figure 4.12: Pyridylimine-Ni(II) complexes **VIII** and **IX** bearing electron withdrawing substituents

4.3.2 Aims and Objectives

As can be seen from this brief review of the literature, NN-pyridylimines as ligands for nickel-based oligo-/polymerisation catalysts have been the subject of numerous reports. So far most emphasis has been placed on modifying the steric and electronic properties of the N-aryl groups, the substituents on the imino carbon and the 2-position of the pyridine unit. On the other hand, the introduction of a proton responsive OH group to the 4-position of the pyridine has not, to the knowledge of the author, been examined. In this section we explore the use of the NN-nickel(II) complexes, **HL3**$_a$**NiBr**$_2$ (**47**), **HL3**$_b$**NiBr**$_2$ (**48**), and **HL3**$_c$**NiBr**$_2$ (**49**), described in Chapter 3, as Ni(II) pre-catalysts for ethylene oligo-/polymerisation with a view to determining the effect of the 4-OH group on the catalytic performance (Figure 4.13).
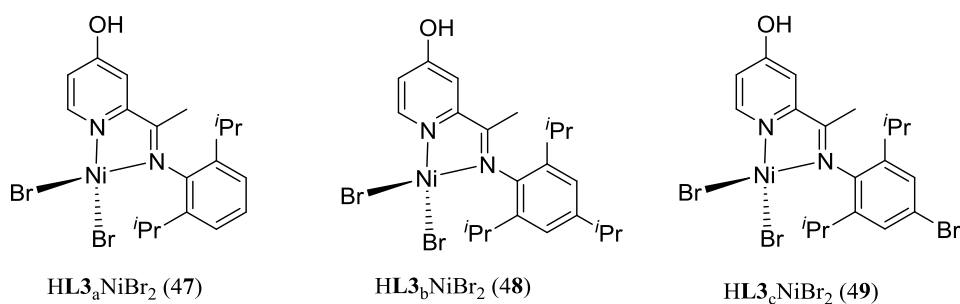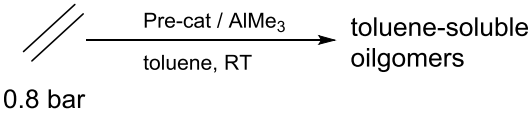

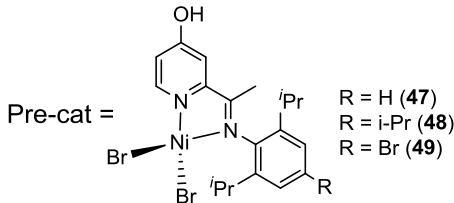**Figure 4.13**: Nickel(II) bromide pre-catalysts to be screened

4.3.3 Results and discussion

Complexes **47 - 49** have all been evaluated as pre-catalysts for oligo-/polymerisation of ethylene using trimethylaluminium (TMA) as the co-catalyst. Typically, the selected Ni(II) complex (0.01 mmol) was treated with either 2, 10 or 100 molar equivalents of TMA in toluene and ethylene gas (0.8 bar) introduced over 30 minutes at room temperature; the results are collected in Table 4.4. All the complexes were active catalysts affording toluene-soluble oligomeric waxes and no polymeric materials could be detected.

Table 4.4: Catalytic evaluation of **47-49** as pre-catalysts for ethylene polymerisation[a]
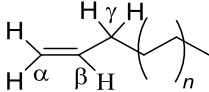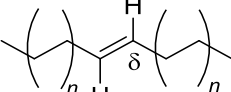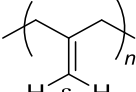
Entry	Pre-catalyst	AlMe$_3$/Ni	Mass of oligomer (g)[b]	Activity (g mmol^{-1}h^{-1}bar^{-1})
1	**47**	2	0.041	10
2	**48**	2	0.010	3
3	**49**	2	0.462	116
4	**47**	10	0.052	13
5	**48**	10	0.009	2
6	**49**	10	0.082	21
7	**47**	100	0.063	16
8	**48**	100	0.015	4
9	**49**	100	0.132	33

[a] *General conditions: pre-catalyst (0.01 mmol), 0.8 bar ethylene pressure, toluene, RT, 30 min.*
[b] *Isolated mass.*

With the amount of TMA set at two equivalents, **47-49** all gave low to good activities (3 – 116 g mmol^{-1}h^{-1}bar^{-1}) with para-bromo-containing **49** giving the highest productivity of 116 g mmol^{-1}h^{-1}bar^{-1} (entry 3, Table 4.4). The ^{1}H NMR spectrum of the oligomeric wax obtained using **49**/2TMA revealed the presence of a mixture of alkene-containing compounds including alpha-olefins and vinylidenes (Table 4.5); both **47**/2TMA and **48**/2TMA gave a similar mixture of hydrocarbons. With regard to relative amounts of these structural types **49**/2TMA gave 93% α-olefins and 7% vinylidenes (entry 3, Table 4.4). By contrast, **47**/2TMA (entry 1, Table 4.4) showed less selectivity for α-olefins with 81% evident.

Table 4.5: Oligomeric structures, relative integrations and chemical shifts (in ppm) of the materials obtained using **49**/2TMA[a]

α-olefin internal olefin vinylidene

Structural type	Int.	α (ppm)	Int.	β (ppm)	Int.	γ (ppm)	Int.	δ (ppm)	Int.	ε (ppm)
α-olefin	2H	4.7-5.1	1H	5.6-5.9	2H	2.05	-	-	-	-
Internal olefin	-	-	-	-	-	-	2H	5.40	-	-
Vinylidene	-	-	-	-	-	-	-	-	2H	4.6-4.7

[a] **Detected by ^{1}H NMR spectroscopy; recorded in CDCl₃ at room temperature**

Using ten equivalents of TMA, **49** again showed the higher activity but notably lower than that observed with two equivalents (entries 4-6, Table 4.4). Likewise using 100 equivalents of trimethylaluminium, **49** gave the highest catalytic activity but once again less than that seen with two equivalents (entries 7-9, Table 4.4). With respect to the runs performed with two molar equivalents of TMA, it is clear the nature of para-substituent of the N-aryl group of the pre-catalyst has a notable effect on catalytic activity with **49** > **47** > **48**. In particular, the electron withdrawing group (Br) is beneficial for catalytic activity.

It is uncertain as to the precise details of activation of the pre-catalyst but it would seem reasonable to assume the OH group is involved. Scheme 4.4 shows a proposed route involving firstly OH deprotonation an elimination of AlMe₂Br and methane. The second equivalent of TMA can then methylate the remaining bromide to generate the active catalyst and eliminate a further equivalent of AlMe₂Br. Coordination and insertion of the ethylene then follows during propagation before termination occurs by β-H elimination.
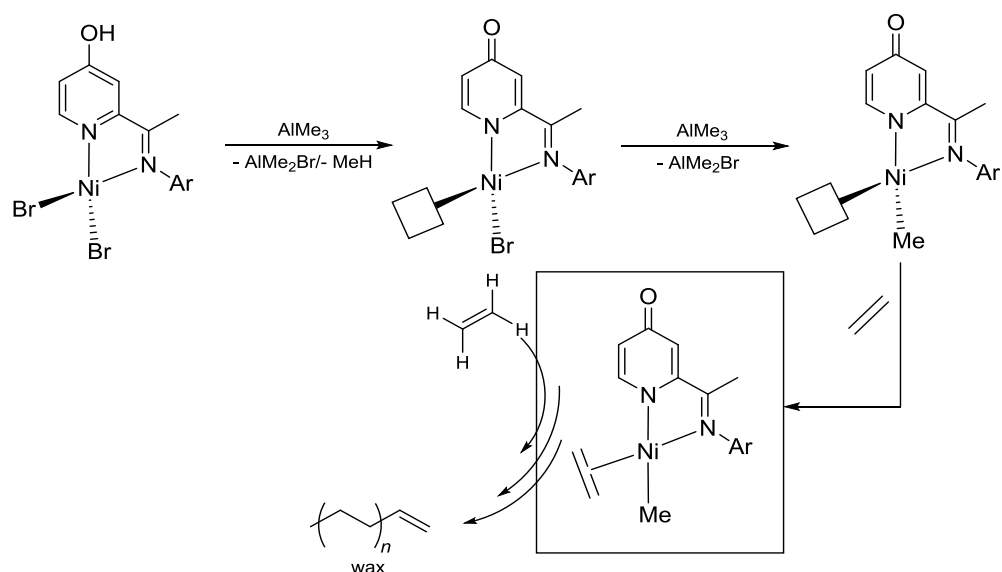
Scheme 4.4: Proposed activation of catalyst and propagation step; □ = vacant coordination site

4.3.4 Conclusions

The three nickel(II) complexes, **47-49**, bearing 4-hydroxy-6-iminopyridine bidentate ligands have all proved active catalysts for ethylene oligomerisation on treatment with trimethylaluminium forming mixtures of α-olefins and vinylidenes. Notably, bromide-containing **49** on activation with two equivalents of trimethylaluminium proved the most active system followed by **47** and then **48**, highlighting the importance of the ligand's electronic properties. We have proposed a mechanism for initiation of the catalyst that involves deprotonation of the OH group, bromide abstraction and methylation of the remaining nickel-bromide to form an active species of the type '[4-pyridinote-imine]NiMe', notably free of counterion. However, it is worth emphasising that the catalytic activity of these systems is an order of magnitude lower than that reported for [pyridylimine]NiX$_2$/MAO catalysts.[26b] Notably, nickel(II) complexes containing 2-hydroxy-6-iminopyridines (*i.e.*, (**HL2**$_{a-c}$)$_2$NiBr$_2$ developed in Chapter 3) have been previously tested by our group as pre-catalysts for ethylene oligomerisation/polymerisation have been found to exhibit much lower catalytic activity.[32]

References

1. M. J. Palmer and M. Wills, *Tetrahedron: Asymmetry*, 1999, **10**, 2045.

2. R. Noyori and S. Hashiguchi, *Acc. Chem. Res.*, 1997, **30**, 97.

3. P. S.Hallman, D. Evans, J. A. Osborn and G. Wilkinson, *Chem. Commun.*, 1967, **197**, 305.

4. D. N. Lawson, J. A. Osborn and G. Wilkinson, *J. Chem. Soc. A.,* 1966, 1733.

5. J. T. Mague and G. Wilkinson, *J. Chem. Soc. A.,* 1966, 1736.

6. J. Ito and H. Nishiyama, *Tetrahedron Lett.,* 2014, **55**, 3133.

7. R. Noyori, M. Yamakawa and S. Hashiguchi, *J. Org. Chem.*, 2001, **66**, 7931.

8. G. Zeng, S. Sakaki, K. Fujita, H. Sano and R. Yamaguchi, *ACS Catal.*, 2014, **4**, 1010.

9. W. Jin, L. Wang and Z. Yu, *Organometallics*, 2012, **31**, 5664.

10. C. M. Moor and N. K.Szymczak, *Chem. Commun.*, 2013, **49**, 400.

11. C. M. Moor, B. Bark and N. K. Szymczak, *ACS Catal.,* 2016, **6**, 1981.

12. J. Shi, B. Hu, D. Gong, S. Shang, G. Hou and D. Chen, *Dalton Trans*., 2016, **45**, 4828.

13. (a) L. Wang, N. Onishi, K. Murata, T. Hirose, J. T. Muckerman, E. Fujita and Y. Himeda, *ChemSusChem.,* 2017, **10**, 1071. (b) S. Xu, N. Onishi, A. Taurusaki, Y. Manaka, W-H. Wang, J. T. Muckerman, E. Fujita and Y. Himeda, *Eur. J. Inorg. Chem.,* 2015, 5591.

14. (a) B. Paul, K. Chahrabarti and S. Kundu, *Dalton Trans.,* 2016, **45**, 11162. (b) J. Shi, B. Hu, S. Shang, D. Deng, Y. Sun, W. Shi, X. Yang, X. Chen and D. Chen, *ACS Omega*, 2017, **2**, 3406. (c) I. Nieto, M. S. Livings, J. B. Sacci, L. E. Reuther, M. Zeller and E. T. Papish, *Organometallics,* 2011, **30**, 6339.

15. T. Yoshida, Y. Imori, R. Yamaguchi and K. Fujita, *Org. Lett.,* 2011, **13**, 2278.

16. J. Yu, X. Hu, Y. Zeng, L. Zhang, X. Hao, C. Ni and W-H. Sun, *New J. Chem.,* 2011, **35**, 178.

17. (a) W. J. Marshall and Z. Guan, *Organometallics*, 2002, **21**, 3580. (b) L. Saussine, R. Welter, F. Speiser and P. Braunstein, *Organometallics*, 2004, **23**, 2613. (c) Z. Weng, S. Teo and T. S. A. Hor, *Organometallics*, 2006, **25**, 4878.

18. (a) T. R. Younkin, E. F. Connor, J. I. Henderson, S. K. Friedrich, D. A. Bansleben and R. H. Grubbs, *Science*, 2000, **287**, 460. (b) D.-P. Song, J.-Q. Wu, W.-P. Ye, H.-L. Mu and Y.-S. Li, *Organometallics*, 2010, **29**, 2306. (c) D.-P. Song, W.-P. Ye, Y.-X. Wang, J.-Y. Liu and Y.-S. Li, *Organometallics*, 2009, **28**, 5697.

19. (a) N. Peulecke, M. Kohler, M. He, W. Keim and J. Heinicke, *J. Organomet. Chem.,* 2005, **690**, 2449. (b) M. Stefan, *Angew. Chem. Int. Ed.,* 2001, **40**, 534.

20. (a) C. M. Killian, D. J. Tempel, L. K. Johnson and M. Brookhart, *J. Am. Chem. Soc.,* 1996, **118**, 11664. (b) S. A. Svejda and M. Brookhart, *Organometallics,* 1999, **18**, 65. (c) P. Hao, S. Zhang, Q. Shi, S. Adewuyi, X. Lu, P. Li and W.-H. Sun, *Organometallics,* 2007, **26**, 2439. (d) J. D. Azoulay, Y. Schneider, G. B. Galland and G.C. Bazan, *Chem. Commun.,* 2009, **41**, 6177. (e) D. H. Camacho and Z. Guan, *Chem. Commun.,* 2010, **46**, 7879. (f) S. Song, T. Xiao, T. Liang, F. Wang, C. Redshaw and W-H. Sun, *Catal. Sci. Technol.,* 2011, **1**, 69. (g) H. Liu, W. Zhao, X. Hao, W. Huang, C. Redshaw and W.-H. Sun, *Organometallics,* 2011, **30**, 2418. (h) S. Song, Y. Li, F. Wang, C. Redshaw and W.-H. Sun, *J. Organomet. Chem.,* 2012, **699**, 18.

21. B. L. Small and M. Brookhart, *J. Am. Chem. Soc*. 1998, **120**, 7143.

22. L. K. Johnson, C. M. Killian and M. Brookhart, *J. Am. Chem. Soc.,* 1995, **117**, 6414.

23. (a) V. C. Gibson and S. K. Spitzmesser, *Chem. Rev.,* 2003, **103**, 283. (b) L. Saussine, F. Speiser and P. Braunstein, *Acc. Chem. Res.,* 2005, **38**, 784. (c) V. C. Gibson, C. Redshaw and G. A. Solan, *Chem. Rev.,* 2007, **107**, 1745. (d) G. Giambastiani, L. Luconi, A. Meli and C. Bianchini, *Coord. Chem. Rev.,* 2010, **254**, 431.

24. D. P. Gates, S. A. Svejda, E. Onate, C. M. Killian, L. K. Johnson, P. S. White and M. Brookhart, *Macromolecules*, 2000, **33**, 2320.

25. Z. Wang, Q. Liu, G. A. Solan and W-H. Sun, *Coord. Chem. Rev.,* 2017, **350**, 68.

26. (a) K. Lappalainen, J. Liimatta, E. Aitola, B. Lofgren, M. Leskela and T. V. Laine, *Macromol. Rapid Commun.,* 1999, **20**, 487. (b) U. Piironen, K. Lappalainen, M. Klinga, E. Aitola, M. Leskela and T. V. Laine, *J. Organomet. Chem.,* 2000, **606**, 118.

27. X. Huang, W. Zhang, X. Hong, Z. Jing and J. Yi, *J. Nat. Gas. Chem.,* 2003, **12**, 98.

28. S. Song, B. Li, X. Hao, Y-S. Li, F. Wang, C. Redshaw and W.-H. Sun, *Dalton Trans.,* 2012, **41**, 11999.

29. S. Song, T. Xiao, L. Wang, F. Wang, C. Redshaw and W.-H. Sun, *J. Organomet. Chem.,* 2012, **699**, 18.

30. Q. Dai, X. Jia, F. Yang, C. Bai, Y. Hu and X. Zhang, *Polymer,* 2016, **8**, 12.

31. A. A. Antonov, N. V. Semikolenova, E. P. Talsi, M. A. Matsko, V. A. Zakharov and K. P. Bryliakov, *J. Organomet. Chem.,* 2016, **822**, 241.

32. M. H. Alhalafi, M. Urbonaite and G. A. Solan, 2015, Unpublished work.

Chapter Five

Experimental Section

5.1 General

All reactions were carried out using standard Schlenk conditions under an atmosphere of nitrogen. All solvents, diethyl ether, toluene, acetonitrile and methanol were dried using appropriate drying agents and distilled prior to use under nitrogen and collected by a degassed syringe. All NMR spectroscopic data (^{1}H, ^{13}C, ^{31}P, ^{19}F) were recorded on Bruker DPX 300 MHz, 400 MHz and 500 MHz using $CDCl_3$, CD_2Cl_2, CD_3CN and CD_3OD as solvent. Chemical shifts (ppm) are referred to the residual protic solvents peaks and coupling constants are expressed in hertz (Hz). Electrospray ionization mass spectrometry (ESIMS) data were obtained on a Micromass Quattra LC mass spectrometer using MeOH or MeCN as a solvent. High-resolution FAB (fast atom bombardment) mass spectra were recorded using a Kratos Concept spectrometer with NBA (3-nitrobenzyl alcohol) as a matrix; TOF mass spectra were recorded on a Kratos Concept spectrometer with NBA. Infra-Red (IR) data were recorded using Perkin Elmer Spectrum One instrument in the solid state. Elemental analyses were performed at the Science Technical Support Unit, London Metropolitan University. Melting points (Mp) were measured on a Gallenkamp melting point apparatus (model MFB-595) in open capillary tubes.

The reagents, 2,6-dibromopyridine, N,N-dimethylacetamide (DMA), *n*-butyl-lithium (1.6 M in hexane), palladium(II) acetate, 2,6-diisopropylaniline, 2,4,6-trimethylaniline, potassium hexafluorophosphate, silver hexafluorophosphate, silver trifluoromethanesulfonate, silver oxide, nickel(II) dibromide 1,2-dimethoxyethane ((DME)NiBr$_2$), trimethylaluminium solution (2 M in toluene) and dichlorotris(triphenylphosphine)ruthenium(II) were purchased from Sigma Aldrich and used without any purification. Tributyltin chloride was distilled under reduced pressure. 2,4,6-trisopropylaniline,[1a] 2,6-diisopropyl-4-bromoaniline,[1a] bis (acetonitrile) palladium(II) chloride,[1b] bis(dimethylsulfoxide) platinum(II) chloride[1b] and tetrakistriphenylphosphine palladium(0)[1c] were previously prepared by the research group using literature routes.[1]

5.2 Experimental procedures for Chapter 2

5.2.1 Synthesis of 2-bromo-6-methoxypyridine
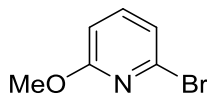
A 100 ml three necked around-bottom flask, equipped with stir bar and a reflux condenser, was evacuated and backfilled with nitrogen. The flask was charged with dry methanol (14 ml) and small pieces of sodium metal (1.33 g, 58.00 mmol). Once the majority of sodium had reacted, 2,6-dibromopyridine (8.00 g, 34.00 mmol) was added followed by more methanol (22 ml). The resulting mixture was stirred and heated to reflux for 24 h. After cooling to room temperature, cold aqueous 5% $NaHCO_3$ (25 ml) was added and the mixture extracted with diethyl ether (3×100 ml). The organic layers were washed with brine (1×30 ml), dried over $MgSO_4$ and concentrated under reduced pressure to give the title compound as a yellow oil (5.51 g, 86%). **^{1}H NMR (400 MHz; CDCl$_3$):** δ 7.40 (1 H, t, $^3J_{HH}$ = 8.0 Hz, Py-H), 7.04 (1H, d, $^3J_{HH}$ = 7.8 Hz, Py-H), 6.67 (1H, d, $^3J_{HH}$ = 8.0 Hz, Py-H), 3.92 (3H, s, OCH$_3$).

The ^{1}H NMR data is consistent with that described by Snieckus *et al.*[2]

5.2.2 Synthesis of 2-bromo-6-acetyl-pyridine [**II**]
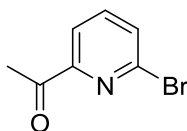
A one litre three necked round-bottom flask, equipped with stir bar and dropping funnel, was evacuated and backfilled with nitrogen. The flask was charged with dry diethyl ether (300 ml), 2,6-dibromopyridine (25.00 g, 105.5 mmol). The mixture was cooled to -78 °C and *n*-BuLi (66 ml, 105.53 mmol, 1.6 M in hexanes) added dropwise over 30 min. The solution was warmed to -40 °C for 15 min and then re-cooled to -78 °C and N,N-dimethylacetamide (10.8 ml, 116.08 mmol, 1.1 eq) introduced. The solution was stirred under an atmosphere of nitrogen for 1 h at -78 °C, then 2 h at -40 °C. The reaction was quenched by the addition of saturated aqueous ammonium chloride solution (100 ml) and stirred overnight at room temperature. The aqueous layer was separated and washed with diethyl ether (2×100 ml). The combined organic extracts were dried over magnesium sulphate, the solvent removed by rotary evaporation and then hexane added until the solution became cloudy. The suspension was placed in the freezer overnight, then filtered to give 2-bromo-6-acetylpyridine as a yellow solid (18.00 g, 88%). **^{1}H NMR (400 MHz;**

CDCl₃): δ 7.90 (1H, dd, $^3J_{HH}$ = 7.2 Hz, $^4J_{HH}$ = 1.2 Hz, Py-H), 7.57-7.64 (2H, m, Py-H), 2.62 (3H, s, CH₃).

The ^{1}H NMR data is consistent with that described by Parks *et al.*[3]

5.2.3 Synthesis of 2-bromo-6-(2-methyl-1, 3-dioxolan-2-yl)-pyridine [III]
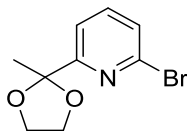
A one litre three necked round-bottom flask, equipped with stir bar and Dean-stark apparatus, was charged with 2-bromo-6-acetylpyridine (34.50 g, 172.48 mmol), 1,2-ethanediol (12.80 g, 206.45 mmol, 1.2 eq.), *p*-toluenesulfonic acid (3.43 g, 19.80 mmol, 0.11 eq.) and benzene (390 ml). The mixture was stirred and heated under reflux for 48 h, after which it was cooled to room temperature, aqueous sodium hydroxide solution added (70 ml, 0.5 M) and then extracted with toluene (3 x 70 ml). The combined organic extracts were washed with aqueous sodium hydroxide (3 x 70 ml, 0.5 M) and with water (2 x 70 ml). The organic phase was dried over magnesium sulphate and the solvent removed by rotary evaporation to give 6-bromo-2-(2-methyl-1,3-dioxolan-2-yl)pyridine as a black oil (39.84 g, 95%). **^{1}H NMR (400 MHz; CDCl₃):** δ 7.41-7.48 (2H, m, Py-H), 7.34 (1H, dd, $^3J_{HH}$ = 7.2 Hz, $^4J_{HH}$ = 1.2 Hz , Py-H), 4.04 (2H, m, CH₂), 3.78-3.85 (2H, m, CH₂), 1.65 (3H, s, CH₃).

The ^{1}H NMR data is consistent with that described by Parks *et al.*[3]

5.2.4 Synthesis of 2-(tributylstannyl)-6-(2-methyl-1, 3-dioxolan-2-yl)-pyridine [IV]
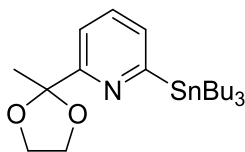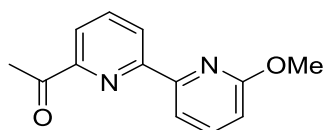

A one litre three necked round-bottom flask, equipped with stir bar, was evacuated and backfilled with nitrogen then charged with a solution of 6-bromo-2-(2-methyl-1,3-dioxolan-2-yl)pyridine (39.84 g, 163.35 mmol) and dry diethyl ether (350 ml) and cooled to -100 °C. *n*-BuLi (107.8 ml, 172.48 mmol, 1.05 eq.; 1.6 M in hexanes) was added dropwise over 30 min. The solution was stirred at -100 °C for 15 min, warmed to -78 °C for 30 min and then re-cooled to -100 °C before the addition of tributyltinchloride (50.5 ml, 186.22 mmol, 1.14 eq.). The solution was stirred for 1 h at -100 °C under an atmosphere of nitrogen then warmed to room temperature and stirred overnight. The

mixture was filtered through celite and the solvent removed by rotary evaporation to give 6-tributylstannyl-2-(2-methyl-1,3-dioxolan-2-yl)pyridine as a dark brown oil (56.90 g, 77%). **^{1}H NMR (400 MHz; CDCl$_3$):** δ 7.40 (1H, t, $^3J_{HH}$ = 7.6 Hz, Py-H), 7.21-7.29 (2H, m, Py-H), 4.00-4.04 (2H, m, CH$_2$), 3.86-3.91 (2H, m, CH$_2$), 1.71 (3H, s, CH$_3$), 1.49 (6H, m, CH$_2$), 1.25 (6H, sext, $^3J_{HH}$ = 7.3 Hz, CH$_2$), 1.02 (6H, dd, $^3J_{HH}$ = 8.0 Hz, $^4J_{HH}$ = 0.2 Hz, CH$_2$), 0.79 (9H, t, $^3J_{HH}$ = 7.4 Hz, CH$_3$).

The ^{1}H NMR data is consistent with that described by Solan et al.[4]

5.2.5 Synthesis of 1-(6'-methoxy-2, 2'-bipyridin-6-yl)-ethanone (**a**)

A 500 ml Schlenk flask, equipped with stir bar, was evacuated and backfilled with nitrogen then charged with dry toluene (120 ml) and degassed by three freeze-thaw pump cycles. 2-Bromo-6-methoxypyridine (2.0 g, 10.637 mmol), 6-tributylstannyl-2-(2-methyl-1,3-dioxolan-2-yl)pyridine (5.79 g, 12.762 mmol, 1.2 eq.) and tetrakistriphenylphosphine palladium(0) (0.49 g, 0.424 mmol, 0.04 eq.) were then added. The solution was stirred for 72 h at 100 °C under an atmosphere of nitrogen, after which the reaction mixture was cooled and the solvent removed under reduced pressure and 4M HCl (66 ml) added. The contents were then stirred overnight at 60 °C. The mixture was cooled to room temperature and carefully neutralised by adding a 2M aqueous solution of NaHCO$_3$. The mixture was extracted with chloroform (3 × 70 ml) and the organic layer washed with water (3 × 70 ml) and with brine (1 × 50 ml). The combined extracts were dried over magnesium sulphate and evaporated under reduced pressure. The crude product was recrystallized from methanol at -30 °C overnight and filtered to give 1-(6-methoxy-2,2-bipyridine-6-yl)ethanone (**a**) as a light brown solid (2.036 g, 83%). **Mp:** 117-119 °C. **^{1}H NMR (400 MHz; CDCl$_3$):** δ 8.60 (1H, dd, $^3J_{HH}$ = 7.8 Hz, $^4J_{HH}$ = 1.2 Hz, Py-H), 8.13 (1H, dd, $^3J_{HH}$ = 7.4 Hz, $^4J_{HH}$ = 0.7 Hz, Py-H), 8.02 (1H, dd, $^3J_{HH}$ = 7.7 Hz, $^4J_{HH}$ =1.2 Hz, Py-H), 7.93 (1H, t, $^3J_{HH}$ = 7.7 Hz, Py-H), 7.74 (1H, t, $^3J_{HH}$ = 7.8 Hz, Py-H), 6.82 (1H, dd, $^3J_{HH}$ = 8.2 Hz, $^4J_{HH}$ = 0.7 Hz, Py-H), 4.06 (3H, s, OCH$_3$), 2.82 (3H, s, CCH$_3$). **^{13}C NMR (100 MHz; CDCl$_3$):** δ 24.7 (OCH$_3$), 52.2 (CCH$_3$), 110.6 (CH), 112.6 (CH), 120.1 (CH), 123.1 (CH), 133.64 (CH), 138.4 (CH), 151.7 (C), 151.9 (C), 154.3 (C), 162.6 (C), 199.3 (C=O). **IR (cm^{-1}):** 1023 (medium, sharp), 1470 (medium, sharp), 1574 (medium, sharp, C=N (pyridine)), 1701 (medium, sharp, C=O). ESIMS: (+) m/z 229

[M+H]. ESIMS: (-) m/z 227 [M-H]. HRMS (FAB): calcd for $C_{13}H_{13}N_2O_2$ [M+H] 229.0977, found 229.0974.

5.2.6 Synthesis of 1-(6'-hydroxy-2, 2'-bipyridin-6-yl)-ethanone (**b**)
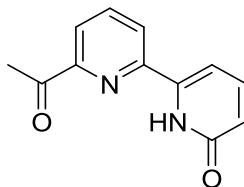
A 250 ml one necked round-bottomed flask, equipped with stir bar and reflux condenser, was charged with 1-(6-methoxy-2,2-bipyridine-6-yl)ethanone (1.12 g, 4.895 mmol) and 48% aqueous HBr (22 ml). The reaction mixture was stirred and heated to reflux for 4 h, after which it was cooled to room temperature and neutralised with a saturated aqueous NaHCO₃ solution. The mixture was extracted with dichloromethane (3 × 30 ml). The combined organic layers washed with water (1 × 40 ml) and dried over MgSO₄. The solvent was removed by rotary evaporation to give 1-(6-hydroxy-2,2-bipyridine-6-yl)ethanone (**b**) as a light yellow solid (1.03 g, 98%). **Mp**: 148-150 °C. **¹H NMR (400 MHz; CDCl₃):** δ 10.79 (1H, s, NH), 8.12 (1H, dd, $^3J_{HH}$ = 7.0 Hz, $^4J_{HH}$ = 1.8 Hz, Py-H), 8.01 (2H, m, Py-H), 7.52-7.60 (1H, m, Py-H), 6.89 (1H, d, $^3J_{HH}$ = 7.8 Hz, Py-H), 6.71 (1H, dd, $^3J_{HH}$ = 9.2 Hz, $^4J_{HH}$ = 0.8 Hz, Py-H), 2.81 (3H, s, CCH₃). **¹³C NMR (100 MHz; CDCl₃):** δ 26.0 (CH₃), 103.9 (CH), 122.5 (CH), 122.8 (CH), 123.2 (CH), 138.7 (CH), 140.6 (CH), 141.1 (C), 147.7 (C), 153.0 (C), 162.9 (C), 198.8 (C=O). **IR (cm⁻¹):** 1238 (medium, sharp), 1595 (medium, sharp, C=N (pyridine)), 1698 (medium, sharp, C=O), 3080 (weak, sharp). ESIMS: (+) *m/z* 215 [M+H]. ESIMS: (-) *m/z* 213 [M-H]. HRMS (FAB): calcd for $C_{12}H_{11}N_2O_2$ [M+H] 215.0821, found 215.0822.
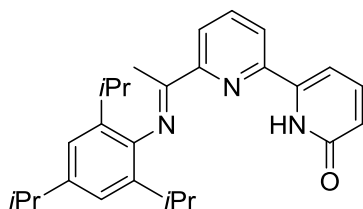
5.2.7 Synthesis of H**L1**ₐ
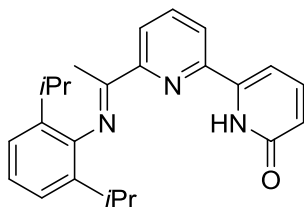
A 50 ml round-bottom flask, equipped with stir bar, was charged with 1-(6'-hydroxy-2,2'-bipyridin-6-yl) ethanone (0.50 g, 2.34 mmol), 2,6-diisopropylaniline (0.62 g, 3.50 mmol, 1.5 eq.) and dry toluene (10 ml). A Dean Stark apparatus with condenser was then attached to the flask. The reaction was stirred at reflux for approximately 30 min before

the addition of 2 drops of formic acid. The reaction mixture was left to stir at reflux for 3 days. After cooling to room temperature the solvent was removed by rotary evaporation. The resulting oil was recrystallized from methanol at -30 °C overnight and filtered to give H**L1$_a$** as a bright yellow solid (0.71 g, 80%). **Mp:** 190-192 °C. ^{1}**H NMR (400 MHz; CDCl$_3$):** δ 10.52 (1H, s, NH), 8.43 (1H, dd, $^3J_{HH}$ =7.2 Hz, $^4J_{HH}$ = 1.6 Hz, Py/Ar-H), 7.96 (2H, m, Py/Ar-H), 7.53 (1H, m, Py/Ar-H), 7.18 (2H, m, Ar-H), 7.12 (1H, m, Ar-H), 6.87 (1H, dd, $^3J_{HH}$ = 7.0 Hz, $^4J_{HH}$ = 0.7 Hz, Py/Ar-H), 6.66 (1H, dd, $^3J_{HH}$ = 9.0 Hz, $^4J_{HH}$ = 0.7 Hz, Py/Ar-H), 2.71 (2H, sept., $^3J_{HH}$ = 6.8 Hz, CH(CH$_3$)$_2$), 2.29 (3H, s, CH$_3$), 1.16 (12H, d, $^3J_{HH}$ = 6.2 Hz, (CH(CH$_3$)$_2$)$_2$). ^{13}**C NMR (100 MHz; CDCl$_3$):** δ 16.5 (CCH$_3$), 21.8 (CH(CH$_3$)$_2$), 22.2 (CH(CH$_3$)$_2$), 27.4 (CH-CH$_3$)$_2$), 102.2 (CH), 119.8 (CH), 121.3 (CH), 122.1 (CH), 122.9 (CH), 134.6 (C), 137.1 (CH), 139.6 (CH), 140.5 (CH), 145.0 (C), 145.9 (C), 155.1 (C), 161.8 (C), 165.1 (C). **IR (cm^{-1}):** 1314 (medium, sharp),1436 (strong, sharp), 1463 (medium, sharp), 1566 (medium, sharp), 1644 (medium, sharp, C=N$_{imine}$), 2961 (medium, sharp, C-H), 3332 (medium, sharp, NH). ESIMS: (+) *m/z* 374 [M+H]. ESIMS: (-) *m/z* 372 [M-H]. HRMS (FAB): calcd for C$_{24}$H$_{27}$N$_3$O [M+H] 374.2232, found 374.2221.

5.2.8 Synthesis of H**L1$_b$**

A 50 ml round-bottom flask, equipped with stir bar, was charged with 1-(6'-hydroxy-2, 2'-bipyridin-6-yl)ethanone (0.50 g, 2.34 mmol), 2,4,6-triisopropylaniline (0.80 g, 3.50 mmol, 1.5 eq.) and dry toluene (10 ml). A Dean Stark apparatus with condenser was then attached to the flask. The reaction mixture was stirred and heated to reflux for approximately 30 min before the addition of 2 drops of formic acid. The reaction mixture was left to stir at reflux for 3 days. After cooling to room temperature the solvent was removed by rotary evaporation. The resulting oil was recrystallized from methanol at -30 °C overnight and filtered to give H**L1$_a$** as a greenish yellow solid (0.70 g, 72%). **Mp:** 235-237 °C. ^{1}**H NMR (400 MHz; CDCl$_3$):** δ 10.52 (1H, s, NH), 8.42 (1H, dd, $^3J_{HH}$ = 7.0 Hz, $^4J_{HH}$ = 1.6 Hz, Py/Ar-H), 7.93 (2H, m, Py/Ar-H), 7.52 (1H, m, Py/Ar-H), 7.02 (2H, s, Ar-H), 6.88 (1H, dd, $^3J_{HH}$ = 6.9 Hz, $^4J_{HH}$ = 0.8 Hz, Py/Ar-H), 6.68 (1H, dd, $^3J_{HH}$ = 9.2 Hz, $^4J_{HH}$ = 0.7 Hz, Py/Ar-H), 2.9 (1H, sept., $^3J_{HH}$ = 6.8 Hz, CH(CH$_3$)$_2$), 2.68 (2H, sept.,

$^3J_{HH}$ = 6.6 Hz, CH(CH$_3$)$_2$), 2.27 (3H, s, CH$_3$), 1.29 (6H, d, $^3J_{HH}$ = 6.9 Hz, (CH(CH$_3$)$_2$)$_2$), 1.15 (12H, d, $^3J_{HH}$ = 6.9 Hz, (CH(CH$_3$)$_2$)$_2$). **^{13}C NMR (100 MHz; CDCl$_3$):** δ 17.5 (CCH$_3$), 23.0 (CH(CH$_3$)$_2$), 23.3 (CH(CH$_3$)$_2$), 24.3 (CH(CH$_3$)$_2$), 28.5 (CH(CH$_3$)$_2$), 34.0 (CH(CH$_3$)$_2$), 103.2 (CH), 120.7 (CH), 121.0 (CH), 122.2 (CH), 122.4 (CH), 135.2 (C), 138.0 (CH), 140.7 (CH), 141.5 (C), 143.8 (C), 144.0 (C), 146.8 (C), 156.2 (C), 162.8 (C), 166 (C). **IR (cm^{-1}):** 1456 (medium, sharp), 1571 (strong, sharp), 1649 (strong, sharp, C=N$_{imine}$), 2958 (medium, sharp, C-H), 3384 (medium, broad, N-H). ESIMS: (+) *m/z* 416 [M+H]. HRMS (FAB): calcd for C$_{27}$H$_{33}$N$_3$O [M+H] 416.2702, found 416.2684.

5.2.9 Synthesis of HL1$_c$
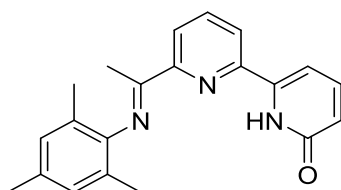
A 50 ml round-bottom flask, was charged with 1-(6-hydroxy-2,2-bipyridine-6-yl)ethanone (0.84 g, 3.925 mmol, 1 eq.), trimethylaniline (0.794 g, 5.88 mmol, 1.5 eq.) and dry toluene (20 ml). A Dean Stark apparatus with condenser was then attached to the flask. The reaction mixture was stirred and heated to reflux for approximately 30 min before the addition of 2 drops of formic acid. The reaction mixture was left to stir at reflux for 3 days. After cooling to room temperature the solvent was removed by rotary evaporation. The resulting oil was recrystallized from methanol at -30 °C overnight and filtered to give H**L1$_c$** as a yellow solid (0.678 g, 52%). **Mp:** 190-192 °C. **^{1}H NMR δ (400 MHz; CDCl$_3$):** 10.44 (1H, s, NH), 8.37 (1H, dd, $^4J_{HH}$ = 6.8 Hz, $^3J_{HH}$ = 1.6 Hz, Py-H), 7.85 (2H, m, Py-H), 7.45 (1H, m, Py-H), 6.83 (2H, s, Ar-H), 6.80 (1H, d, $^3J_{HH}$ = 6 Hz, Py-H), 6.61 (1H, d, $^3J_{HH}$ = 8.4 Hz, Py-H), 2.23 (3H, s, CCH$_3$), 2.17 (3H, s, Ar-CH$_3$), 1.93 (6H, s, Ar-CH$_3$). **^{13}C NMR (100 MHz; CDCl$_3$):** δ 15.74 (CCH$_3$), 16.80 (CH$_3$), 19.71 (CH$_3$), 102.16 (CH), 119.76 (CH), 121.29 (CH), 124.07 (CH), 127.65 (CH), 131.59 (C), 137.01 (CH), 139.67 (C), 140.48 (C), 144.82 (C), 145.81 (C), 155.21 (C), 161.77 (C), 165.44 (C). **IR (cm^{-1}):** 1258 (medium, sharp), 1568 (medium, sharp), 1651 (medium, sharp, C=N), 3314 (weak, broad). ESIMS: (+) *m/z* 332 [M+H]. ESIMS: (-) *m/z* 330 [M-H]. HRMS (FAB): calcd for C$_{21}$H$_{22}$N$_3$O [M+H] 332.1763, found 332.1754.

5.2.10 Synthesis of **L1$_{OMe}$**
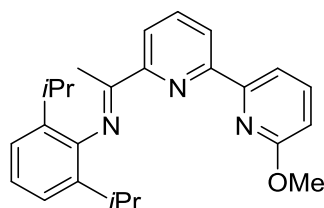
A 50 ml one necked round-bottom flask, was charged with compound **a** (0.800 g, 3.51 mmol, 1 eq.), 2,6-diisopropylaniline (0.93 g, 5.26 mmol, 1.5 eq.) and dry toluene (40 ml). A Dean Stark apparatus with condenser was then attached to the flask. The reaction mixture was stirred and heated to reflux for approximately 30 min before the addition of 2 drops of formic acid. The reaction mixture was left to stir and reflux for 3 days. After cooling to room temperature, the solvent was removed by rotary evaporation. The resulting oil was recrystallized from methanol at -30 °C overnight and filtered to give **L1$_{OMe}$** as a pale yellow solid (1.21 g, 89%). **Mp:** 191-193 °C. **^{1}H NMR δ (400 MHz; CDCl$_3$):** 8.44 (1H, dd, $^4J_{HH}$ = 7.8 Hz, $^3J_{HH}$ = 0.9 Hz, Py/Ar-H), 8.29 (1H, dd, $^4J_{HH}$ = 7.9 Hz, $^3J_{HH}$ = 1.0 Hz, Py/Ar-H), 8.07 (1H, d, $^4J_{HH}$ = 6.9 Hz, PyAr-H), 7.84 (1H, t, $^4J_{HH}$ = 7.8 Hz, Py/Ar-H), 7.65 (1H, t, $^4J_{HH}$ = 7.4 Hz, Py/Ar-H), 7.11 (2H, dd, $^4J_{HH}$ = 6.9 Hz, $^3J_{HH}$ = 1.3 Hz, PyAr-H), 7.03 (1H, t, $^4J_{HH}$ = 7.4 Hz, Py/Ar-H), 6.73 (1H, dd, $^4J_{HH}$ = 6.7 Hz, $^3J_{HH}$ = 0.6 Hz, Py/Ar-H), 4.00 (3H, s, OMe), 2.71 (2H, sept., $^4J_{HH}$ = 6.9 Hz, CH(CH$_3$)$_2$), 2.25 (3H, s, CCH$_3$), 1.09 (12H, d, $^3J_{HH}$ = 6.9 Hz, (CH(CH$_3$)$_2$)$_2$). **^{13}C NMR (100 MHz; CDCl$_3$):** δ 17.2 (CCH$_3$), 22.9 (CH(CH$_3$)$_2$), 23.2 (CH(CH$_3$)$_2$), 28.3 (CH-CH$_3$)$_2$), 53.3 (OMe), 114.1 (CH), 113.7 (CH), 120.9 (CH), 121.2 (CH), 121.8 (CH), 123.5 (CH), 135.8 (C), 137.2 (CH), 139.3 (CH), 146.6 (C), 153.4 (C), 154.8 (C), 155.6 (C), 163.6 (C), 167.2 (C). **IR (cm^{-1}):** 1258 (medium, sharp), 1568 (medium, sharp), 1649 (medium, sharp, C=N). ESIMS: (+) *m/z* 388 [M+H].

5.2.11 Synthesis of **1**
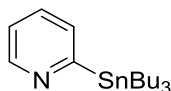
A 250 ml three necked round-bottom flask, equipped with a stir bar, was evacuated, backfilled with nitrogen then charged with a solution of 2-bromopyridine (4.98 g, 31.5 mmol) and dry diethyl ether (150 ml). The solution was then cooled to -78 °C and *n*-BuLi (19.6 ml, 31.5 mmol, 1 eq.; 1.6 M in hexanes) added dropwise over 10 min. The solution was stirred at -78 °C for 15 min before tributyltinchloride (9 ml, 31.8 mmol, 1.01 eq.)

was added. The solution was stirred for 2 h at -78 °C under an atmosphere of nitrogen then warmed to room temperature and treated with 60 ml of a saturated NH$_4$Cl aqueous solution. The organic layer was extracted with Et$_2$O (3 × 30 ml). The combined organic extracts were dried over magnesium sulphate and evaporated under reduced pressure to give the product as a pale orange oil (10.4 g, 90%)

^{1}H-NMR (400 MHz; CDCl$_3$): δ 8.66 (1H, ddd, $^3J_{HH}$ = 4.9 Hz, $^4J_{HH}$ = 2.8 Hz, $^6J_{HH}$ = 1.0 Hz, Py-H), 7.40 (1H, ddd, $^3J_{HH}$ = 7.5 Hz, $^4J_{HH}$ = 3.3 Hz, $^6J_{HH}$ = 1.9 Hz, Py-H), 7.31 (1H, t, $^3J_{HH}$ = 7.3 Hz, Py-H), 7.03(1H, ddd, $^3J_{HH}$ = 6.4 Hz, $^4J_{HH}$ = 4.9 Hz, $^6J_{HH}$ = 1.5 Hz, Py-H), 1.49 (4H, m, Bu$_3$), 1.26 (8H, m, Bu$_3$), 1.05 (6H, m, Bu$_3$), 0.80 (9H, t, $^3J_{HH}$ = 7.2 Hz, Bu$_3$). The ^{1}H NMR data are consistent with that described by Bianchini *et al.* [5]

5.2.12 Synthesis of **2**
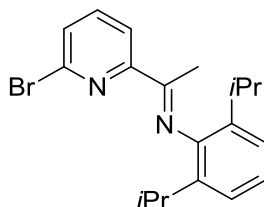
A 50 ml round-bottom flask, equipped with a stir bar, was charged with 2-bromo-6-acetylpyridine (2.40 g, 12.0 mmol), 2,6-diisopropylaniline (3.54 g, 18.0 mmol, 1.5 eq.), formic acid (2 drops) and MeOH (20 ml). The reaction mixture was stirred and heated to reflux overnight. After cooling to room temperature the reaction mixture was allowed to stand for 24 h. During this time, yellow crystals precipitated, which were separated by filtration and washed with cold MeOH to give **2** as a bright yellow solid (3.69 g, 85%).

^{1}H NMR (400 MHz; CDCl$_3$): δ 8.34 (1H, dd, $^3J_{HH}$ = 7.7 Hz, $^4J_{HH}$ = 0.8 Hz, Py/Ar-H), 7.68 (1H, t, $^3J_{HH}$ = 7.6 Hz, Py/Ar-H), 7.60 (1H, dd, $^3J_{HH}$ = 7.6 Hz, $^4J_{HH}$ = 0.8 Hz, Py/Ar-H), 7.12 (3H, m, Py/Ar-H), 2.71 (2H, sept., $^3J_{HH}$ = 6.6 Hz, CH(CH$_3$)$_2$), 2.21 (3H, s, CCH$_3$), 1.16 (12H, d, $^3J_{HH}$ = 6.9 Hz, CH(CH$_3$)$_2$).

The ^{1}H NMR data are consistent with that described by Bianchini *et al.* [5]

5.2.13 Synthesis of **L1$_H$**
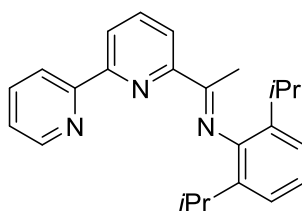
A 100 ml Schlenk flask, equipped with a stir bar, was evacuated and backfilled with nitrogen. Then charged with **1** (0.57 g, 1.59 mmol), **2** (0.247 g, 1.67 mmol, 1.2 eq.), toluene (20 ml) and tetrakistriphenylphosphine palladium(0) (0.055 g, 0.048 mmol, 0.03 eq.). The solution was stirred for 18 h at 95 °C under an atmosphere of nitrogen. After the reaction mixture was cooled to room temperature, the solvent was removed under reduced pressure to give the crude product. The residue was suspended in the minimal methanol, filtered, washed with more cold MeOH and dried to give **L1$_H$** as a yellow powder (0.51 g, 89%). **^{1}H NMR (400 MHz; CDCl$_3$):** δ 8.63 (1H, ddd, $^3J_{HH}$ = 4.7 Hz, $^4J_{HH}$ = 1.7 Hz, $^6J_{HH}$ = 0.8 Hz, Py/Ar-H), 8.47 (2H, td, $^3J_{HH}$ = 6.7 Hz, $^4J_{HH}$ = 1.1 Hz, Py/Ar-H), 8.32 (1H, dd, $^3J_{HH}$ = 7.8 Hz, $^4J_{HH}$ = 1.0 Hz, Py/Ar-H), 7.87 (1H, t, $^3J_{HH}$ = 7.8 Hz, Py/Ar-H), 7.76 (1H, td, $^3J_{HH}$ = 7.6 Hz, $^4J_{HH}$ = 1.7 Hz, Py/Ar-H), 7.26 (1H, ddd, $^3J_{HH}$ = 7.4 Hz, $^4J_{HH}$ = 4.7 Hz, $^6J_{HH}$ = 1.1 Hz, Py/Ar-H), 7.03 (3H, m, Py/Ar-H), 2.71 (2H, sept., $^3J_{HH}$ = 6.8 Hz, CH(CH$_3$)$_2$), 2.25 (3H, s, CCH$_3$), 1.09 (12H, d, $^3J_{HH}$ = 7.0 Hz, CH(CH$_3$)$_2$).

The ^{1}H NMR data are consistent with that described by Bianchini *et al.* [5]

5.2.14 Synthesis of **L1$_a$PdOAc**
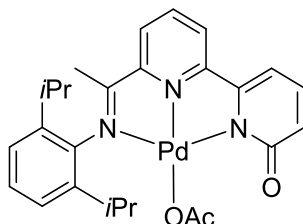
A 100 ml Schlenk flask, equipped with a stir bar, was evacuated, backfilled with nitrogen then charged with H**L1$_a$** (0.70 g, 1.88 mmol, 1 eq.), palladium(II) acetate (0.42 g, 1.88 mmol, 1 eq.) and dry toluene (30 ml). The reaction was stirred at room temperature overnight under an atmosphere of nitrogen affording a red precipitate, which was filtered through celite and washed with toluene. The precipitate was then extracted with dichloromethane and the solvent removed by rotary evaporation affording **L1$_a$PdOAc** as a red powder (0.94 g, 94%). Mp: 250 °C (decomp). **^{1}H NMR (400 MHz; MeOD):** δ 8.37 (1H, t, $^3J_{HH}$ = 8.2 Hz, Py/Ar-H), 8.24 (1H, d, $^3J_{HH}$ = 8.2 Hz, Py/Ar-H), 8.11 (1H, d, $^3J_{HH}$ = 7.6 Hz, Py/Ar-H), 7.60 (1H, t, $^3J_{HH}$ = 7.9 Hz, Py/Ar-H), 7.08 (1H, t, $^3J_{HH}$ = 7.4 Hz, Py/Ar-H), 7.34 (2H, d, $^3J_{HH}$ = 7.4 Hz, Py/Ar-H), 7.29 (1H, d, $^3J_{HH}$ = 7.0 Hz, Py/Ar-H), 6.53 (1H, d, $^3J_{HH}$ = 8.8 Hz, Py/Ar-H), 3.24 (2H, sept., $^3J_{HH}$ = 6.4 Hz, CH(CH$_3$)$_2$), 1.86 (3H, s, OAc), 1.36 (6H, d, $^3J_{HH}$ = 6.8 Hz, (CH(CH$_3$)$_2$)$_2$), 1.17 (6H, d, $^3J_{HH}$ = 6.8 Hz, (CH(CH$_3$)$_2$)$_2$). **^{13}C NMR (100 MHz; MeOD):** Not soluble enough. IR (cm^{-1}): 1052

(weak, sharp), 1319 (medium, sharp), 1362 (medium, sharp), 1483 (strong, sharp), 1550 (medium, sharp), 1620 (medium, sharp, C=N), 2961 (medium, sharp, C-H). ESIMS: (+) m/z 478 [M-OAc]. FABMS: m/z 478 [M-OAc]. Anal. calc. for ($C_{26}H_{29}N_3O_3Pd \cdot 3H_2O$): C 52.75, H 5.96, N 7.10. Found C 52.98, H 5.29, N 7.11%.

5.2.15 Synthesis of **L1$_b$PdOAc**
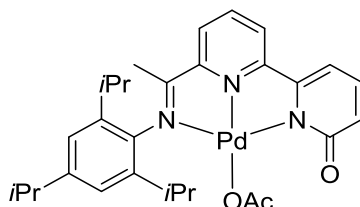
A 100 ml Schlenk flask, equipped with a stir bar, was evacuated, backfilled with nitrogen then charged with H**L1$_b$** (0.50 g, 1.20 mmol, 1 eq.), palladium(II) acetate (0.27 g, 1.20 mmol, 1 eq.) and dry toluene (30 ml). The reaction was stirred at room temperature overnight under an atmosphere of nitrogen affording a red precipitate which was then filtered through celite and washed with toluene. The precipitate was then extracted with dichloromethane and the solvent removed by rotary evaporation to give **L1$_b$PdOAc** as a red powder (0.67 g, 96%). **Mp**: 250 °C (decomp). **^{1}H NMR (400 MHz; CDCl$_3$):** δ 8.42 (1H, d, $^3J_{HH}$ = 8.4 Hz, Py/Ar-H), 8.19 (1H, t, $^3J_{HH}$ = 8.0 Hz, Py/Ar-H), 7.54 (1H, d, $^3J_{HH}$ = 7.6 Hz, Py/Ar-H), 7.18 (1H, d, $^3J_{HH}$ = 6.4 Hz, Py/Ar-H), 7.08 (2H, s, Ar-H), 6.95 (1H, m, Py/Ar-H), 6.18 (1H, d, $^3J_{HH}$ = 8.6 Hz, Py/Ar-H), 3.21 (2H, sept., $^3J_{HH}$ = 6.7 Hz, CH(CH$_3$)$_2$), 2.92 (1H, sept., $^3J_{HH}$ = 7.1 Hz, CH(CH$_3$)$_2$), 2.29 (3H, s, CH$_3$), 1.6 (3H, s, OAc), 1.49 (6H, d, $^3J_{HH}$ = 6.6 Hz, (CH(CH$_3$)$_2$), 1.28 (6H, d, $^3J_{HH}$ = 6.9 Hz, (CH(CH$_3$)$_2$), 1.16 (6H, d, $^3J_{HH}$ = 6.9 Hz, (CH(CH$_3$)$_2$). **^{13}C NMR (125 MHz; CDCl$_3$):** δ 18.4 (CCH$_3$), 22.1 (OAc), 23.8 (CH(CH$_3$)$_2$), 24.0 (CH(CH$_3$)$_2$), 24.3 (CH(CH$_3$)$_2$), 29.0 (CH(CH$_3$)$_2$), 34.3 (CH(CH$_3$)$_2$), 119.5 (CH), 121.7 (CH), 124.0 (CH), 126.1 (CH), 126.8 (CH), 128.2 CH), 135.2 (C), 136.6 (CH), 140.2 (C), 149.2 (C), 151.8 (C), 153.9 (C), 158.6 (C), 168.9 (C), 177.2 (C). **IR (cm^{-1}):** 1319 (medium, sharp), 1483 (strong, sharp), 1599 (medium, sharp), 1621 (medium, sharp, C=N), 2961 (medium, sharp, C-H). ESIMS: (+) m/z 520 [M-OAc]. FABMS: m/z 520 [M-OAc], 579 [M]. Anal. calc. for ($C_{29}H_{35}N_3O_3Pd \cdot 0.8CH_2Cl_2$): C 55.24, H 5.69, N 6.48. Found C 55.38, H 5.29, N 6.91%.

5.2.16 Synthesis of **L1$_c$**PdOAc
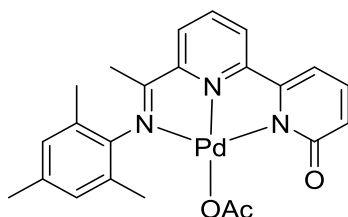
A 100 ml Schlenk flask, equipped with a stir bar, was evacuated, backfilled with nitrogen then charged with H**L1$_c$** (0.10 g, 0.302 mmol), palladium(II) acetate (0.068 g, 0.302 mmol) and dry toluene (20 ml). The reaction was stirred at room temperature overnight under an atmosphere of nitrogen affording a red precipitate was then filtered through celite, washed with toluene and then extracted with dichloromethane. The solvent was removed by rotary evaporation to give **L1$_c$**PdOAc as a dark red powder (0.102 g, 68%). **Mp:** 265 °C (decomp). **^{1}H NMR (400 MHz; CDCl$_3$):** δ 8.33 (1H, d, $^3J_{HH}$ = 8.4 Hz, Py-H), 8.10 (1H, t, $^3J_{HH}$ = 8 Hz, Py-H), 7.47 (1H, d, $^3J_{HH}$ = 7.6 Hz, Py-H), 7.10 (2H, m, Py-H), 6.87 (2H, s, Ar-H), 6.15 (1H, d, $^3J_{HH}$ = 8.6 Hz, Py-H), 2.28 (3H, s, Ar-CH$_3$), 2.27 (6H, s, Ar-CH$_3$), 2.23 (3H, s, OAc), 2.13 (3H, s, CCH$_3$). **^{13}C NMR (100MHz; CDCl$_3$):** the sample was insufficiently soluble to give an assignable spectrum. **IR (cm^{-1}):** 793 (strong, sharp), 1012 (medium, sharp), 1259 (medium, sharp), 1567 (medium, sharp,C=O), 1618 (medium, sharp, C=N). ESIMS: (+) *m/z* 436 [M$^+$- OAc]. ESIMS: (-) *m/z* 494 [M$^+$-H]. FABMS: *m/z* 436 [M$^+$- OAc].


5.2.17 Synthesis of **L1$_a$**PdCl from **L1$_a$**PdOAc
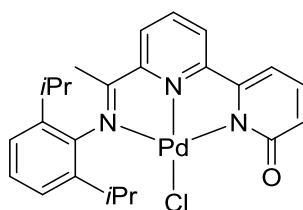
A 100 ml round-bottom flask, equipped with stir bar, was charged with **L1$_a$**PdOAc (0.10 g, 0.186 mmol), brine (6 ml) and chloroform (10 ml). The reaction was stirred vigorously at room temperature overnight. The mixture was separated, the aqueous layer extracted with chloroform (3 × 10 ml) and the combined organic layers dried over MgSO$_4$. The solvent was removed by rotary evaporation to give **L1$_a$**PdCl as a reddish orange solid (0.096 g, 100%). **Mp**: 250 °C (decomp). **^{1}H NMR δ (400 MHz; CD$_3$CN):** δ 8.23 (1H, m, Py/Ar-H), 8.07 (1H, d, $^3J_{HH}$ = 8.4 Hz, Py/Ar-H), 7.9 (1H, d, $^3J_{HH}$ = 7.8 Hz, Py/Ar-H), 7.33 (2H, m, Py/Ar-H), 7.25 (2H, d, $^3J_{HH}$ = 8.6 Hz, Py/Ar-H), 7.03 (1H, dd, $^3J_{HH}$ = 6.8

Hz, $^4J_{HH}$ = 1.2 Hz, Py/Ar-H), 6.52 (1H, d, $^3J_{HH}$ = 8.6 Hz, Py/Ar-H), 3.13 (2H, sept., $^3J_{HH}$ = 6.7 Hz, CH(CH₃)₂), 2.24 (3H, s, CCH₃), 1.34 (6H, d, $^3J_{HH}$ = 6.8 Hz, CH(CH₃)₂), 1.14 (6H, d, $^3J_{HH}$ = 6.8 Hz, CH(CH₃)₂). The remaining data was as reported as above.

5.2.18 Synthesis of **L1ᵦPdCl** from **L1ᵦPdOAc**
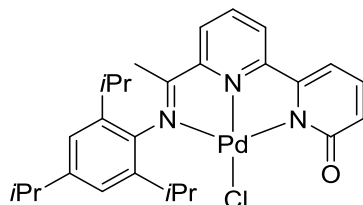
A 100 ml round-bottom flask, equipped with stir bar, was charged with **L1ᵦPdOAc** (0.15 g, 0.26 mmol), brine (15 ml) and chloroform (30 ml). The reaction was stirred vigorously at room temperature overnight. The mixture was separated, the aqueous layer extracted with chloroform (3 × 10 ml) and the combined organic layers dried over MgSO₄. The solvent was removed by rotary evaporation to give **L1ᵦPdCl** as a dark orange solid (0.144 g, 100%). **Mp**: 250 °C (decomp). **¹H NMR (400 MHz; CD₃CN):** δ 8.23 (1H, t, $^3J_{HH}$ = 7.8 Hz, Py-H), 8.06 (1H, d, $^3J_{HH}$ = 8.4 Hz, Py-H), 7.90 (1H, d, $^3J_{HH}$ = 7.6 Hz, Py-H), 7.33 (1H, m, Py-H), 7.10 (2H, s, Ar-H), 6.92 (1H, d, $^3J_{HH}$ = 7.6 Hz, Py-H), 6.42 (1H, d, $^3J_{HH}$ = 8.9 Hz, Py-H), 3.13 (2H, sept., $^3J_{HH}$ = 6.8 Hz, CH(CH₃)₂), 2.91 (1H, sept., $^3J_{HH}$ = 6.8 Hz, CH(CH₃)₂), 2.33 (3H, s, CH₃), 1.34 (6H, d, $^3J_{HH}$ = 6.9 Hz, CH(CH₃)₂), 1.26 (6H, d, $^3J_{HH}$ = 6.9 Hz, (CH(CH₃)₂), 1.14 (6H, d, $^3J_{HH}$ = 6.9 Hz, (CH(CH₃)₂). **¹³C NMR (100 MHz; CD₃CN):** the sample was insufficiently soluble to give an assignable spectrum. **IR (cm⁻¹):** 1051 (medium, sharp), 1260 (medium, sharp), 1554 (medium, sharp), 1619 (medium, sharp, C=N), 2961 (medium, sharp, C-H). ESIMS: (+) *m/z* 520 [M-Cl]. FABMS: *m/z* 520 [M-Cl], 556 [M].
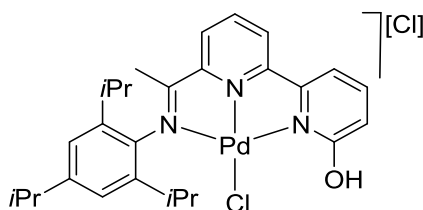
5.2.19 Synthesis of [H**L1ₐ**PdCl][Cl]
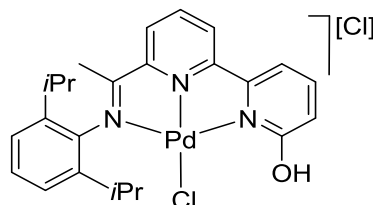
A 100 ml Schlenk flask, equipped with a stir bar, was evacuated, backfilled with nitrogen then charged with H**L1ₐ** (0.20 g, 0.54 mmol, 1 eq.), bis(acetonitrile)palladium(II) chloride (0.14 g, 0.54 mmol, 1 eq.) and dry toluene (20 ml). The reaction was stirred at room

temperature for 18 h under an atmosphere of nitrogen. The resulting precipitate was filtered through celite and washed with toluene. The brown solid was then extracted with methanol and the solvent removed under reduced pressure to give [H**L1ₐ**PdCl][Cl] as a reddish brown powder (0.24 g, 81%). **Mp**: 260 °C (decomp). **¹H NMR (400 MHz; MeOD):** δ 8.43 (2H, m, Py/Ar-H), 8.19 (1H, dd, $^3J_{HH}$ = 7.0 Hz, $^4J_{HH}$ = 1.8 Hz, Py/Ar-H) 8.06 (1H, t, $^3J_{HH}$ = 8.0 Hz, Py/Ar-H), 7.91 (1H, dd, $^3J_{HH}$ = 7.4 Hz, $^4J_{HH}$ =1.0 Hz, Py/Ar-H), 7.34 (1H, t, $^3J_{HH}$ = 7.8 Hz, Py/Ar-H), 7.23 (2H, d, $^3J_{HH}$ = 7.8 Hz, Py/Ar-H), 7.09 (1H, dd, $^3J_{HH}$ = 8.6 Hz, $^4J_{HH}$ = 1.0 Hz, Py/Ar-H), 3.21 (2 H, sept., $^3J_{HH}$ = 6.6 Hz, CH(CH₃)₂), 2.37 (3H, s, CCH₃), 1.31 (6H, d, $^3J_{HH}$ = 6.8 Hz, CH(CH₃)₂), 1.12 (6H, d, $^3J_{HH}$ = 6.8 Hz, CH(CH₃)₂). **¹³C NMR (100 MHz; MeOD):** the sample was insufficiently soluble to give an assignable spectrum. **IR (cm⁻¹):** 1233 (strong, sharp), 1570 (medium, sharp), 1613 (medium, sharp, C=N), 3644 (medium, broad, OH). ESIMS: (+) *m/z* 478 [M⁺- 2Cl]. FABMS: *m/z* 478 [M⁺- 2Cl].

5.2.20 Synthesis of [H**L1ᵦ**PdCl][Cl]

A 100 ml Schlenk flask, equipped with a stir bar, was evacuated, backfilled with nitrogen then charged with H**L1ᵦ** (0.20 g, 0.482 mmol, 1 eq.), bis(acetonitrile)palladium(II) chloride (0.125 g, 0.482 mmol, 1 eq.) and dry toluene (20 ml). The reaction was stirred at room temperature for 18 h under an atmosphere of nitrogen. The resulting precipitate was filtered through celite and washed with toluene. The yellow brown solid was then extracted with methanol and the solvent removed under reduced pressure to give [H**L1ᵦ**PdCl][Cl] as a yellow brown powder (0.28 g, 98%). **Mp**: 260 °C (decomp). **¹H NMR (400 MHz; MeOD):** δ 8.44 (2H, m, Py-H), 8.18 (1H, dd, $^3J_{HH}$ = 6.4 Hz, $^4J_{HH}$ = 2.3 Hz , Py-H), 8.05 (1H, t, $^3J_{HH}$ = 7.4, Py-H), 7.92 (1H, d, $^3J_{HH}$ = 7.4, Py-H), 7.07 (2H, s, Ar-H), 7.06 (1H, d, $^3J_{HH}$ = 8.5 Hz, Py-H), 3.11 (2 H, sept., $^3J_{HH}$ = 6.7 Hz, CH(CH₃)₂), 2.86 (1H, sept., $^3J_{HH}$ = 6.7 Hz, CH(CH₃)₂), 2.37 (3H, s, CCH₃), 1.29 (6H, d, $^3J_{HH}$ = 6.8 Hz, CH(CH₃)₂), 1.19 (6H, d, $^3J_{HH}$ = 6.8 Hz, CH(CH₃)₂), 1.13 (6H, d, $^3J_{HH}$ = 6.8 Hz, CH(CH₃)₂). **¹³C NMR (100MHz; MeOD):** δ 19.3 (CH₃), 24.1 (CH(CH₃)₂), 24.2 (CH(CH₃)₂), 24.3 (CH(CH₃)₂), 30.1 (CH(CH₃)₂), 35.6 (CH(CH₃)₂), 119.2 (CH), 119.4

(CH), 123.1 (CH), 127.0 (CH), 129.6 (CH), 138.6 (C), 141.6 (C), 143.9 (CH), 145.3 (CH), 151.4 (C), 155.6 (C), 155.9 (C), 157.9 (C), 168.8 (C), 186.9 (C). **IR (cm^{-1}):** 1570 (medium, sharp), 1619 (medium, sharp, C=N), 2961 (sharp, C-H), 3510 (medium, broad, OH). ESIMS: (+) *m/z* 521 [M$^+$- 2Cl]. FABMS: *m/z* 592 [M$^+$]. TOFMS: calcd for C$_{27}$H$_{33}$N$_3$OPdCl$_2$ [M$^+$-Cl] 560.1862, Found 560.1872.

5.2.21 Synthesis of [H**L1$_c$**PdCl][Cl]
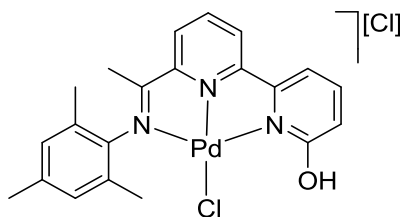
A 100 ml Schlenk flask, was evacuated, backfilled with nitrogen, then charged with H**L1$_c$** (0.040 g, 0.121 mmol, 1.1 eq.) and bis(acetonitrile) palladium(II) chloride (0.029 g, 0.11 mmol, 1 eq.) and dry toluene (10 ml). The reaction was stirred at room temperature overnight under an atmosphere of nitrogen. The resulting precipitate was filtered through celite and washed with toluene. The yellow brown solid was then extracted with methanol and the solvent removed under reduced pressure to give [H**L1$_c$**PdCl][Cl] as yellow solid (0.043 g, 70%). **Mp:** 260 °C (decomp). **^{1}H NMR (400 MHz; MeOD):** δ 8.44 (2H, m, Py-CH), 8.17 (1H, d, $^3J_{HH}$ = 7.2 Hz, Py-H), 8.05 (1H, t, $^3J_{HH}$ = 8 Hz, Py-H), 7.91 (1H, d, $^3J_{HH}$ = 7.2 Hz, Py-H), 7.09 (1H, d, $^3J_{HH}$ = 8.4 Hz, Py-H), 6.92 (2H, s, Ar-H), 2.31 (3H, s, CCH$_3$), 2.22 (3H, s, CH$_3$), 2.20 (6H, s, CH$_3$). **^{13}C NMR (100MHz; MeOD):** the sample was insufficiently soluble to give an assignable spectrum. **IR (cm^{-1}):** 817 (strong, sharp), 1233 (strong, sharp), 1570 (medium, sharp), 1623 (medium, sharp, C=N), 3605 (medium, broad, OH). ESIMS: (+) *m/z* 436 [M$^+$- Cl]. FABMS: *m/z* 436 [M$^+$- Cl].
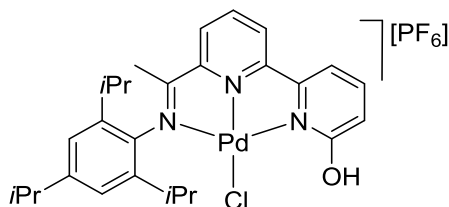
5.2.22 Synthesis of [H**L1$_a$**PdCl][PF$_6$]
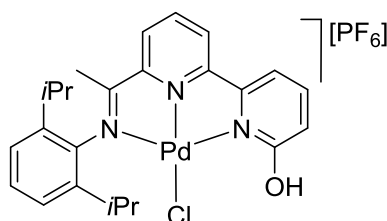
A 100 ml round-bottom flask, was charged with [H**L1$_a$**PdCl][Cl] (0.18 g, 0.33 mmol, 1 eq.), dichloromethane (20 ml) and a potassium hexafluorophosphate solution (10 ml). The reaction was stirred at room temperature overnight. The mixture was separated and the

aqueous phase extracted with dichloromethane (3×20 ml). The combined organic layers were dried over MgSO$_4$. The solvent was removed by rotary evaporation to give [H**L1$_a$**PdCl][PF$_6$] as a reddish orange solid (0.20 g, 93%). **Mp:** 250 °C (decomp). **^{1}H NMR (400 MHz; CD$_3$CN):** δ 10.76 (1H, s, OH), 8.39 (1H, t, $^3J_{HH}$ = 4.1 Hz, Py/Ar-H), 8.21 (1H, dd, $^3J_{HH}$ = 8.4 Hz, $^4J_{HH}$ = 0.9Hz, Py/Ar-H), 8.01 (2H, m, Py/Ar-H), 7.76 (1H, dd, $^3J_{HH}$ = 7.4 Hz, $^4J_{HH}$ =1.0 Hz, Py/Ar-H), 7.39 (1H, t, $^3J_{HH}$ = 7.8 Hz, Ar-H), 7.25 (2H, d, $^3J_{HH}$ = 7.9 Hz, Ar-H), 7.05 (1H, dd, $^3J_{HH}$ = 8.6 Hz, $^4J_{HH}$ =1.0 Hz, Py/Ar-H), 3.13 (2H, sept., $^3J_{HH}$ = 6.6 Hz, CH(CH$_3$)$_2$), 2.29 (3H, s, CCH$_3$), 1.28 (6H, d, $^3J_{HH}$ = 6.8 Hz, CH(CH$_3$)$_2$), 1.10 (6H, d, $^3J_{HH}$ = 6.8 Hz, CH(CH$_3$)$_2$). **^{13}C NMR (100 MHz; CD$_3$CN):** δ 20.1 (CCH$_3$), 24.3 (CH(CH$_3$)$_2$), 24.3 (CH(CH$_3$)$_2$), 30.0 (CH(CH$_3$)$_2$), 119.7 (CH), 119.8 (CH), 125.59 (CH), 127.6 (CH), 130.1 (CH), 130.9 (C), 140.7 (CH), 141.9 (CH), 144.1 (C), 145.6 (C), 155.9 (C), 157.6 (C), 168.6 (C), 187.0 (C). **^{19}F NMR (376MHz; CD$_3$CN):** δ -71.9 (6F, d, J -707.2, PF$_6$). **^{31}P NMR (202MHz; CD$_3$CN):** δ -144.63 (P, sept., J -703.9, PF$_6$). **IR (cm^{-1}):** 1625 (strong, sharp, C=N), 2963 (medium, sharp, C-H), 3690 (medium, broad, OH). ESIMS: (+) m/z 515 [M-PF$_6$]. ESIMS: (-) *m/z* 145 [PF$_6$]. FABMS: *m/z* 516 [M-PF$_6$].

5.2.23 Synthesis of [H**L1$_a$**PdCl][PF$_6$]

A 100 ml round-bottom flask, was charged with [H**L1$_b$**PdCl][Cl] (0.050 g, 0.084 mmol, 1 eq.), dichloromethane (20 ml) and a solution of potassium hexafluorophosphate (10 ml) was added. The reaction was stirred at room temperature overnight and separated; the aqueous phase was extracted with dichloromethane (3×20 ml). The combined organic layers were dried over MgSO$_4$ and the solvent removed by rotary evaporation to give [H**L1$_b$**PdCl][PF$_6$] as an orange solid (0.058 g, 98%). **Mp:** 250 °C (decomp). **^{1}H NMR (400 MHz; CDCl$_3$):** δ 11.02 (1H, s, OH), 8.43 (1H, t, $^3J_{HH}$ = 8.0 Hz, Py-H), 8.34 (1H, d, $^3J_{HH}$ = 8.0 Hz 8.0, Py-H), 8.13 (1H, d, $^3J_{HH}$ = 7.8 Hz, Py-H), 7.94 (1H, t, $^3J_{HH}$ = 7.5 Hz, Py-H), 7.78 (1H, d, $^3J_{HH}$ = 6.6 Hz, Py-H), 7.01 (2H, s, Ar-H), 7.00 (1H, d, $^3J_{HH}$ = 7.8 Hz, Py-H), 3.02 (2H, sept., $^3J_{HH}$ = 6.6 Hz, CH(CH$_3$)$_2$), 2.85 (1H, sept., $^3J_{HH}$ = 6.6 Hz, CH(CH$_3$)$_2$), 2.36 (3H, s, CCH$_3$), 1.32 (6H, d, $^3J_{HH}$ = 6.7 Hz, CH(CH$_3$)$_2$), 1.21 (6H, d, $^3J_{HH}$

= 6.7 Hz, CH(CH$_3$)$_2$), 1.13 (6H, d, $^3J_{HH}$ = 6.7 Hz, CH(C$\underline{H}_3$)$_2$). **^{13}C NMR (125 MHz; CDCl$_3$):** δ 17.78 (CH$_3$), 22.6 (CH(C$\underline{H}_3$)$_2$), 22.7 (CH(C$\underline{H}_3$)$_2$), 22.8 (CH(C$\underline{H}_3$)$_2$), 28.1 (C$\underline{H}$(CH$_3$)$_2$), 33.1 (C$\underline{H}$(CH$_3$)$_2$), 117.0 (CH), 117.8 (CH), 121.0 (CH), 125.6 (CH), 126.1 (CH), 127.9 (CH), 135.9 (C), 138.9 (C), 142.7 (CH), 149.2 (C), 152.6 (C), 152.8 (C), 154.9 (C), 166.5 (C), 183.6 (C). **^{19}F NMR (376 MHz; CDCl$_3$):** δ -72.2 (F, d, J -714.8, PF$_6$). **^{31}P NMR (161.9 MHz; CDCl$_3$):** δ -145.0 (P, sept., J -701.2, PF$_6$). **IR (cm^{-1}):** 1626 (strong, sharp, C=N), 2963 (medium, sharp, C-H), 3682 (medium, broad). ESIMS: (+) m/z 521 [M-(Cl+PF$_6$)], 557 [M- PF$_6$]. ESIMS: (-) m/z 145 [PF$_6$]. FABMS: m/z 556 [M-PF$_6$]. TOFMS: calcd for C$_{27}$H$_{33}$N$_3$OPdClPF$_6$ [M$^+$-(Cl+PF$_6$)] 522.1584, Found 522.1592. Anal. calc. for (C$_{27}$H$_{33}$N$_3$OPdClPF$_6$·(CH$_3$)$_2$CO): C 47.38, H 5.17, N 5.53. Found C 47.40, H 5.70, N 5.30%.

5.2.24 Synthesis of [**L1$_a$**PdCl] from [H**L1$_a$**PdCl][PF$_6$]
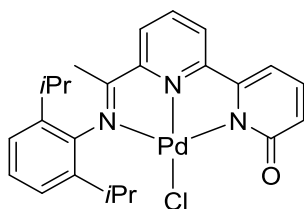
A 100 ml round-bottom flask was charged with [H**L1$_a$**PdCl][PF$_6$] (0.040 g, 0.073 mmol, 1 eq.), triethylamine (0.029 g, 0.292 mmol, 4 eq.) and chloroform (10 ml). The reaction was stirred at room temperature overnight forming a reddish orange precipitate. The mixture was filtered through celite, washed with chloroform and then extracted with methanol to give the product. The solvent was removed by rotary evaporation to give **L1$_a$**PdCl as a reddish orange solid (0.03 g, 84%). **Mp**: 250 °C (decomp). **^{1}H NMR (400 MHz; CD$_3$CN):** δ 8.23 (1H, m, Py/Ar-H), 8.07 (1H, d, $^3J_{HH}$ = 8.4 Hz, Py/Ar-H), 7.9 (1H, d, $^3J_{HH}$ = 7.8 Hz, Py/Ar-H), 7.33 (2H, m, Py/Ar-H), 7.25 (2H, d, $^3J_{HH}$ = 8.6 Hz, Py/Ar-H), 7.03 (1H, dd, $^3J_{HH}$ = 6.8 Hz, $^4J_{HH}$ = 1.2 Hz, Py/Ar-H), 6.93 (1H, d, $^3J_{HH}$ = 8.6 Hz, Py/Ar-H), 3.13 (2H, sept., $^3J_{HH}$ = 6.7 Hz, CH(CH$_3$)$_2$), 2.24 (3H, s, CCH$_3$), 1.34 (6H, d, $^3J_{HH}$ = 6.8 Hz, CH(CH$_3$)$_2$), 1.14 (6H, d, $^3J_{HH}$ = 6.8 Hz, CH(CH$_3$)$_2$). **^{1}H NMR (400 MHz; MeOD):** δ 8.36 (1H, t, $^3J_{HH}$ = 7.9 Hz, Py/Ar-H), 8.22(1H, d, $^3J_{HH}$ = 7.7 Hz, Py/Ar-H), 8.09 (1H, d, $^3J_{HH}$ = 7.7 Hz, Py/Ar-H), 7.57 (1H, t, $^3J_{HH}$ = 7.8 Hz, Py/Ar-H), 7.43 (1H, t, $^3J_{HH}$ = 7.4 Hz, Ar-H), 7.33 (2H, d, $^3J_{HH}$ = 7.0 Hz, Ar-H), 7.27 (1H, d, $^3J_{HH}$ = 7.4 Hz, Py/Ar-H), 6.52 (1H, d, $^3J_{HH}$ = 8.9 Hz, Ar-H), 3.21 (2H, sept., $^3J_{HH}$ = 7.1 Hz, CH(CH$_3$)$_2$), 1.37 (6H, d, $^3J_{HH}$ = 6.5 Hz, CH(CH$_3$)$_2$), 1.18 (6H, d, $^3J_{HH}$ = 6.5 Hz, CH(CH$_3$)$_2$). **^{13}C NMR**

(100 MHz; MeOD): the sample was insufficiently soluble to give an assignable spectrum. **IR (cm⁻¹):** 1046 (weak, sharp), 1379 (medium, sharp), 1549 (medium, sharp), 1620 (strong, sharp, C=N), 2958 (medium, sharp, C-H). ESIMS: (+) m/z 478 [M-Cl]. FABMS: *m/z* 516 [M+H], 478 [M- Cl]. Anal. calc. for (C$_{24}$H$_{26}$N$_3$OPdCl·CHCl$_3$·6MeOH): C 45.08, H 6.22, N 5.09. Found C 45.09, H 6.72 N 4.74%.

5.2.25 Synthesis of [**L1$_a$**Pd(NCCH$_3$)][PF$_6$]
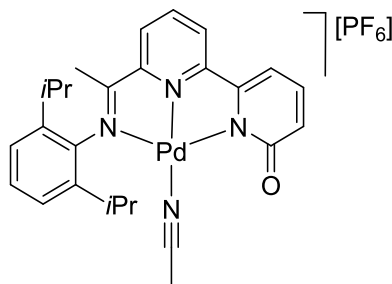
A 100 ml Schlenk flask, equipped with stir bar, was evacuated and backfilled with nitrogen and then charged with **L1$_a$**PdCl (0.110 g, 0.214 mmol, 1 eq.), silver hexafluorophosphate (0.081 g, 0.321 mmol, 1.5 eq.) and dry acetonitrile (20 ml). The reaction was stirred at room temperature overnight under an atmosphere of nitrogen. The mixture was filtered through celite and the celite cake washed with acetonitrile. The solvent was removed by rotary evaporation to give [**L1$_a$**Pd(NCCH$_3$)][PF$_6$] as a red powder (0.135 g, 95%). **Mp**: 250 °C (decomp). **¹H NMR (400 MHz; CD$_3$CN):** δ 8.38 (1H, t, $^3J_{HH}$ = 8.2 Hz, Py/Ar-H), 8.13 (1H, d, $^3J_{HH}$ = 8.5 Hz, Py/Ar-H), 8.01 (1H, dd, $^3J_{HH}$ = 7.8 Hz, $^4J_{HH}$ = 0.7 Hz, Py/Ar-H), 7.47 (2H, d, $^3J_{HH}$ = 6.8 Hz, Py/Ar-H), 7.4 (2H, d, $^3J_{HH}$ = 7.7 Hz, Ar-H), 7.02 (1H, m, Py/Ar-H), 6.49 (1H, d, $^3J_{HH}$ = 6.7 Hz, Py/Ar-H), 3.25 (2H, sept., $^3J_{HH}$ = 6.8 Hz, CH(CH$_3$)$_2$), 2.38 (3H, s, CH$_3$), 1.88 (3H, s, NCCH$_3$), 1.42 (6H, d, $^3J_{HH}$ = 6.7 Hz, CH(CH$_3$)$_2$), 1.23 (6H, d, $^3J_{HH}$ = 6.7 Hz, CH(CH$_3$)$_2$).**¹⁹F NMR (376 MHz; CD$_3$CN):** δ -71.9 (F, d, J -707.2, PF$_6$). **³¹P NMR (202 MHz; CD$_3$CN):** δ -144.63 (P, sept., J -703.9, PF$_6$). **IR (cm⁻¹):** 1011 (medium, sharp), 1573 (medium, sharp,C=O), 1618 (medium, sharp, C=N), 2965 (medium, sharp, C-H). ESIMS: (+) *m/z* 478 [M-(NCCH$_3$)-(PF$_6$)], (-) *m/z* 145 [PF$_6$]. HRMS (FAB): calcd for C$_{26}$H$_{29}$N$_4$OPdPF$_6$ [M-PF$_6$] 519.1376, Found 519.1393. Anal. calc. for (C$_{26}$H$_{29}$N$_4$OPdPF$_6$·3CHCl$_3$·H$_2$O): C 35.42, H 3.90, N 5.16. Found C 35.92, H 3.87 N 5.25%.
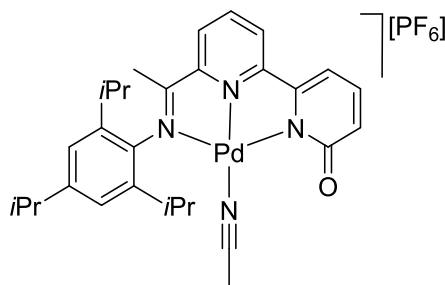
5.2.26 Synthesis of [**L1ₐ**Pd(NCCH₃)][OTf]
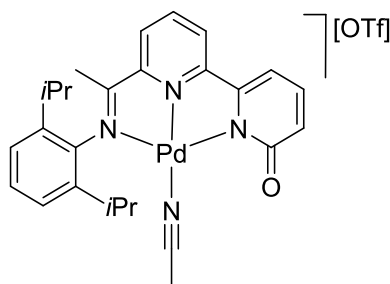
A 100 ml Schlenk flask, equipped with stir bar, was evacuated and backfilled with nitrogen tand hen charged with **L1ₐ**PdCl (0.090 g, 0.175 mmol, 1 eq.), silver trifluoromethanesulfonate (0.067 g, 0.263 mmol, 1.5 eq.) and dry acetonitrile (20 ml). The reaction was stirred at room temperature overnight under an atmosphere of nitrogen. The mixture was filtered through celite and the celite cake washed with acetonitrile. The solvent was removed by rotary evaporation to give [**L1ₐ**Pd(NCCH₃)][OTf] as a dark red powder (0.112 g, 96%). **Mp**: 250 °C (decomp). **¹H NMR (400 MHz; CD₃CN):** δ 8.40 (1H, t, $^3J_{HH}$ = 8.1 Hz, Py/Ar-H), 8.18 (1H, d, $^3J_{HH}$ = 8.6 Hz, Py/Ar-H), 7.97 (2H, m, Py/Ar-H), 7.58 (H, d, $^3J_{HH}$ = 6.6 Hz, Py/Ar-H), 7.41 (H, t, $^3J_{HH}$ = 7.6 Hz, Py/Ar-H), 7.12 (1H, d, $^3J_{HH}$ = 6.8 Hz, Py/Ar-H), 6.58 (1H, d, $^3J_{HH}$ = 6.6 Hz, Py/Ar-H), 3.15 (2H, sept., $^3J_{HH}$ = 6.8 Hz, CH(CH₃)₂), 2.37 (3H, s, CH₃), 1.88 (3H, s, NCCH₃), 1.32 (6H, d, $^3J_{HH}$ = 6.8 Hz, CH(CH₃)₂), 1.13 (6H, d, $^3J_{HH}$ = 6.8 Hz, CH(CH₃)₂).**¹⁹F NMR (376 MHz; CD₃CN):** δ -80.2 (F, s, OTf). **IR (cm⁻¹):** 1011 (medium, sharp), 1570 (medium, sharp,C=O), 1620 (medium, sharp, C=N), 2965 (medium, sharp, C-H). ESIMS: (+) *m/z* 519 [M- OTf]. ESIMS: (-) *m/z* 149 [OTf].

5.2.27 Synthesis of [**L1ᵦ**Pd(NCCH₃)][PF₆]

A 100 ml Schlenk flask, equipped with stir bar, was evacuated and backfilled with nitrogen and then charged with **L1ᵦ**PdCl (0.10 g, 0.180 mmol, 1 eq.), silver hexafluorophosphate (0.068 g, 0.27 mmol, 1.5 eq.) and dry acetonitrile (30 ml). The reaction was stirred at room temperature overnight under an atmosphere of nitrogen. The reaction mixture was filtered through celite and the celite cake washed with acetonitrile.

The solvent was removed by rotary evaporation to give [**L1$_b$Pd(NCCH$_3$)**][PF$_6$] as a red powder (0.123 g, 97%). **Mp**: 250 °C (decomp). **^{1}H NMR (400 MHz; CD$_3$CN):** δ 8.34 (1H, t, $^3J_{HH}$ = 7.2 Hz , Py-H), 8.11 (1H, d, $^3J_{HH}$ = 8.6 Hz, Py -H), 7.96 (1H, d, $^3J_{HH}$ = 7.8 Hz, Py -H), 7.71 (2H, m Py-H), 7.19 (2H, s, Ar-H), 6.89 (1H, d, $^3J_{HH}$ = 7.8 Hz, Py-H), 3.13 (2H, sept., $^3J_{HH}$ = 6.8 Hz, CH(CH$_3$)$_2$), 2.89 (1H, sept., $^3J_{HH}$ = 6.8 Hz, CH(CH$_3$)$_2$), 2.33 (3H, s, CH$_3$), 1.88 (3H, s, NCCH$_3$), 1.32 (6H, d, $^3J_{HH}$ = 6.9 Hz, CH(CH$_3$)$_2$), 1.19 (6H, d, $^3J_{HH}$ = 6.9 Hz, CH(CH$_3$)$_2$) 1.14 (6H, d, $^3J_{HH}$ = 6.9 Hz, CH(CH$_3$)$_2$). **^{19}F NMR (376 MHz; CD$_3$CN):** δ -72.9 (F, d, J -707.2, PF$_6$). **^{31}P NMR (202 MHz; CD$_3$CN):** δ -144.63 (P, sept., J -701.24, PF$_6$). **IR (cm^{-1}):** 1135 (medium, sharp), 1574 (medium, sharp,C=O), 1619 (medium, sharp, C=N), 2964 (medium, sharp, C-H). ESIMS: (+) *m/z* 520 [M-(NCCH$_3$+PF$_6$)], (-) *m/z* 145 [PF$_6$]. ASAP: (+) *m/z* 561 [M$^+$-(PF$_6$)].

5.2.28 Synthesis of [**L1$_a$Pd(3,5-Me$_2$Py)**][PF$_6$]
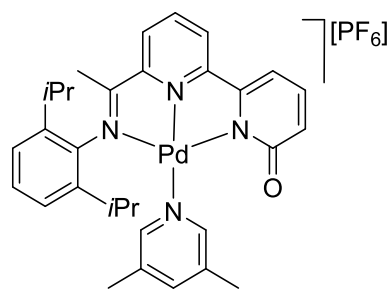
A 100 ml Schlenk flask, equipped with stir bar, was evacuated and backfilled with nitrogen and then charged with **L1$_a$PdCl** (0.050 g, 0.097 mmol, 1 eq.), silver hexafluorophosphate (0.037 g, 0.146 mmol, 1.5 eq.) and dry MeOH (10 ml). The reaction was stirred for 0.5 h before 3,5-lutidine was added (0.011 g, 0.097 mmol, 1 eq.). The reaction mixture was left to stir at room temperature overnight under an atmosphere of nitrogen. The mixture was filtered through celite and celite cake washed with MeOH. The solvent was removed by rotary evaporation to give [**L1$_a$Pd(3,5-Me$_2$Py)**][PF$_6$] as a red solid (0.064 g, 90%). **Mp**: 250 °C (decomp). **^{1}H NMR (400 MHz; MeOD):** δ 8.34 (1H, t, $^3J_{HH}$ = 7.9 Hz , Py/Ar-H), 8.24 (1H, d, $^3J_{HH}$ = 8.4 Hz, Py/Ar-H), 8.11 (1H, d, $^3J_{HH}$ = 8.0 Hz, Py/Ar-H), 7.88 (2H, s, Py-H), 7.42 (1H, t, $^3J_{HH}$ = 8.8 Hz , Py/Ar-H), 7.36 (1H, s, Py-H), 7.22 (IH, t, $^3J_{HH}$ = 7.7 Hz, Py/Ar-H), 7.09 (1H, d, $^3J_{HH}$ = 7.8 Hz, Py/Ar-H) 6.29 (1H, d, $^3J_{HH}$ = 8.8 Hz, Py/Ar-H), 3.10 (2H, sept., $^3J_{HH}$ = 6.3 Hz, CH(CH$_3$)$_2$), 2.44 (3H, s, CH$_3$), 2.02 (6H, s, CH$_3$), 1.14 (6H, d, $^3J_{HH}$ = 6.6 Hz, CH(CH$_3$)$_2$), 1.05 (6H, d, $^3J_{HH}$ = 6.6 Hz, CH(CH$_3$)$_2$). **^{13}C NMR (100 MHz; MeOD):** δ18.2 (CH$_3$-Py), 18.4 (CCH$_3$), 23.6 (CH(CH$_3$)$_2$), 24.9 (CH(CH$_3$)$_2$), 29.8 (CH(CH$_3$)$_2$), 111.9 (CH), 125.5 (CH), 125.7 (CH),

126.5 (CH), 128.5 (CH), 130.6 CH), 135.9 (C), 136.2 (C), 140.1 (CH), 140.6 (C), 141.7 (CH), 143.4 (CH), 149.6 (CH), 154.7 (C), 155.8 (C), 160.2 (C), 171.6 (C), 185.0 (C). **^{19}F NMR (376 MHz; MeOD):** δ -72.1 (F, d, J -707.2, PF$_6$). **^{31}P NMR (202 MHz; MeOD):** δ -144.57 (P, sept., J -702.4, PF$_6$). **IR (cm^{-1}):** 759 (strong, sharp), 1017 (medium, sharp), 1616 (medium, sharp, C=N), 2923 (medium, sharp, C-H). ESIMS: (+) *m/z* 585 [M- PF$_6$], (-) *m/z* 145 [PF$_6$]. HRMS (FAB): C$_{31}$H$_{35}$N$_4$OPdPF$_6$ [M-PF$_6$] 585. Anal. calc. for (C$_{31}$H$_{35}$N$_4$OPd(PF$_6$)$_{1.5}$·8H$_2$O): C 39.29, H 5.42, N 5.91. Found C 39.12, H 5.37 N 4.56%.
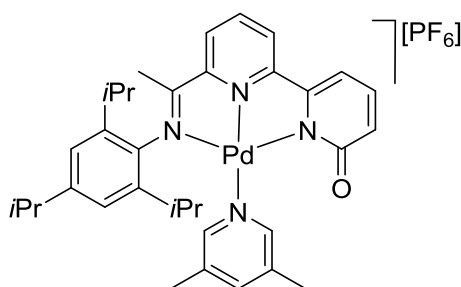
5.2.29 Synthesis of [**L1$_b$**Pd(3,5-Me$_2$Py)][PF$_6$]

A 100 ml Schlenk flask, equipped with stir bar, was evacuated and backfilled with nitrogen and then charged with **L1$_b$**PdCl (0.050 g, 0.090 mmol, 1 eq.), silver hexafluorophosphate (0.034 g, 0.135 mmol, 1.5 eq.) and dry MeOH (10 ml). The reaction was stirred for 0.5 h before 3,5-lutidine (0.010 g, 0.090 mmol, 1 eq.) was added and the mixture left to stir at room temperature overnight under an atmosphere of nitrogen. Then mixture was filtered through celite and the celite cake washed with MeOH. The solvent was removed by rotary evaporation to give [**L1$_b$**Pd(3,5-Me$_2$Py)][PF$_6$] as a red solid (0.018 g, 90%). **Mp**: 250 °C (decomp). **^{1}H NMR (400MHz; MeOD):** δ 8.33 (1H, t, $^3J_{HH}$ = 7.87 Hz, Py-H), 8.22 (IH, dd, $^3J_{HH}$ = 8.4 Hz, $^4J_{HH}$ = 0.9 Hz, Py-H), 8.08 (1H, dd, $^3J_{HH}$ = 7.8 Hz, $^4J_{HH}$ = 0.9 Hz, Py-H), 7.90(2H, s, Py-H), 7.38 (1H,t, $^3J_{HH}$ = 7.9 Hz Py-H), 7.33 (1H, s, Py-H), 7.09 (1H, dd, $^3J_{HH}$ = 6.9 Hz, $^4J_{HH}$ = 1.09 Hz Py-H), 6.94 (2H, s, Ar-H), 6.31 (1H, dd, $^3J_{HH}$ = 8.7 Hz, $^4J_{HH}$ = 1.09 Hz, Py-H), 3.08 (2H, sept., $^3J_{HH}$ = 6.9 Hz, CH(CH$_3$)$_2$), 2.67 (1H, sept., $^3J_{HH}$ = 6.9 Hz, CH(CH$_3$)$_2$), 2.26 (3H, s, CH$_3$), 2.03 (6H, s, CH$_3$), 1.15 (6H, d, $^3J_{HH}$ = 6.7 Hz, CH(CH$_3$)$_2$), 1.11 (6H, d, $^3J_{HH}$ = 6.9 Hz, CH(CH$_3$)$_2$) 1.05 (6H, d, $^3J_{HH}$ = 6.7 Hz, CH(CH$_3$)$_2$). **^{13}C NMR (100 MHz; MeOD):** δ18.2 (CH$_3$-Py), 18.3 (CCH$_3$), 23.6 (CH(CH$_3$)$_2$), 24.9 (CH(CH$_3$)$_2$), 29.8 (CH(CH$_3$)$_2$) 35.4 (CH(CH$_3$)$_2$), 111.9 (CH), 123.4 (CH), 125.4 (CH), 126.4 (CH), 128.4 (CH), 130.7 (C), 140.1 (CH), 140.6 (CH), 141.1 (CH), 141.5 (C), 143.3 (CH), 151.6 (C), 154.7 (C), 171.6 (C), 185.0 (C). **^{19}F NMR (376 MHz; MeOD):** δ -74.73 (F, d, J -718.85, PF$_6$). **^{31}P NMR (202 MHz; MeOD):** δ -144.63

(P, sept., J -701.24, PF$_6$). **IR (cm^{-1}):** 1008 (strong, sharp), 1258 (medium, sharp), 1620 (medium, sharp, C=N), 2963 (medium, sharp, C-H). ESIMS: (+) *m/z* 627 [M-(PF$_6$)], (-) *m/z* 145 [PF$_6$]. HRMS (FAB): C$_{34}$H$_{41}$N$_4$OPdPF$_6$ [M-PF$_6$] 627.
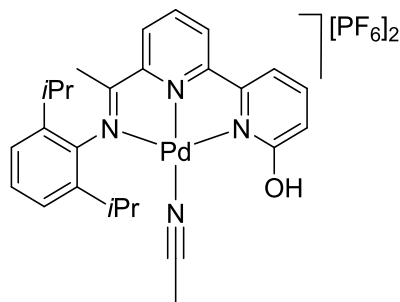

5.2.30 Synthesis [H**L1$_a$**Pd(NCMe)][PF$_6$]$_2$

A 50 ml Schlenk flask, equipped with stir bar, was evacuated and backfilled with nitrogen and then charged was charged with bis(acetonitrile)palladium(II) chloride (0.014 g, 0.054 mmol, 1 eq.), AgPF$_6$ (0.041 g, 0.16 mmol, 3 eq.) and dry acetonitrile (5 ml). The reaction mixture was stirred at room temperature for 1 h before H**L1$_a$** (0.020 g, 0.054 mmol, 1 eq.) was added. The reaction was stirred at room temperature overnight and the resulting filtered through celite. The solvent was removed by rotary evaporation to give [H**L1$_a$**Pd(NCMe)][PF$_6$]$_2$ as a yellow solid (0.039 g, 90%).

Mp: 250 °C (decomp). **^{1}H NMR (400 MHz; CD$_3$CN):** δ 10.77 (1H, s, OH), 8.28 (1H, t, $^3J_{HH}$ = 8.2 Hz, Py-H), 8.06 (1H, d, $^3J_{HH}$ = 8.2 Hz, Py-H), 7.88 (1H, d, $^3J_{HH}$ = 7.9 Hz, Py-H), 7.84 (1H, t, $^3J_{HH}$ = 7.8 Hz, Py-H), 7.51 (1H, , $^3J_{HH}$ = 7.3 Hz, Py-H), 7.29 (1H, t, $^3J_{HH}$ = 7.6 Hz, Ar-H), 7.19 (2H, m, Ar-H), 7.09 (1H, d, $^3J_{HH}$ = 8.4 Hz, Py-H), 3.05 (2H, sept., $^3J_{HH}$ = 6.8 Hz, (CH(CH$_3$)$_2$), 2.23 (3H, s, CCH$_3$), 1.88 (3H, s, NCMe), 1.18 (6H, d, $^3J_{HH}$ = 6.6 Hz, CH(CH$_3$)$_2$), 1.00 (6H, d, $^3J_{HH}$ = 6.6 Hz, CH(CH$_3$)$_2$). **^{13}C NMR (125 MHz; CDCl$_3$):** δ 1.9 (NCCH$_3$), 18.4 (CCH$_3$), 22.5 (CH(CH$_3$)$_2$), 22.8 (CH(CH$_3$)$_2$)), 28.2 CH(CH$_3$)$_2$), 117.1 (CH), 117.4 (CH), 123.9 (CH), 124.6 (CH), 125.9 (CH), 126.2 (CH), 138.8 (C), 139.9 (C), 142.5 (CH), 143.5 (CH), 153.7 (C), 154.8 (C), 157.0 (C), 166.2 (C), 186.2 (C). **^{19}F NMR (376 MHz; CD$_3$CN):** δ -72.8 (F, d, J -704.8, PF$_6$). **^{31}P NMR (161.9 MHz; CD$_3$CN):** δ -144.6 (P, sept., J -707.7, PF$_6$).

IR (cm^{-1}): 1619 (strong, sharp, C=N), 2964 (medium, sharp, C-H), 3415 (medium, broad, O-H). ESIMS: (+) m/z 520 [M-PF$_6$-(HPF$_6$)]. FABMS: *m/z* 480 [M$^+$-(NCMe+PF$_6$+HPF$_6$]. TOFMSASAP: calcd for C$_{26}$H$_{30}$N$_4$OPd(PF$_6$)$_2$ [M$^+$-PF$_6$-(HPF$_6$)]. PF$_6$)$_2$] 521.1380, found 521.1389.

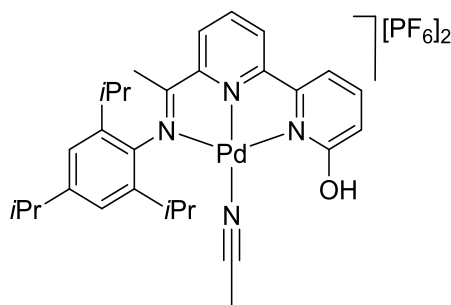5.2.31 Synthesis [H**L1_b**Pd(NCMe)][PF$_6$]$_2$

A 50 ml Schlenk flask, equipped with stir bar, was evacuated and backfilled with nitrogen and then charged with bis(acetonitrile)palladium(II) chloride (0.012 g, 0.048 mmol, 1 eq.), AgPF$_6$ (0.036 g, 0.145 mmol, 3 eq.) and dry acetonitrile (3 ml). The reaction was stirred at room temperature for 1 h before H**L1_b** (0.020g, 0.048 mmol, 1 eq.) was added. The mixture was stirred at room temperature overnight and the resulting precipitate filtered through celite. The solvent was removed by rotary evaporation to give [H**L1_b**Pd(NCMe)][PF$_6$]$_2$ as a yellow solid (0.040 g, 98%).

Mp: 250 °C (decomp). **^{1}H NMR (400 MHz; CD$_3$CN):** δ 10.82 (1H, s, OH), 8.41 (1H, t, $^3J_{HH}$ = 8.2 Hz, Py-H), 8.19 (1H, d, $^3J_{HH}$ = 8.4 Hz, Py-H), 8.02 (1H, d, $^3J_{HH}$ = 7.9 Hz, Py-H), 7.97 (1H, t, $^3J_{HH}$ = 8.2 Hz, Py-H), 7.65 (1H,d , $^3J_{HH}$ = 7.3 Hz, Py-H), 7.20 (2H,s, Ar-H), 7.19 (1H, d, $^3J_{HH}$ = 7.4 Hz, Py-H), 3.16 (2H, sept., $^3J_{HH}$ = 6.8 Hz, CH(CH$_3$)$_2$), 2.89 (1H, sept., $^3J_{HH}$ = 6.8 Hz, CH(CH$_3$)$_2$), 2.36 (3H, s, CCH$_3$), 1.88 (3H, s, NCMe), 1.32 (6H, d, $^3J_{HH}$ = 6.6 Hz, CH(CH$_3$)$_2$), 1.19 (6H, d, $^3J_{HH}$ = 6.8 Hz, CH((C$\underline{H}_3$)$_2$), 1.14 (6H, d, $^3J_{HH}$ = 6.6 Hz, CH(CH$_3$)$_2$). **^{13}C NMR (125 MHz; CDCl$_3$):** δ 1.9 (NC$\underline{C}$H$_3$), 18.3 (C$\underline{C}$H$_3$), 22.5 (CH($\underline{C}$H$_3$)$_2$), 22.7 (CH($\underline{C}$H$_3$)$_2$), 22.8 (CH($\underline{C}$H$_3$)$_2$), 28.2 ($\underline{C}$H(CH$_3$)$_2$), 33.2 ($\underline{C}$H(CH$_3$)$_2$), 117.1 (CH), 122.5 (CH),125.6 (CH), 128.9 (CH), 136.8(C), 137.2 (CH), 139.8 (C) 142.5 (CH), 143.5 (CH), 150.8 (C), 153.8 (C), 154.8 (C), 156.9 (C), 166.1 (C), 186.2 (C). **^{19}F NMR (376 MHz; CD$_3$CN):** δ -72.4 (F, d, J -704.4, PF$_6$). **^{31}P NMR (161.9 MHz; CD$_3$CN):** δ -145.6 (P, sept., J -707.7, PF$_6$). **IR (cm^{-1}):** 1620 (strong, sharp, C=N), 2968 (medium, sharp, C-H), 3612 (medium, broad, O-H). ESIMS: (+) m/z 563 [M$^+$-PF$_6$-(HPF$_6$)]. FABMS: *m/z* 563 [M$^+$-PF$_6$-(HPF$_6$)]. TOFMSASAP: calcd for C$_{29}$H$_{36}$N$_4$OPd(PF$_6$)$_2$ [M$^+$-PF$_6$-(HPF$_6$)] 563.1850, Found 563.1879.

Anal. calc. for (C$_{29}$H$_{36}$N$_4$OPd(PF$_6$)$_2$·3.5CHCl$_3$·8H$_2$O): C 27.59, H 3.95, N 3.96. Found C 27.07, H 3.46 N 4.23%.
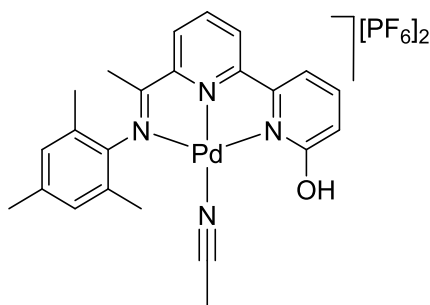
5.2.32 Synthesis [H**L1_c**Pd(NCMe)][PF₆]₂

A 50 ml Schlenk flask, equipped with stir bar, was evacuated and backfilled with nitrogen and then charged was charged with bis(acetonitrile)palladium(II) chloride (0.012g, 0.045 mmol, 1 eq.), AgPF$_6$ (0.034 g, 0.135 mmol, 3 eq.) and dry acetonitrile (5 ml). The reaction was stirred at room temperature for 1 h before H**L1$_c$** (0.015 g, 0.045 mmol, 1 eq.) was added. The mixture was stirred at room temperature overnight and the resulting precipitate filtered through celite. The solvent was removed by rotary evaporation to give [H**L1$_c$**Pd(NCMe)][PF$_6$]$_2$ as a yellow solid (0.029 g, 83%).

Mp: 250 °C (decomp). **^{1}H NMR (400 MHz; CD$_3$CN):** δ 10.58 (1H, s, OH), 8.26 (1H, t, $^3J_{HH}$ = 8.1 Hz, Py-H), 8.04 (1H, d, $^3J_{HH}$ = 8.3 Hz, Py-H), 7.87 (1H, d, $^3J_{HH}$ = 7.4 Hz, Py-H), 7.84 (1H, t, $^3J_{HH}$ = 8.0 Hz, Py-H), 7.51 (1H,d , $^3J_{HH}$ = 7.2 Hz, Py-H), 7.05 (1H, d, $^3J_{HH}$ = 8.4 Hz, Py-H), 6.88 (2H,s, Ar-H), 2.18 (3H, s, CCH$_3$), 2.12 (6H, s, CH$_3$), 2.09 (3H, s, CH$_3$), 1.88 (3H, s, NCMe). **^{13}C NMR (125 MHz; CD$_3$CN):** δ 1.9 (NCCH$_3$), 16.5 (CH$_3$, Ar), 17.4 (CCH$_3$), 19.7 (CH$_3$, Ar), 115.3 (CH), 117.1 (CH), 126.1 (CH), 128.7 (CH), 129.1 (CH), 129.3 (C), 139.2(C), 141.8 (C), 142.6 (C), 143.5 (CH), 144.1 (CH), 153.7 (C), 154.8 (C), 157.0 (C), 165.6 (C), 186.1 (C). **^{19}F NMR (376 MHz; CD$_3$CN):** δ -72.6 (F, d, J -698.0, PF$_6$). **^{31}P NMR (161.9 MHz; CD$_3$CN):** δ -144.51 (P, sept., J -707.5, PF$_6$). **IR (cm^{-1}):** 1619 (strong, sharp, C=N), 2962 (medium, sharp, C-H), 3622 (medium, broad, O-H). ESIMS: (+) m/z 437 [M-(NCCH$_3$+PF$_6$+HPF$_6$)]. ESIMS: (-) m/z 145 [PF$_6$]. FABMS: *m/z* 437 [M-(NCCH$_3$+PF$_6$+HPF6)]. TOFMSASAP: calcd for C$_{23}$H$_{34}$N$_4$OPd(PF$_6$)$_2$ [M$^+$-(PF$_6$+HPF$_6$)] 479.0911, found 479.0942.

5.2.33 Synthesis [H**L1_a**Pd(3,5-Me₂Py)][PF₆]₂
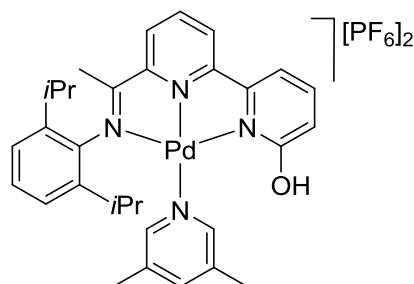
A 50 ml round-bottom flask, equipped with stir bar, was charged with [H**L1_a**Pd(NCMe)][PF₆]₂ (0.012 g, 0.016 mmol), methanol (3 ml) and HPF₆ (1 ml). The reaction mixture was stirred at room temperature overnight and the solvent then removed by rotary evaporation to give [H**L1_a**Pd(3,5-Me₂Py)][PF₆]₂ as a yellow solid (80% conversion). **Mp:** 250 °C (decomp). **¹H NMR (400 MHz; MeOD):** δ 8.24 (2H, m, Py/Ar-H), 8.17 (1H, d, ³J_{HH} = 7.2 Hz, Py/Ar-H), 8.05 (1H, t, ³J_{HH} = 7.9 Hz, Py/Ar-H), 7.90 (1H, d, ³J_{HH} = 7.4 Hz, Py/Ar-H), 7.79 (2H, s, Py-H), 7.34 (1H, t, ³J_{HH} = 7.2 Hz, Py/Ar-H), 7.23 (1H, s, Py-H), 7.21 (1H, d, ³J_{HH} = 7.7 Hz, Py/Ar-H), 7.08 (1H, d, ³J_{HH} = 8.6 Hz, Py/Ar-H), 3.14 (2H, sept., ³J_{HH} = 6.8 Hz, CH(CH₃)₂), 2.71 (3H, s, CCH₃), 2.44 (6H, s, CH₃) 1.29 (6H, d, ³J_{HH} = 6.6 Hz, CH(CH₃)₂), 1.13 (6H, d, ³J_{HH} = 6.6 Hz, CH(CH₃)₂). **¹³C NMR (125 MHz; MeOD):** 18.3 (CCH₃), 23.1 (CH₃-Py), 23.9 (CH(<u>C</u>H₃)₂), 24.2 (CH(<u>C</u>H₃)₂), 29.8 (<u>C</u>H(CH₃)₂), 39.1 (CH), 119.1 (CH), 119.40 (CH), 125.3 (CH), 126.3 (CH), 126.6 (CH), 127.4 (CH) 128.9 (CH), 129.6 (CH), 130.6 (C), 141.8 (CH), 143.9 (C), 145.3 (C), 155.3 (C), 157.9 (C), 168.9 (C), 187.1 (C). **¹⁹F NMR (376 MHz; MeOD):** δ -74.5 (F, d, J -708.06, PF₆). **³¹P NMR (161.9 MHz; MeOD):** δ -144.2 (P, sept., J -703.2, PF₆). **IR (cm⁻¹):** 1629 (strong, sharp, C=N), 2963 (medium, sharp, C-H), 3327 (medium, broad, O-H). ESIMS: (+) m/z 479 [M-(3,5Me₂Py+PF₆+HPF₆]. ESIMS: (-) m/z 145 [PF₆]. TOFMSASAP: calcd for C₃₁H₃₆N₄OPd(PF₆)₂ [M-{(3,5Me₂Py+ PF₆+HPF₆}] 479.1189, found 479.1152.
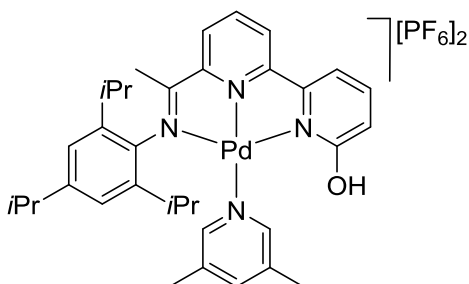
5.2.34 Synthesis [H**L1b**Pd(3,5-Me₂Py)][PF₆]₂

A 50 ml round-bottom flask, equipped with stir bar, was charged with [H**L1b**Pd(NCMe)][PF₆]₂ (0.015 g, 0.019 mmol), methanol (5 ml) and HPF₆ (1 ml). The reaction was stirred at room temperature overnight and the solvent then removed by rotary evaporation to give [H**L1b**Pd(3,5-Me₂Py)][PF₆]₂ as a yellow solid (83% conversion). **Mp:** 250 °C (decomp). **^{1}H NMR (400 MHz; MeOD):** δ 8.41 (2H, m, Py-H), 8.16 (1H, dd, $^3J_{HH}$ = 7.2 Hz, $^4J_{HH}$ = 1.4 Hz, Py-H), 8.04 (1H, t, $^3J_{HH}$ = 8.2 Hz, Py-H), 7.93 (2H, s, Py-H), 7.89 (1H, dd, $^3J_{HH}$ = 7.4 Hz, $^4J_{HH}$ = 0.9 Hz, Py-H), 7.36 (IH, s, Py-H), 7.07 (2H, s, Ar-H), 7.06 (1H, dd, $^3J_{HH}$ = 8.6 Hz, $^4J_{HH}$ = 1.0 Hz, Py-H), 3.12 (2H, sept., $^3J_{HH}$ = 6.9 Hz, CH(CH₃)₂), 2.85 (1H, sept., $^3J_{HH}$ = 6.9 Hz, CH(CH₃)₂), 2.42 (3H, s, CCH₃), 2.35 (6H, s, CH₃) 1.29 (6H, d, $^3J_{HH}$ = 6.8 Hz, CH(CH₃)₂), 1.19 (6H, d, $^3J_{HH}$ = 6.8 Hz, CH(CH₃)₂) 1.13 (6H, d, $^3J_{HH}$ = 6.8 Hz, CH(CH₃)₂). **^{13}C NMR (125 MHz; MeOD):** δ 18.3 (CCH₃), 23.7 (CH₃-Py), 24.2 (CH(<u>C</u>H₃)₂), 24.3 (CH(<u>C</u>H₃)₂), 24.9 (CH(<u>C</u>H₃)₂), 29.8 (<u>C</u>H(CH₃)₂), 35.4 (<u>C</u>H(CH₃)₂), 119.1 (CH), 123.1 (CH), 123.5 (CH), 127.4 (CH), 129.6 (CH), 138.6 (C) 141.4 (CH), 141.6 (C), 143.9 (CH), 145.3 (CH), 149.6 (C), 151.4 (C), 155.6 (C), 157.9 (C), 168.9 (C), 186.9 (C).**^{19}F NMR (376 MHz; MeOD):** δ -74.13 (F, d, J -708.13, PF₆).**^{31}P NMR (161.9 MHz; MeOD):** δ -144.4 (P, sept., J -701.3, PF₆). **IR (cm⁻¹):** 1629 (strong, sharp, C=N), 2963 (medium, sharp, C-H), 3327 (medium, broad, O-H). FABMS: m/z 628 [M-(PF₆+HPF₆)]. TOFMSASAP: calcd for C₃₁H₃₆N₄OPd(PF₆)₂ [M-{(3,5Me₂Py+PF₆+HPF₆)}] 522.1584, found 522.1623.

5.2.35 Synthesis of [H**L1a**PtCl][PtCl₃(DMSO)]
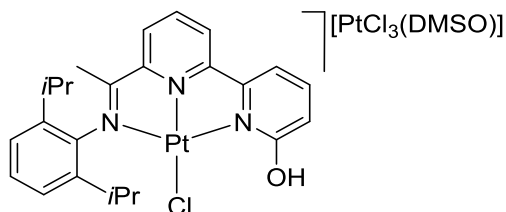
A 50 ml round-bottom flask, was charged with H**L1a** (0.020 g, 0.054 mmol, 1 eq.), chloroform (5 ml) and bis(dimethylsulfoxide)platinum dichloride (0.023 g, 0.054 mmol,

1 eq.). The reaction was stirred at 57 °C overnight and the solvent removed by rotary evaporation to give [H**L1$_a$**PtCl][DMSOPtCl$_3$] as a red solid (0.050 g, 92%).

Mp: 230 °C (decomp). **^{1}H NMR (400 MHz; CDCl$_3$):** δ 11.05 (1H, s, OH), 8.89 (2H, m, Py/Ar-H), 8.58 (1H, d, $^3J_{HH}$ = 7.4 Hz, Py/Ar-H), 8.22 (1H, d, $^3J_{HH}$ = 6.8 Hz, Py/Ar-H), 8.11 (1H, t, $^3J_{HH}$ = 8.6 Hz, Py/Ar-H), 7.42 (1H, t, $^3J_{HH}$ = 8 Hz, Py/Ar-H), 7.30 (2H, d, $^3J_{HH}$ = 7.8 Hz, Py/Ar-H), 7.11 (1H, d, $^3J_{HH}$ = 8.6 Hz, Py/Ar-H), 3.36 (6H, s, DMSO), 3.07 (2H, sept., $^3J_{HH}$ = 6.8 Hz, CH(CH$_3$)$_2$), 2.53 (3H, s, CCH$_3$), 1.35 (6H, d, $^3J_{HH}$ = 6.8 Hz, CH(CH$_3$)$_2$), 1.21 (6H, d, $^3J_{HH}$ = 6.8 Hz, CH(CH$_3$)$_2$). **^{13}C NMR (125 MHz; CDCl$_3$):** δ 19.37 (CCH$_3$), 23.6 (CH(CH$_3$)$_2$), 23.9 (CH(CH$_3$)$_2$), 28.6 (CH(CH$_3$)$_2$), 44 (DMSO), 119.0 (CH), 120.1 (CH), 124.3 (CH), 128.2 (CH), 129.8 (CH), 138.2 (C), 140.7 (C), 143.7 (CH), 144.1 (CH), 156.1 (C), 168.5 (C). **IR (cm^{-1}):** 1630 (strong, sharp, C=N), 2969 (medium, sharp, C-H), 3663 (medium, broad, O-H). ESIMS: (+) m/z 604 [M-(DMSOPtCl$_3$)]. FABMS: *m/z* 604 [M$^+$-(DMSOPtCl$_3$)]. TOFMSASAP: calcd for C$_{24}$H$_{27}$N$_3$OPt$_2$Cl$_4$DMSO [M$^+$-(DMSOPtCl$_3$)] 604.1492, Found 604.1478. Anal. calc. for (C$_{26}$H$_{33}$N$_3$O$_2$Pt$_2$Cl$_4$S·1.5 NCMe): C 33.33, H 3.62, N 6.0. Found C 33.62, H 3.24, N 4.95%.

5.2.36 Synthesis of [H**L1$_b$**PtCl][PtCl$_3$(DMSO)]

A 50 ml round-bottom flask, was charged with H**L1$_b$** (0.020 g, 0.048 mmol, 1 eq.), chloroform (5 ml) and bis(dimethylsulfoxide)platinum dichloride (0.020g, 0.048 mmol, 1 eq.). The reaction was stirred at 57 °C overnight and the solvent then removed by rotary evaporation to give [H**L1$_b$**PtCl][PtCl$_3$(DMSO)] as a red solid (0.048 g, 96%).

Mp: 230 °C (decomp). **^{1}H NMR (400 MHz; CDCl$_3$):** δ 10.99 (1H, s, OH), 8.85 (1H, d, $^3J_{HH}$ = 8.4 Hz, Py/Ar-H), 8.83 (1H, t, $^3J_{HH}$ = 8 Hz 8, Py/Ar-H), 8.57 (1H, d, $^3J_{HH}$ = 7.5 Hz, Py/Ar-H), 8.24 (1H, d, $^3J_{HH}$ = 7.4 Hz, Py/Ar-H), 8.06 (1H, t, $^3J_{HH}$ = 7.8 Hz, Py/Ar-H), 7.04 (2H, s, Ar-H), 7.01 (1H, d, $^3J_{HH}$ = 6.8 Hz, Py/Ar-H), 3.30 (6H, s, DMSO), 2.96 (2H, sept., $^3J_{HH}$ = 6.8 Hz, CH(CH$_3$)$_2$), 2.88 (1H, sept., $^3J_{HH}$ = 6.8 Hz, CH(CH$_3$)$_2$) 2.47 (3H, s, CCH$_3$), 1.27 (6H, d, $^3J_{HH}$ = 6.8 Hz, CH(CH$_3$)$_2$), 1.22 (6H, d, $^3J_{HH}$ = 6.8 Hz, CH((CH$_3$)$_2$), 1.13 (6H, d, $^3J_{HH}$ = 6.8 Hz, CH(CH$_3$)$_2$). **^{13}C NMR (125 MHz; CDCl$_3$):** δ 19.4 (CCH$_3$), 23.7 (CH(CH$_3$)$_2$), 23.9 (CH(CH$_3$)$_2$), 24.1 (CH(CH$_3$)$_2$), 28.6 (CH(CH$_3$)$_2$), 34.1

(C̲H(CH$_3$)$_2$), 44 (DMSO), 118.9 (CH), 119.9 (CH), 122.0 (CH), 127.9 (CH), 129.7 (CH), 136.2 (C), 140.3 (C), 143.7 (CH), 144.1 (CH), 150.2 (C), 153.3 (C), 154.5 (C), 155.9 (C), 168.5 (C), 184.6 (C). **IR (cm^{-1}):** 1631 (strong, sharp, C=N), 2987 (medium, sharp, C-H), 3693 (medium, broad, O-H). ESIMS: (+) m/z 645 [M-(DMSOPtCl$_3$)]. ESIMS: (-) *m/z* 644 [M-(DMSOPtCl$_3$)]. FABMS: *m/z* 646 [M$^+$-(DMSOPtCl$_3$)]. TOFMSASAP: calcd for C$_{27}$H$_{33}$N$_3$OPt$_2$Cl$_4$DMSO [M$^+$-(DMSOPtCl$_3$)] 646.1962, Found 646.1982. Anal. calc. for (C$_{29}$H$_{39}$N$_3$O$_2$Pt$_2$Cl$_4$S): C 33.96, H 3.83, N 4.10. Found C 34.03, H 3.85, N 4.15%.

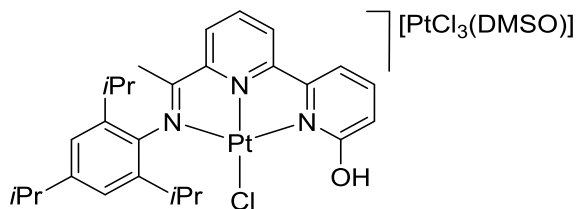## 5.2.37 Synthesis of [H**L1$_c$**PtCl][PtCl$_3$(DMSO)]
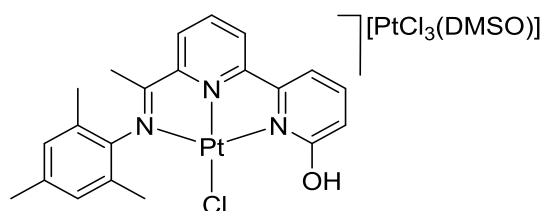
A 50 ml round-bottom flask, was charged with H**L1$_c$** (0.023 g, 0.054 mmol, 1 eq.), chloroform (5 ml) and bis(dimethylsulfoxide)platinum dichloride (0.023 g, 0.054 mmol, 1 eq.). The reaction was stirred at 57 °C for 2 days and the solvent then removed by rotary evaporation to give [H**L1$_c$**PtCl][PtCl$_3$(DMSO)] as a red solid (60% conversion).

Mp: 230 °C (decomp). **^{1}H NMR (400 MHz; CDCl$_3$):** δ 11.01 (1H, s, OH), 8.03 (1H, d, $^3J_{HH}$ = 6.6 Hz Py/Ar-H), 7.94 (1H, m, Py/Ar-H), 7.46 (1H, t, $^3J_{HH}$ = 7.9 Hz, Py/Ar-H), 6.81 (1H, d, $^3J_{HH}$ = 6.7 Hz, Py/Ar-H), 6.69 (2H, s, Ar), 6.63 (1H, d, $^3J_{HH}$ = 8.4 Hz, Ar-H), 2.54 (6H, s, DMSO), 2.17 (3H, s, CCH$_3$), 2.13 (3H, s, CH$_3$), 2.09 (6H, s, CH$_3$). **IR (cm^{-1}):** 1629 (strong, sharp, C=N), 2962 (sharp, C-H), 3350 (medium, broad, O-H). ESIMS: (+) m/z 526 [M-(Cl+DMSOPtCl$_3$)]. FABMS: *m/z* 526 [M$^+$-(Cl+DMSOPtCl$_3$)]. TOFMSASAP: calcd for C$_{21}$H$_{21}$N$_3$OPt$_2$Cl$_4$DMSO [M-(Cl+DMSOPtCl$_3$)] 526.1256, Found 526.1283.

5.2.38 Synthesis of H**L1$_a$**RuCl$_2$(PPh$_3$)
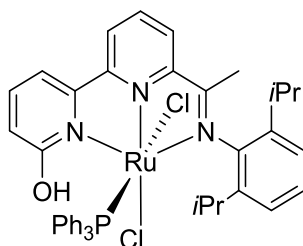
A 50 ml Schlenk flask, equipped with stir bar, was evacuated and backfilled with nitrogen and then charged with H**L1$_a$** (0.030 g, 0.080 mmol, 1 eq.),

dichlorotris(triphenylphosphine) ruthenium(II) (0.077 g, 0.080 mmol, 1 eq.) and dry toluene (10 ml). The reaction was stirred and heated to reflux overnight under an atmosphere of nitrogen affording a purple precipitate which was then filtered through celite and washed with toluene. The precipitate was extracted with dichloromethane and the solvent removed by rotary evaporation to give $HL1_aRuCl_2(PPh_3)$ as a purple powder (0.062 g, 95%). **M.P**: > 260°C. **^{1}H NMR (400 MHz; CDCl$_3$):** δ 11.73 (1H, s, OH), 8.01 (1H, dd, $^3J_{HH}$ = 6.1 Hz, $^4J_{HH}$ = 1.3 Hz, Py/Ar-H), 7.77 (IH, d, $^3J_{HH}$ = 6.2 Hz, Py/Ar-H), 7.76 (1H, m, Ar-H), 7.50 (1H, d, $^3J_{HH}$ = 7.6 Hz, Py/Ar-H), 7.34 (4H, m, PPh$_3$), 7.15 (4H, m, Py/Ar-H), 6.90 (11H, m, PPh$_3$),6.29 (1H, dd, $^3J_{HH}$ = 8.1 Hz, $^4J_{HH}$ = 1.2 Hz, Py/Ar-H), 4.89 (1H, sept., $^3J_{HH}$ = 6.6 Hz, CH(CH$_3$)$_2$), 2.59 (3H, s, CH$_3$), 2.12 (1H, sept., $^3J_{HH}$ = 6.7 Hz, CH(CH$_3$)$_2$), 1.59 (3H, d, $^3J_{HH}$ = 6.5 Hz, CH(CH$_3$)$_2$), 0.99 (3H, d, $^3J_{HH}$ = 6.7 Hz, CH(CH$_3$)$_2$), 0.85 (3H, d, $^3J_{HH}$ = 6.5 Hz, CH(CH$_3$)$_2$), - 0.44 (3H, d, $^3J_{HH}$ = -6.6 Hz, CH(CH$_3$)$_2$). **^{31}P NMR (161 MHz; CDCl$_3$):** δ 40.9(1P, s). **IR (cm^{-1}):** 1265 (medium, sharp), 1362 (medium, sharp), 1483 (strong, sharp), 1554 (medium, sharp), 1635 (medium, sharp, C=N), 2987 (medium, sharp, C-H), 3694 (weak, sharp, O-H). **ESIMS**: (+) *m/z* 738 [M-2Cl] $^+$. **FABMS**: *m/z* 738 [M-2Cl]$^+$. **HRMS (FAB)**: calcd for C$_{42}$H$_{42}$N$_3$ORuCl$_2$P [M-2Cl]$^+$ 738.2041, Found 738.2064. Anal. calc. for (C$_{42}$H$_{42}$N$_3$ORuCl$_2$·CHCl$_3$·NCCH$_3$): C 55.77, H 4.89, N 5.78. Found C 55.72, H 4.32, N 5.31%.

5.2.39 Synthesis of $HL1_bRuCl_2(PPh_3)$

A 50 ml Schlenk flask, equipped with stir bar, was evacuated and backfilled with nitrogen then charged with $HL1_b$ (0.030 g, 0.072 mmol, 1 eq.), dichlorotris(triphenylphosphine) ruthenium(II) (0.069 g, 0.072 mmol, 1 eq.) and dry toluene (10 ml). The reaction was stirred and heated to reflux overnight under an atmosphere of nitrogen affording a purple precipitate which was then filtered through celite and washed with toluene. The precipitate was extracted with dichloromethane and the solvent removed by rotary evaporation to give $HL1_bRuCl_2(PPh_3)$ as a purple powder (0.058 g, 97%). **M.P**: > 260°C. **^{1}H NMR (400 MHz; CDCl$_3$):** δ 11.76 (1H, s, OH), 7.99 (1H, t, $^3J_{HH}$ = 4.4 Hz, Py/Ar-H),

7.76 (IH, d, $^3J_{HH}$ =7.1 Hz, Py/Ar-H), 7.75 (1H, s, Ar-H), 7.33 (2H, m, Py/Ar-H), 7.14 (5H, m, PPh₃), 6.99 (1H, s, Ar-H), 6.89 (10H, m, PPh₃), 6.69 (1H, d, $^3J_{HH}$ = 6.2 Hz, Py/Ar-H), 6.29 (1H, d, $^3J_{HH}$ = 6.9 Hz, Py/Ar-H), 4.87 (1H, sept., $^3J_{HH}$ = 6.6 Hz, CH(CH₃)₂), 2.97 (1H, sept., $^3J_{HH}$ = 6.7 Hz, CH(CH₃)₂), 2.56 (3H, s, CH₃), 2.09 (1H, sept., $^3J_{HH}$ = 6.7 Hz, CH(CH₃)₂), 1.59 (3H, d, $^3J_{HH}$ = 6.6 Hz, CH(CH₃)₂), 1.35 (3H, d, $^3J_{HH}$ = 7.0 Hz, CH(CH₃)₂), 1.34 (3H, d, $^3J_{HH}$ = 7.0 Hz, CH(CH₃)₂), 0.98 (3H, d, $^3J_{HH}$ = 6.7 Hz, CH(CH₃)₂), 0.86 (3H, d, $^3J_{HH}$ = 6.5 Hz, CH(CH₃)₂), - 0.46 (3H, d, $^3J_{HH}$ = 6.7 Hz, CH(CH₃)₂). **^{31}P NMR (161 MHz; CDCl₃):** δ 40.9 (1P, s). **IR (cm^{-1}):** 1319 (medium, sharp), 1362 (medium, sharp), 1483 (strong, sharp), 1599 (medium, sharp), 1633 (medium, sharp, C=N), 2987 (medium, sharp, C-H), 3687 (weak, sharp, O-H). **ESIMS**: (+) *m/z* 778 [M-2Cl]. **FABMS**: *m/z* 778 [M-2Cl]. **HRMS (FAB):** calcd. for C₄₅H₄₈N₃ORuCl₂P [M-2Cl] 778.2500, Found 778.2493.
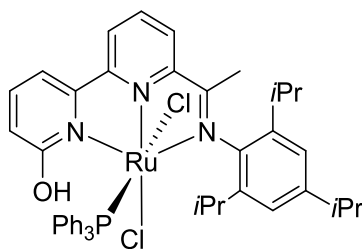
5.2.40 Synthesis of H**L1c**RuCl₂(PPh₃)

 A 50 ml Schlenk flask, equipped with stir bar, was evacuated and backfilled with nitrogen then charged with H**L1c** (0.030 g, 0.084 mmol, 1 eq.), dichlorotris(triphenylphosphine) ruthenium(II) (0.080 g, 0.084 mmol, 1 eq.) and dry toluene (10 ml). The reaction was stirred and heated at reflux overnight under an atmosphere of nitrogen affording a purple precipitate which was then filtered through celite and washed with toluene. The precipitate was then extracted with dichloromethane and the solvent removed by rotary evaporation to give H**L1c**RuCl₂(PPh₃) as a purple powder (0.040 g, 60%). **M.P**: > 260 °C. **^{1}H NMR (400 MHz; CDCl₃):** δ 11.43 (1H, s, OH), 7.92 (1H, d, $^3J_{HH}$ = 7.2 Hz, Py-H), 7.72 (2H, m, Py-H), 7.45 (1H, t, $^3J_{HH}$ = 7.6 Hz, Py-H), 7.32 (1H, d, $^3J_{HH}$ = 6.67 Hz, Py-H), 7.19 (5H, m, PPh₃), 7.08 (1H, s, Ar-H), 6.93 (10H, m, PPh₃), 6.42 (1H, d, $^3J_{HH}$ = 8.0 Hz, Py-H), 6.31 (1H, s, Ar-H), 2.80 (3H, s, CCH₃), 2.41 (3H, s, CH₃), 2.32 (3H, s, CH₃), 0.98 (3H, s, CH₃). **^{31}P NMR (161 MHz; CDCl₃):** δ 40.8 (1P, s). **IR (cm^{-1}):** 1262 (medium, sharp), 1554 (medium, sharp), 1637 (medium, sharp, C=N), 2981 (medium, sharp, C-H), 3636 (weak, sharp, O-H). **ESIMS**: (+) *m/z* 694 [M-2Cl]$^+$. **FABMS**: *m/z* 730

[M-Cl]⁺. **HRMS (TOF)**: calcd for $C_{39}H_{36}N_3ORuCl_2P$ [M-2Cl]⁺ 694.1561, Found 694.1598.
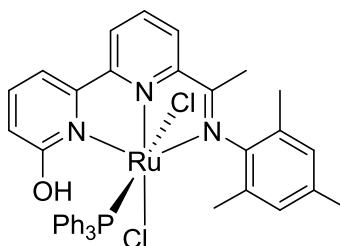
5.2.41 Synthesis of **L1$_H$**RuCl$_2$(PPh$_3$)
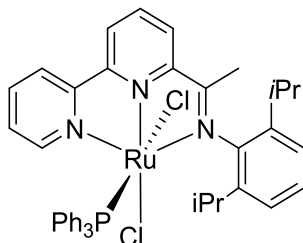
A 50 ml Schlenk flask, equipped with stir bar, was evacuated and backfilled with nitrogen and then charged with **L1$_H$** (0.025 g, 0.076 mmol, 1 eq.), dichlorotris(triphenylphosphine) ruthenium(II) (0.072 g, 0.076 mmol, 1 eq.) and dry toluene (5 ml). The reaction was stirred and heated to reflux overnight under an atmosphere of nitrogen affording a purple precipitate was then filtered through celite and washed with toluene. The precipitate was then extracted with dichloromethane. The solvent was removed by rotary evaporation to give **L1$_H$**RuCl$_2$(PPh$_3$) as a purple powder (0.040 g, 69%). **M.P**: > 260 °C. **¹H NMR (400 MHz; CDCl$_3$):** δ 8.35 (1H, dd, $^3J_{HH}$ = 6.4 Hz, Py-H), 7.96 (IH, d, $^3J_{HH}$ = 7.3 Hz, Py/Ar-H), 7.80 (1H, d, $^3J_{HH}$ = 7.2 Hz, Py/Ar-H), 7.67 (3H, m, Py/Ar-H), 7.44 (1H, dd, $^3J_{HH}$ = 6.4 Hz, $^4J_{HH}$ = 1.4 Hz, Py/Ar-H), 7.39 (1H, td, $^3J_{HH}$ = 7.6 Hz, $^4J_{HH}$ = 1.6 Hz, Py/Ar-H), 7.25 (1H, t, $^3J_{HH}$ = 7.8 Hz, Py/Ar-H), 7.10 (7H, m, PPh$_3$), 6.8 (8H, m, PPh$_3$), 6.55 (1H, td, $^3J_{HH}$ = 7.1 Hz, $^4J_{HH}$ = 1.3 Hz, Py/Ar-H), 4.82 (1H, sept., $^3J_{HH}$ = 6.4 Hz, CH(CH$_3$)$_2$), 2.49 (3H, s, CH$_3$), 2.04 (1H, sept., $^3J_{HH}$ = 6.6 Hz, CH(CH$_3$)$_2$), 1.54 (3H, d, $^3J_{HH}$ = 6.6 Hz, CH(CH$_3$)$_2$), 0.93 (3H, d, $^3J_{HH}$ = 7.1 Hz, CH(CH$_3$)$_2$), 0.76 (3H, d, $^3J_{HH}$ = 6.6 Hz, CH(CH$_3$)$_2$), - 0.55 (3H, d, $^3J_{HH}$ = -6.6 Hz, CH(CH$_3$)$_2$). **³¹P NMR (161 MHz; CDCl$_3$):** δ 40.1 (1P, s). **IR (cm⁻¹):** 1388 (medium, sharp), 1563 (medium, sharp), 1625 (medium, sharp, C=N), 2898 (medium, sharp, C-H). **ESIMS**: (+) *m/z* 756 [M-Cl]⁺. **FABMS**: *m/z* 756 [M-Cl]⁺. **HRMS (TOF)**: calcd for $C_{42}H_{42}N_3RuCl_2P$ [M-Cl]⁺ 756.1848, found 756.1879.

5.3 Experimental procedures for Chapter 3

PART 1

5.3.1 Synthesis of 2-bromo-6-methoxypyridine (**I**)

See 5.2.1 for the experiment.

5.3.2 Synthesis of 1-(6-methoxypyridin-2-yl)ethanone (**III**)
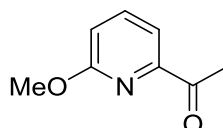
A 250 ml three necked round-bottom flask, equipped with stir bar and dropping funnel, was evacuated and backfilled with nitrogen. The flask was charged with dry THF (80 ml), 2-bromo-6-methoxypyridine (6.00 g, 31.91 mmol) under a nitrogen atmosphere. The mixture was cooled to -78 °C before n-BuLi (21.9 ml, 35.11 mmol, 1.1 eq) was added dropwise over 30 min using the attached drop-in funnel affording a dark-green solution. The reaction mixture was stirred for 1 h at -78 °C before freshly distilled DMA (3.4 ml, 35.11 mmol, 1.1 eq) was added dropwise. The reaction mixture was stirred for another 1 h at -78 °C before cooling was stopped and stirring was continued at room temperature overnight forming an orange solution. Upon reaction completion, the reaction was quenched with the addition of aqueous NH$_4$Cl (20%, 50 ml) solution. The reaction mixture was extracted with Et$_2$O (3 x 50 ml). The combined organic layers were washed with water (3 x 50 ml) and then dried over MgSO$_4$. The organic liquid was then concentrated under reduced pressure to give a red/brown oil (4.4 g, 92%). **^{1}H NMR (400 MHz; CDCl$_3$):** δ 7.68 (1H, t, $^3J_{HH}$ = 8.0 Hz, Py-H), 7.62 (1H, d, $^3J_{HH}$ = 7.9 Hz, Py-H), 6.92 (1H, d, $^3J_{HH}$ = 7.8 Hz, Py-H), 4.00 (3H, s, O<u>Me</u>), 2.67 (3H, s, CC<u>H</u>$_3$). The ^{1}H NMR data is consistent with that in the literature.[6,7]

5.3.3 Synthesis of 6-acetylpyridin-2(1H)-one (**IV**)
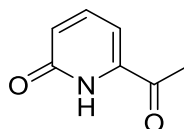
A 100 ml round-bottom flask, equipped with stir bar and condenser, was charged with 1-(6-methoxypyridin-2-yl)ethanone (**III**) (4.00 g, 26.5 mmol) and HBr in glacial AcOH (45%) (60 ml, 318 mmol, 12.0 eq) under an atmosphere open to the air. The reaction mixture was stirred and heated to reflux for 4 h. Upon reaction completion, the mixture

was cooled to room temperature, poured into an ice/water bath and neutralised (pH 6-7) using a solution of aqueous NaOH (20%). The solution was extracted with Et_2O (6 x 100 ml) and the aqueous layer concentrated to give a green solid. The residue was extracted with reagent grade acetone (5 x 50 ml) and concentrated under reduced pressure to give a beige dusty solid (3.30 g, 92%). **^{1}H NMR (400 MHz; MeOD):** δ 7.70 (1H, t, $^3J_{HH}$ = 8.0 Hz, Py-H), 7.20 (1H, d, $^3J_{HH}$ = 8.0 Hz, Py-H), 6.78 (1H, d, $^3J_{HH}$ = 8.0 Hz, Py-H), 2.56 (3H, s, CCH_3). **^{1}H NMR (400 MHz; CDCl₃):** δ 7.48 (1H, t, $^3J_{HH}$ = 8.0 Hz, Py-H), 6.87 (1H, d, $^3J_{HH}$ = 8.0 Hz, Py-H), 6.82 (1H, d, $^3J_{HH}$ = 8.0 Hz, Py-H), 2.52 (3H, s, CCH_3). The ^{1}H NMR data is consistent with that previously reported.[6,8]

5.3.4 Synthesis of H**L2**$_a$
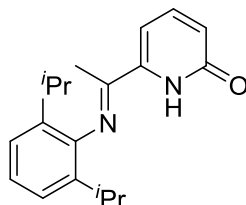
A 50 ml round-bottom flask, equipped with stir bar, was charged with **IV** (1.00 g, 7.3 mmol, 1 eq) and *n*-BuOH (20 ml). 2,6-Diisopropylaniline (1.90 g, 10.9 mmol, 1.5 eq) and *p*-toluenesulfonic acid (0.01 g, 0.073 mmol, 0.01 eq.) were then added. A Dean Stark apparatus with condenser was then attached to the flask and the reaction mixture stirred and heated to reflux for 3 days. Upon reaction completion, the mixture was cooled to room temperature and the solvent concentrated under reduced pressure. Petroleum ether (25 ml) was then added to induce precipitation of a yellow solid. The solid was filtered, washed with more petroleum ether and dried to give H**L2**$_a$ as a yellow powder (1.80 g, 82%). **^{1}H NMR (400 MHz; CDCl₃):** δ 10.33 (1H, s, NH), 7.48 (1H, t, $^3J_{HH}$ = 8 Hz, Py/Ar-H), 7.15 (3H, m, Py/Ar-H), 6.75 (1H, d, $^3J_{HH}$ = 7.5 Hz, Py/Ar-H), 6.64 (1H, d, $^3J_{HH}$ = 7.8 Hz, Py/Ar-H), 2.56 (2H, sept., $^3J_{HH}$ = 6.5 Hz, $CH(CH_3)_2$), 2.00 (3H, s, CCH_3), 1.11 (12H, d, $^3J_{HH}$ = 6.6 Hz, $CH(CH_3)_2$).

The ^{1}H NMR data are consistent with that described by Huang *et al*.[8]

5.3.5 Synthesis of H**L2**_b

5.3.5 Synthesis of HL2$_b$

A 50 ml round-bottom flask, equipped with stir bar, was charged with **IV** (1.00 g, 7.3 mmol, 1 eq), *n*-BuOH (20 ml), 2,4,6-triisopropylaniline (2.40 g, 10.9 mmol, 1.5 eq) and *p*-toluenesulfonic acid (0.01 g, 0.073 mmol, 0.01 eq.). A Dean Stark apparatus with condenser was then attached to the flask and the reaction mixture stirred and heated to reflux for 3 days. Upon reaction completion, the mixture was cooled to room temperature and the solvent concentrated under reduced pressure. Petroleum ether (25 ml) was then added to induce precipitation of a yellow solid. The solid was filtered, washed with more petroleum ether and dried to give HL2$_b$ as a yellow powder (2.20 g, 89%). **M.P**: 161-163 °C. **^{1}H NMR (400 MHz; CDCl$_3$):** δ 10.33 (1H, s, NH), 7.48 (1H, t, $^3J_{HH}$ = 8.2 Hz, Py-H), 6.99 (2H, s, Ar-H), 6.75 (1H, d, $^3J_{HH}$ = 8 Hz, Py-H), 6.64 (1H, d, $^3J_{HH}$ = 7.7 Hz, Py-H), 2.89 (1H, sept., $^3J_{HH}$ = 6.9 Hz, CH(CH$_3$)$_2$), 2.54 (2H, $^3J_{HH}$ = 6.9 Hz, CH(CH$_3$)$_2$), 2.01 (3H, s, CCH$_3$), 1.27 (6H, d, $^3J_{HH}$ = 6.8 Hz, CH(CH$_3$)$_2$), 1.11 (12H, d, $^3J_{HH}$ = 6.9 Hz, CH(CH$_3$)$_2$). **^{13}C NMR (100 MHz; CDCl$_3$):** δ 16.3 (CCH$_3$), 23.3 (CH(CH$_3$)$_2$), 23.8 (CH(CH$_3$)$_2$), 24.6 (CH(CH$_3$)$_2$), 28.8 (CH(CH$_3$)$_2$), 34.4 (CH(CH$_3$)$_2$), 107.1 (CH), 121.4 (CH), 125.3 (CH), 136.1 (C), 140.5 (CH), 141.2 (C), 142.3 (C), 145.3 (C), 158.3 (C), 162.8 (C). **IR (cm^{-1}):** 2958 (medium, sharp, C-H), 1651 (strong, sharp, C=N$_{imine}$), 1454 (medium, sharp), 1289 (medium, strong). ESIMS: (+) *m/z* 339 [M+H]. HRMS (TOF): calculated for C$_{22}$H$_{31}$N$_2$O [M+H], 339.2436, found: 339.2430.

5.3.6 Synthesis of H**L2**_c
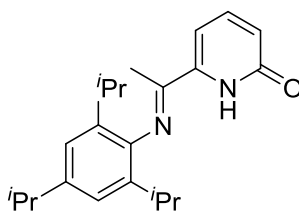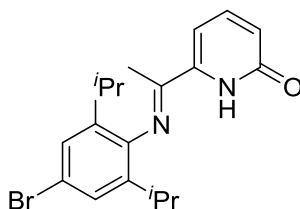
5.3.6 Synthesis of HL2$_c$

A 50 ml round-bottom flask, equipped with stir bar, was charged with **IV** (1.00 g, 7.3 mmol, 1 eq), *n*-BuOH (20 ml), 2,6-diisopropyl-4-bromoaniline (2.8 g, 10.9 mmol, 1.5 eq) and *p*-toluenesulfonic acid (0.01 g, 0.073 mmol, 0.01 eq.). A Dean Stark apparatus with condenser was then attached to the flask and the reaction mixture stirred and heated to

reflux for 3 days. Upon reaction completion, the mixture was cooled to room temperature and the solvent concentrated under reduced pressure. Petroleum ether (25 ml) was then added to induce precipitation of a yellow solid. The solid was filtered, washed with more petroleum ether and dried to give H**L2**$_c$ as a brown powder (2.30 g, 85%). **M.P**: 161-162 °C. **^{1}H NMR (400 MHz; CDCl$_3$):** δ 10.17 (1H, s, NH), 7.42 (1H, t, $^3J_{HH}$ = 8 Hz, Py-H), 7.19 (2H, s, Ar-H), 6.70 (1H, d, $^3J_{HH}$ = 8.6 Hz, Py-H), 6.59 (1H, d, $^3J_{HH}$ = 6.8 Hz, Py-H), 2.46 (2H, sept., $^3J_{HH}$ = 6.8 Hz, CH(CH$_3$)$_2$), 1.94 (3H, s, CCH$_3$), 1.04 (12H, d, $^3J_{HH}$ = 6.9 Hz, CH(CH$_3$)2). **^{13}C NMR (100 MHz; CDCl$_3$):** δ 15.9 (CCH$_3$), 22.6 (CH(CH$_3$)$_2$), 23.2 (CH(CH$_3$)$_2$), 28.5 (CH(CH$_3$)$_2$), 107.1 (CH), 118.2 (C), 125.4 (CH), 126.5 (CH), 138.6 (CH), 139.9 (C), 140.4 (C), 143.2 (C), 158.7 (C), 162.2 (C). **IR (cm^{-1}):** 2963 (medium, sharp, C-H), 1652 (strong, sharp, C=N$_{imine}$), 1454 (medium, sharp), 1368 (medium, strong), 1289 (m, C-O), 877 (w, C-N), 794 (strong, sharp). ESIMS: (+) *m/z* 377 [M+H]. ESIMS: (-) *m/z* 375 [M-H]. HRMS (TOF+ESI) calculated for C$_{19}$H$_{23}$N$_2$OBr [M] 375.1072, Found: 375.1066.

5.3.7 Synthesis of (**L2**$_a$Pd)$_2$(OH)(OAc)
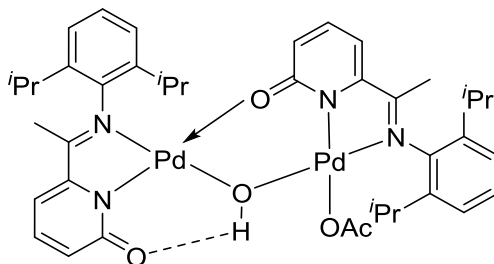
A small dry Schlenk flask, equipped with stir bar, was charged with H**L2**$_a$ (0.070 g, 0.236 mmol), Pd(OAc)$_2$ (0.053 g, 0.236 mmol) and dry distilled toluene (10 ml). The reaction mixture was stirred overnight at room temperature resulting in a red solution after 24 h. The solvent was removed by rotary evaporation to give a red powder (0.020 g, 98%). **M.P**: > 250 °C. **^{1}H NMR (400 MHz; CD$_2$Cl$_2$):** δ 7.44 (1H, s, OH), 7.24 (3H, m, Py/Ar-H), 7.23 (1H, d, $^3J_{HH}$ = 7.5 Hz, Py/Ar-H), 7.21 (2H, m, Py/Ar-H), 7.17 (2H, m, Py/Ar-H), 6.64 (1H, d, $^3J_{HH}$ = 7.8 Hz, Py/Ar-H), 6.62 (1H, d, $^3J_{HH}$ = 6.9 Hz, Py/Ar-H), 6.59 (1H, d, $^3J_{HH}$ = 7.7 Hz, Py/Ar-H), 6.56 (1H, d, $^3J_{HH}$ = 7.9 Hz, Py/Ar-H), 3.23 (2H, sept., $^3J_{HH}$ = 6.7 Hz, CH(CH$_3$)$_2$), 3.18 (2H, sept., $^3J_{HH}$ = 6.7 Hz, CH(CH$_3$)$_2$), 1.94 (3H, s, CCH$_3$), 1.93 (3H, s, CCH$_3$), 1.87 (3H, s, OAc), 1.37 (6H, d, $^3J_{HH}$ = 7.0 Hz, CH(CH$_3$)$_2$), 1.22 (6H, d, $^3J_{HH}$ = 6.8 Hz, CH(CH$_3$)$_2$), 1.17 (6H, d, $^3J_{HH}$ = 6.8 Hz, CH(CH$_3$)$_2$), 1.73 (6H, d, $^3J_{HH}$ = 7.0 Hz, CH(CH$_3$)$_2$). **^{13}C NMR (125 MHz; CD$_2$Cl$_2$):** δ 16.4 (CCH$_3$), 17.5 (CCH$_3$), 18.1

(OAc), 20.9 (CH($\underline{C}$H$_3$)$_2$), 22.5 (CH($\underline{C}$H$_3$)$_2$), 22.7 (CH($\underline{C}$H$_3$)$_2$), 23.2 (CH($\underline{C}$H$_3$)$_2$), 27.6 ($\underline{C}$H(CH$_3$)$_2$), 27.8 ($\underline{C}$H(CH$_3$)$_2$), 111.1 (CH), 113.6 (CH), 122.5 (CH),122.8 (CH), 125.2 (CH), 126.9 (CH), 127.0 (CH), 135.2 (C), 136.0 (CH), 139.2 (CH), 140.0 (C), 152.3 (C), 153.3 (C), 175.9 (C), 176.5 (C). **IR (cm^{-1}):** 1614 (strong, sharp, C=N), 2962 (medium, sharp, C-H), 3670 (medium, broad). ESIMS: (+) m/z 819 [M$^+$-OAc]. FABMS: *m/z* 819 [M$^+$-OAc]. HRMS (TOF+ASAP) *m/z* calculated for C$_{40}$H$_{52}$O$_5$N$_4$Pd$_2$ [M-OAc] 819.2656, Found 819.2786. Anal. calc. for (C$_{40}$H$_{52}$N$_4$O$_5$Pd$_2$·2.2CH$_3$CO$_2$H): C 52.71, H 5.86, N 5.54, Found: C 52.63, H 6.10, N 5.34%.

5.3.8 Synthesis of (**L2$_b$**Pd)$_2$(OH)(OAc)

A small dry Schlenk flask, equipped with stir bar, was charged with **HL2$_b$** (0.10 g, 0.296 mmol), Pd(OAc)$_2$ (0.066 g, 0.296 mmol) and dry distilled toluene (15 ml). The reaction mixture was stirred overnight at room temperature resulting in a red solution after 24 h. The solvent was removed by rotary evaporation and then the red solid crystallised from dichloromethane/hexane to give orange crystals (0.19 g, 70%). **M.P:** > 250 °C. **^{1}H NMR (400 MHz; CD$_2$Cl$_2$):** δ 7.24 (1H, t, $^3J_{HH}$ = 6.8 Hz, Py-H), 7.22 (1H, s, OH), 6.97 (1H, t, $^3J_{HH}$ = 6.9 Hz , Py-H), 6.93 (2H, s, Ar), 6.91 (2H, s, Ar), 6.61 (1H, dd, $^3J_{HH}$ = 6.9 Hz, $^4J_{HH}$ = 1.2 Hz, Py-H), 6.55 (1H, dd, $^3J_{HH}$ = 6.8 Hz, $^4J_{HH}$ = 1.0 Hz, Py-H), 6.37 (1H, dd, $^3J_{HH}$ = 9.0 Hz, $^4J_{HH}$ = 1.2 Hz, Py-H), 5.47 (1H, dd, $^3J_{HH}$ = 8.6 Hz, $^4J_{HH}$ = 1.0 Hz, Py-H), 3.17 (4H, sept., $^3J_{HH}$ = 6.8 Hz, CH(CH$_3$)$_2$), 2.78 (1H, sept., $^3J_{HH}$ = 6.8 Hz, CH(CH$_3$)$_2$), 2.83 (1H, sept., $^3J_{HH}$ = 6.8 Hz, CH(CH$_3$)$_2$), 1.95 (3H, s, CCH$_3$), 1.87 (3H, s, CCH$_3$), 1.36 (6H, d, $^3J_{HH}$ = 6.7 Hz, CH(CH$_3$)$_2$), 1.23 (6H, d, $^3J_{HH}$ = 6.7 Hz, CH(CH$_3$)$_2$), 1.19 (6H, d, $^3J_{HH}$ = 6.9 Hz, CH(CH$_3$)$_2$), 1.14 (6H, d, $^3J_{HH}$ = 6.9Hz, CH(CH$_3$)$_2$), 1.13 (3H, s, OAc), 1.06 (6H, d, $^3J_{HH}$ = 6.9 Hz, CH(CH$_3$)$_2$), 0.96 (6H, d, $^3J_{HH}$ = 6.9 Hz, CH(CH$_3$)$_2$). **^{13}C NMR (125 MHz; CD$_2$Cl$_2$):** δ 16.4 (C$\underline{C}$H$_3$), 16.6 (C$\underline{C}$H$_3$), 17.5 (OAc), 22.2 (CH($\underline{C}$H$_3$)$_2$), 22.6 (CH($\underline{C}$H$_3$)$_2$), 22.7 (CH($\underline{C}$H$_3$)$_2$), 22.8 (CH($\underline{C}$H$_3$)$_2$), 22.9 (CH($\underline{C}$H$_3$)$_2$), 23.2 (CH($\underline{C}$H$_3$)$_2$), 27.7 ($\underline{C}$H(CH$_3$)$_2$), 27.9($\underline{C}$H(CH$_3$)$_2$), 33.2 ($\underline{C}$H(CH$_3$)$_2$), 33.6 ($\underline{C}$H(CH$_3$)$_2$), 110.9 CH, 113.5

(CH), 120.6 (CH), 120.8 (CH), 122.4 (CH), 125.0 (CH), 135.2 (C), 135.8 (CH), 136.8 (CH), 139.8 (C), 139.8 (C), 147.5 (C), 152.3 (C), 153.3 (C), 168.3 (C), 171.0 (C), 175.1 (C), 175.9 (C), 176.5(C). **IR (cm^{-1}):** 1615 (strong, sharp, C=N), 2963 (medium, sharp, C-H), 3670 (medium, broad). ESIMS: (+) m/z 905 [M$^+$-OAc]. FABMS: *m/z* 905 [M$^+$-OAc]. HRMS (TOF): calcd for C$_{44}$H$_{59}$N$_4$O$_3$Pd$_2$OAc [M-OAc] 903.2657, found 903.2668. Anal. calc. for (C$_{44}$H$_{59}$N$_4$O$_3$Pd$_2$OAc): C 57.32, H 6.48, N 5.81, Found: C 57.28, H 6.39, N 5.71 %.
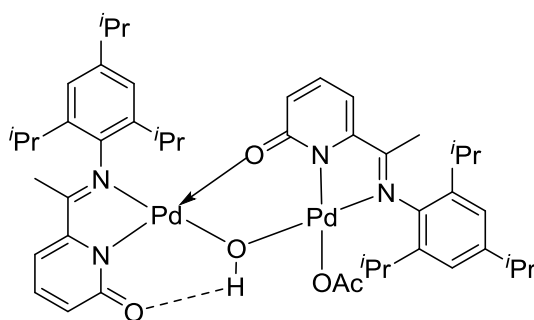
5.3.9 Synthesis of (**L2$_c$**Pd)$_2$(OH)(OAc)
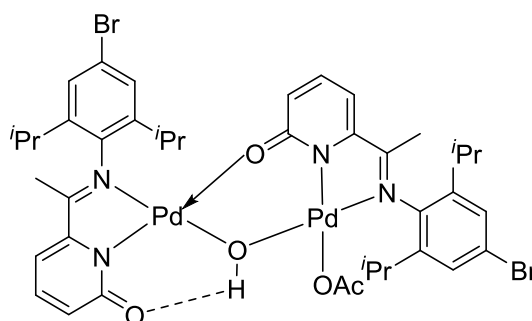
A small dry Schlenk flask, equipped with stir bar, was charged with H**L2$_c$** (0.080 g, 0.21 mmol), Pd(OAc)$_2$ (0.048 g, 0.21 mmol) and dry distilled toluene (10 ml). The reaction mixture was stirred overnight at room temperature affording an orange precipitate which was then filtered through celite, washed with toluene and then extracted with dichloromethane. The solvent was removed by rotary evaporation to give an orange powder (0.21 g, 97%). **M.P:** > 250 °C. **^{1}H NMR (400 MHz; CDCl$_3$):** δ 8.12 (1H, s, OH), 7.25 (2H, s, Ar), 7.24 (2H, s, Ar), 7.17 (2H, m, Py-H), 6.68 (1H, dd, $^3J_{HH}$ = 7.0 Hz, $^4J_{HH}$ = 1.1 Hz, Py-H), 6.58 (1H, dd, $^3J_{HH}$ = 7.0 Hz, $^4J_{HH}$ = 1.1 Hz, Py-H), 6.51 (1H, dd, $^3J_{HH}$ = 8.7 Hz, $^4J_{HH}$ = 0.1 Hz, Py-H), 5.83 (1H, dd, $^3J_{HH}$ = 8.7 Hz, $^4J_{HH}$ = 0.1 Hz, Py-H), 3.30 (4H, sept., $^3J_{HH}$ = 6.9 Hz, CH(CH$_3$)$_2$), 2.02 (3H, s, CCH$_3$), 1.97 (3H, s, CCH$_3$), 1.45 (3H, s, OAc), 1.43 (6H, d, $^3J_{HH}$ = 7.0 Hz, CH(CH$_3$)$_2$), 1.36 (6H, d, $^3J_{HH}$ = 6.8 Hz, CH(CH$_3$)$_2$), 1.14 (6H, d, $^3J_{HH}$ = 6.8 Hz, CH(CH$_3$)$_2$), 1.03 (6H, d, $^3J_{HH}$ = 7.0 Hz, CH(CH$_3$)$_2$). **^{13}C NMR (125 MHz; CDCl$_3$):** δ 17.2 (C$\underline{C}$H$_3$), 18.2 (C$\underline{C}$H$_3$), 21.2 (OAc), 23.3 (CH($\underline{C}$H$_3$)$_2$), 23.4 (CH($\underline{C}$H$_3$)$_2$), 23.5 (CH($\underline{C}$H$_3$)$_2$), 24.0 (CH($\underline{C}$H$_3$)$_2$), 28.7 ($\underline{C}$H(CH$_3$)$_2$), 28.8 ($\underline{C}$H(CH$_3$)$_2$), 112.3 (CH), 114.2 (CH), 121.5 (C), 123.4 (CH), 125.3 (C), 126.8 (CH), 126.9 (CH), 128.2 (CH), 129.0 (C), 135.7 (CH), 136.7 (CH), 138.8 (C), 143.4 (C), 152.6 (C), 153.4 (C), 168.8 (C), 171.8 (C), 176.4 (C), 177.1 (C), 177.2 (C). IR (cm^{-1}): 1487 (strong, sharp), 1614 (strong, sharp, C=N), 2961 (medium, sharp, C-H). ESIMS: (+) m/z

977 [M-OAc]. FABMS: *m/z* 978 [M$^+$-OAc]. HRMS(TOF): calculated for C$_{40}$H$_{48}$N$_4$O$_5$Br$_2$Pd$_2$ [M-OAc] 977.0129, Found 976.9932

5.3.10 Synthesis of H**L2**$_a$PdCl$_2$
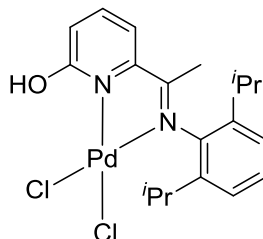
A small Schlenk tube, equipped with stir bar, was evacuated and backfilled with nitrogen and then charged with H**L2**$_a$ (0.100 g, 0.34 mmol, 1 eq.), bis(acetonitrile)palladium(II) chloride (0.09 g, 0.34 mmol, 1 eq.) and dry toluene (20 ml). The reaction was stirred at room temperature for 18 h under an atmosphere of nitrogen. The resulting precipitate was filtered through celite and washed with toluene. The yellow solid was then extracted with dichloromethane and the solvent removed under reduced pressure to give H**L2**$_a$PdCl$_2$ as a yellow powder (0.16 g, 100%). **Mp**: 260 °C (decomp). **^{1}H NMR (400 MHz; CD$_2$Cl$_2$):** *δ* 12.49 (1H, s, OH), 7.95 (1H, t, $^3J_{HH}$ = 7.9Hz, Py/Ar-H), 7.42 (1H, dd, $^3J_{HH}$ = 6.8 Hz, $^4J_{HH}$ = 2.0 Hz, Py/Ar-H), 7.35 (1H, t, $^3J_{HH}$ = 7.9Hz, Py/Ar-H), 7.20 (2H, d, $^3J_{HH}$ = 7.7 Hz, Py/Ar-H), 7.12 (1H, dd, $^3J_{HH}$ = 6.9 Hz, $^4J_{HH}$ = .9 Hz, Py/Ar-H), 3.11 (2H, sept., $^3J_{HH}$ = 6.9 Hz, CH(CH$_3$)$_2$), 2.15 (3H, s, CCH$_3$), 1.40 (6H, d, $^3J_{HH}$ = 6.8 Hz, CH(CH$_3$)$_2$), 1.12 (6H, d, $^3J_{HH}$ = 6.8 Hz, CH(CH$_3$)$_2$). **^{13}C NMR (125 MHz; CD$_2$Cl$_2$):** *δ* 19.4 (C$\underline{C}$H$_3$), 23.9 (CH($\underline{C}$H$_3$)$_2$), 24.1 (CH($\underline{C}$H$_3$)$_2$), 29.5 ($\underline{C}$H(CH$_3$)$_2$), 120.6 (CH), 121.3 (CH), 124.3 (CH), 129.1 (CH), 140.7 (CH), 141.6 (C), 141.9 (CH), 153.3 (C), 168.7 (C), 180.1 (C). **IR (cm$^-$^{1}):** 1455 (strong, sharp), 1625 (strong, sharp, C=N), 2965 (medium, sharp, C-H). ESIMS: (+) m/z 402 [M-Cl]. FABMS: *m/z* 402 [M-Cl]. HRMS (TOF): calcd for C$_{19}$H$_{24}$N$_2$OPdCl$_2$ [M$^+$-Cl] 439.3720, Found 439.3710. Anal. calc. for (C$_{19}$H$_{24}$Cl$_2$N$_2$OPd.0.56CH$_2$Cl$_2$): C 45.07, H 4.86, N 5.37, Found: C 45.00, H 5.18, N 5.15%.

5.3.11 Synthesis of H**L2**$_b$PdCl$_2$
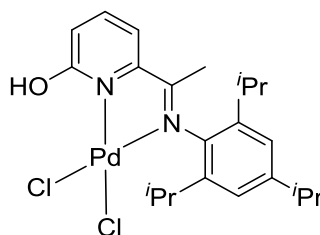
A small Schlenk tube, equipped with stir bar, was evacuated and backfilled with nitrogen and then charged with H$L2_b$ (0.080, 0.24 mmol), bis(acetonitrile)palladium(II) chloride (0.06 g, 0.24 mmol, 1 eq.) and dry toluene (10 ml). The reaction was stirred at room temperature for 18 h under an atmosphere of nitrogen. The resulting precipitate was filtered through celite and washed with toluene. The yellow solid was then extracted with dichloromethane and the solvent removed under reduced pressure to give H$L2_b$PdCl$_2$ as a yellow powder (0.12 g, 99%). **Mp**: 260 °C (decomp). **^{1}H NMR (400 MHz; CD$_2$Cl$_2$):** δ 12.44 (1H, s, OH), 7.86 (1H, t, $^3J_{HH}$ = 7.8 Hz, Py-H), 7.33 (1H, d, $^3J_{HH}$ = 7.5 Hz, Py-H), 7.04 (1H, d, $^3J_{HH}$ = 7.9 Hz, Py-H), 6.97 (2H, s, Ar-H), 3.03 (2H, sept., $^3J_{HH}$ = 6.7 Hz, CH(CH$_3$)$_2$), 2.85 (2H, sept., $^3J_{HH}$ = 6.7 Hz, CH(CH$_3$)$_2$), 2.06 (3H, s, CCH$_3$), 1.33 (6H, d, $^3J_{HH}$ = 6.5 Hz, CH(CH$_3$)$_2$), 1.19 (6H, d, $^3J_{HH}$ = 6.5 Hz, CH(CH$_3$)$_2$), 1.05 (6H, d, $^3J_{HH}$ = 6.5 Hz, CH(CH$_3$)$_2$). **^{13}C NMR (125 MHz; CD$_2$Cl$_2$):** δ 19.7 (C$\underline{C}$H$_3$), 23.8 (CH($\underline{C}$H$_3$)$_2$), 23.9 (CH($\underline{C}$H$_3$)$_2$), 29.4 ($\underline{C}$H(CH$_3$)$_2$), 34.4 ($\underline{C}$H(CH$_3$)$_2$), 120.4 (CH), 120.9 (CH), 121.9 (CH), 139.5 (C), 140.2 (C), 141.8 (CH), 149.4 (C), 153.2 (C), 168.5 (C), 178.1 (C). **IR (cm^{-1}):** 1457 (strong, sharp), 1621 (strong, sharp, C=N), 2962 (medium, sharp, C-H). ESIMS: (+) m/z 444 [M-Cl]. HRMS (TOF): calcd for C$_{22}$H$_{30}$N$_2$OPdCl$_2$ [M$^+$-Cl] 479.5320, Found 479.5210. Anal. calc. for (C$_{22}$H$_{30}$Cl$_2$N$_2$OPd.0.41CH$_2$Cl$_2$): C 48.88, H 5.64, N 5.09, Found: C 48.83, H 5.68, N 4.89%.

5.3.12 Synthesis of H$L2_c$PdCl$_2$
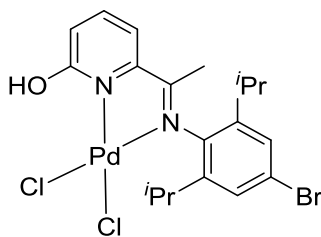
A small Schlenk tube, equipped with stir bar, was evacuated and backfilled with nitrogen and then charged with H$L2_c$ (0.090, 0.24 mmol), bis(acetonitrile)palladium(II) chloride (0.062 g, 0.24 mmol, 1 eq.) and dry toluene (10 ml). The reaction was stirred at room temperature for 18 h under an atmosphere of nitrogen. The resulting precipitate was filtered through celite and washed with toluene. The brown solid was then extracted with dichloromethane and the solvent removed under reduced pressure to give H$L2_c$PdCl$_2$ as a brown powder (0.129 g, 98%). **Mp**: 260 °C (decomp). **^{1}H NMR (400 MHz; CDCl$_3$):** δ 12.61 (1H, s, OH), 7.8 (1H, t, $^3J_{HH}$ = 7.8 Hz, Py-H), 7.35 (1H, d, $^3J_{HH}$ = 7.5 Hz, Py-H), 7.24 (2H, s, Ar-H), 7.08 (1H, d, $^3J_{HH}$ = 8.6 Hz, Py-H), 3.05 (2H, sept., $^3J_{HH}$ = 6.7 Hz,

CH(CH$_3$)$_2$), 2.12 (3H, s, CCH$_3$), 1.36 (6H, d, $^3J_{HH}$ = 6.8 Hz, CH(CH$_3$)$_2$), 1.06 (6H, d, $^3J_{HH}$ = 6.8 Hz, CH(CH$_3$)$_2$). ^{13}C NMR (125 MHz; CD$_2$Cl$_2$): δ 19.5 (CCH$_3$), 23.5 (CH(CH$_3$)$_2$), 23.7 (CH(CH$_3$)$_2$), 29.2 (CH(CH$_3$)$_2$), 120.0 (CH), 121.2 (CH), 123.0 (C), 127.3 (CH), 139.8 (C), 141.3 (CH), 142.4 (C), 152.4 (C), 168.3 (C), 179.4 (C). IR (cm^{-1}): 1448 (strong, sharp), 1622 (strong, sharp, C=N), 2961 (medium, sharp, C-H), 3569 (broad, OH). ESIMS: (+) m/z 519 [M$^+$-Cl]. ESIMS: (-) m/z 515 [M$^-$-Cl]. FABMS: m/z 518 [M-Cl]. HRMS (TOF): calcd for C$_{19}$H$_{23}$N$_2$OBrPdCl$_2$ [M-Cl] 480.9930, found 480.9953.

5.3.13 Synthesis of (L2$_a$Pd)$_2$(OH)(Cl)
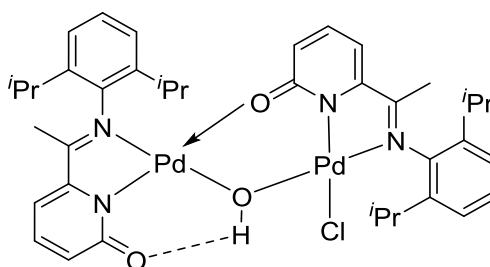
A small round-bottom flask, equipped with stir bar, was charged with HL2$_a$PdCl$_2$ (0.050 g, 0.11 mmol), Ag$_2$O (0.097 g, 0.42 mmol, 4 eq.) and dichloromethane (5 ml). The reaction mixture was left to stir at room temperature for 18 h. Upon reaction completion, the mixture was filtered through celite and the solvent removed under reduced pressure to give (L2$_a$Pd)$_2$(OH)(Cl) as a yellow powder (0.077 g, 82%). Mp: 250 °C (decomp). ^{1}H NMR (400 MHz; CD$_2$Cl$_2$): δ 7.38 (1H, s, OH), 7.32 (2H, m, Py/Ar-H), 7.23 (1H, d, $^3J_{HH}$ = 7.6 Hz, Py/Ar-H), 7.19 (3H, m, Py/Ar-H), 7.13 (2H, m, Py/Ar-H), 6.75 (1H, d, $^3J_{HH}$ = 7.5 Hz, Py/Ar-H), 6.66 (1H, d, $^3J_{HH}$ = 6.9 Hz, Py/Ar-H), 6.56 (1H, d, $^3J_{HH}$ = 7.8 Hz, Py/Ar-H), 6.54 (1H, d, $^3J_{HH}$ = 8 Hz, Py/Ar-H), 3.30 (2H, sept., $^3J_{HH}$ = 6.8 Hz, CH(CH$_3$)$_2$), 3.16 (2H, sept., $^3J_{HH}$ = 6.8 Hz, CH(CH$_3$)$_2$), 2.02 (3H, s, CCH$_3$), 1.83 (3H, s, CCH$_3$), 1.44 (6H, d, $^3J_{HH}$ = 7.0 Hz, CH(CH$_3$)$_2$), 1.29 (6H, d, $^3J_{HH}$ = 6.8 Hz, CH(CH$_3$)$_2$), 1.16 (6H, d, $^3J_{HH}$ = 6.8 Hz, CH(CH$_3$)$_2$), 1.08 (6H, d, $^3J_{HH}$ = 7.0 Hz, CH(CH$_3$)$_2$). ^{13}C NMR (125 MHz; CD$_2$Cl$_2$): δ 17.7 (CCH$_3$), 18.8 (CCH$_3$), 23.8 (CH(CH$_3$)$_2$), 24.0 (CH(CH$_3$)$_2$), 24.1 (CH(CH$_3$)$_2$), 24.2 (CH(CH$_3$)$_2$), 29.2 (CH(CH$_3$)$_2$), 29.3 (CH(CH$_3$)$_2$), 112.3 (CH), 115.7 (CH), 123.7 (CH), 123.8 (CH), 126.3 (CH), 127.8 (CH), 136.6 (CH), 136.9 (CH), 140.0 (C), 140.7 (CH), 140.9 (CH), 141.4 (C), 141.5 (C), 142.5 (C), 153.3 (C), 154.3 (C), 154.5 (C), 177.9 (C), 178.5 (C), 178.7 (C). IR (cm^{-1}): 1616 (strong, sharp, C=N), 2960 (medium, sharp, C-H), 3668 (medium, broad). ESIMS: (+) m/z 819 [M-Cl]. FABMS: *m/z* 856 [M$^+$]. HRMS (TOF+ASAP) *m/z* calculated for C$_{38}$H$_{47}$O$_3$N$_4$Pd$_2$Cl [M-Cl] 818.9920,

Found 818.9911. Anal. calc. for ($C_{38}H_{47}N_4O_3Pd_2Cl \cdot 2CH_2Cl_2$): C 46.83, H 5.01, N 5.46 Found: C 46.69, H 3.64, N 5.68%.

5.3.14 Synthesis of ($L2_b$Pd)$_2$(OH)(Cl)
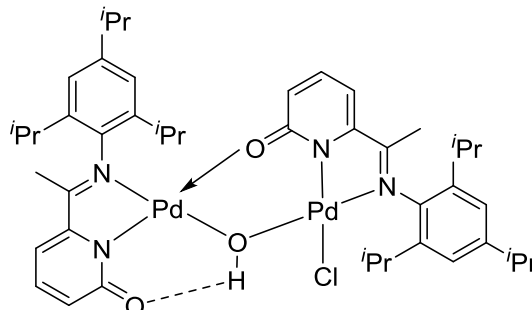
A small round-bottom flask, equipped with a stir bar, was charged with $HL2_b$PdCl$_2$ (0.100 g, 0.19 mmol), Ag$_2$O (0.17 g, 0.76 mmol, 4 eq.) and dichloromethane (10 ml). The reaction mixture was left to stir at room temperature for 18 h. Upon reaction completion, the mixture was filtered through celite and the solvent removed under reduced pressure to give ($L2_b$Pd)$_2$(OH)(Cl) as a yellow solid (0.15 g, 88%). **Mp**: 250 °C (decomp). **¹H NMR (400 MHz; CDCl₃):** δ 7.49 (1H, s, OH), 7.16 (1H, m, Py-H), 6.95 (1H, m, Py-H), 6.92 (2H, s, Ar-H), 6.87 (2H, s, Ar-H), 6.59 (1H, d, $^3J_{HH}$ = 7.0 Hz, Py-H), 6.54 (1H, d, $^3J_{HH}$ = 8.0 Hz, Py-H), 6.49 (1H, d, $^3J_{HH}$ = 6.7 Hz, Py-H), 5.52 (1H, d, $^3J_{HH}$ = 8 Hz, Py-H), 3.19 (2H, sept., $^3J_{HH}$ = 6.9 Hz, CH(CH₃)₂), 3.05 (2H, sept., $^3J_{HH}$ = 6.9 Hz, CH(CH₃)₂), 2.81 (1H, sept., $^3J_{HH}$ = 6.9 Hz, CH(CH₃)₂), 2.80 (1H, sept., $^3J_{HH}$ = 6.9 Hz, CH(CH₃)₂), 1.96 (3H, s, CCH₃), 1.80 (3H, s, CCH₃), 1.38 (6H, d, $^3J_{HH}$ = 6.7 Hz, CH(CH₃)₂), 1.22 (6H, d, $^3J_{HH}$ = 6.9 Hz, CH(CH₃)₂), 1.21 (6H, d, $^3J_{HH}$ = 6.7 Hz, CH(CH₃)₂), 1.15 (6H, d, $^3J_{HH}$ = 6.9 Hz, CH(CH₃)₂), 1.08 (6H, d, $^3J_{HH}$ = 6.7 Hz, CH(CH₃)₂). 0.99 (6H, d, $^3J_{HH}$ = 6.9 Hz, CH(CH₃)₂). **¹³C NMR (125 MHz; CDCl₃):** δ 17.2 (C$\underline{C}$H₃), 18.2 (C$\underline{C}$H₃), 23.5 (CH($\underline{C}$H₃)₂), 23.7 (CH($\underline{C}$H₃)₂), 23.8 (CH($\underline{C}$H₃)₂), 23.9 (CH($\underline{C}$H₃)₂), 24.0 (CH($\underline{C}$H₃)₂), 24.1 (CH($\underline{C}$H₃)₂), 28.5 ($\underline{C}$H(CH₃)₂), 28.7 ($\underline{C}$H(CH₃)₂), 33.9 ($\underline{C}$H(CH₃)₂), 34.4 ($\underline{C}$H(CH₃)₂), 111.6 (CH), 113.7 (CH), 121.3 (CH), 121.4 (CH), 123.7 (CH), 127.0 (CH), 136.2 (CH), 137.7 (CH), 139.8 (C), 140.6 (C), 147.8 (C), 148.1 (C), 152.8 (C), 153.7 (C), 168.4 (C), 171.5 (C), 176.9 (C), 177.4 (C). **IR (cm⁻¹):** 1618 (strong, sharp, C=N), 2961 (medium, sharp, C-H), 3664 (medium, broad). ESIMS: (+) m/z 903 [M-Cl]. FABMS: *m/z* 904 [M⁺-Cl]. HRMS (TOF+ASAP) *m/z* calculated for $C_{44}H_{59}O_3N_4Pd_2Cl$ [M⁺-Cl] 905.2661, found 905.2742.

5.3.15 Synthesis of (**L2**$_c$Pd)$_2$(OH)(Cl)
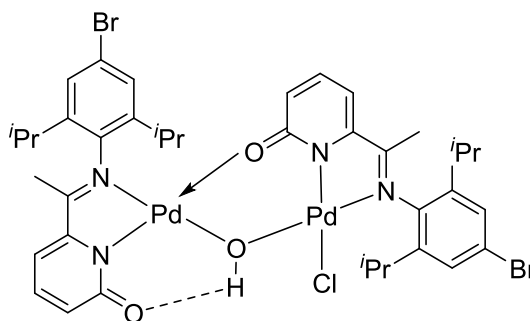
A small round-bottom flask, equipped with stir bar, was charged with H**L2**$_c$PdCl$_2$ (0.090 g, 0.16 mmol), Ag$_2$O (0.15 g, 0.64 mmol, 4 eq.) and dichloromethane (10 ml). The reaction mixture was left to stir at room temperature for 18 h. Upon reaction completion, the mixture was filtered through celite and the solvent removed under reduced pressure to give (**L2**$_c$Pd)$_2$(OH)(Cl) as a sandy powder (0.14 g, 87%). **Mp**: 250 °C (decomp). **^{1}H NMR (400 MHz; CDCl$_3$):** δ 7.77 (1H, s, OH), 7.23 (1H, m, Py-H), 7.21 (2H, s, Ar-H), 7.15 (2H, s, Ar-H), 7.12 (1H, m, Py-H), 6.72 (1H, d, $^3J_{HH}$ = 7.0 Hz, Py-H), 6.57 (1H, d, $^3J_{HH}$ = 6.8 Hz, Py-H), 6.53 (1H, d, $^3J_{HH}$ = 7.8 Hz, Py-H), 5.69 (1H, d, $^3J_{HH}$ = 7.8 Hz, Py-H), 3.19 (2H, sept., $^3J_{HH}$ = 6.9 Hz, CH(CH$_3$)$_2$), 3.05 (2H, sept., $^3J_{HH}$ = 6.9 Hz, CH(CH$_3$)$_2$), 1.96 (3H, s, CCH$_3$), 1.84 (3H, s, CCH$_3$), 1.34 (6H, d, $^3J_{HH}$ = 6.6 Hz, CH(CH$_3$)$_2$), 1.22 (6H, d, $^3J_{HH}$ = 6.8 Hz, CH(CH$_3$)$_2$), 1.08 (6H, d, $^3J_{HH}$ = 6.8 Hz, CH(CH$_3$)$_2$), 0.98 (6H, d, $^3J_{HH}$ = 6.8 Hz, CH(CH$_3$)$_2$). **^{13}C NMR (125 MHz; CDCl$_3$):** δ 17.3 (C$\underline{C}$H$_3$), 18.4 (C$\underline{C}$H$_3$), 23.3 (CH($\underline{C}$H$_3$)$_2$), 23.5 (CH($\underline{C}$H$_3$)$_2$), 23.6 (CH($\underline{C}$H$_3$)$_2$), 23.7 (CH($\underline{C}$H$_3$)$_2$), 28.7 ($\underline{C}$H(CH$_3$)$_2$), 28.8 ($\underline{C}$H(CH$_3$)$_2$), 112.5 (CH), 114.7 (CH), 121.6 (CH), 121.8 (C), 124.1 (CH), 126.9 (CH), 127.4 (CH), 135.7 (CH), 136.9 (CH), 138.8 (C), 140.8 (C), 142.3 (C), 143.3 (C), 143.4 (C), 152.5 (C), 153.3 (C), 167.7 (C), 171.5 (C), 177.4 (C), 178.0 (C). **IR (cm^{-1}):** 1617 (strong, sharp, C=N), 2963 (medium, sharp, C-H). ESIMS: (+) m/z 1017 [M$^+$]. FABMS: *m/z* 1016 [M$^+$]. HRMS(TOF) calculated for C$_{38}$H$_{45}$N$_4$O$_3$Br$_2$PdCl [M-Cl] 980.5561, Found 981.0115.

5.3.16 Synthesis of **L2$_a$**PdCl(PPh$_3$)
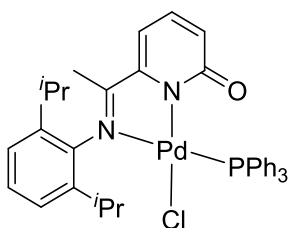
Route one

A small Schlenk tube, equipped with stir bar, was evacuated, backfilled with nitrogen and then charged with H**L2**$_a$ (0.050 g, 0.17 mmol), NaH (0.016 g, 0.68 mmol, 4 eq.) and dry THF (10 ml). The reaction mixture was stirred and heated to 40 °C overnight under a nitrogen atmosphere. After cooling to room temperature, the solution was filtered via cannula into another Schlenk flask containing (MeCN)$_2$PdCl$_2$ (0.044 g, 0.17 mmol) and PPh$_3$ (0.045 g, 0.17 mmol). The reaction mixture was then left to stir for 18 h at room temperature and then filtered through celite. The solvent was removed by rotary evaporation to give **L2**$_a$PdCl(PPh$_3$) as a yellow solid (0.12 g, 100%). **Mp**: > 250 °C. **^{1}H NMR (400 MHz; CDCl$_3$):** δ 7.67 (7H, m, Py/Ar-H), 7.33 (4H, m, Py/Ar-H), 7.22 (6H, m, Py/Ar-H), 7.09 (2H, m, Py/Ar-H), 6.57 (1H, d, $^3J_{HH}$ = 6.8 Hz, Py/Ar-H), 6.15 (1H, d, $^3J_{HH}$ = 8 Hz, Py/Ar-H), 3.09 (2H, sept., $^3J_{HH}$ = 6.7 Hz, CH(CH$_3$)$_2$), 2.02 (3H, s, CCH$_3$), 1.24 (6H, d, $^3J_{HH}$ = 6.8 Hz, CH(CH$_3$)$_2$), 1.09 (6H, d, $^3J_{HH}$ = 6.8 Hz, CH(CH$_3$)$_2$). **^{13}C NMR (125 MHz; CDCl$_3$):** δ 18.2 (CC̲H$_3$), 23.5 (CH(C̲H$_3$)$_2$), 24.0 (CH(C̲H$_3$)$_2$), 28.8 (C̲H(CH$_3$)$_2$), 111.5 (CH), 123.3 (CH), 124.4 (CH), 127.4 (CH), 127.5 (CH), 128.0 (CH), 128.1 (CH), 128.2 (CH), 129.7 (CH), 130.5 (CH), 133.5 (CH), 133.6 (CH), 134.5 (CH), 135.1 (CH), 135.2 (CH), 139.8 (C), 141.3 (C), 153.9 (C), 166.4 (C), 176.3 (C). **^{31}P NMR (202 MHz; CDCl$_3$):** δ 25.3 (IP, s, PPh$_3$). **IR (cm^{-1}):** 1467 (medium, sharp), 1586 (medium, strong), 1623 (strong, sharp, C=N), 2960 (medium, sharp, C-H). ESIMS: (+) m/z 699 [M$^+$]. FABMS: m/z 699 [M$^+$]. HRMS (TOF+ESI) m/z calculated for C$_{37}$H$_{38}$ON$_2$PdP [M$^+$] 699.1330, Found 699.1274. Anal. cal. for C$_{37}$H$_{38}$ON$_2$PdP: C 63.53, H 5.48, N 4.00 Found: C 63.69, H 5.64, N 3.68%.

Route two

A small Schlenk tube, equipped with a stir bar, was charged with (**L2**$_a$Pd)$_2$(OH)(Cl) (0.050 g, 0.059 mmol), PPh$_3$ (0.015 g, 0.059 mmol) and dichloromethane (5 ml). The reaction mixture was left to stir at room temperature for 18 h and the solvent then removed by rotary evaporation to give **L2**$_a$PdCl(PPh$_3$) as a yellow solid (0.020 g, 48%). The analytical and spectroscopic properties were as above.

5.3.17 Synthesis of **L2ₑPdCl(PPh₃)**
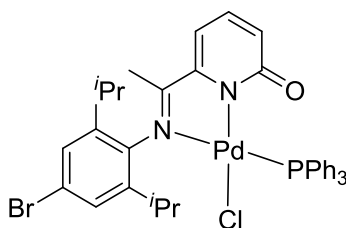
A small Schlenk tube, equipped with a stir bar, was charged with (**L2ₐPd**)₂(OH)(Cl) (0.050 g, 0.049 mmol), PPh₃ (0.013 g, 0.049 mmol) and dichloromethane (5 ml). The reaction mixture was left to stir at 47 °C for 7 days. After cooling to room temperature, the solvent was removed by rotary evaporation to give **L2ₑPdClPPh₃** as a yellow solid (0.010 g, 26%). **Mp**: > 250 °C. **¹H NMR (400 MHz; CD₂Cl₂):** δ 7.55 (7H, m, PPh₃), 7.39 (4H, m, PPh₃), 7.30 (4H, m, PPh₃), 7.20 (2H, s, Ar-H), 7.07 (1H, t, $^3J_{HH}$ = 7.4 Hz, Py-H), 6.58 (1H, d, $^3J_{HH}$ = 6.8 Hz, Py-H), 6.07 (1H, d, $^3J_{HH}$ = 8 Hz, Py-H), 3.07 (2H, sept., $^3J_{HH}$ = 6.8 Hz, C$\underline{H}$(CH₃)₂), 2.25 (3H, s, CCH₃), 1.23 (6H, d, $^3J_{HH}$ = 6.8 Hz, CH(CH₃)₂), 1.08 (6H, d, $^3J_{HH}$ = 6.8 Hz, CH(CH₃)₂). **¹³C NMR (125 MHz; CD₂Cl₂):** δ 20.4 (C$\underline{C}$H₃), 22.2 (CH($\underline{C}$H₃)₂), 22.4 (CH($\underline{C}$H₃)₂), 27.7 ($\underline{C}$H(CH₃)₂), 111.4 (CH), 123.4 (CH), 125.6 (CH), 126.4 (CH), 127.1 (CH), 127.7 (CH), 128.2 (CH), 131.1 (CH), 131.2 (CH), 131.7 (CH), 132.4 (CH), 132.5 (CH), 133.8 (CH), 139.1 (C), 139.7 (C), 141.8 (C), 153.2 (C), 165.1 (C), 179.4 (C). **³¹P NMR (161 MHz; CD₂Cl₂):** δ 25.61 (1P, s, PPh₃). **IR (cm⁻¹):** 1434 (strong, sharp), 1618 (strong, sharp, C=N), 2961 (medium, sharp, C-H). ESIMS: (+) m/z 742 [M-Cl]. HRMS(TOF): calculated for C₁₉H₂₂N₂OBrPdClPPh₃ [M-Cl] 743.0866, Found 743.0873.

5.3.18 Synthesis of [H**L2ₐ**Pd(NCMe)₂][PF₆]₂
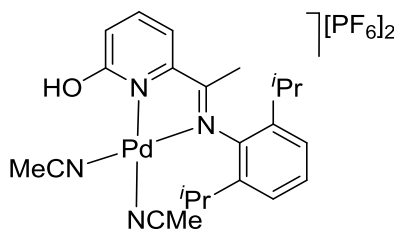
A 50 ml Schlenk tube, equipped with stir bar, was evacuated and backfilled with nitrogen and then charged was charged with bis(acetonitrile)palladium(II) chloride (0.026 g, 0.10 mmol, 1 eq.), AgPF₆ (0.077 g, 0.30 mmol, 3 eq.) and dry acetonitrile (5 ml). The reaction was stirred at room temperature for 1 h before the addition of H**L2ₐ** (0.030 g, 0.10 mmol, 1 eq.). The reaction was stirred at room temperature for an additional 18 h and then filtered through celite. The solvent was removed by rotary evaporation to give

[H**L2**a**Pd(NCMe)₂][[PF₆]₂** as a yellow solid (0.076 g, 97%). **Mp:** 250 °C (decomp). **¹H NMR (400 MHz; CD₃CN):** δ 10.15 (1H, s, OH), 8.67 (1H, t, $^3J_{HH}$ = 7.6 Hz, Py/Ar-H), 8.30 (1H, dd, $^3J_{HH}$ = 7.6 Hz, $^4J_{HH}$ = 0.9 Hz, Py/Ar-H), 7.92 (1H, dd, $^3J_{HH}$ = 8.6 Hz, $^4J_{HH}$ = 1.0 Hz Py/Ar-H), 7.51 (2H, m, Py/Ar-H), 7.40 (1H, d, $^3J_{HH}$ = 7.6 Hz, Py/Ar-H), 3.06 (2H, sept., $^3J_{HH}$ = 6.7 Hz, CH(CH₃)₂), 2.52 (3H, s, CCH₃), 1.87 (6H, s, NCMe), 1.37 (6H, d, $^3J_{HH}$ = 6.7 Hz, CH(CH₃)₂), 1.19 (6H, d, $^3J_{HH}$ = 6.7 Hz, CH(CH₃)₂). **¹³C NMR (125 MHz; CD₃CN):** δ 0.5 (NC$\underline{C}$H₃), 19.5 (C$\underline{C}$H₃), 23.9 (CH($\underline{C}$H₃)₂), 24.1 (CH($\underline{C}$H₃)₂), 29.5 ($\underline{C}$H(CH₃)₂), 118.5 (CH), 122.2 (CH), 125.9 (CH), 129.6 (CH), 131.3 (CH), 140.5 (C), 141.2 (C), 147.5 (CH), 152.9 (C), 155.2 (C), 174.9 (C), 183.4 (C). **¹⁹F NMR (376 MHz; CD₃CN):** δ -72.9 (F, d, J -709.4, PF₆). **³¹P NMR (202 MHz; CD₃CN):** δ -144.6 (P, sept., J -714.6, PF₆). **IR (cm⁻¹):** 1621 (strong, sharp, C=N), 2946 (medium, sharp, C-H), 3309 (medium, broad, O-H). ESIMS: (+) m/z 485 [M⁺- PF₆]. ESIMS: (-) m/z 145 [PF₆]. FABMS: *m/z* 485 [M⁺-(PF₆+HPF₆)]. HRMS(TOF+ASAP): calcd for C₂₃H₃₀N₄OPd(PF₆)₂ [M⁺-(NCMe+PF₆+HPF₆)] 444.1115, Found 444.1114.

5.3.19 Synthesis of [H**L2**b**Pd(NCMe)₂][PF₆]₂**
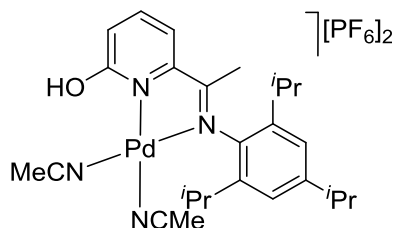
A 50 ml Schlenk tube, equipped with stir bar, was evacuated, backfilled with nitrogen and then charged with bis(acetonitrile)palladium(II) chloride (0.031 g, 0.12 mmol, 1 eq.), AgPF₆ (0.091 g, 0.36 mmol, 3 eq.) and dry acetonitrile (10 ml). The reaction was stirred at room temperature for 1 h before the addition of H**L2**b (0.040 g, 0.12 mmol, 1 eq.). The reaction was stirred at room temperature for 18 h and then filtered through celite. The solvent was removed by rotary evaporation to give [H**L2**b**Pd(NCMe)₂][PF₆]₂** as a yellow solid (0.096 g, 99%). **Mp:** 250 °C (decomp). **¹H NMR (400 MHz; CD₃CN):** δ 11.06 (1H, s, OH), 8.68 (1H, t, $^3J_{HH}$ = 7.8 Hz, Py-H), 8.32 (1H, d, $^3J_{HH}$ = 7.4 Hz, Py-H), 7.92 (1H, d, $^3J_{HH}$ = 7.6 Hz, Py-H), 7.30 (2H, s, Ar-H), 3.08 (2H, sept., $^3J_{HH}$ = 6.8 Hz, CH(CH₃)₂), 3.00 (1H, sept., $^3J_{HH}$ = 6.8 Hz, CH(CH₃)₂), 2.53 (3H, s, CCH₃), 1.85 (6H, s, NCMe), 1.38 (6H, d, $^3J_{HH}$ = 6.8 Hz, CH(CH₃)₂), 1.29 (6H, d, $^3J_{HH}$ = 6.8 Hz, CH(CH₃)₂) 1.21 (6H, d, $^3J_{HH}$ = 6.7 Hz, CH(CH₃)₂). **¹³C NMR (125 MHz; CD₃CN):** δ 0.5 (NC$\underline{C}$H₃), 19.6 (C$\underline{C}$H₃), 23.9 (CH($\underline{C}$H₃)₂), 24.5 (CH($\underline{C}$H₃)₂), 24.6 (CH($\underline{C}$H₃)₂), 30.1 ($\underline{C}$H(CH₃)₂), 35.3 ($\underline{C}$H(CH₃)₂),

122.2 (CH), 124.0 (CH), 129.5 (CH), 138.5 (C), 141.2 (C), 147.4 (CH), 152.3 (C), 153.1 (C), 155.4 (C), 166.7(C). **^{19}F NMR (376 MHz; CD$_3$CN):** δ -72.6 (F, d, J -110.5, PF$_6$). **^{31}P NMR (202 MHz; CD$_3$CN):** δ -144.6 (P, sept., J -731.6, PF$_6$). **IR (cm^{-1}):** 1620 (strong, sharp, C=N), 2966 (medium, sharp, C-H), 3311 (medium, broad, O-H). ESIMS: (+) m/z 527 [M-(PF$_6$+HPF$_6$)], ESIMS: (-) m/z 145 [PF$_6$]. FABMS: *m/z* 527 [M-(PF$_6$+HPF$_6$)]. HRMS (TOF+ASAP): calcd for C$_{26}$H$_{36}$N$_4$OPd(PF$_6$)$_2$ [M-(PF$_6$+HPF$_6$)] 527.1850, found 527.1848.

5.3.20 Synthesis of [H**L2**$_c$Pd(NCMe)$_2$][PF$_6$]$_2$
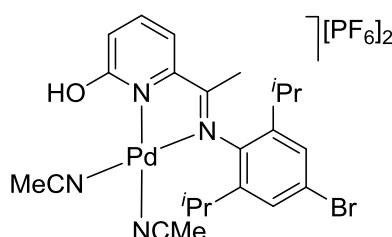
A 50 ml Schlenk tube, equipped with stir bar, was evacuated, backfilled with nitrogen and then charged with bis(acetonitrile)palladium(II) chloride (0.021 g, 0.12 mmol, 1 eq.), AgPF$_6$ (0.061 g, 0.24 mmol, 3 eq.) and dry acetonitrile (5 ml). The reaction was stirred at room temperature for 1 h before the addition of H**L2**$_c$ (0.030 g, 0.08 mmol, 1 eq.). The resulting mixture was stirred at room temperature for an additional 18 h and then filtered through celite. The solvent was removed by rotary evaporation to give [H**L2**$_c$Pd(NCMe)$_2$][PF$_6$]$_2$ as a yellow solid (0.066 g, 97%). **Mp:** 250 °C (decomp). **^{1}H NMR (400 MHz; CD$_3$CN):** δ 11.07 (1H, s, OH), 8.68 (1H, t, $^3J_{HH}$ = 8.4 Hz, Py-H), 8.33 (1H, d, $^3J_{HH}$ = 7.6 Hz, Py-H), 7.93 (1H, d, $^3J_{HH}$ = 8.6 Hz, Py-H), 7.59 (2H, s, Ar-H), 3.09 (2H, sept., $^3J_{HH}$ = 6.8 Hz, CH(CH$_3$)$_2$), 2.54 (3H, s, CCH$_3$), 1.86 (6H, s, NCMe), 1.36 (6H, d, $^3J_{HH}$ = 6.7 Hz, CH(CH$_3$)$_2$), 1.20 (6H, d, $^3J_{HH}$ = 6.7 Hz, CH(CH$_3$)$_2$). **^{13}C NMR (125 MHz; CD$_3$CN):** δ 0.5 (NC$\underline{C}$H$_3$), 19.7 (C$\underline{C}$H$_3$), 23.7 (CH($\underline{C}$H$_3$)$_2$), 24.0 (CH($\underline{C}$H$_3$)$_2$), 30.0 ($\underline{C}$H(CH$_3$)$_2$), 118.6 (CH), 122.3 (CH), 124.9 (CH), 129.9 (CH), 139.9 (C), 144.2 (C), 147.3 (C), 153.0 (C), 155.1 (C), 166.6 (C). **^{19}F NMR (376 MHz; CD$_3$CN):** δ -72.6 (F, d, J -110.5, PF$_6$). **^{31}P NMR (202 MHz; CD$_3$CN):** δ -144.6 (P, sept., J -716.7, PF$_6$). **IR (cm^{-1}):** 1621 (strong, sharp, C=N), 2973 (medium, sharp, C-H), 3306 (medium, broad, O-H). ESIMS: (+) m/z 481 [M$^+$- (NCMe+PF$_6$+HPF$_6$], ESIMS: (-) m/z 145 [PF$_6$]. FABMS: *m/z* 522 [M-(PF$_6$+HPF$_6$)].

5.3.21 Synthesis of [(**L2**ₐPd)₂OH(NCMe)][PF₆]
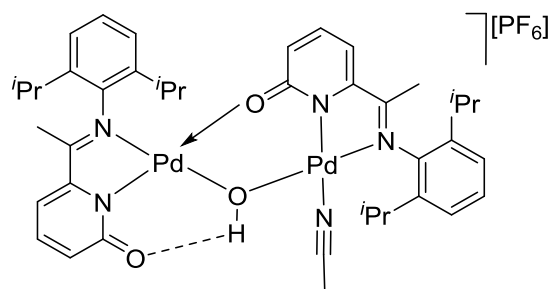
Route one

A small dry Schlenk tube, equipped with stir bar, was charged with (**L2**ₐPd)₂OH(Cl) (0.020 g, 0.023 mmol, 1 eq.), AgPF₆ (0.009 g, 0.035 mmol, 1.5 eq.) and dry distilled acetonitrile (5 ml). The reaction mixture was stirred overnight at room temperature affording a white precipitate. This precipitate (AgCl) was filtered through celite and the solvent removed by rotary evaporation to give [(**L2**ₐPd)₂OH(NCMe)][PF₆] as a yellow solid (0.023 g, 98%). **Mp:** 250 °C (decomp). **^{1}H NMR (400 MHz; CD₃CN):** δ 9.06 (1H, s, OH), 7.40 (1H, t, $^3J_{HH}$ = 7.0 Hz, Py/Ar-H), 7.29 (5H, m, Py/Ar-H), 7.13 (2H, d, $^3J_{HH}$ = 7.6 Hz. Py/Ar-H), 6.92 (1H, d, $^3J_{HH}$ = 7.0 Hz, Py/Ar-H), 6.83 (1H, d, $^3J_{HH}$ = 7.0 Hz, Py/Ar-H), 6.38 (1H, d, $^3J_{HH}$ = 8.8 Hz, Py/Ar-H), 5.69 (1H, d, $^3J_{HH}$ = 8.8 Hz, Py/Ar-H), 3.18 (2H, sept., $^3J_{HH}$ = 6.8 Hz, CH(CH₃)₂), 3.08 (2H, sept., $^3J_{HH}$ = 6.8 Hz, CH(CH₃)₂), 2.08 (3H, s, CCH₃), 2.01 (3H, s, CCH₃), 1.99 (3H, s, NCMe), 1.38 (6H, d, $^3J_{HH}$ = 6.8 Hz, CH(CH₃)₂), 1.18 (6H, d, $^3J_{HH}$ = 6.8 Hz, CH(CH₃)₂), 1.10 (6H, d, $^3J_{HH}$ = 6.8 Hz, CH(CH₃)₂), 1.08 (6H, d, $^3J_{HH}$ = 6.8 Hz, CH(CH₃)₂). **^{13}C NMR (125 MHz; CD₃CN):** δ 0.6 (NCMe), 17.2 (CCH₃), 17.7 (CCH₃), 21.3 (CH(CH₃)₂), 21.8 (CH(CH₃)₂), 22.4 (CH(CH₃)₂), 22.6 (CH(CH₃)₂), 27.8 (CH(CH₃)₂), 28.2 (CH(CH₃)₂), 113.6 (CH), 113.7 (CH), 117.0 (CH), 123.3 (CH), 124.2 (CH), 124.3 (CH), 124.7 (CH), 124.8 (CH), 128.0 (CH), 128.6 (CH), 137.3 (CH), 138.4 (CH), 138.8 (C), 139.2 (C), 140.3 (C), 141.2 (C), 152.7 (C), 153.6 (C), 169.3 (C), 171.6 (C), 179.3 (C), 181.2 (C). **^{19}F NMR (376 MHz; CD₃CN):** δ -73.2 (F, d, J -718.6, PF₆). **^{31}P NMR (202 MHz; CD₃CN):** δ -144.6 (P, sept., J -716.7, PF₆). **IR (cm^{-1}):** 1475 (strong, sharp), 1618 (strong, sharp, C=N), 2969 (medium, sharp, C-H). ESIMS: (+) m/z 860 [M-PF₆], ESIMS: (-) m/z 145 [PF₆]. FABMS: *m/z* 860 [M-PF₆]. HRMS (TOF): calcd for C₄₀H₅₀N₅O₃Pd₂PF₆ [M-PF₆] 860.1983, Found 860.1994.

Route two

A 25 ml round-bottom flask, equipped with stir bar, was charged with [H**L2**ₐPd(NCMe)₂][PF₆]₂ (0.050 g, 0.065 mmol), silver oxide (0.060 g, 0.26 mmol) and

acetonitrile (5 ml). The reaction mixture was left to stir at room temperature for 18 h at which point the mixture was filtered through celite. The solvent was then removed by rotary evaporation to give [(**L2**$_a$Pd)$_2$OH(NCMe)][PF$_6$] as a yellow solid (0.065 g, 100%). The analytical and spectroscopic properties were as above.

5.3.22 Synthesis of [(**L2**$_b$Pd)$_2$OH(NCMe)][PF$_6$]
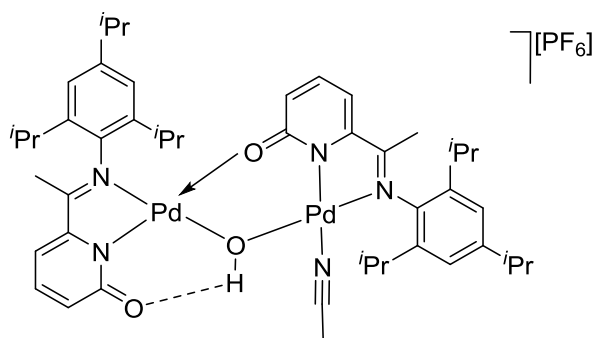
A small dry Schlenk tube was charged with (**L2**$_b$Pd)$_2$OH(Cl) (0.030 g, 0.032 mmol, 1 eq.), AgPF$_6$ (0.012 g, 0.048 mmol, 1.5 eq.) and dry distilled acetonitrile (5 ml). The reaction mixture was stirred overnight at room temperature affording a white precipitate. This precipitate (AgCl) was filtered through celite and the solvent removed by rotary evaporation to give [(**L2**$_b$Pd)$_2$OH(NCMe)][PF$_6$] as a yellow solid (0.034 g, 98%). **Mp:** 250 °C (decomp). **^{1}H NMR (400 MHz; CD$_3$CN):** δ 8.86 (1H, s, OH), 7.40 (1H, t, $^3J_{HH}$ = 7.8 Hz, Py-H), 7.19 (1H, t, $^3J_{HH}$ = 7.9 Hz, Py-H), 7.11 (2H, s, Ar-H), 7.00 (2H, s, Ar-H), 6.89 (1H, dd, $^3J_{HH}$ = 7.1 Hz, $^4J_{HH}$ = 1.2 Hz, Py-H), 6.82 (1H, dd, $^3J_{HH}$ = 6.8 Hz, $^4J_{HH}$ = 1.1 Hz, Py-H), 6.37 (1H, dd, $^3J_{HH}$ = 8.8 Hz, $^4J_{HH}$ = 1.0 Hz, Py-H), 5.64 (1H, dd, $^3J_{HH}$ = 8.8 Hz, $^4J_{HH}$ = 1.2 Hz, Py-H), 3.13 (2H, sept., $^3J_{HH}$ = 6.7 Hz, CH(CH$_3$)$_2$), 3.05 (2H, sept., $^3J_{HH}$ = 6.7 Hz, CH(CH$_3$)$_2$), 2.84 (2H, sept., $^3J_{HH}$ = 6.7 Hz, CH(CH$_3$)$_2$), 2.09 (3H, s, CCH$_3$), 2.00 (3H, s, CCH$_3$), 1.99 (3H, s, NCMe), 1.38 (6H, d, $^3J_{HH}$ = 6.8 Hz, CH(CH$_3$)$_2$), 1.19 (6H, d, $^3J_{HH}$ = 6.9 Hz, CH(CH$_3$)$_2$), 1.17 (6H, d, $^3J_{HH}$ = 6.9 Hz, CH(CH$_3$)$_2$), 1.16 (6H, d, $^3J_{HH}$ = 6.9 Hz, CH(CH$_3$)$_2$), 1.10 (6H, d, $^3J_{HH}$ = 6.8 Hz, CH(CH$_3$)$_2$), 1.07 (6H, d, $^3J_{HH}$ = 6.9 Hz, CH(CH$_3$)$_2$). **^{13}C NMR (125 MHz; CDCl$_3$):** δ 0.6 (NCMe), 16.7 (C$\underline{C}$H$_3$), 17.2 (C$\underline{C}$H$_3$), 22.3 (CH($\underline{C}$H$_3$)$_2$), 22.4 (CH($\underline{C}$H$_3$)$_2$), 22.6 (CH($\underline{C}$H$_3$)$_2$), 22.7 (CH($\underline{C}$H$_3$)$_2$), 22.8 (CH($\underline{C}$H$_3$)$_2$), 23.0 (CH($\underline{C}$H$_3$)$_2$), 28.2 ($\underline{C}$H(CH$_3$)$_2$), 28.3 ($\underline{C}$H(CH$_3$)$_2$), 33.7 ($\underline{C}$H(CH$_3$)$_2$), 33.8 ($\underline{C}$H(CH$_3$)$_2$), 113.0 (CH), 116.9 (CH), 117.0 (CH), 117.3 (CH), 121.4 (CH), 122.0 (CH), 124.1 (CH), 124.6 (CH), 136.6 (C), 137.2 (C), 137.3 (C), 139.5 (C), 140.1 (C), 148.7 (C), 149.8 (C), 152.7 (C), 153.6 (C), 169.4 (C), 179.2 (C), 181.2 (C). **^{19}F NMR (376 MHz; CD$_3$CN):** δ -72.9 (F, d, J -705.1, PF$_6$). **^{31}P NMR (202 MHz; CD$_3$CN):** δ -144.6 (P, sept.,

J -716.7, PF$_6$). **IR (cm^{-1}):** 1489 (strong, sharp), 1618 (strong, sharp, C=N), 2962 (medium, sharp, C-H). ESIMS: (+) m/z 944 [M-PF$_6$], ESIMS: (-) m/z 145 [PF$_6$]. FABMS: *m/z* 944 [M-PF$_6$]. HRMS (TOF): calcd for C$_{46}$H$_{62}$N$_5$O$_3$Pd$_2$PF$_6$ [M-PF$_6$] 944.2922, Found 944.3015.

5.3.23 Synthesis of [(L2$_c$Pd)$_2$OH(NCMe)][PF$_6$]
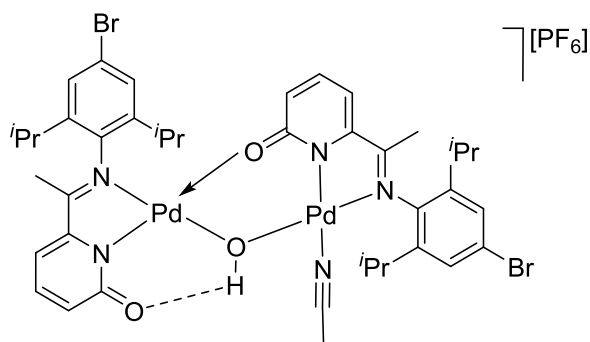
A small dry Schlenk tube, equipped with a stir bar, was charged with (L2$_b$Pd)$_2$OH(Cl) (0.035 g, 0.035 mmol, 1 eq.), AgPF$_6$ (0.013 g, 0.053 mmol, 1.5 eq.) and dry distilled acetonitrile (5 ml). The reaction mixture was stirred overnight at room temperature affording a white precipitate. Theis precipitate (AgCl) was filtered through celite and the solvent removed by rotary evaporation to give [(L2$_c$Pd)$_2$OH(NCMe)][PF$_6$] as a yellow solid (0.039 g, 97%). **Mp:** 250 °C (decomp). **^{1}H NMR (400 MHz; CD$_3$CN):** δ 9.20 (1H, s, OH), 7.42 (1H, t, $^3J_{HH}$ = 7.8 Hz, Py-H), 7.40 (2H, s, Ar-H), 7.31 (1H, t, $^3J_{HH}$ = 7.8 Hz, Py-H), 7.29 (2H, s, Ar-H), 6.95 (1H, dd, $^3J_{HH}$ = 7.0 Hz, $^4J_{HH}$ = 1.2 Hz, Py-H), 6.84 (1H, dd, $^3J_{HH}$ = 7.0 Hz, $^4J_{HH}$ = 1.2 Hz, Py-H), 6.40 (1H, dd, $^3J_{HH}$ = 8.8 Hz, $^4J_{HH}$ = 1.0 Hz, Py-H), 5.83 (1H, dd, $^3J_{HH}$ = 8.6 Hz, $^4J_{HH}$ = 1.1 Hz, Py-H), 3.15 (2H, sept., $^3J_{HH}$ = 6.8 Hz, CH(CH$_3$)$_2$), 3.05 (2H, sept., $^3J_{HH}$ = 6.8 Hz, CH(CH$_3$)$_2$), 2.02 (3H, s, CCH$_3$), 2.01 (3H, s, CCH$_3$), 1.99 (3H, s, NCMe), 1.37 (6H, d, $^3J_{HH}$ = 6.8 Hz, CH(CH$_3$)$_2$), 1.18 (6H, d, $^3J_{HH}$ = 6.8 Hz, CH(CH$_3$)$_2$), 1.09 (6H, d, $^3J_{HH}$ = 6.9 Hz, CH(CH$_3$)$_2$), 1.07 (6H, d, $^3J_{HH}$ = 6.9 Hz, CH(CH$_3$)$_2$). **^{13}C NMR (125 MHz; CD$_3$CN):** δ 0.6 (NCMe), 16.9 (C$\underline{C}$H$_3$), 17.4 (C$\underline{C}$H$_3$), 22.1 (CH($\underline{C}$H$_3$)$_2$), 22.2 (CH($\underline{C}$H$_3$)$_2$), 22.3 (CH($\underline{C}$H$_3$)$_2$), 22.74 (CH($\underline{C}$H$_3$)$_2$), 28.2 ($\underline{C}$H(CH$_3$)$_2$), 28.3 ($\underline{C}$H(CH$_3$)$_2$), 114.1 (CH), 117.0 (CH), 117.9 (CH), 124.4 (CH), 125.0 (CH), 126.7 (CH), 127.5 (CH), 137.3 (CH), 137.3 (C), 138.3 (C), 139.5 (C), 142.4 (C), 143.1 (C), 152.6 (C), 169.3 (C), 181.2 (C). **^{19}F NMR (376 MHz; CD$_3$CN):** δ -72.9 (F, d, J -705.1, PF$_6$). **^{31}P NMR (202 MHz; CD$_3$CN):** δ -144.6 (P, sept., J -716.7, PF$_6$). **IR (cm^{-1}):** 1488 (strong, sharp), 1619 (strong, sharp, C=N), 2970 (medium, sharp, C-H). ESIMS: (+) m/z 1018 [M-PF$_6$], ESIMS: (-) m/z 145 [PF$_6$]. FABMS: *m/z* 1018 [M-PF$_6$].

5.3.24 Synthesis of H**L2**$_a$PtCl$_2$
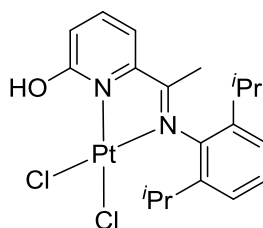
A 25 ml round-bottom flask, equipped with stir bar, was charged with H**L2**$_a$ (0.020 g, 0.067 mmol), chloroform (5 ml) and bis(dimethylsulfoxide)platinum dichloride (0.028 g, 0.067 mmol). The reaction was stirred and heated to 57 °C overnight resulting in a colour change from yellow to dark red after 24 h. A fine white precipitate formed upon cooling to room temperature. The mixture was filtered through celite and the solvent removed by rotary evaporation to give H**L2**$_a$PtCl$_2$ as a red solid (0.038 g, 100%). **Mp:** 230 °C (decomp). **^{1}H NMR (400 MHz; CD$_2$Cl$_2$):** δ 12.55 (1H, s, OH), 7.99 (1H, t, $^3J_{HH}$ = 7.7 Hz, Py/Ar-H), 7.47 (1H, dd, $^3J_{HH}$ = 7.8 Hz, $^4J_{HH}$ = 1.8 Hz, Py/Ar-H), 7.36 (1H, t, $^3J_{HH}$ = 6.8 Hz, Py/Ar-H), 7.24 (2H, d, $^3J_{HH}$ = 7.5 Hz, Py/Ar-H), 7.18 (1H, dd, $^3J_{HH}$ = 6.9 Hz, $^4J_{HH}$ = 0.9 Hz, Py/Ar-H), 3.10 (2H, sept., $^3J_{HH}$ = 6.8 Hz, C$\underline{H}$(CH$_3$)$_2$), 1.99 (3H, s, CC$\underline{H}_3$), 1.36 (6H, d, $^3J_{HH}$ = 6.6 Hz, CH(C$\underline{H}_3$)$_2$), 1.11 (6 H, d, $^3J_{HH}$ = 6.6 Hz, CH(C$\underline{H}_3$)$_2$). **^{13}C NMR (125 MHz; CD$_2$Cl$_2$):** δ 19.7 (C$\underline{C}$H$_3$), 23.8 (CH($\underline{C}$H$_3$)$_2$), 24.1 (CH($\underline{C}$H$_3$)$_2$), 28.8 ($\underline{C}$H(CH$_3$)$_2$), 117.0 (CH), 121.1 (CH), 121.7 (CH), 124.3 (CH), 129.4 (CH), 127.5 (CH), 137.3 (C), 138.3 (C), 139.5 (C), 141.3 (C), 179.2 (C). **IR (cm^{-1}):** 1625 (strong, sharp, C=N), 2968 (medium, sharp, C-H), 3665 (medium, broad). ESIMS: (+) m/z 491 [M-Cl]. Anal. calc. for C$_{19}$H$_{24}$N$_2$OPtCl$_2$: C 40.58, H 4.30, N 4.98 Found: C 40.39, H 4.36, N 4.95%.

5.3.25 Synthesis of H**L2**$_b$PtCl$_2$
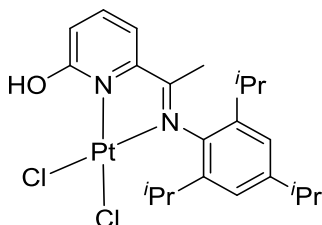
A 25 ml round-bottom flask, equipped with stir bar, was charged with H**L2**$_b$ (0.025 g, 0.074 mmol), chloroform (5 ml) and bis(dimethylsulfoxide)platinum dichloride (0.031 g, 0.074 mmol). The reaction was stirred and heated to 57 °C overnight resulting in a change in the colour of the solution from yellow to dark red after 24 h. A fine white precipitate formed upon cooling to room temperature. The mixture was filtered through celite and

the solvent removed by rotary evaporation to give $HL2_bPtCl_2$ as a red solid (0.044 g, 98%). **Mp:** 230 °C (decomp). **^{1}H NMR (400 MHz; CD$_2$Cl$_2$):** δ 12.50 (1H, s, OH), 8.00 (1H, t, $^3J_{HH}$ = 7.8 Hz, Py-H), 7.45 (1H, d, $^3J_{HH}$ = 7.9 Hz, Py-H), 7.18 (1H, d, $^3J_{HH}$ = 7.0 Hz, Py-H), 7.10 (2H, s, Ar-H), 3.06 (2H, sept., $^3J_{HH}$ = 6.9 Hz, CH(CH$_3$)$_2$), 2.95 (1H, sept., $^3J_{HH}$ = 6.9 Hz, CH(CH$_3$)$_2$), 1.98 (3H, s, CCH$_3$), 1.37 (6H, d, $^3J_{HH}$ = 6.8 Hz, CH(CH$_3$)$_2$), 1.27 (6 H, d, $^3J_{HH}$ = 6.8 Hz, CH(CH$_3$)$_2$), 1.12 (6 H, d, $^3J_{HH}$ = 6.8 Hz, CH(CH$_3$)$_2$). **^{13}C NMR (125 MHz; CD$_2$Cl$_2$):** δ 19.7 (C$\underline{C}$H$_3$), 23.7 (CH($\underline{C}$H$_3$)$_2$), 23.9 (CH($\underline{C}$H$_3$)$_2$), 24.3 (CH($\underline{C}$H$_3$)$_2$), 28.4 ($\underline{C}$H(CH$_3$)$_2$), 34.2 ($\underline{C}$H(CH$_3$)$_2$) 120.4 (CH), 121.1 (CH), 121.6 (CH), 124.5 (CH), 140.7 (C), 141.6 (C), 149.6 (C), 154.2 (C), 169.4 (C), 178.7 (C). **IR (cm^{-1}):** 1624 (strong, sharp, C=N), 2964 (medium, sharp, C-H), 3660 (medium, broad). ESIMS: (+) m/z 533 [M-Cl]. HRMS (TOF+ASAP) *m/z* calculated for C$_{24}$H$_{33}$ON$_2$PtCl$_2$ [M-Cl] 568.1697, found 568.1652.

5.3.26 Synthesis of $HL2_cPtCl_2$
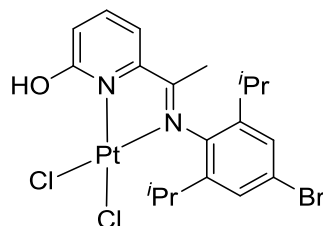
A 25 ml round-bottom flask, equipped with stir bar, was charged with $HL2_c$ (0.020 g, 0.053 mmol), chloroform (5 ml) and bis(dimethylsulfoxide)platinum dichloride (0.022 g, 0.053 mmol). The reaction was stirred and heated to 57 °C overnight resulting in a change in colour of the solution from yellow to dark red after 24 h. A fine white precipitate formed upon cooling to room temperature. The mixture was filtered through celite and the solvent removed by rotary evaporation to give $HL2_cPtCl_2$ as a red solid (0.032 g, 95%). **Mp:** 230 °C (decomp). **^{1}H NMR (400 MHz; CDCl$_3$):** *δ* 12.62 (1H, s, OH), 7.92 (1H, t, $^3J_{HH}$ = 7.8 Hz, Py-H), 7.42 (1H, dd, $^3J_{HH}$ = 7.4 Hz, $^4J_{HH}$ = 1.1 Hz, Py-H), 7.27 (2H, s, Ar-H), 7.12 (1H, dd, $^3J_{HH}$ = 8.6 Hz, $^4J_{HH}$ = 1.1 Hz, Py-H), 3.01 (2H, sept., $^3J_{HH}$ = 6.8 Hz, CH(CH$_3$)$_2$), 1.95 (3H, s, CCH$_3$), 1.32 (6H, d, $^3J_{HH}$ = 6.6 Hz, (CH(CH$_3$)$_2$), 1.04 (6H, d, $^3J_{HH}$ = 6.6 Hz, (CH(CH$_3$)$_2$). **^{13}C NMR (125 MHz; CDCl$_3$):** δ 19.3 (C$\underline{C}$H$_3$), 23.4 (CH($\underline{C}$H$_3$)$_2$), 23.8 (CH($\underline{C}$H$_3$)$_2$), 28.5 ($\underline{C}$H(CH$_3$)$_2$), 120.4 (CH), 121.8 (CH), 123.0 (CH), 127.5 (CH), 139.4 (C), 140.5 (CH), 143.1 (C), 154.1 (C). **IR (cm^{-1}):** 1441 (strong, sharp), 1623 (strong, sharp, C=N), 2966 (medium, sharp, C-H), 3500 (medium, sharp, OH). ESIMS: (+) m/z 570 [M-2Cl]. FABMS: *m/z* 606 [M-Cl].

5.3.27 Synthesis of (H**L2**ₐ)₂NiBr₂
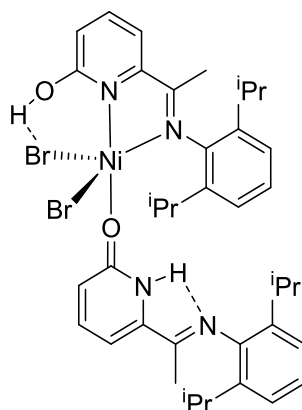
A small Schlenk flask, equipped with a stir bar, was evacuated and backfilled with nitrogen and then charged with (DME)NiBr₂ (0.026 g, 0.084 mmol, 1 eq.) and dichloromethane (5 ml). H**L2ₐ** (0.050 g, 0.169 mmol, 2 eq.) in dichloromethane (5 ml) were then introduced and the reaction mixture left to stir at room temperature for 18 h. The resulting precipitate was filtered and dried affording the product as a yellow powder (0.134 g, 98%). **M.p**: > 250 °C. **IR (cm⁻¹):** 3329 (sharp, O-H), 2968 (strong, C-H), 1632 (Strong, sharpe, C=N$_{imine}$), 1598 (s, C=N). ESIMS: m/z 652 [M-Br}. FABMS: *m/z* 731 [M-Br]. HRMS (TOF+ASAP) *m/z* calculated for C₁₉H₂₄BrN₂NiO [M-(HL2+Br)] 435.0405, Found 435.0411. μ$_{eff}$ = 2.82 BM.

5.3.28 Synthesis of (H**L2**ᵦ)₂NiBr₂
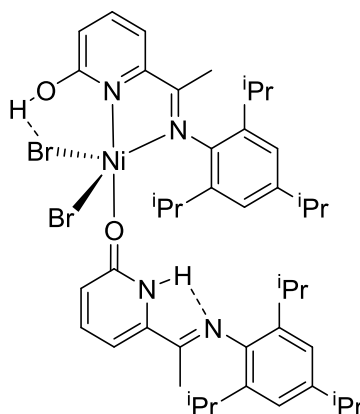
A small Schlenk flask, equipped with stir bar, was evacuated and backfilled with nitrogen and then charged with (DME)NiBr₂ (0.023 g, 0.075 mmol, 1 eq.) and dichloromethane (5 ml). H**L2ᵦ** (0.050 g, 0.15 mmol, 2 eq.) in dichloromethane (5 ml) was introduced and the mixture left to stir at room temperature for 18 h. The resulting precipitate was filtered and dried affording the product as a yellow powder (0.13 g, 97%). **M.p**: > 250 °C. **IR (cm⁻¹):** 3253 (sharp, O-H), 2954 (strong, C-H), 1635 (sharpe, C=N$_{imine}$), 1598 (s, C=N). ESIMS:

m/z 735 [M-Br]. FABMS: *m/z* 815 [M-Br]. HRMS (TOF+ASAP) *m/z* calculated for $C_{44}H_{60}N_4NiO_2$ [M-Br] 735.3946, found 735.4029. μ_{eff} = 2.72 BM. Anal. calc. for $C_{44}H_{60}N_4O_2NiBr_2$: C 59.02, H 6.75, N 6.26. Found: C 58.93, H 6.86, N 6.24%.

5.3.29 Synthesis of $(HL2_c)_2NiBr_2$
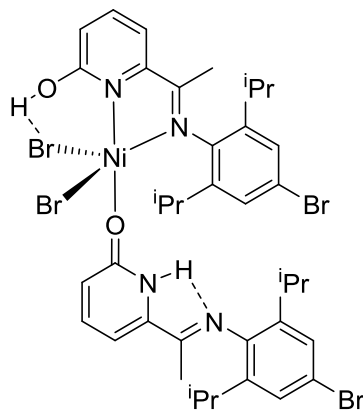
A small Schlenk flask, equipped with a stir bar, was evacuated and backfilled with nitrogen and then charged with $(DME)NiBr_2$ (0.020 g, 0.066 mmol, 1 eq.) and dichloromethane (5 ml). $HL2_c$ (0.050 g, 0.132 mmol, 2 eq.) in dichloromethane (5 ml) was introduced and the reaction mixture left to stir at room temperature for 18 h. The resulting precipitate was filtered and dried affording the product as a yellow powder (0.122 g, 95%). **M.p**: > 250 °C. **IR (cm^{-1}):** 3648 (sharp, O-H), 2942 (strong, C-H), 1634 (sharpe, C=N$_{imine}$), 1594 (s, C=N). ESIMS: m/z 810 [M-Br]. FABMS: *m/z* 810 [M-Br]. μ_{eff} = 2.86 BM. Anal. calc. for $C_{38}H_{46}N_4O_2NiBr_4 \cdot 3H_2O \cdot 5CH_2Cl_2$: C 35.67, H 4.32, N 3.87 Found: C 35.36, H 4.75, N 4.05%.

PART 2

5.3.30 Synthesis of 4-methoxypyridine N-oxide (**A**)
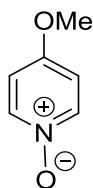
A 250 ml three necked round-bottom flask, equipped with a stir bar and reflux condenser, was evacuated and backfilled with nitrogen. Sodium metal (2.36 g, 102.78 mmol, 1.8 eq.) was added to dry MeOH (170 mL) at 0 °C under a positive pressure of nitrogen. 4-Nitropyridine N-oxide (8.00 g, 57.10 mmol) was added and the reaction mixture stirred under reflux (100 °C) for 18 h under an atmosphere of nitrogen. Upon reaction completion, the reaction mixture was cooled to room temperature and quenched with saturated aqueous NH_4Cl (50 mL). The methanol was removed from the reaction mixture at this point on a rotary evaporator. The remaining mixture was then extracted using $CHCl_3$ (4 x 100 mL). The organic layers were combined and dried over $MgSO_4$ and the solvent concentrated under reduced pressure to give 4-methoxypyridine N-oxide as a yellow-white solid (6.90 g, 98%). **^{1}H NMR (400 MHz; CDCl$_3$):** δ 8.13 (2H, d, $^3J_{HH}$ = 7.7 Hz, Py-H), 6.83 (2H, d, $^3J_{HH}$ = 7.7 Hz, Py-H), 3.87 (3H, s, O<u>Me</u>).

The ^{1}H NMR data is consistent with that described by Hegarty *et al.*[9]

5.3.31 Synthesis of 2-cyano-4-methoxypyridine (**B**)
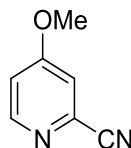
A 250 ml three necked round-bottom flask, equipped with a stir bar and pressure equalised dropping funnel (50 mL), was evacuated and backfilled with nitrogen. Trimethylsilyl cyanide (4.4 ml, 35.2 mmol, 1.1 eq.) was added to a solution of 4-methoxypyridine N-oxide (**A**) (4.00 g, 32 mmol. 1 eq.) in dry dichloromethane (60 ml) under a positive pressure of nitrogen. Dimethylcarbamyl chloride (3.2 ml, 35.2 mmol, 1.1 eq.) in dry dichloromethane (6 ml) was added dropwise using the attached dropping funnel. The mixture was stirred for 72 h under an atmosphere of nitrogen. A 10% aqueous potassium carbonate solution (35 ml) was added through the dropping funnel and stirred for 1 h. The organic layer was separated and the aqueous layer extracted with dichloromethane (4 x 50 ml); the organic layers were combined and dried over $MgSO_4$ and filtered. The solvent

was concentrated on the rotary evaporator to give 2-cyano-4-methoxypyridine (**B**) as a yellow solid (3.90 g, 92%). **¹H NMR (400 MHz; CDCl₃):** δ 8.51 (1H, d, $^3J_{HH}$ = 6.8 Hz, Py-H), 7.23 (1H, d, $^3J_{HH}$ = 6.5 Hz, Py-H), 6.83 (1H, q, $^4J_{HH}$ = 2.6 Hz, Py-H), 3.91 (3H, s, O<u>Me</u>).

The ¹H NMR data is consistent with that described by Bilcer *et al.*[10]

5.3.32 Synthesis of 2-acetyl-4-methoxypyridine (**C**)
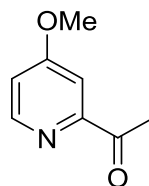
A 500 ml Schlenk tube, equipped with a stir bar, was evacuated, backfilled with nitrogen and then charged with 2-cyano-4-methoxypyridine (**B**) (4.00 g, 29.85 mmol) and dry toluene (100 ml). A 2 M solution of trimethylaluminium in toluene (30 ml, 59.7 mmol, 2 eq.) was added dropwise to the Schlenk flask and the reaction mixture stirred and heated at 60 °C for 18 h. Upon completion, the reaction was cooled to room temperature and concentrated under vacuum to give a red oil. The flask was cooled to 0 °C in an ice bath and diluted with chloroform (50 ml). Deionised water (*ca.* 50 ml) was added dropwise until the generation of gas was no longer observed. The mixture was diluted further with chloroform (30 ml) and stirred for 2 h. The aqueous layer was separated and washed with chloroform (4 x 50 ml), dried over MgSO₄ and then the solvent removed under reduced pressure to give 2-acetyl-4-methoxypyridine (**C**) as a brown oil (3.60 g, 80%). **¹H NMR (400 MHz; CDCl₃):** δ 8.40 (1H, d, $^3J_{HH}$ = 6.8 Hz, Py-H), 7.49 (1H, d, $^3J_{HH}$ = 6.6 Hz, Py-H), 6.89 (1H, d, $^3J_{HH}$ = 7.2 Hz, Py-H), 3.82 (3H, s, O<u>Me</u>), 2.64 (3H, s, CC<u>H</u>₃).

The ¹H NMR data is consistent with that described by Zuo *et al.*[11]

5.3.33 Synthesis of 2-acetyl-4-pyridone (**D**)
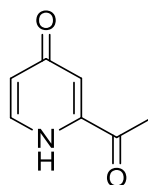
A 150 ml one neck round-bottom flask, equipped with stir bar and reflux condenser, was charged with 2-acetyl-4-methoxypyridine (3.00 g, 19.87 mmol) and 45% HBr in acetic acid (54 ml, 238.44 mmol, 12 eq.). The reaction mixture was stirred and heated at 115 °C

for 18 h. Upon completion, the mixture was cooled to room temperature and then poured into ice/water (50 ml). An aqueous solution of sodium hydroxide (20%) was added dropwise until the resultant solution was raised to pH 6-7. The solution was then washed with diethyl ether (6 x 50 ml) and the aqueous phase concentrated under reduced pressure. The remaining green solid was taken up in hot acetone (100 ml) and filtered. The filtrate was collected and the acetone was removed by rotary evaporation to give 2-acetyl-4-pyridone (**D**) as a pale brown solid (2.15 g, 79%). **^{1}H NMR (400 MHz; MeOD):** δ 7.81 (1H, d, $^3J_{HH}$ = 6.7 Hz, Py-H), 7.04 (1H, s, Py-H), 6.50 (1H, dd, $^3J_{HH}$ = 6.7 Hz, $^4J_{HH}$ = 2.2 Hz, Py-H), 2.50 (3H, s, CCH$_3$). **^{1}H NMR (400 MHz; CDCl$_3$):** δ 8.95 (IH, s, NH), 7.47 (1H, d, $^3J_{HH}$ = 6.4 Hz, Py-H), 6.94 (1H, s, Py-H), 6.43 (1H, d, $^3J_{HH}$ = 6.2 Hz, Py-H), 2.52 (3H, s, CCH$_3$). **^{13}C NMR (100 MHz; CDCl$_3$):** δ 25.5 (CCH$_3$), 106.5 (CH), 113.5 (CH), 149.7 (CH), 155.0 (C), 166.0 (C), 199.5 (C). ESIMS: (+) m/z 137 [M]. HRMS (TOF): calculated for C$_7$H$_8$NO$_2$ [M+H], 138.0555, Found: 138.0548.

5.3.34 Synthesis of H**L3**$_a$
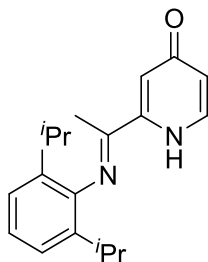
A 50 ml round-bottom flask, equipped with a stir bar, was charged with 2-acetyl-4-pyridone (**D**) (1.00 g, 7.3 mmol, 1 eq) and n-BuOH (20 ml). 2,6-Diisopropylaniline (1.90 g, 10.9 mmol, 1.5 eq) and p-toluenesulfonic acid (0.01 g, 0.073 mmol, 0.01 eq.) were then added. A Dean Stark apparatus with condenser was attached to the flask and the reaction mixture stirred and heated at reflux for 3 days. Upon completion, the mixture was cooled to room temperature, the solvent concentrated under reduced pressure and petroleum ether (25 ml) added to induce precipitation. The solid was filtered and dried to give H**L3**$_a$ as yellow solid (1.70 g, 78%). **M.P**: 132-135 °C. **^{1}H NMR (400 MHz; CDCl$_3$):** δ 9.95 (1H, s, NH), 7.54 (1H, d, $^3J_{HH}$ = 6.2 Hz, Py/Ar-H), 7.03 (3H, m, Py/Ar-H), 6.80 (1H, s, Py-H), 6.42 (1H, d, $^3J_{HH}$ = 6.5 Hz, Py/Ar-H), 2.49 (2H, sept., $^3J_{HH}$ = 6.8 Hz, CH(CH$_3$)$_2$), 1.95 (3H, s, CCH$_3$), 1.06 (12H, d, $^3J_{HH}$ = 6.8 Hz, CH(CH$_3$)$_2$).). **^{13}C NMR (100 MHz; CDCl$_3$):** δ 15.0 (CCH$_3$), 21.9 (CH(CH$_3$)$_2$), 22.3 (CH(CH$_3$)$_2$), 27.3 (CH(CH$_3$)$_2$), 116.7 (CH), 117.2 (CH), 122.3 (CH), 123.9 (CH), 135.1 (C), 136.0 (CH), 141.9 (C), 142.9 (C),

159.3 (C), 180.1 (C). **IR (cm⁻¹):** 2960 (medium, sharp, C-H), 1648 (strong, sharp, C=N_{imine}), 1372 (medium, sharp), 1199 (medium, strong). ESIMS: (+) *m/z* 297 [M+H]. HRMS (TOF): calculated for $C_{19}H_{24}N_2O$ [M+H], 297.1967, found: 297.1977.

5.3.35 Synthesis of H**L3**_b
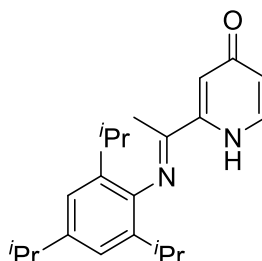
A 50 ml round-bottom flask, equipped with stir bar, was charged with 2-acetyl-4-pyridone (**D**) (0.90 g, 6.6 mmol, 1 eq) and *n*-BuOH (20 ml). 2,4,6-Triisopropylaniline (2.20 g, 9.9 mmol, 1.5 eq) and *p*-toluenesulfonic acid (0.01 g, 0.066 mmol, 0.01 eq.) were then added. A Dean Stark apparatus with condenser was attached to the flask and the reaction mixture stirred and heated to reflux for 3 days. Upon completion, the mixture was cooled to room temperature, the solvent concentrated under reduced pressure and petroleum ether (25 ml) added to induce precipitation. The solid was filtered and dried to give H**L3**_b as a yellow-white solid (1.80 g, 82%). **M.P**: 158-160 °C. **¹H NMR (400 MHz; CDCl₃):** δ 10.05 (1H, s, NH), 7.52 (1H, d, $^3J_{HH}$ = 7.5 Hz, Py-H), 6.93 (2H, s, Ar-H), 6.77 (1H, d, $^4J_{HH}$ = 1.9 Hz, Py-H), 6.39 (1H, dd, $^3J_{HH}$ = 7.8 Hz, $^4J_{HH}$ = 1.9 Hz, Py-H), 2.82 (1H, sept., $^3J_{HH}$ = 6.8 Hz, CH(CH₃)₂), 2.47 (2H, $^3J_{HH}$ = 6.8 Hz, CH(CH₃)₂), 1.92 (3H, s, CCH₃), 1.19 (6H, d, $^3J_{HH}$ = 6.8 Hz, CH(CH₃)₂), 1.05 (12H, d, $^3J_{HH}$ = 6.8 Hz, CH(CH₃)₂). **¹³C NMR (100 MHz; CDCl₃):** δ 15.0 (CCH₃), 21.9 (CH(CH₃)₂), 22.4 (CH(CH₃)₂), 23.1 (CH(CH₃)₂), 27.4 (CH(CH₃)₂), 33.0 (CH(CH₃)₂), 116.7 (CH), 117.1 (CH), 120.2 (CH), 134.7 (C), 135.7 (CH), 140.6 (C), 141.9 (C), 144.2 (C), 159.3 (C), 180.0 (C). **IR (cm⁻¹):** 2959 (medium, sharp, C-H), 1650 (strong, sharp, C=N_{imine}), 1540 (medium, sharp), 1262 (medium, strong). ESIMS: (+) *m/z* 339 [M+H]. HRMS (TOF): calculated for $C_{22}H_{31}N_2O$ [M+H], 339.2435, Found: 339.2449.

5.3.36 Synthesis of H**L3**$_c$
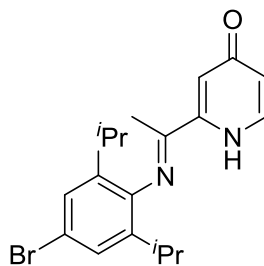
A 50 ml round-bottom flask, equipped with stir bar, was charged with 2-acetyl-4-pyridone (**D**) (1.00 g, 7.3 mmol, 1 eq) and *n*-BuOH (20 ml). 2,6-Diisopropyl-4-bromoaniline (2.80 g, 10.9 mmol, 1.5 eq) and *p*-toluenesulfonic acid (0.01 g, 0.073 mmol, 0.01 eq.) were then added. A Dean Stark apparatus with condenser was then attached to the flask and the reaction mixture stirred and heated at reflux for 3 days. Upon completion, the mixture was cooled to room temperature, the solvent concentrated under reduced pressure and petroleum ether (25 ml) added to induce precipitation. The solid was filtered and dried to give H**L3**$_c$ as a brown powder (2.20 g, 82%). **M.P**: 161-163 °C. **^{1}H NMR (400 MHz; CDCl$_3$):** δ 9.78 (1H, s, NH), 7.52 (1H, d, $^3J_{HH}$ = 6.6 Hz, Py-H), 7.20 (2H, s, Ar-H), 6.79 (1H, s, Py-H), 6.42 (1H, d, $^3J_{HH}$ = 6.4 Hz, Py-H), 2.46 (2H, sept., $^3J_{HH}$ = 6.8 Hz, CH(CH$_3$)$_2$), 1.97 (3H, s, CCH$_3$), 1.05 (12H, d, $^3J_{HH}$ = 6.8 Hz, CH(CH$_3$)2). **^{13}C NMR (100 MHz; CDCl$_3$):** δ 16.3 (CCH$_3$), 22.7 (CH(CH$_3$)$_2$), 23.1 (CH(CH$_3$)$_2$), 28.0 (CH(CH$_3$)$_2$), 117.6 (CH), 118.4 (CH), 123.3 (C), 125.8 (CH), 138.6 (CH), 142.9 (C), 143.2 (C). **IR (cm^{-1}):** 3663 (sharp, NH), 2957 (medium, sharp, C-H), 1647 (strong, sharp, C=N$_{imine}$), 1454 (medium, sharp). ESIMS: (+) *m/z* 377 [M+H]. ESIMS: (-) *m/z* 375 [M-H]. HRMS (TOF+ESI) calculated for C$_{19}$H$_{23}$N$_2$OBr [M+H] 377.1052, Found: 377.1062.

5.3.37 Synthesis of (**L3**$_a$)$_2$Pd
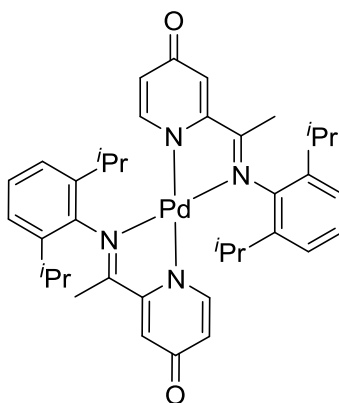
A small Schlenk flask, equipped with stir bar, was evacuated, backfilled with nitrogen and then charged with H**L3**$_a$ (0.100 g, 0.34 mmol, 2 eq.), palladium(II) acetate (0.38 g, 0.17 mmol, 1 eq.) and dry toluene (15 ml). The reaction mixture was left to stir at room temperature overnight under an atmosphere of nitrogen affording a red precipitate. This precipitate was then filtered through celite, washed with toluene and then extracted with dichloromethane. The solvent was removed by rotary evaporation to give (**L3**$_a$)$_2$Pd as a dark red powder (2.14 g, 89%). **Mp:** 265 °C (decomp). **^{1}H NMR (400 MHz; CDCl$_3$):** δ 7.45 (2H, d, $^3J_{HH}$ = 7.8 Hz, Py/Ar-H), 7.28 (2H, s, Py-H), 7.25 (2H, d, $^3J_{HH}$ = 6.8 Hz, Py/Ar-H), 6.99 (2H, d, $^3J_{HH}$ = 6.9 Hz, Py/Ar-H), 5.89 (2H, dd, $^3J_{HH}$ = 7.4 Hz, $^4J_{HH}$ = 2.9 Hz, Py/Ar-H), 5.29 (2H, d, $^3J_{HH}$ = 7.4 Hz, Py/Ar-H), 3.10 (4H, sept., $^3J_{HH}$ = 6.7 Hz, C$\underline{H}$(CH$_3$)$_2$), 2.15 (6H, s, CC$\underline{H}_3$), 1.15 (12H, d, $^3J_{HH}$ = 6.8 Hz, CH(C$\underline{H}_3$)$_2$), 1.08 (12H, d, $^3J_{HH}$ = 6.8 Hz, CH(C$\underline{H}_3$)$_2$). **^{13}C NMR (100 MHz; CDCl$_3$):** δ 18.9 (C$\underline{C}$H$_3$), 22.7 (CH($\underline{C}$H$_3$)$_2$), 23.6 (CH(CH$_3$)$_2$), 28.9 ($\underline{C}$H(CH$_3$)$_2$), 118.7 (CH), 123.5 (CH), 125.6 (CH), 130.3 (CH), 139.4 (C), 140.9 (C), 145.9 (CH), 153.8(C), 178.0 (C), 184.2 (C). **IR (cm^{-1}):** 1370 (strong, sharp), 1463 (medium, sharp), 1614 (strong, sharp, C=N), 2961 (medium, sharp, C-H). ESIMS: (+) *m/z* 698 [M+H]. ESIMS: (-) *m/z* 695 [M-H]. FABMS: *m/z* 697 [M+H]. HRMS(TOF): calculated for C$_{38}$H$_{46}$N$_4$O$_2$Pd [M] 696.2767, Found: 696.2750.

5.3.38 Synthesis of (**L3**$_b$)$_2$Pd
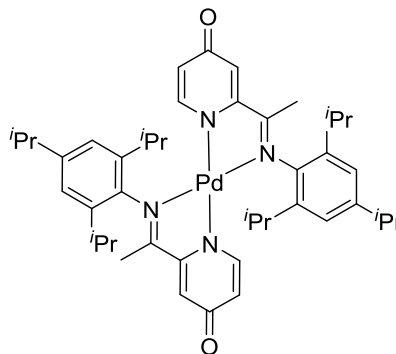
A small Schlenk flask, equipped with a stir bar, was evacuated, backfilled with nitrogen and then charged with H**L3**$_b$ (0.050 g, 0.15 mmol, 2 eq.), palladium(II) acetate (0.017 g, 0.075 mmol, 1 eq.) and dry toluene (10 ml). The reaction mixture was left to stir at room temperature overnight under an atmosphere of nitrogen affording a red precipitate. The precipitate was filtered through celite, washed with toluene and then extracted with dichloromethane. The solvent was removed by rotary evaporation to give (**L3**$_b$)$_2$Pd as a red powder (0.108 g, 90%). **Mp:** 265 °C (decomp). **^{1}H NMR (400 MHz; CDCl$_3$):** δ The

spectrum was very abroad peak hard to analyse. **IR (cm^{-1}):** 1357 (strong, sharp), 1453 (medium, sharp), 1616 (strong, sharp, C=N), 2960 (medium, sharp, C-H). ESIMS: (+) *m/z* 781 [M+H]. FABMS: *m/z* 782 [M+H]. HRMS(TOF): calculated for $C_{44}H_{58}N_4O_2Pd$ [M] 780.1250, Found:780.1220.

5.3.39 Synthesis of (**L3**$_c$)$_2$Pd
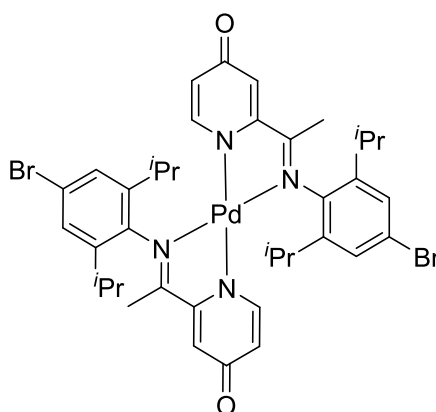
A small Schlenk flask, equipped with a stir bar, was evacuated, backfilled with nitrogen and then charged with H**L3**$_c$ (0.080 g, 0.21 mmol, 2 eq.), palladium(II) acetate (0.024 g, 0.105 mmol, 1 eq.) and dry toluene (10 ml). The reaction mixture was left to stir at room temperature overnight under an atmosphere of nitrogen affording a red precipitate. This precipitate was filtered through celite, washed with toluene and then extracted with dichloromethane. The solvent was removed by rotary evaporation to give (**L3**$_c$)$_2$Pd as a red powder (0.15 g, 85%). **Mp:** 265 °C (decomp). **^{1}H NMR (400 MHz; CDCl$_3$):** δ The spectrum was very abroad peak and hard to analyse. **IR (cm^{-1}):** 1370 (strong, sharp), 1463 (medium, sharp), 1615 (strong, sharp, C=N), 2962 (medium, sharp, C-H). ESIMS: (+) *m/z* 855 [M+H]. HRMS(TOF): calculated for $C_{38}H_{44}N_4O_2PdBr_2$ [M] 856.0101, Found: 856.0112.

5.3.40 Synthesis of H**L3**$_a$PdCl$_2$
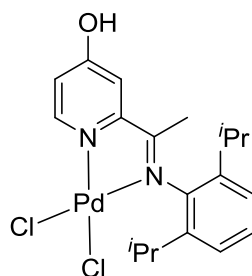
A small Schlenk tube, equipped with stir bar, was evacuated, backfilled with nitrogen and then charged with H**L3**$_a$ (0.090 g, 0.30 mmol, 1 eq.), bis(acetonitrile)palladium(II) chloride (0.09 g, 0.30 mmol, 1 eq.) and dry toluene (15 ml). The reaction was stirred at room temperature for 18 h under an atmosphere of nitrogen. The resulting precipitate was filtered through celite and washed with toluene. The yellow brown solid was then extracted with methanol and the solvent removed under reduced pressure to give H**L3**$_a$PdCl$_2$ as a yellow brown solid (0.125 g, 89%). **Mp**: 260 °C (decomp). **^{1}H NMR (400 MHz; CD$_3$CN):** δ 9.48 (1H, s, OH), 8.85 (1H, d, $^3J_{HH}$ = 7.6 Hz, Py/Ar-H), 7.84 (1H, d, $^4J_{HH}$ =2.7 Hz, Py-H), 7.32 (1H, t, $^3J_{HH}$ = 7.6 Hz, Ar-H), 7.22 (2H, dd, $^3J_{HH}$ = 7.6 Hz, $^4J_{HH}$ = 2.7 Hz, Py/Ar-H), 7.19 (1H, t, $^3J_{HH}$ =7.6 Hz, Py/Ar-H), 3.09 (2H, sept., $^3J_{HH}$ = 6.7 Hz, CH(CH$_3$)$_2$), 2.23 (3H, s, CCH$_3$), 1.36 (6H, d, $^3J_{HH}$ = 6.7 Hz, CH(CH$_3$)$_2$), 1.11 (6H, $^3J_{HH}$ = 6.7 Hz, CH(CH$_3$)$_2$). **^{1}H NMR (400 MHz; MeOD):** δ 8.79 (1H, d, $^3J_{HH}$ = 6.7 Hz, Py/Ar-H), 7.43 (1H, d, $^4J_{HH}$ = 2.7 Hz, Py-H), 7.23 (1H, t, $^3J_{HH}$ = 7.6 Hz, Ar-H), 7.14 (2H, d, $^3J_{HH}$ = 7.4 Hz, Py/Ar-H), 7.05 (1H, dd, $^3J_{HH}$ = 6.7 Hz, $^4J_{HH}$ = 2.7 Hz, Py-H), 3.09 (2H, sept., $^3J_{HH}$ = 6.8 Hz, CH(CH$_3$)$_2$), 2.16 (3H, s, CCH$_3$), 1.30 (6H, d, $^3J_{HH}$ = 6.7 Hz, CH(CH$_3$)$_2$), 1.07 (6H, $^3J_{HH}$ = 6.7 Hz, CH(CH$_3$)$_2$). **^{13}C NMR (125 MHz; MeOD):** δ 19.2 (C$\underline{C}$H$_3$), 23.9 (CH($\underline{C}$H$_3$)$_2$), 24.2 (CH(CH$_3$)$_2$), 30.1 ($\underline{C}$H(CH$_3$)$_2$), 115.9 (CH), 118.5 (CH), 125.1 (CH), 129.1 (CH), 129.7 (CH), 152.8 (C), 178.1 (C). **IR (cm^{-1}):** 1333 (strong, sharp), 1617 (strong, sharp, C=N), 2958 (medium, sharp, C-H), 3411 (medium, broad, O-H). ESIMS: (+) m/z 437 [M-Cl]. ESIMS: (-) m/z 473 [M]. FABMS: *m/z* 437 [M-Cl]. Anal Calc. for C$_{19}$H$_{24}$Cl$_2$N$_2$OPd.0.56CH$_2$Cl$_2$: C 45.07, H 4.86, N 5.37, found: C 45.00, H 5.18, N 5.15%.

5.3.41 Synthesis of H**L3**$_b$PdCl$_2$
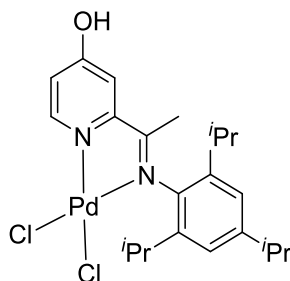
A small Schlenk tube, equipped with stir bar, was evacuated, backfilled with nitrogen and then charged with H**L3**$_b$ (0.100 g, 0.30 mmol, 1 eq.), bis(acetonitrile)palladium(II) chloride (0.09 g, 0.30 mmol, 1 eq.) and dry toluene (20 ml). The reaction was stirred at room temperature for 18 h under an atmosphere of nitrogen. The resulting precipitate was

filtered through celite and washed with toluene. The yellow solid was then extracted with methanol and the solvent removed under reduced pressure to give H$\mathbf{L3}_b$PdCl$_2$ as a yellow solid (0.136 g, 91%). **Mp**: 260 °C (decomp). **^{1}H NMR (400 MHz; MeOD):** δ 8.78 (1H, d, $^3J_{HH}$ = 6.5 Hz, Py-H), 7.45 (1H, d, $^4J_{HH}$ = 2.6 Hz, Py-H), 7.06 (1H, dd, $^3J_{HH}$ = 6.6 Hz, $^4J_{HH}$ = 2.6 Hz, Py-H), 6.99 (2H, s, Ar-H), 3.06 (2H, sept., $^3J_{HH}$ = 6.8 Hz, CH(CH$_3$)$_2$), 2.81 (1H, sept., $^3J_{HH}$ = 6.8 Hz, CH(CH$_3$)$_2$), 2.16 (3H, s, CCH$_3$), 1.29 (6H, d, $^3J_{HH}$ = 6.7 Hz, CH(CH$_3$)$_2$), 1.17 (6H, $^3J_{HH}$ = 6.9 Hz, CH(CH$_3$)$_2$), 1.07 (6H, $^3J_{HH}$ = 6.7 Hz, CH(CH$_3$)$_2$). **^{13}C NMR (125 MHz; MeOD):** δ 19.1 (C$\underline{C}$H$_3$), 24.0 (CH($\underline{C}$H$_3$)$_2$), 24.6 (CH($\underline{C}$H$_3$)$_2$), 24.8 (CH($\underline{C}$H$_3$)$_2$), 30.2 ($\underline{C}$H(CH$_3$)$_2$), 35.7 ($\underline{C}$H(CH$_3$)$_2$) 116.0 (CH), 117.9 (CH), 122.8 (CH), 152.2 (CH), 140.4 (C), 141.4 (C), 150.0 (C), 159.3 (C), 169.6 (C), 181.8 (C). **IR (cm^{-1}):** 1338 (strong, sharp), 1624 (strong, sharp, C=N), 2959 (medium, sharp, C-H), 3450 (medium, broad, O-H). ESIMS: (+) m/z 443 [M-Cl]. ESIMS: (-) m/z 515 [M]. FABMS: *m/z* 479 [M-Cl]. HRMS (TOF) calculated for C$_{22}$H$_{30}$ClN$_2$OPd [M-Cl] 479.5520, found 479.5311. Anal Calc. for C$_{21}$H$_{30}$Cl$_2$N$_2$OPd·0.41CH$_2$Cl$_2$: C 48.88, H 5.64, N 5.09. Found: C 48.83, H 5.68, N 4.89%.

5.3.42 Synthesis of H$\mathbf{L3}_c$PdCl$_2$
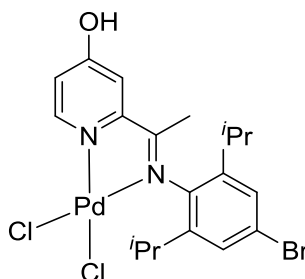
A small Schlenk tube, equipped with stir bar, was evacuated, backfilled with nitrogen and then charged with H$\mathbf{L3}_c$ (0.060 g, 0.16 mmol, 1 eq.), bis(acetonitrile)palladium(II) chloride (0.041 g, 0.16 mmol, 1 eq.) and dry toluene (10 ml). The reaction was stirred at room temperature for 18 h under an atmosphere of nitrogen. The resulting precipitate was filtered through celite and washed with toluene. The solid was then extracted with methanol and the solvent removed under reduced pressure to give H$\mathbf{L3}_c$PdCl$_2$ as a brown solid (0.08 g, 90%). **Mp**: 260 °C (decomp). **^{1}H NMR (400 MHz; MeOD):** δ 8.78 (1H, d, $^3J_{HH}$ = 6.6 Hz, Py-H), 7.46 (1H, d, $^4J_{HH}$ = 2.7 Hz, Py-H), 7.25 (2H, s, Ar-H), 7.07 (1H, dd, $^3J_{HH}$ = 6.6 Hz, $^4J_{HH}$ = 2.7 Hz, Py-H), 3.05 (2H, sept., $^3J_{HH}$ = 6.8 Hz, CH(CH$_3$)$_2$), 2.20 (3H, s, CCH$_3$), 1.29 (6H, d, $^3J_{HH}$ = 6.6 Hz, CH(CH$_3$)$_2$), 1.06 (6H, $^3J_{HH}$ = 6.6 Hz, CH(CH$_3$)$_2$). **^{13}C NMR (125 MHz; MeOD):** δ 19.2 (C$\underline{C}$H$_3$), 23.8 (CH($\underline{C}$H$_3$)$_2$), 23.9

(CH(C$\underline{H}_3$)$_2$), 30.2 (C$\underline{H}$(CH$_3$)$_2$), 116.0 (CH), 118.1 (CH), 123.3 (CH), 128.1 (CH), 141.3 (C), 144.2 (C), 152.6 (C), 169.6 (C). **IR (cm^{-1}):** 1333 (strong, sharp), 1620 (strong, sharp, C=N), 2963 (medium, sharp, C-H), 3645 (medium, broad, O-H). ESIMS: (+) m/z 481 [M-Cl]. ESIMS: (-) m/z 551 [M].

5.3.43 Synthesis of [H**L3**$_a$Pd(NCMe)$_2$][PF$_6$]$_2$
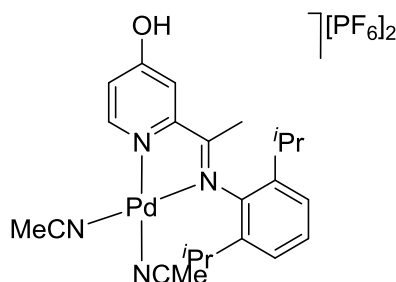
A small Schlenk tube, equipped with stir bar, was evacuated, backfilled with nitrogen and then charged with bis(acetonitrile)palladium(II) chloride (0.041 g, 0.14 mmol, 1 eq.), AgPF$_6$ (0.11 g, 0.42 mmol, 3 eq.) and dry acetonitrile (5 ml). The reaction was stirred at room temperature for 1 h before the addition of H**L3**$_a$ (0.040 g, 0.14 mmol, 1 eq.). The reaction mixture was then stirred at room temperature for an additional 18 h and the resulting precipitate (AgCl) filtered through celite. The solvent was removed by rotary evaporation to give [H**L3**$_a$Pd(NCMe)$_2$][PF$_6$]$_2$ as a yellow solid (0.099 g, 90%). **Mp:** 250 °C (decomp). **^{1}H NMR (400 MHz; CD$_3$CN):** δ 10.51 (1H, s, OH), 8.07 (1H, d, $^3J_{HH}$ = 6.0 Hz, Py/Ar-H),7.56 (1H, s, Py-H), 7.44 (1H, t, $^3J_{HH}$ = 7.7 Hz, Py/Ar-H), 7.32 (2H, d, $^3J_{HH}$ = 7.6 Hz, Py/Ar-H), 7.16 (1H, d, $^3J_{HH}$ = 6.6 Hz, Py/Ar-H), 3.13 (2H, sept., $^3J_{HH}$ = 6.8 Hz, CH(CH$_3$)$_2$), 2.30 (3H, s, CCH$_3$), 1.89 (6H, s, NCMe), 1.34 (6H, d, $^3J_{HH}$ = 6.6 Hz, CH(CH$_3$)$_2$), 1.11 (6H, d, $^3J_{HH}$ = 6.6 Hz, CH(CH$_3$)$_2$). **^{13}C NMR (125 MHz; CD$_3$CN):** δ 0.7 (NCC$_3$), 19.6 (CC$_3$), 23.3 (CH(C$\underline{H}_3$)$_2$), 24.0 (CH(C$\underline{H}_3$)$_2$), 29.5 (C$\underline{H}$(CH$_3$)$_2$), 117.4 (CH), 120.7 (CH), 125.8 (CH), 131.8 (CH), 140.8 (C), 141.7 (C), 154.2 (CH), 158.8 (C), 171.0 (C), 188.4 (C). **^{19}F NMR (376 MHz; CD$_3$CN):** δ -72.8 (F, d, J -693.1, PF$_6$). **^{31}P NMR (202 MHz; CD$_3$CN):** δ -144.6 (P, sept., J -710.9, PF$_6$). **IR (cm^{-1}):** 1620 (strong, sharp, C=N), 2942 (medium, sharp, C-H), 3310 (medium, broad, O-H). ESIMS: (+) m/z 402 [M$^+$- (NCMe+PF$_6$+HPF$_6$)], ESIMS: (-) m/z 145 [PF$_6$]. FABMS: *m/z* 443 [M-(PF$_6$+HPF$_6$)].

5.3.44 Synthesis of [HL3ᵦPd(NCMe)₂][PF₆]₂
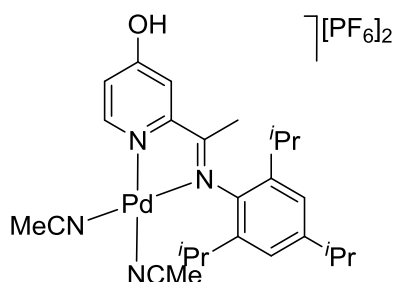
A small Schlenk tube, equipped with stir bar, was evacuated, backfilled with nitrogen and then charged with bis(acetonitrile)palladium(II) chloride (0.031 g, 0.12 mmol, 1 eq.), AgPF₆ (0.091 g, 0.36 mmol, 3 eq.) and dry acetonitrile (10 ml). The reaction was stirred at room temperature for 1 h before the addition of **HL3**$_b$ (0.040 g, 0.12 mmol, 1 eq.). The reaction mixture was stirred at room temperature for 18 h and the resulting precipitate (AgCl) filtered through celite. The solvent was removed by rotary evaporation to give [**HL3**$_b$Pd(NCMe)₂][PF₆]₂ as a yellow solid (0.095 g, 97%). **Mp:** 250 °C (decomp). **^{1}H NMR (400 MHz; CD₃CN):** δ 11.01 (1H, s, OH), 8.07 (1H, d, $^3J_{HH}$ = 6.3 Hz, Py-H), 7.53 (1H, s, Py-H), 7.18 (2H, s, Ar-H), 7.15 (1H, d, $^3J_{HH}$ = 6.2 Hz, Py-H), 3.10 (2H, sept., $^3J_{HH}$ = 6.7 Hz, CH(CH₃)₂), 2.88 (1H, sept., $^3J_{HH}$ = 6.7 Hz, CH(CH₃)₂), 2.29 (3H, s, CCH₃), 1.89 (6H, s, NCMe), 1.33 (6H, d, $^3J_{HH}$ = 6.6 Hz, CH(CH₃)₂), 1.18 (6H, d, $^3J_{HH}$ = 6.8 Hz, CH(CH₃)₂) 1.11 (6H, d, $^3J_{HH}$ = 6.8 Hz, CH((C$\underline{H}$₃)₂). **^{13}C NMR (125 MHz; CD₃CN):** δ 0.7 (NCCH₃), 19.6 (C$\underline{C}$H₃), 23.3 (CH($\underline{C}$H₃)₂), 23.9 (CH($\underline{C}$H₃)₂), 24.3 (CH($\underline{C}$H₃)₂), 29.8 ($\underline{C}$H(CH₃)₂), 35.2 ($\underline{C}$H(CH₃)₂), 117.3 (CH), 120.6 (CH), 124.0 (CH), 138.9 (C), 141.6 (CH), 152.7 (C), 154.3 (C), 158.9 (C), 170.7(C), 188.4 (C). **^{19}F NMR (376 MHz; CD₃CN):** δ -72.6 (F, d, J -751.7, PF₆). **^{31}P NMR (202 MHz; CD₃CN):** δ -144.6 (P, sept., J -695.3, PF₆). **IR (cm^{-1}):** 1622 (strong, sharp, C=N), 2965 (medium, sharp, C-H), 3312 (medium, broad, O-H). ESIMS: (+) m/z 527 [M⁺- (PF₆+HPF₆)], ESIMS: (-) m/z 145 [PF₆]. FABMS: *m/z* 526 [M- (PF₆+HPF₆)].

5.3.45 Synthesis of [HL3$_c$Pd(NCMe)₂][PF₆]₂
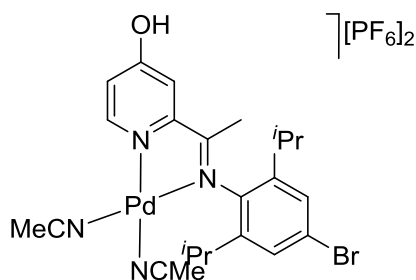
A small Schlenk tube, equipped with stir bar, was evacuated, backfilled with nitrogen and then charged with bis(acetonitrile)palladium(II) chloride (0.021 g, 0.12 mmol, 1 eq.), AgPF$_6$ (0.061 g, 0.24 mmol, 3 eq.) and dry acetonitrile (5 ml). The reaction was stirred at room temperature for 1 h before the addition of H**L3**$_c$ (0.030g, 0.08 mmol, 1 eq.). The reaction mixture was then stirred at room temperature for 18 h and the resulting precipitate (AgCl) filtered through celite. The solvent was removed by rotary evaporation to give [H**L3**$_c$Pd(NCMe)$_2$][PF$_6$]$_2$ as a yellow solid (0.063 g, 93%). **Mp:** 250 °C (decomp). **^{1}H NMR (400 MHz; CD$_3$CN):** δ 10.59 (1H, s, OH), 8.17 (1H, d, $^3J_{HH}$ = 6.6 Hz, Py-H), 7.60 (1H, d, $^4J_{HH}$ = 2.5 Hz, Py-H), 7.57 (2H, s, Ar-H), 7.25 (1H, d, $^3J_{HH}$ = 6.6 Hz, Py-H), 3.21 (2H, sept., $^3J_{HH}$ = 6.7 Hz, CH(CH$_3$)$_2$), 2.40 (3H, s, CCH$_3$), 1.89 (6H, s, NCMe), 1.42 (6H, d, $^3J_{HH}$ = 6.8 Hz, CH(CH$_3$)$_2$), 1.20 (6H, d, $^3J_{HH}$ = 6.8 Hz, CH(CH$_3$)$_2$). **^{13}C NMR (125 MHz; CD$_3$CN):** δ 0.7 (NCCH$_3$), 19.7 (CCH$_3$), 23.7 (CH(CH$_3$)$_2$), 23.9 (CH(CH$_3$)$_2$), 29.9 (CH(CH$_3$)$_2$), 117.1 (CH), 121.0 (CH), 125.4 (CH), 129.0 (CH), 140.2 (C), 144.6 (C), 153.8 (C), 158.7 (C), 170.6 (C), 189.1 (C). **^{19}F NMR (376 MHz; CD$_3$CN):** δ -72.8 (F, d, J -706.9, PF$_6$). **^{31}P NMR (202 MHz; CD$_3$CN):** δ -144.6 (P, sept., J -695.3, PF$_6$). **IR (cm^{-1}):** 1626 (strong, sharp, C=N), 2966 (medium, sharp, C-H), 3306 (medium, broad, O-H). ESIMS: (+) m/z 563 [M-(PF$_6$+HPF$_6$)], ESIMS: (-) m/z 145 [PF$_6$]. FABMS: *m/z* 563 [M-(PF$_6$+HPF$_6$)].

5.3.46 Synthesis of H**L3**$_a$PtCl$_2$
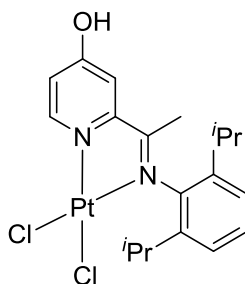
A 25 ml round-bottom flask, equipped with stir bar, was charged with H**L3**$_a$ (0.030 g, 0.10 mmol), chloroform (5 ml) and bis(dimethylsulfoxide)platinum dichloride (0.042 g, 0.10 mmol). The reaction was stirred and heated at 57 °C for 3 days resulting in a colour change from pale yellow to dark orange. The reaction was cooled to room temperature and any remaining Pt(DMSO)$_2$Cl$_2$ removed by filtration through a celite plug. The filtrate was dried to give H**L3**$_a$PtCl$_2$ as a red solid (0.049 g, 87%). **Mp:** 240 °C (decomp). **^{1}H NMR (400 MHz; CDCl$_3$):** δ 11.39 (1H, s, OH), 9.25 (1H, d, $^3J_{HH}$ = 6.6 Hz, Py/Ar-H), 7.62 (1H, d, $^4J_{HH}$ = 1.8 Hz, Py-H), 7.32 (2H, m, Py/Ar-H), 7.23 (2H, d, $^3J_{HH}$ = 6.7 Hz,

Py/Ar-H), 3.08 (2H, sept., $^3J_{HH}$ = 6.8 Hz, CH(CH$_3$)$_2$), 1.98 (3H, s, CCH$_3$), 1.33 (6H, d, $^3J_{HH}$ = 6.8 Hz, CH(CH$_3$)$_2$), 1.10 (6H, d, $^3J_{HH}$ = 6.8 Hz, CH(CH$_3$)$_2$). **^{13}C NMR (125 MHz; CDCl$_3$):** δ 18.6 (CCH$_3$), 23.4 (CH(CH$_3$)$_2$), 23.6 (CH(CH$_3$)$_2$), 28.4 (CH(CH$_3$)$_2$), 115.8 (CH), 116.6 (CH), 123.3 (CH), 123.7 (CH), 128.8 (CH), 140.3 (C), 150.3 (C), 158.3 (C), 167.5 (C), 177.6 (C). **IR (cm^{-1}):** 1343 (strong, sharp), 1617 (strong, sharp, C=N), 2962 (medium, sharp, C-H), 3630 (medium, broad, O-H). ESIMS: (+) m/z 561 [M-H]. ESIMS: 525 [M-Cl].

5.3.47 Synthesis of H**L3**$_b$PtCl$_2$
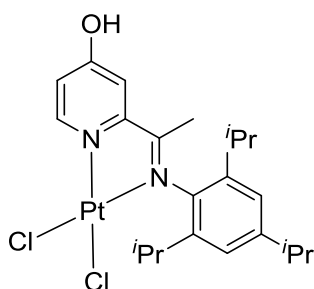
A 25 ml round-bottom flask was charged with H**L3**$_b$ (0.035 g, 0.104 mmol), chloroform (5 ml) and bis(dimethylsulfoxide)platinum dichloride (0.044 g, 0.104 mmol). The reaction was stirred and heated at 57 °C for 3 days resulting in a colour change from pale yellow to dark orange. The reaction was cooled to room temperature and any remaining Pt(DMSO)$_2$Cl$_2$ removed by filtration through a celite plug. The filtrate was dried to give H**L3**$_b$PtCl$_2$ as a red solid (0.057 g, 90%). **Mp:** 240 °C (decomp). **^{1}H NMR (400 MHz; CDCl$_3$):** δ 11.37 (1H, s, OH), 9.18 (1H, d, $^3J_{HH}$ = 6.7 Hz, Py-H), 7.57 (1H, d, $^4J_{HH}$ = 2.6 Hz, Py-H), 7.18 (1H, dd, $^3J_{HH}$ = 6.7 Hz, $^4J_{HH}$ = 2.5 Hz, Py-H), 7.00 (2H, s, Ar-H), 2.99 (2H, sept., $^3J_{HH}$ = 6.9 Hz, CH(CH$_3$)$_2$), 2.84 (1H, sept., $^3J_{HH}$ = 6.9 Hz, CH(CH$_3$)$_2$), 1.90 (3H, s, CCH$_3$), 1.24 (6H, d, $^3J_{HH}$ = 6.7 Hz, CH(CH$_3$)$_2$), 1.19 (6H, d, $^3J_{HH}$ = 6.9 Hz, CH(CH$_3$)$_2$), 1.02 (6H, d, $^3J_{HH}$ = 6.9 Hz, CH(CH$_3$)$_2$). **^{13}C NMR (125 MHz; CDCl$_3$):** δ 17.6 (CCH$_3$), 22.0 (CH(CH$_3$)$_2$), 22.6 (CH(CH$_3$)$_2$), 22.9 (CH(CH$_3$)$_2$), 27.1 (CH(CH$_3$)$_2$), 32.9 (CH(CH$_3$)$_2$), 114.5 (CH), 115.5 (CH), 120.4 (CH), 134.6 (C), 137.3 (CH), 139.2 (C), 147.9 (C), 157.4 (C), 166.5 (C), 176.6 (C). **IR (cm^{-1}):** 1343 (strong, sharp), 1615 (strong, sharp, C=N), 2960 (medium, sharp, C-H), 3640 (medium, broad, O-H). ESIMS: (+) m/z 608 [M+H]. ESIMS: 567 [M-Cl].

5.3.48 Synthesis of HL3cPtCl2
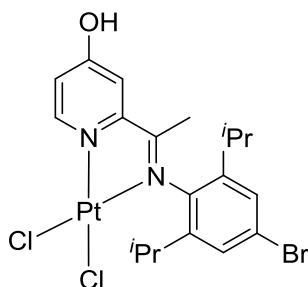
A 25 ml round-bottom flask was charged with **HL3**c (0.030 g, 0.08 mmol), chloroform (5 ml) and bis(dimethylsulfoxide)platinum dichloride (0.034 g, 0.08 mmol). The reaction was stirred and heated at 57 °C for 3 days resulting in a colour change from pale yellow to dark orange. The reaction was cooled to room temperature and any Pt(DMSO)$_2$Cl$_2$ removed by filtration through a celite plug. The filtrate was dried to give **HL3**cPtCl$_2$ as a red solid (0.045 g, 89%). **Mp:** 240 °C (decomp). **^{1}H NMR (400 MHz; CDCl$_3$):** δ 11.38 (1H, s, OH), 9.26 (1H, d, $^3J_{HH}$ = 6.6 Hz, Py-H), 7.60 (1H, d, $^4J_{HH}$ = 2.2 Hz, Py-H), 7.33 (2H, s, Ar-H), 7.30 (1H, d, $^3J_{HH}$ = 6.4 Hz, Py-H), 3.06 (2H, sept., $^3J_{HH}$ = 6.7 Hz, CH(CH$_3$)$_2$), 1.99 (3H, s, CCH$_3$), 1.32 (6H, d, $^3J_{HH}$ = 6.7 Hz, CH(CH$_3$)$_2$), 1.09 (6H, d, $^3J_{HH}$ = 6.7 Hz, CH(CH$_3$)$_2$). **^{13}C NMR (125 MHz; CDCl$_3$):** δ 18.8 (CCH$_3$), 23.3 (CH(CH$_3$)$_2$), 23.9 (CH(CH$_3$)$_2$), 28.3 (CH(CH$_3$)$_2$), 116.0 (CH), 117.0 (CH), 127.2 (CH), 139.3 (C), 142.9 (C), 143.3 (CH), 150.4 (C), 158.1 (C), 167.5 (C), 178.0 (C). **IR (cm^{-1}):** 1343 (strong, sharp), 1617 (strong, sharp, C=N), 2962 (medium, sharp, C-H), 3633 (medium, broad, O-H). ESIMS: (+) m/z 644 [M+H]. ESIMS: 570 [M-Cl].

5.3.49 Synthesis of L3aNiBr2
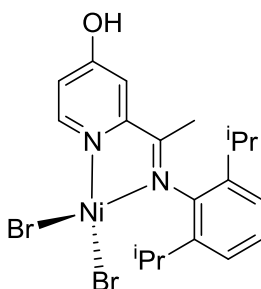
A small Schlenk flask, equipped with a stir bar, was evacuated, backfilled with nitrogen and then charged with (DME)NiBr$_2$ (0.052 g, 0.169 mmol) and dichloromethane (5 ml). **HL2**a (0.050 g, 0.169 mmol) in dichloromethane (5 ml) was introduced to the solution at 0 °C and the reaction mixture left to stir at room temperature for an additional 18 h. The resulting precipitate was filtered and dried to give the product as a green solid (0.045 g,

90%). **M.p**: > 250 °C. **IR (cm^{-1}):** 2967 (strong, C-H), 1605 (sharpe, C=N$_{imine}$), 1598 (s, C=N). ESIMS: m/z 434 [M-Br]. FABMS: *m/z* 434 [M-Br]. μ_{eff} = 2.73 BM.

5.3.50 Synthesis of **L3$_b$NiBr$_2$**
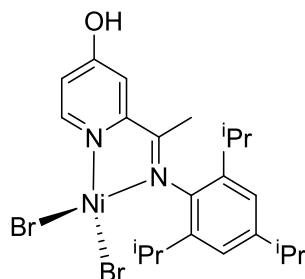
A small Schlenk flask, equipped with stir bar was evacuated, backfilled with nitrogen and then charged with (DME)NiBr$_2$ (0.046 g, 0.148 mmol) and dichloromethane (5 ml). H**L2$_b$** (0.050 g, 0.148 mmol) in dichloromethane (5 ml) was introduced to the solution at 0 °C and the reaction mixture left to stir at room temperature for an additional 18 h. The resulting precipitate was filtered and dried to give the product as a brown powder (0.044 g, 88%). **M.p**: > 250 °C. **IR (cm^{-1}):** 2963 (strong, C-H), 1606 (sharpe, C=N$_{imine}$), 1596 (s, C=N). ESIMS: m/z 477 [M-Br]. μ_{eff} = 2.69 BM.

5.3.51 Synthesis of **L3$_c$NiBr$_2$**
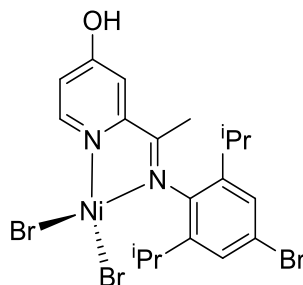
A small Schlenk flask, equipped with stir bar, was evacuated, backfilled with nitrogen and then charged with (DME)NiBr$_2$ (0.041 g, 0.13 mmol) and dichloromethane (5 ml). H**L2$_c$** (0.050 g, 0.13 mmol) in dichloromethane (5 ml) was introduced to the solution at 0 °C and the reaction mixture left to stir at room temperature for an additional 18 h. The resulting precipitate was filtered and dried to give the product as a brown powder (0.042 g, 84%). **M.p**: > 250 °C. **IR (cm^{-1}):** 2966 (strong, C-H), 1605 (sharpe, C=N$_{imine}$), 1595 (s, C=N). ESIMS: m/z 541 [M-Br]. FABMS: *m/z* 514 [M-Br]. μ_{eff} = 2.87 BM.

5.3.52 Synthesis of [(HL3$_a$)$_2$NiBr][Br]
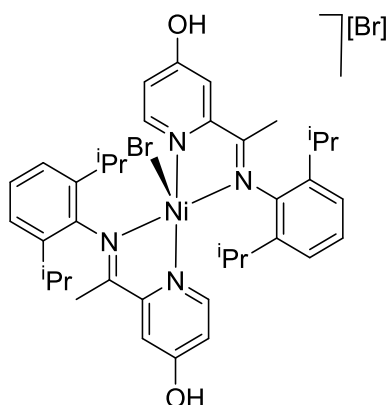
A small Schlenk flask, equipped with a stir bar, was evacuated, backfilled with nitrogen and then charged with (DME)NiBr$_2$ (0.026 g, 0.085 mmol) and dichloromethane (5 ml). HL2$_a$ (0.050 g, 0.169 mmol, 2 eq.) in dichloromethane (5 ml) was introduced to the solution at 0 °C and the reaction mixture left to stir at room temperature for an additional 18 h. The resulting precipitate was filtered and dried to give the product as a green solid (0.46 g, 92%). **M.p**: above 250 °C. **IR (cm^{-1}):** 3368 (strong, OH), 2972 (strong, C-H), 1604 (sharpe, C=N$_{imine}$), 1589 (s, C=N). ESIMS: m/z 652 [M-Br]. μ_{eff} = 2.64 BM.

5.4 Experimental procedures for Chapter 4
PART 1
5.4.1 Transfer hydrogenation

All the ketones and aldehydes, acetophenone, *p*-methoxyacetophenone, *p*-bromoacetophenone, *p*-methylacetophenone, benzophenone and benzylaldehyde were purchased from Sigma-Aldrich and used as received (Figure 5.1).
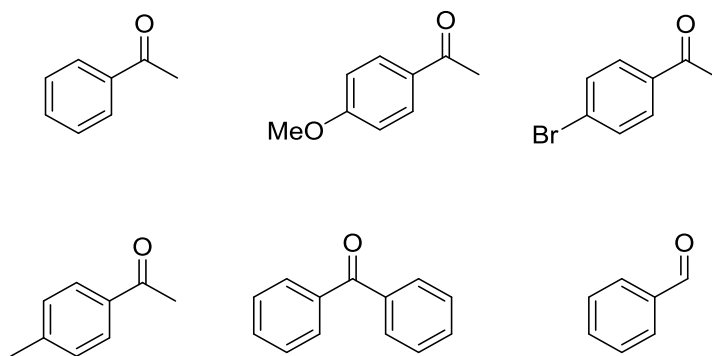
Figure 5.1: Substrates used for catalytic transfer hydrogenation

Typical procedure for the catalytic transfer hydrogenation

A stock solution of [H**L1**aRuCl$_2$(PPh$_3$)] (**41**) was first prepared in a 10 ml volumetric flask by dissolving **41** (0.033 g, 0.041 mmol) in isopropanol (10 ml). Under a nitrogen purged atmosphere a small Schlenk flask was loaded with a mixture of acetophenone (0.100 g, 0.83 mmol), the solution of **41** (1.0 ml, 0.0041 mmol, 0.5 mol%), base (0.009 g, 0.083 mmol) and isopropanol (10 ml). The reaction mixture was stirred at 80 °C for 6 h (with the tap open to the nitrogen bubbler) and then allowed to cool to room temperature. After removal of the solvent under reduced pressure, the ^{1}H NMR spectrum was recorded to determine the conversion. The crude product was purified by column chromatography on silica gel (100% dichloromethane) to give 1-phenyl ethanol (0.101 g, 99% yield) as a colourless oil.

The screening of H**L1**$_b$RuCl$_2$(PPh$_3$) (**42**), H**L1**$_c$RuCl$_2$(PPh$_3$) (**43**), **L1**$_H$RuCl$_2$(PPh$_3$) (**44**), [H**L1**$_a$PdNCMe][PF$_6$]$_2$ (**45**) and [H**L2**$_a$Pd(NCMe)$_2$][PF$_6$]$_2$ (**46**) was conducted in a similar manner. Likewise all the organic substrates were evaluated using the procedure described with **41** as the catalyst throughout.

1-Phenyl ethanol
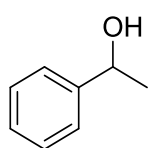
(0.100 g, 0.82 mmol, 98%) **^{1}H NMR (400 MHz, CDCl$_3$):** δ 7.38 (5H, m, CH), 4.84 (1H, d, $^3J_{HH}$ = 6.4 Hz, CH), 2.05 (IH, s, OH), 1.48 (3H, d, $^3J_{HH}$ = 6.8 Hz, CH$_3$).

4-Methoxy-α-methylbenzylalcohol
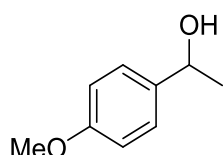
Colorless oil (0.109 g, 0.72 mmol, 87%) **^{1}H NMR (400 MHz, CDCl$_3$):** δ 7.20 (2H, d, $^3J_{HH}$ = 8.0 Hz, CH), 6.70 (2H, d, $^3J_{HH}$ = 8.0 Hz, CH), 4.82 (IH, q, $^3J_{HH}$ = 6.0 Hz, CH), 3.70 (3H, s, OMe), 1.38 (3H, d, $^3J_{HH}$ = 6.4 Hz, CH$_3$).

4-Bromo-α-methylbenzylalcohol
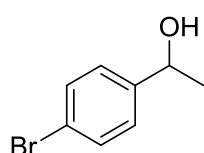
Cololess oil (0.163 g, 0.81 mmol, 98%) **^{1}H NMR (400 MHz, CDCl$_3$):** δ 7.36 (2H, d, $^3J_{HH}$ = 8.6 Hz, CH), 7.13 (2H, d, $^3J_{HH}$ = 8.6 Hz, CH), 4.73 (IH, q, $^3J_{HH}$ = 6.5 Hz, CH), 2.39 (IH, s, OH), 1.36 (3H, d, $^3J_{HH}$ = 6.5 Hz, CH$_3$).

1-(p-Tolyl)ethanol
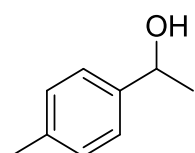
Colorless oil (0.093 g, 0.68 mmol, 82%) **^{1}H NMR (400 MHz, CDCl$_3$):** δ 7.14(2H, d, $^3J_{HH}$ = 7.9 Hz, CH), 7.05 (2H, d, $^3J_{HH}$ = 7.9 Hz, CH), 4.82 (1H, q, $^3J_{HH}$ = 6.5 Hz, CH), 2.15 (1H, s, OH), 2.25 (3H, s, *p*-Me), 1.36 (3H, d, $^3J_{HH}$ = 6.5 Hz, CH$_3$).

Diphenylmethanol
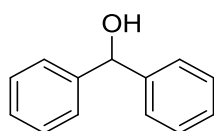
White solid (0.073 g, 0.39 mmol, 48%) **^{1}H NMR (400 MHz, CDCl$_3$):** δ 7.26 (4H, m, CH), 7.22 (4H, m, CH), 7.16 (2H, m, CH), 5.70 (1H, d, $^3J_{HH}$ = 4.0 Hz, CH), 2.19 (1H, d, $^3J_{HH}$ = 4.0 Hz, OH).

Benzyl alcohol
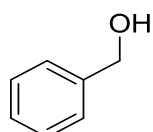
Colorless oil (0.085 g, 0.79 mmol, 95%) **^{1}H NMR (400 MHz, CDCl$_3$):** δ 7.25 (5H, m, CH), 4.59 (2H, d, $^3J_{HH}$ = 6.0 Hz, CH$_2$), 2.62 (IH, s, OH).

PART 2

5.4.2 Ethylene oligomerisation with two equivalents of trimethylaluminium

a) A large Schlenk tube, equipped with a stir bar, was evacuated and backfilled with nitrogen and then charged with **L3$_a$NiBr$_2$** (**47**) (0.005 g, 0.01 mmol), and a freshly preprared stock solution of trimethylaluminium (4.0 ml, 0.02 mmol, 2 eq.) and dry toluene (36 ml). The reaction mixture was left to stir for 5 min before ethylene gas was introduced at 0.8 bar. After 30 min of stirring at room temperature the ethylene pressure was vented to the bubbler and the reaction mixture quenched with a 2 M aqueous solution of HCl (15 ml). The organic layer was separated, dried over MgSO$_4$ and then the solvent removed by rotary evaporation to give an oligomeric wax (0.041 g). ^{1}H NMR (400 MHz; CDCl$_3$): 5.9 (1H, m, CH$_2$=C$\underline{H}$-), 4.7 (2H, m, C$\underline{H}_2$=C-), 1.1 (12H, s, n-C$\underline{H}_2$), 0.8 (3H, s, C$\underline{H}_3$). The catalytic activity is 10 g mmol^{-1} h^{-1} bar^{-1}.

b) Using a similar procedure to that described for **47**, using **L3$_b$NiBr$_2$** (**48**) (0.006 g, 0.01 mmol) as the pre-catalyst, afforded an oligomeric wax (0.010 g). ^{1}H NMR (400 MHz; CDCl$_3$): could not be record. The catalytic activity is 3 g mmol^{-1} h^{-1} bar^{-1}.

c) Using a similar procedure to that described for **47**, using **L3$_c$NiBr$_2$** (**49**) (0.006 g, 0.01 mmol) as the pre-catalyst, afforded an oligomeric wax (0.462 g). ^{1}H NMR (400 MHz; CDCl$_3$): 5.8 (1H, m, CH$_2$=C$\underline{H}$-), 5.1 (2H, m, C$\underline{H}_2$=CH-), 4.6 (2H, m, C$\underline{H}_2$=C-), 1.2 (12H, s, n-C$\underline{H}_2$), 0.9 (3H, s, C$\underline{H}_3$). The catalytic activity is 116 g mmol^{-1} h^{-1} bar^{-1}.

5.4.3 Ethylene uligomerisation with ten equivalents of trimethylaluminium

a) A large Schlenk tube, equipped with a stir bar, was evacuated and backfilled with nitrogen and then charged with **47** (0.005 g, 0.01 mmol), a freshly prepared stock solution of trimethylaluminium (20 ml, 0.1 mmol, 10 eq.) and dry toluene (20 ml). The reaction mixture was left to stir for 5 min before ethylene gas was introduced at 0.8 bar. After 30 min of stirring at room temperature the ethylene pressure was vented to the bubbler and the reaction mixture quenched with a 2 M aqueous solution of HCl (15 ml). The organic layer was separated, dried over MgSO$_4$ and then the solvent removed by rotary evaporation to give an oligomeric wax (0.052 g). ^{1}H NMR (400 MHz; CDCl$_3$): 4.7 (2H, m, C$\underline{H}_2$=C-), 1.1 (12H, s, n-C$\underline{H}_2$), 0.9 (3H, s, C$\underline{H}_3$). The catalytic activity is 13 g mmol^{-1} h^{-1} bar^{-1}.

b) Using a similar procedure to that described for **47**, using **48** (0.006 g, 0.01 mmol) as the pre-catalyst, afforded an oligomeric wax (0.009 g). ^{1}H NMR (400 MHz; CDCl$_3$): could not be recorded. The catalytic activity is 2 g mmol^{-1} h^{-1} bar^{-1}.

c) Using a similar procedure to that described for **47**, using **49** (0.006 g, 0.01 mmol) as the pre-catalyst, afforded an oligomeric wax (0.082 g). ^{1}H NMR (400 MHz; CDCl$_3$): 5.2 (1H, m, CH$_2$=C$\underline{H}$), 4.6 (2H, m, C$\underline{H}_2$=C-), 1.2 (12H, s, *n*-C$\underline{H}_2$), 0.8 (3H, s, C$\underline{H}_3$). The catalytic activity is 21 g mmol^{-1} h^{-1} bar^{-1}.

5.4.4 Ethylene oligomerisation with 100 equivalents of trimethylaluminium

a) A large Schlenk tube, equipped with a stir bar, was evacuated and backfilled with nitrogen and then charged with **47** (0.005 g, 0.01 mmol), a solution 2M trimethylaluminium (0.5 ml, 1 mmol, 100 eq.) and dry toluene (40 ml). The reaction mixture was left to stir for 5 min before ethylene gas was introduced at 0.8 bar. After 30 min of stirring at room temperature the ethylene pressure was vented to the bubbler and the reaction mixture quenched with a 2 M aqueous solution of HCl (15 ml). The organic layer was separated, dried over MgSO$_4$ and then the solvent removed by rotary evaporation to give an oligomeric wax (0.063 g). The catalytic activity is 16 g mmol^{-1} h^{-1} bar^{-1}.

b) Using a similar procedure to that described for **47**, using **48** (0.006 g, 0.01 mmol) as the pre-catalyst, afforded an oligomeric wax (0.015 g). The catalytic activity is 4 g mmol^{-1} h^{-1} bar^{-1}.

c) Using a similar procedure to that described for **47**, using **49** (0.006 g, 0.01 mmol) as the pre-catalyst, afforded an oligomeric wax (0.132 g). The catalytic activity is 33 g mmol^{-1} h^{-1} bar^{-1}.

5.5 Crystallographic Studies

Data for all crystallographically characterised samples were collected on a Bruker APEX 2000 CCD diffractometer. The data were corrected for Lorentz and polarisation effects and empirical absorption corrections applied. Structure solution by direct methods and

structure refinement based on full-matrix least-squares on F^2 employed SHELXTL version 6.10.[12] Hydrogen atoms were included in calculated positions (C-H = 0.95 – 1.00 Å) riding on the bonded atom with isotropic displacement parameters set to 1.5 Ueq(C) for methyl H atoms and 1.2 Ueq(C) for all other H atoms. All non-H atoms were refined with anisotropic displacement parameters. Details of data collection, refinement and crystal data are listed in Tables A.1 – A.42 in the Appendix.

References

1. (a) J. Liu, Y. Li, Y. Li and N. Hu, *J. Appl. Polym. Sci.,* 2008, **109**, 700. (b) C. J. Mathews, P.J. Smith and T. Welton, *J. Mol. Catal. A: Chem.,* 2003, **206**, 77. (c) D. R. Coulson, C. L. Satek, O. S. Grim, *Inorg. Synth.,* 1972, **13**: 121

2. T. Nguyen, M. A. Wicki and V. Snieckus, *J. Org. Chem.,* 2004, **69**, 7816.

3. B. E. Wagner, R. H. Holm and J. E. Parks, *J. Organomet. Chem.,* 1974, **56**, 53.

4. Y. D. M. Champouret, R. K. Chaggar, I. Dadhiwala, J. Fawcett and G. A. Solan, *Tetrahedron,* 2006, **62**, 79.

5. F. Vizza, A. Toti, L. Sorace, A. Meli, C. Mealli, F. Laschi, I. G. Rios, G. Giambastiani, D. Gatteschi and C. Bianchini, *Organometallics*, 2007, **26**, 726.

6. O. K. and and G. Wassilios, *World Pat.*, WO9730032 (A1), 1996.

7. B. M. L.and B. M. M., *USA Pat.*, WO2007017754 (A2), 2007.

8. D. Peng, Y. Zhang, X. Du, L. Zhang, X. Leng, M. D. Walter and Z. Huang, *J. Am. Chem. Soc*, 2013, **135**, 19154.

9. S. J. Connon and A. F. Hegarty, *Eur. J. Org. Chem.,* 2004, **16**, 3477.

10. A. K. Ghosh, N. Kumaragurnbaran, C. Liu, T. Devasamudram, H. Lei, L.Swanson, S. Ankala, J. Tang and G. Bilcer, *World Pat*, WO2006110668 A1, 2006.

11. W. H. Sun, S. Zhang and W. Zuo, *C. R. Chimie*, 2008, **11**, 307.

12. a) J. Huang, E. D. Stevens, S. P. Nolan and J. L. Peterson, *J. Am. Chem. Soc*., 1999, **121**, 2674. (b) M. Scholl, T. M. Trnka, J. P. Morgan and R. H. Grubbs, *Tet. Lett*., 1999, **40**, 2247 (c) M. Scholl, S. Ding, C. W. Lee and R. H. Grubbs, *Org. Lett*., 1999, **6**, 953.

Appendix

Crystal data and structure refinements

Additional figures

Table A.1. Crystal data and structure refinement for **b**

Identification code	11049
Empirical formula	C13 H14 N2 O3
Formula weight	246.26
Temperature	150(2) K
Wavelength	0.71073 Å
Crystal system	Monoclinic
Space group	P2(1)/n
Unit cell dimensions	a = 3.953(2) Å α= 90°.
	b = 15.086(9) Å β= 94.430(13)°.
	c = 20.069(12) Å γ = 90°.
Volume	1193.1(12) Å^3
Z	4
Density (calculated)	1.371 Mg/m^3
Absorption coefficient	0.099 mm^{-1}
F(000)	520
Crystal size	0.42 x 0.13 x 0.07 mm^3
Theta range for data collection	1.69 to 25.00°.
Index ranges	-4<=h<=4, -17<=k<=17, -23<=l<=23
Reflections collected	8525
Independent reflections	2108 [R(int) = 0.1562]
Completeness to theta = 25.00°	100.0 %
Absorption correction	Empirical
Max. and min. transmission	0.969 and 0.231
Refinement method	Full-matrix least-squares on F^2
Data / restraints / parameters	2108 / 0 / 146
Goodness-of-fit on F^2	0.859
Final R indices [I>2sigma(I)]	R1 = 0.0769, wR2 = 0.1788
R indices (all data)	R1 = 0.1537, wR2 = 0.2073
Largest diff. peak and hole	0.316 and -0.282 e.Å^{-3}

Table A.2. Crystal data and structure refinement for **HL1$_a$**

Identification code	11039
Empirical formula	C24 H27 N3 O
Formula weight	373.49
Temperature	150(2) K
Wavelength	0.71073 Å
Crystal system	Monoclinic
Space group	C2/c
Unit cell dimensions	a = 24.131(11) Å $\alpha = 90°$.
	b = 11.422(5) Å $\beta = 113.953(9)°$.
	c = 16.373(7) Å $\gamma = 90°$.
Volume	4124(3) Å^3
Z	8
Density (calculated)	1.203 Mg/m^3
Absorption coefficient	0.075 mm^{-1}
F(000)	1600
Crystal size	0.27 x 0.18 x 0.10 mm^3
Theta range for data collection	1.85 to 25.00°.
Index ranges	-28<=h<=28, -13<=k<=13, -19<=l<=19
Reflections collected	14531
Independent reflections	3628 [R(int) = 0.0853]
Completeness to theta = 25.00°	99.9 %
Absorption correction	Empirical
Max. and min. transmission	0.981 and 0.439
Refinement method	Full-matrix least-squares on F^2
Data / restraints / parameters	3628 / 0 / 258
Goodness-of-fit on F^2	0.945
Final R indices [I>2sigma(I)]	R1 = 0.0530, wR2 = 0.1132
R indices (all data)	R1 = 0.0827, wR2 = 0.1248
Largest diff. peak and hole	0.194 and -0.222 e.Å^{-3}

Table A.3. Crystal data and structure refinement for **HL2$_a$**

Identification code	15126
Empirical formula	C19 H24 N2 O
Formula weight	296.40
Temperature	150(2) K
Wavelength	0.71073 Å
Crystal system	Triclinic
Space group	P-1
Unit cell dimensions	a = 8.866(2) Å α= 91.980(4)°.
	b = 12.571(3) Å β= 100.619(4)°.
	c = 15.275(3) Å γ = 94.830(4)°.
Volume	1665.2(6) Å^3
Z	4
Density (calculated)	1.182 Mg/m^3
Absorption coefficient	0.073 mm^{-1}
F(000)	640
Crystal size	0.36 x 0.15 x 0.10 mm^3
Theta range for data collection	1.36 to 26.00°.
Index ranges	-10<=h<=10, -15<=k<=15, -18<=l<=18
Reflections collected	13003
Independent reflections	6446 [R(int) = 0.0453]
Completeness to theta = 26.00°	98.7 %
Absorption correction	Empirical
Max. and min. transmission	0.831 and 0.507
Refinement method	Full-matrix least-squares on F^2
Data / restraints / parameters	6446 / 0 / 427
Goodness-of-fit on F^2	0.932
Final R indices [I>2sigma(I)]	R1 = 0.0536, wR2 = 0.1234
R indices (all data)	R1 = 0.0801, wR2 = 0.1341
Largest diff. peak and hole	0.339 and -0.306 e.Å^{-3}

Table A.4. Crystal data and structure refinement for **HL2$_b$**

Identification code	14057
Empirical formula	C22 H30 N2 O
Formula weight	338.48
Temperature	150(2) K
Wavelength	0.71073 Å
Crystal system	Triclinic
Space group	P-1
Unit cell dimensions	a = 6.049(5) Å α= 88.854(13)°.
	b = 8.791(7) Å β= 82.228(15)°.
	c = 19.261(14) Å γ = 80.046(15)°.
Volume	999.4(13) Å^3
Z	2
Density (calculated)	1.125 Mg/m^3
Absorption coefficient	0.069 mm^{-1}
F(000)	368
Crystal size	0.43 x 0.10 x 0.05 mm^3
Theta range for data collection	2.13 to 25.00°.
Index ranges	-7<=h<=7, -10<=k<=10, -22<=l<=22
Reflections collected	7310
Independent reflections	3495 [R(int) = 0.2299]
Completeness to theta = 25.00°	99.1 %
Absorption correction	Empirical
Max. and min. transmission	0.969 and 0.004
Refinement method	Full-matrix least-squares on F^2
Data / restraints / parameters	3495 / 6 / 234
Goodness-of-fit on F^2	0.849
Final R indices [I>2sigma(I)]	R1 = 0.1259, wR2 = 0.2420
R indices (all data)	R1 = 0.2951, wR2 = 0.3154
Extinction coefficient	0.010(5)
Largest diff. peak and hole	0.317 and -0.346 e.Å^{-3}

Table A.5. Crystal data and structure refinement for **HL3$_a$**

Identification code	16005
Empirical formula	C19.75 H27 N2 O1.75
Formula weight	320.43
Temperature	150(2) K
Wavelength	0.71073 Å
Crystal system	Orthorhombic
Space group	Fdd2
Unit cell dimensions	a = 27.539(11) Å α= 90°.
	b = 11.448(4) Å β= 90°.
	c = 23.285(9) Å γ = 90°.
Volume	7341(5) Å^3
Z	16
Density (calculated)	1.160 Mg/m^3
Absorption coefficient	0.074 mm^{-1}
F(000)	2776
Crystal size	0.43 x 0.28 x 0.15 mm^3
Theta range for data collection	2.12 to 25.00°.
Index ranges	-32<=h<=32, -13<=k<=13, -27<=l<=27
Reflections collected	12773
Independent reflections	1666 [R(int) = 0.1185]
Completeness to theta = 25.00°	100.0 %
Absorption correction	Empirical
Max. and min. transmission	0.981 and 0.410
Refinement method	Full-matrix least-squares on F^2
Data / restraints / parameters	1666 / 1 / 204
Goodness-of-fit on F^2	1.002
Final R indices [I>2sigma(I)]	R1 = 0.0514, wR2 = 0.1104
R indices (all data)	R1 = 0.0619, wR2 = 0.1142
Absolute structure parameter	?
Largest diff. peak and hole	0.215 and -0.261 e.Å^{-3}

Table A.6. Crystal data and structure refinement for **HL3$_b$**

Identification code	17019
Empirical formula	C23 H31 Cl3 N2 O
Formula weight	457.85
Temperature	150(2) K
Wavelength	0.71073 Å
Crystal system	Orthorhombic
Space group	P2(1)2(1)2
Unit cell dimensions	a = 22.640(6) Å α= 90°.
	b = 33.822(9) Å β= 90°.
	c = 6.4791(18) Å γ = 90°.
Volume	4961(2) Å^3
Z	8
Density (calculated)	1.226 Mg/m^3
Absorption coefficient	0.385 mm^{-1}
F(000)	1936
Crystal size	0.45 x 0.14 x 0.08 mm^3
Theta range for data collection	1.20 to 26.00°.
Index ranges	-27<=h<=27, -41<=k<=40, -7<=l<=7
Reflections collected	39327
Independent reflections	9725 [R(int) = 0.2211]
Completeness to theta = 26.00°	100.0 %
Absorption correction	Empirical
Max. and min. transmission	0.981 and 0.645
Refinement method	Full-matrix least-squares on F^2
Data / restraints / parameters	9725 / 463 / 537
Goodness-of-fit on F^2	0.899
Final R indices [I>2sigma(I)]	R1 = 0.0973, wR2 = 0.2170
R indices (all data)	R1 = 0.2230, wR2 = 0.2668
Absolute structure parameter	0.48(14)
Largest diff. peak and hole	1.098 and -0.553 e.Å^{-3}

Table A.7. Crystal data and structure refinement for **HL3_c**

Identification code	16138
Empirical formula	C39 H47 Br2 Cl3 N4 O2
Formula weight	869.98
Temperature	150(2) K
Wavelength	0.71073 Å
Crystal system	Monoclinic
Space group	P2(1)/c
Unit cell dimensions	$a = 20.845(4)$ Å $\quad\alpha= 90°$.
	$b = 12.811(3)$ Å $\quad\beta= 103.141(4)°$.
	$c = 15.493(3)$ Å $\quad\gamma = 90°$.
Volume	4028.8(14) Å^3
Z	4
Density (calculated)	1.434 Mg/m^3
Absorption coefficient	2.249 mm^{-1}
F(000)	1784
Crystal size	0.46 x 0.06 x 0.02 mm^3
Theta range for data collection	1.88 to 27.00°.
Index ranges	-26<=h<=26, -16<=k<=16, -19<=l<=19
Reflections collected	33060
Independent reflections	8773 [R(int) = 0.0667]
Completeness to theta = 27.00°	99.8 %
Absorption correction	Empirical
Max. and min. transmission	0.894 and 0.614
Refinement method	Full-matrix least-squares on F^2
Data / restraints / parameters	8773 / 7 / 461
Goodness-of-fit on F^2	0.844
Final R indices [I>2sigma(I)]	R1 = 0.0445, wR2 = 0.0843
R indices (all data)	R1 = 0.0850, wR2 = 0.0916
Largest diff. peak and hole	0.780 and -0.790 e.Å^{-3}

Table A.8. Crystal data and structure refinement for **L1$_a$PdOAc**

Identification code	16136
Empirical formula	C29 H44 N3 O7.50 Pd
Formula weight	661.07
Temperature	150(2) K
Wavelength	0.71073 Å
Crystal system	Triclinic
Space group	P-1
Unit cell dimensions	a = 10.229(3) Å $\quad$ α= 73.740(5)°.
	b = 10.656(4) Å $\quad$ β= 89.364(5)°.
	c = 15.883(5) Å $\quad$ γ = 67.539(5)°.
Volume	1527.0(9) Å^3
Z	2
Density (calculated)	1.438 Mg/m^3
Absorption coefficient	0.658 mm^{-1}
F(000)	690
Crystal size	0.45 x 0.23 x 0.14 mm^3
Theta range for data collection	1.34 to 26.00°.
Index ranges	-12<=h<=12, -13<=k<=13, -19<=l<=19
Reflections collected	11885
Independent reflections	5912 [R(int) = 0.0684]
Completeness to theta = 26.00°	98.4 %
Absorption correction	Empirical
Max. and min. transmission	0.831 and 0.394
Refinement method	Full-matrix least-squares on F^2
Data / restraints / parameters	5912 / 0 / 304
Goodness-of-fit on F^2	0.974
Final R indices [I>2sigma(I)]	R1 = 0.0559, wR2 = 0.1289
R indices (all data)	R1 = 0.0713, wR2 = 0.1341
Largest diff. peak and hole	1.447 and -0.849 e.Å^{-3}

Table A.9. Crystal data and structure refinement for **L1**$_a$**PdCl**

Identification code	11056n
Empirical formula	C24 H40 Cl N3 O8 Pd
Formula weight	640.44
Temperature	150(2) K
Wavelength	0.71073 Å
Crystal system	Tetragonal
Space group	P4/nnc
Unit cell dimensions	a = 23.179(3) Å $\quad$ α= 90°.
	b = 23.179(3) Å $\quad$ β= 90°.
	c = 20.125(4) Å $\quad$ γ = 90°.
Volume	10812(3) Å^3
Z	16
Density (calculated)	1.574 Mg/m^3
Absorption coefficient	0.837 mm^{-1}
F(000)	5312
Crystal size	0.37 x 0.21 x 0.08 mm^3
Theta range for data collection	1.24 to 26.00°.
Index ranges	0<=h<=20, 0<=k<=28, 0<=l<=24
Reflections collected	5328
Independent reflections	5328 [R(int) = 0.0000]
Completeness to theta = 26.00°	100.0 %
Absorption correction	Empirical
Max. and min. transmission	0.862 and 0.287
Refinement method	Full-matrix least-squares on F^2
Data / restraints / parameters	5328 / 0 / 276
Goodness-of-fit on F^2	0.870
Final R indices [I>2sigma(I)]	R1 = 0.0833, wR2 = 0.2068
R indices (all data)	R1 = 0.1778, wR2 = 0.2406
Largest diff. peak and hole	0.715 and -0.474 e.Å^{-3}

Table A.10. Crystal data and structure refinement for [**HL1**c PdCl][Cl]

Identification code	11053
Empirical formula	C21 H23 Cl2 N3 O2 Pd
Formula weight	526.72
Temperature	150(2) K
Wavelength	0.71073 Å
Crystal system	Monoclinic
Space group	P2(1)/c
Unit cell dimensions	a = 8.2511(11) Å $\quad$ α= 90°.
	b = 35.253(5) Å $\quad$ β= 97.421(4)°.
	c = 7.4344(11) Å $\quad$ γ = 90°.
Volume	2144.4(5) Å^3
Z	4
Density (calculated)	1.631 Mg/m^3
Absorption coefficient	1.137 mm^{-1}
F(000)	1064
Crystal size	0.12 x 0.11 x 0.08 mm^3
Theta range for data collection	2.31 to 26.00°.
Index ranges	-10<=h<=10, -43<=k<=43, -8<=l<=9
Reflections collected	15744
Independent reflections	4181 [R(int) = 0.1384]
Completeness to theta = 26.00°	99.1 %
Absorption correction	Empirical
Max. and min. transmission	0.862 and 0.576
Refinement method	Full-matrix least-squares on F^2
Data / restraints / parameters	4181 / 0 / 266
Goodness-of-fit on F^2	0.859
Final R indices [I>2sigma(I)]	R1 = 0.0603, wR2 = 0.1025
R indices (all data)	R1 = 0.1122, wR2 = 0.1182
Largest diff. peak and hole	1.200 and -0.735 e.Å^{-3}

Table A.11. Crystal data and structure refinement for [**HL1_a**PdCl][PF$_6$]

Identification code	14031
Empirical formula	C51 H57 Cl11 F12 N6 O2 P2 Pd2
Formula weight	1678.72
Temperature	150(2) K
Wavelength	0.71073 Å
Crystal system	Monoclinic
Space group	P2(1)/c
Unit cell dimensions	a = 20.135(4) Å $\quad$ α= 90°.
	b = 39.205(7) Å $\quad$ β= 93.978(4)°.
	c = 8.3079(15) Å $\quad$ γ = 90°.
Volume	6542(2) Å^3
Z	4
Density (calculated)	1.704 Mg/m^3
Absorption coefficient	1.126 mm^{-1}
F(000)	3352
Crystal size	0.40 x 0.20 x 0.16 mm^3
Theta range for data collection	1.45 to 26.00°.
Index ranges	-24<=h<=24, -48<=k<=48, -10<=l<=10
Reflections collected	50860
Independent reflections	12852 [R(int) = 0.0883]
Completeness to theta = 26.00°	99.8 %
Absorption correction	Empirical
Max. and min. transmission	0.831 and 0.657
Refinement method	Full-matrix least-squares on F^2
Data / restraints / parameters	12852 / 0 / 785
Goodness-of-fit on F^2	1.000
Final R indices [I>2sigma(I)]	R1 = 0.0524, wR2 = 0.0969
R indices (all data)	R1 = 0.0789, wR2 = 0.1051
Largest diff. peak and hole	0.955 and -0.807 e.Å^{-3}

Table A.12. Crystal data and structure refinement for [**HL1ᵦ**PdCl][PF₆]

Identification code	16148
Empirical formula	C28 H35 Cl3 F6 N3 O P Pd
Formula weight	787.31
Temperature	150(2) K
Wavelength	0.71073 Å
Crystal system	Triclinic
Space group	P-1
Unit cell dimensions	a = 15.596(3) Å α= 96.851(4)°.
	b = 15.842(3) Å β= 108.345(4)°.
	c = 16.385(3) Å γ = 117.730(4)°.
Volume	3226.6(10) Å³
Z	4
Density (calculated)	1.621 Mg/m³
Absorption coefficient	0.936 mm⁻¹
F(000)	1592
Crystal size	0.19 x 0.13 x 0.04 mm³
Theta range for data collection	1.38 to 26.00°.
Index ranges	-19<=h<=19, -19<=k<=19, -20<=l<=19
Reflections collected	25572
Independent reflections	12534 [R(int) = 0.1318]
Completeness to theta = 26.00°	98.8 %
Absorption correction	Empirical
Max. and min. transmission	0.831 and 0.628
Refinement method	Full-matrix least-squares on F²
Data / restraints / parameters	12534 / 6 / 789
Goodness-of-fit on F²	0.680
Final R indices [I>2sigma(I)]	R1 = 0.0632, wR2 = 0.0962
R indices (all data)	R1 = 0.1791, wR2 = 0.1207
Largest diff. peak and hole	0.784 and -0.647 e.Å⁻³

Table A.13. Crystal data and structure refinement for [**L1**_aPd(OH₂)][PF₆]

Identification code	14097
Empirical formula	C24 H28 F6 N3 O2 P Pd
Formula weight	641.86
Temperature	150(2) K
Wavelength	0.71073 Å
Crystal system	Triclinic
Space group	P-1
Unit cell dimensions	a = 9.725(4) Å α= 81.271(7)°.
	b = 11.041(4) Å β= 69.631(7)°.
	c = 12.645(5) Å γ = 77.963(7)°.
Volume	1240.2(8) Å³
Z	2
Density (calculated)	1.719 Mg/m³
Absorption coefficient	0.886 mm⁻¹
F(000)	648
Crystal size	0.27 x 0.13 x 0.07 mm³
Theta range for data collection	1.72 to 26.00°.
Index ranges	-11<=h<=11, -13<=k<=13, -15<=l<=15
Reflections collected	9746
Independent reflections	4780 [R(int) = 0.1013]
Completeness to theta = 26.00°	98.5 %
Absorption correction	Empirical
Max. and min. transmission	0.862 and 0.474
Refinement method	Full-matrix least-squares on F²
Data / restraints / parameters	4780 / 3 / 339
Goodness-of-fit on F²	0.935
Final R indices [I>2sigma(I)]	R1 = 0.0690, wR2 = 0.1354
R indices (all data)	R1 = 0.1059, wR2 = 0.1467
Largest diff. peak and hole	1.203 and -1.552 e.Å⁻³

Table A.14. Crystal data and structure refinement for [**L1$_b$**Pd(OH$_2$)][PF$_6$]

Identification code	14109
Empirical formula	C59 H73 Cl15 F12 N6 O4 P2 Pd2
Formula weight	1964.72
Temperature	150(2) K
Wavelength	0.71073 Å
Crystal system	Monoclinic
Space group	P2(1)/n
Unit cell dimensions	a = 8.7790(19) Å α= 90°.
	b = 14.979(3) Å β= 97.227(5)°.
	c = 31.961(7) Å γ = 90°.
Volume	4169.6(16) Å^3
Z	2
Density (calculated)	1.565 Mg/m^3
Absorption coefficient	1.022 mm^{-1}
F(000)	1972
Crystal size	0.46 x 0.16 x 0.12 mm^3
Theta range for data collection	1.28 to 26.00°.
Index ranges	-10<=h<=10, -18<=k<=18, -39<=l<=38
Reflections collected	32241
Independent reflections	8198 [R(int) = 0.1520]
Completeness to theta = 26.00°	100.0 %
Absorption correction	Empirical
Max. and min. transmission	0.831 and 0.441
Refinement method	Full-matrix least-squares on F^2
Data / restraints / parameters	8198 / 3 / 477
Goodness-of-fit on F^2	1.052
Final R indices [I>2sigma(I)]	R1 = 0.1116, wR2 = 0.2828
R indices (all data)	R1 = 0.1713, wR2 = 0.3213
Extinction coefficient	0.0171(16)
Largest diff. peak and hole	2.210 and -0.804 e.Å^{-3}

Table A.15. Crystal data and structure refinement for [**L1**_{**a**}Pd(OH$_2$)][OTf]

Identification code	15083
Empirical formula	C25 H28 F3 N3 O5 Pd S
Formula weight	645.96
Temperature	150(2) K
Wavelength	0.71073 Å
Crystal system	Monoclinic
Space group	P2(1)/c
Unit cell dimensions	a = 10.1352(19) Å $\quad$ α= 90°.
	b = 16.881(3) Å $\quad$ β= 106.234(3)°.
	c = 16.212(3) Å $\quad$ γ = 90°.
Volume	2663.2(9) Å^3
Z	4
Density (calculated)	1.611 Mg/m^3
Absorption coefficient	0.837 mm^{-1}
F(000)	1312
Crystal size	0.38 x 0.17 x 0.06 mm^3
Theta range for data collection	1.78 to 27.00°.
Index ranges	-12<=h<=12, -21<=k<=21, -20<=l<=20
Reflections collected	21786
Independent reflections	5794 [R(int) = 0.0423]
Completeness to theta = 27.00°	99.7 %
Absorption correction	Empirical
Max. and min. transmission	0.831 and 0.584
Refinement method	Full-matrix least-squares on F^2
Data / restraints / parameters	5794 / 25 / 366
Goodness-of-fit on F^2	1.064
Final R indices [I>2sigma(I)]	R1 = 0.0522, wR2 = 0.1255
R indices (all data)	R1 = 0.0595, wR2 = 0.1297
Largest diff. peak and hole	1.645 and -1.480 e.Å^{-3}

Table A.16. Crystal data and structure refinement for [**L1$_a$**Pd(3,5-Me$_2$Py)][PF$_6$]

Identification code	14133n
Empirical formula	C62 H70 F18 N8 O2 P3 Pd2
Formula weight	1606.97
Temperature	150(2) K
Wavelength	0.71073 Å
Crystal system	Monoclinic
Space group	C2/c
Unit cell dimensions	a = 35.148(11) Å α= 90°.
	b = 14.658(5) Å β= 110.928(8)°.
	c = 13.871(4) Å γ = 90°.
Volume	6675(4) Å^3
Z	4
Density (calculated)	1.599 Mg/m^3
Absorption coefficient	0.710 mm^{-1}
F(000)	3252
Crystal size	0.34 x 0.15 x 0.03 mm^3
Theta range for data collection	1.52 to 26.00°.
Index ranges	-43<=h<=40, 0<=k<=18, 0<=l<=17
Reflections collected	6534
Independent reflections	6534 [R(int) = 0.0000]
Completeness to theta = 26.00°	99.7 %
Absorption correction	Empirical
Max. and min. transmission	0.831 and 0.584
Refinement method	Full-matrix least-squares on F^2
Data / restraints / parameters	6534 / 0 / 437
Goodness-of-fit on F^2	0.800
Final R indices [I>2sigma(I)]	R1 = 0.0723, wR2 = 0.0948
R indices (all data)	R1 = 0.2060, wR2 = 0.1219
Largest diff. peak and hole	0.685 and -0.769 e.Å^{-3}

Table A.17. Crystal data and structure refinement for [**HL1**$_a$Pd(3,5-Me$_2$Py)][PF$_6$]$_2$

Identification code	14133
Empirical formula	C62 H71 F18 N8 O2 P3 Pd2
Formula weight	1607.98
Temperature	150(2) K
Wavelength	0.71073 Å
Crystal system	Monoclinic
Space group	Cc
Unit cell dimensions	a = 35.000(7) Å α= 90°.
	b = 14.620(3) Å β= 110.00(3)°.
	c = 13.860(3) Å γ = 90°.
Volume	6664(2) Å^3
Z	4
Density (calculated)	1.603 Mg/m^3
Absorption coefficient	0.712 mm^{-1}
F(000)	3256
Crystal size	0.34 x 0.15 x 0.03 mm^3
Theta range for data collection	1.24 to 26.00°.
Index ranges	-43<=h<=40, 0<=k<=18, 0<=l<=17
Reflections collected	6530
Independent reflections	6530 [R(int) = 0.0000]
Completeness to theta = 26.00°	99.7 %
Absorption correction	Empirical
Max. and min. transmission	0.831 and 0.584
Refinement method	Full-matrix least-squares on F^2
Data / restraints / parameters	6530 / 611 / 570
Goodness-of-fit on F^2	0.795
Final R indices [I>2sigma(I)]	R1 = 0.0688, wR2 = 0.1202
R indices (all data)	R1 = 0.1957, wR2 = 0.1772
Absolute structure parameter	0.02(10)
Largest diff. peak and hole	0.598 and -0.755 e.Å^{-3}

Table A18. Crystal data and structure refinement for [**L1**$_b$Pd(3,5-Me$_2$Py)][PF$_6$]

Identification code	16045
Empirical formula	C68 H84 F18 N8 O2 P3 Pd2
Formula weight	1693.14
Temperature	150(2) K
Wavelength	0.71073 Å
Crystal system	Monoclinic
Space group	C2/c
Unit cell dimensions	a = 36.848(6) Å α= 90°.
	b = 15.671(3) Å β= 106.436(3)°.
	c = 13.186(2) Å γ = 90°.
Volume	7303(2) Å^3
Z	4
Density (calculated)	1.540 Mg/m^3
Absorption coefficient	0.654 mm^{-1}
F(000)	3452
Crystal size	0.20 x 0.14 x 0.06 mm^3
Theta range for data collection	1.42 to 26.00°.
Index ranges	-45<=h<=45, -19<=k<=18, -16<=l<=16
Reflections collected	28145
Independent reflections	7184 [R(int) = 0.0750]
Completeness to theta = 26.00°	99.9 %
Absorption correction	Empirical
Max. and min. transmission	0.831 and 0.709
Refinement method	Full-matrix least-squares on F^2
Data / restraints / parameters	7184 / 5 / 484
Goodness-of-fit on F^2	0.951
Final R indices [I>2sigma(I)]	R1 = 0.0541, wR2 = 0.1327
R indices (all data)	R1 = 0.0822, wR2 = 0.1434
Largest diff. peak and hole	1.182 and -0.760 e.Å^{-3}

Table A.19. Crystal data and structure refinement for [H**L1**$_b$Pd(3,5-Me$_2$Py)][PF$_6$]

Identification code	16045
Empirical formula	C68 H83 F18 N8 O2 P3 Pd2
Formula weight	1692.13
Temperature	150(2) K
Wavelength	0.71073 Å
Crystal system	Monoclinic
Space group	Cc
Unit cell dimensions	a = 36.848(6) Å α= 90°.
	b = 15.671(3) Å β= 106.436(3)°.
	c = 13.186(2) Å γ = 90°.
Volume	7303(2) Å^3
Z	4
Density (calculated)	1.539 Mg/m^3
Absorption coefficient	0.654 mm^{-1}
F(000)	3448
Crystal size	0.20 x 0.14 x 0.06 mm^3
Theta range for data collection	1.42 to 26.00°.
Index ranges	-45<=h<=45, -19<=k<=18, -16<=l<=16
Reflections collected	28144
Independent reflections	13987 [R(int) = 0.0645]
Completeness to theta = 26.00°	99.9 %
Absorption correction	Empirical
Max. and min. transmission	0.831 and 0.709
Refinement method	Full-matrix least-squares on F^2
Data / restraints / parameters	13987 / 897 / 930
Goodness-of-fit on F^2	0.865
Final R indices [I>2sigma(I)]	R1 = 0.0499, wR2 = 0.0908
R indices (all data)	R1 = 0.0862, wR2 = 0.1014
Absolute structure parameter	0.41(5)
Largest diff. peak and hole	0.982 and -0.598 e.Å^{-3}

Table A.20. Crystal data and structure refinement for [H**L1$_a$**PtCl][Cl$_3$Pt(DMSO)]

Identification code	16008
Empirical formula	C28 H35 Cl10 N3 O2 Pt2 S
Formula weight	1222.33
Temperature	150(2) K
Wavelength	0.71073 Å
Crystal system	Triclinic
Space group	P-1
Unit cell dimensions	a = 9.289(4) Å α= 78.628(9)°.
	b = 11.727(5) Å β= 80.146(9)°.
	c = 18.698(8) Å γ = 74.736(10)°.
Volume	1911.0(15) Å^3
Z	2
Density (calculated)	2.124 Mg/m^3
Absorption coefficient	8.098 mm^{-1}
F(000)	1164
Crystal size	0.35 x 0.09 x 0.03 mm^3
Theta range for data collection	1.82 to 26.00°.
Index ranges	-11<=h<=11, -14<=k<=14, -23<=l<=22
Reflections collected	15146
Independent reflections	7444 [R(int) = 0.1123]
Completeness to theta = 26.00°	99.0 %
Absorption correction	Empirical
Max. and min. transmission	0.831 and 0.452
Refinement method	Full-matrix least-squares on F^2
Data / restraints / parameters	7444 / 66 / 386
Goodness-of-fit on F^2	0.792
Final R indices [I>2sigma(I)]	R1 = 0.0665, wR2 = 0.1210
R indices (all data)	R1 = 0.1320, wR2 = 0.1375
Largest diff. peak and hole	2.250 and -2.231 e.Å^{-3}

Table A.21. Crystal data and structure refinement for [H**L1**_b_PtCl][Cl_3Pt(DMSO)]

Identification code	16121
Empirical formula	C31 H47 Cl8 N3 O4 Pt2 S
Formula weight	1231.56
Temperature	150(2) K
Wavelength	0.71073 Å
Crystal system	Triclinic
Space group	P-1
Unit cell dimensions	a = 9.163(3) Å α= 87.568(4)°.
	b = 12.036(3) Å β= 77.428(5)°.
	c = 19.499(5) Å γ = 73.689(4)°.
Volume	2014.0(10) Å^3
Z	2
Density (calculated)	2.031 Mg/m^3
Absorption coefficient	7.560 mm^{-1}
F(000)	1188
Crystal size	0.25 x 0.13 x 0.08 mm^3
Theta range for data collection	1.76 to 26.00°.
Index ranges	-11<=h<=11, -14<=k<=14, -24<=l<=23
Reflections collected	15734
Independent reflections	7802 [R(int) = 0.0534]
Completeness to theta = 26.00°	98.5 %
Absorption correction	Empirical
Max. and min. transmission	0.831 and 0.506
Refinement method	Full-matrix least-squares on F^2
Data / restraints / parameters	7802 / 32 / 379
Goodness-of-fit on F^2	0.934
Final R indices [I>2sigma(I)]	R1 = 0.0396, wR2 = 0.0909
R indices (all data)	R1 = 0.0548, wR2 = 0.0965
Largest diff. peak and hole	2.026 and -0.980 e.Å^{-3}

Table A.22. Crystal data and structure refinement for (**L2$_a$Pd**)$_2$OH(OAc)

Identification code	14013
Empirical formula	C46 H60 Cl9 N10 O10 Pd2
Formula weight	1444.89
Temperature	150(2) K
Wavelength	0.71073 Å
Crystal system	Monoclinic
Space group	P2(1)/c
Unit cell dimensions	a = 12.536(4) Å $\quad$ α= 90°.
	b = 29.194(8) Å $\quad$ β= 92.031(6)°.
	c = 28.167(8) Å $\quad$ γ = 90°.
Volume	10302(5) Å^3
Z	8
Density (calculated)	1.863 Mg/m^3
Absorption coefficient	1.235 mm^{-1}
F(000)	5848
Crystal size	0.38 x 0.28 x 0.18 mm^3
Theta range for data collection	1.00 to 26.00°.
Index ranges	-15<=h<=15, -36<=k<=35, -34<=l<=34
Reflections collected	79222
Independent reflections	20227 [R(int) = 0.1486]
Completeness to theta = 26.00°	99.8 %
Absorption correction	Empirical
Max. and min. transmission	0.831 and 0.592
Refinement method	Full-matrix least-squares on F^2
Data / restraints / parameters	20227 / 884 / 941
Goodness-of-fit on F^2	0.878
Final R indices [I>2sigma(I)]	R1 = 0.0739, wR2 = 0.1618
R indices (all data)	R1 = 0.1386, wR2 = 0.1796
Largest diff. peak and hole	1.341 and -0.716 e.Å^{-3}

Table A.23. Crystal data and structure refinement for (**L2**b**Pd)**₂**OH(OAc)

Identification code	16153
Empirical formula	C48 H66 Cl4 N4 O5 Pd2
Formula weight	1133.65
Temperature	150(2) K
Wavelength	0.71073 Å
Crystal system	Orthorhombic
Space group	P2(1)2(1)2(1)
Unit cell dimensions	$a = 13.827(4)$ Å $\quad \alpha = 90°.$
	$b = 15.771(4)$ Å $\quad \beta = 90°.$
	$c = 23.808(6)$ Å $\quad \gamma = 90°.$
Volume	5192(2) Å^3
Z	4
Density (calculated)	1.450 Mg/m^3
Absorption coefficient	0.945 mm^{-1}
F(000)	2328
Crystal size	0.15 x 0.13 x 0.11 mm^3
Theta range for data collection	1.55 to 27.00°.
Index ranges	-17<=h<=17, -19<=k<=20, -29<=l<=30
Reflections collected	43474
Independent reflections	11305 [R(int) = 0.0728]
Completeness to theta = 27.00°	99.8 %
Absorption correction	Empirical
Max. and min. transmission	0.831 and 0.667
Refinement method	Full-matrix least-squares on F^2
Data / restraints / parameters	11305 / 13 / 583
Goodness-of-fit on F^2	0.964
Final R indices [I>2sigma(I)]	R1 = 0.0423, wR2 = 0.0803
R indices (all data)	R1 = 0.0518, wR2 = 0.0827
Absolute structure parameter	0.00(2)
Largest diff. peak and hole	1.440 and -0.714 e.Å^{-3}

Table A.24. Crystal data and structure refinement for $(\mathbf{L3_a})_2Pd$

Identification code	16085
Empirical formula	C39 H48 Cl2 N4 O2 Pd
Formula weight	782.11
Temperature	150(2) K
Wavelength	0.71073 Å
Crystal system	Monoclinic
Space group	C2/c
Unit cell dimensions	a = 33.952(5) Å $\quad$ α= 90°.
	b = 14.244(2) Å $\quad$ β= 101.979(3)°.
	c = 23.894(4) Å $\quad$ γ = 90°.
Volume	11304(3) Å^3
Z	12
Density (calculated)	1.379 Mg/m^3
Absorption coefficient	0.673 mm^{-1}
F(000)	4872
Crystal size	0.21 x 0.17 x 0.10 mm^3
Theta range for data collection	1.23 to 26.00°.
Index ranges	-41<=h<=41, -17<=k<=17, -29<=l<=29
Reflections collected	43543
Independent reflections	11105 [R(int) = 0.0927]
Completeness to theta = 26.00°	99.9 %
Absorption correction	Empirical
Max. and min. transmission	0.831 and 0.575
Refinement method	Full-matrix least-squares on F^2
Data / restraints / parameters	11105 / 0 / 665
Goodness-of-fit on F^2	0.819
Final R indices [I>2sigma(I)]	R1 = 0.0456, wR2 = 0.0927
R indices (all data)	R1 = 0.0879, wR2 = 0.1029
Largest diff. peak and hole	1.361 and -0.961 e.Å^{-3}

Table A.25. Crystal data and structure refinement for **HL2$_a$PdCl$_2$**

Identification code	14048
Empirical formula	C19 H24 Cl2 N2 O Pd
Formula weight	473.70
Temperature	150(2) K
Wavelength	0.71073 Å
Crystal system	Monoclinic
Space group	P2(1)/n
Unit cell dimensions	a = 9.042(3) Å α= 90°.
	b = 27.393(8) Å β= 118.145(4)°.
	c = 9.169(3) Å γ = 90°.
Volume	2002.7(10) Å^3
Z	4
Density (calculated)	1.571 Mg/m^3
Absorption coefficient	1.203 mm^{-1}
F(000)	960
Crystal size	0.41 x 0.24 x 0.13 mm^3
Theta range for data collection	1.49 to 26.00°.
Index ranges	-11<=h<=11, -33<=k<=33, -11<=l<=11
Reflections collected	15472
Independent reflections	3942 [R(int) = 0.0746]
Completeness to theta = 26.00°	100.0 %
Absorption correction	Empirical
Max. and min. transmission	0.831 and 0.577
Refinement method	Full-matrix least-squares on F^2
Data / restraints / parameters	3942 / 6 / 231
Goodness-of-fit on F^2	1.056
Final R indices [I>2sigma(I)]	R1 = 0.0614, wR2 = 0.1594
R indices (all data)	R1 = 0.0694, wR2 = 0.1658
Largest diff. peak and hole	2.334 and -2.111 e.Å^{-3}

Table A.26. Crystal data and structure refinement for **HL2$_b$PdCl$_2$**

Identification code	14011
Empirical formula	C23 H31 Cl5 N2 O Pd
Formula weight	635.15
Temperature	150(2) K
Wavelength	0.71073 Å
Crystal system	Orthorhombic
Space group	P2(1)2(1)2(1)
Unit cell dimensions	a = 9.149(2) Å $\qquad$ α= 90°.
	b = 14.618(3) Å $\qquad$ β= 90°.
	c = 20.669(4) Å $\qquad$ γ= 90°.
Volume	2764.2(10) Å^3
Z	4
Density (calculated)	1.526 Mg/m^3
Absorption coefficient	1.173 mm^{-1}
F(000)	1288
Crystal size	0.42 x 0.09 x 0.08 mm^3
Theta range for data collection	1.71 to 25.99°.
Index ranges	-11<=h<=11, -18<=k<=17, -25<=l<=25
Reflections collected	21825
Independent reflections	5432 [R(int) = 0.1021]
Completeness to theta = 25.99°	100.0 %
Absorption correction	Empirical
Max. and min. transmission	0.831 and 0.679
Refinement method	Full-matrix least-squares on F^2
Data / restraints / parameters	5432 / 0 / 314
Goodness-of-fit on F^2	0.947
Final R indices [I>2sigma(I)]	R1 = 0.0513, wR2 = 0.0882
R indices (all data)	R1 = 0.0653, wR2 = 0.0923
Absolute structure parameter	-0.01(4)
Largest diff. peak and hole	0.837 and -0.849 e.Å^{-3}

Table A.27. Crystal data and structure refinement for $HL3_aPdCl_2$

Identification code	15133
Empirical formula	C20 H26 Cl4 N2 O Pd
Formula weight	558.63
Temperature	150(2) K
Wavelength	0.71073 Å
Crystal system	Triclinic
Space group	P-1
Unit cell dimensions	a = 9.267(4) Å α= 109.139(8)°.
	b = 10.421(4) Å β= 91.620(8)°.
	c = 13.185(5) Å γ = 100.878(8)°.
Volume	1175.7(8) $Å^3$
Z	2
Density (calculated)	1.578 Mg/m^3
Absorption coefficient	1.257 mm^{-1}
F(000)	564
Crystal size	0.23 x 0.07 x 0.05 mm^3
Theta range for data collection	1.64 to 26.00°.
Index ranges	-11<=h<=11, -12<=k<=12, -16<=l<=16
Reflections collected	9272
Independent reflections	4566 [R(int) = 0.0880]
Completeness to theta = 26.00°	98.7 %
Absorption correction	Empirical
Max. and min. transmission	0.831 and 0.645
Refinement method	Full-matrix least-squares on F^2
Data / restraints / parameters	4566 / 0 / 258
Goodness-of-fit on F^2	0.837
Final R indices [I>2sigma(I)]	R1 = 0.0550, wR2 = 0.0950
R indices (all data)	R1 = 0.0899, wR2 = 0.1038
Largest diff. peak and hole	0.855 and -1.005 e.$Å^{-3}$

Table A.28. Crystal data and structure refinement for **HL3$_b$PdCl$_2$**

Identification code	16024
Empirical formula	C22 H30 Cl2 N2 O Pd
Formula weight	515.78
Temperature	150(2) K
Wavelength	0.71073 Å
Crystal system	Monoclinic
Space group	C2/c
Unit cell dimensions	a = 34.386(15) Å $\quad$ α= 90°.
	b = 8.209(4) Å $\quad$ β= 105.575(7)°.
	c = 16.988(8) Å $\quad$ γ = 90°.
Volume	4619(4) Å^3
Z	8
Density (calculated)	1.483 Mg/m^3
Absorption coefficient	1.049 mm^{-1}
F(000)	2112
Crystal size	0.25 x 0.18 x 0.12 mm^3
Theta range for data collection	2.46 to 26.00°.
Index ranges	-42<=h<=41, -10<=k<=10, -20<=l<=20
Reflections collected	17315
Independent reflections	4527 [R(int) = 0.0902]
Completeness to theta = 26.00°	99.9 %
Absorption correction	Empirical
Max. and min. transmission	0.831 and 0.663
Refinement method	Full-matrix least-squares on F^2
Data / restraints / parameters	4527 / 24 / 278
Goodness-of-fit on F^2	0.909
Final R indices [I>2sigma(I)]	R1 = 0.0427, wR2 = 0.0722
R indices (all data)	R1 = 0.0700, wR2 = 0.0779
Largest diff. peak and hole	0.592 and -0.534 e.Å^{-3}

Table A.29. Crystal data and structure refinement for $HL3_cPdCl_2$

Identification code	17027
Empirical formula	C20 H27 Br Cl2 N2 O2 Pd
Formula weight	584.65
Temperature	150(2) K
Wavelength	0.71073 Å
Crystal system	Triclinic
Space group	P-1
Unit cell dimensions	a = 9.098(3) Å α= 82.090(5)°.
	b = 9.370(3) Å β= 80.849(5)°.
	c = 14.004(4) Å γ = 73.319(4)°.
Volume	1123.7(5) Å^3
Z	2
Density (calculated)	1.728 Mg/m^3
Absorption coefficient	2.860 mm^{-1}
F(000)	584
Crystal size	0.29 x 0.23 x 0.19 mm^3
Theta range for data collection	1.48 to 26.99°.
Index ranges	-11<=h<=11, -11<=k<=11, -17<=l<=17
Reflections collected	9440
Independent reflections	4807 [R(int) = 0.0332]
Completeness to theta = 26.99°	98.1 %
Absorption correction	Empirical
Max. and min. transmission	0.831 and 0.638
Refinement method	Full-matrix least-squares on F^2
Data / restraints / parameters	4807 / 0 / 260
Goodness-of-fit on F^2	0.980
Final R indices [I>2sigma(I)]	R1 = 0.0344, wR2 = 0.0744
R indices (all data)	R1 = 0.0420, wR2 = 0.0768
Largest diff. peak and hole	0.929 and -0.882 e.Å^{-3}

Table A.30. Crystal data and structure refinement for (**L2$_a$**Pd)$_2$OH(Cl)

Identification code	14022
Empirical formula	C157 H201 Cl19 N16 O16 Pd8
Formula weight	4093.09
Temperature	150(2) K
Wavelength	0.71073 Å
Crystal system	Monoclinic
Space group	P2(1)/c
Unit cell dimensions	a = 12.653(3) Å $\quad$ α= 90°.
	b = 18.837(4) Å $\quad$ β= 95.425(4)°.
	c = 20.017(4) Å $\quad$ γ = 90°.
Volume	4749.4(16) Å^3
Z	1
Density (calculated)	1.431 Mg/m^3
Absorption coefficient	1.064 mm^{-1}
F(000)	2074
Crystal size	0.17 x 0.16 x 0.04 mm^3
Theta range for data collection	1.49 to 26.00°.
Index ranges	-15<=h<=15, -23<=k<=23, -24<=l<=24
Reflections collected	36905
Independent reflections	9321 [R(int) = 0.1320]
Completeness to theta = 26.00°	99.9 %
Absorption correction	Empirical
Max. and min. transmission	0.831 and 0.695
Refinement method	Full-matrix least-squares on F^2
Data / restraints / parameters	9321 / 12 / 524
Goodness-of-fit on F^2	0.932
Final R indices [I>2sigma(I)]	R1 = 0.0615, wR2 = 0.1364
R indices (all data)	R1 = 0.1126, wR2 = 0.1527
Largest diff. peak and hole	1.347 and -0.722 e.Å^{-3}

Table A.31. Crystal data and structure refinement for (**L2**$_c$Pd)$_2$OH(Cl)

Identification code	15142
Empirical formula	C50 H75.80 Br2 Cl N4 O4.40 Pd2
Formula weight	1211.42
Temperature	150(2) K
Wavelength	0.71073 Å
Crystal system	Tetragonal
Space group	I4(1)/a
Unit cell dimensions	a = 37.861(6) Å $\alpha = 90°$.
	b = 37.861(6) Å $\beta = 90°$.
	c = 13.302(3) Å $\gamma = 90°$.
Volume	19067(6) Å^3
Z	16
Density (calculated)	1.688 Mg/m^3
Absorption coefficient	2.538 mm^{-1}
F(000)	9888
Crystal size	0.20 x 0.19 x 0.17 mm^3
Theta range for data collection	1.62 to 26.00°.
Index ranges	-46<=h<=45, -46<=k<=46, -16<=l<=16
Reflections collected	73227
Independent reflections	9385 [R(int) = 0.1774]
Completeness to theta = 26.00°	99.9 %
Absorption correction	Empirical
Max. and min. transmission	0.831 and 0.661
Refinement method	Full-matrix least-squares on F^2
Data / restraints / parameters	9385 / 429 / 479
Goodness-of-fit on F^2	0.920
Final R indices [I>2sigma(I)]	R1 = 0.0686, wR2 = 0.1600
R indices (all data)	R1 = 0.1516, wR2 = 0.1782
Largest diff. peak and hole	1.080 and -0.758 e.Å^{-3}

Table A.32. Crystal data and structure refinement for **L2$_a$**PdCl(PPh$_3$)

Identification code	14037
Empirical formula	C38 H40 Cl3 N2 O P Pd
Formula weight	784.44
Temperature	150(2) K
Wavelength	0.71073 Å
Crystal system	Monoclinic
Space group	P2(1)/c
Unit cell dimensions	a = 18.198(4) Å $\quad$ α= 90°.
	b = 11.091(2) Å $\quad$ β= 92.366(5)°.
	c = 17.907(4) Å $\quad$ γ = 90°.
Volume	3611.2(12) Å^3
Z	4
Density (calculated)	1.443 Mg/m^3
Absorption coefficient	0.813 mm^{-1}
F(000)	1608
Crystal size	0.27 x 0.16 x 0.08 mm^3
Theta range for data collection	2.15 to 26.00°.
Index ranges	-21<=h<=22, -13<=k<=13, -22<=l<=22
Reflections collected	27850
Independent reflections	7085 [R(int) = 0.1181]
Completeness to theta = 26.00°	99.8 %
Absorption correction	Empirical
Max. and min. transmission	0.831 and 0.645
Refinement method	Full-matrix least-squares on F^2
Data / restraints / parameters	7085 / 0 / 420
Goodness-of-fit on F^2	0.874
Final R indices [I>2sigma(I)]	R1 = 0.0545, wR2 = 0.0922
R indices (all data)	R1 = 0.0898, wR2 = 0.1031
Largest diff. peak and hole	0.717 and -1.057 e.Å^{-3}

Table A.33. Crystal data and structure refinement for [(**L2**$_b$Pd)$_2$OH(NCMe)][PF$_6$]

Identification code	17003
Empirical formula	C92 H126 F12 N10 O7 P2 Pd4
Formula weight	2199.57
Temperature	150(2) K
Wavelength	0.71073 Å
Crystal system	Monoclinic
Space group	P2(1)/c
Unit cell dimensions	a = 15.115(3) Å α= 90°.
	b = 21.221(4) Å β= 115.755(3)°.
	c = 16.982(3) Å γ = 90°.
Volume	4906.1(15) Å^3
Z	2
Density (calculated)	1.489 Mg/m^3
Absorption coefficient	0.833 mm^{-1}
F(000)	2252
Crystal size	0.26 x 0.14 x 0.08 mm^3
Theta range for data collection	1.50 to 26.00°.
Index ranges	-18<=h<=18, -26<=k<=25, -20<=l<=20
Reflections collected	38043
Independent reflections	9635 [R(int) = 0.1011]
Completeness to theta = 26.00°	99.8 %
Absorption correction	Empirical
Max. and min. transmission	0.831 and 0.725
Refinement method	Full-matrix least-squares on F^2
Data / restraints / parameters	9635 / 3 / 592
Goodness-of-fit on F^2	0.920
Final R indices [I>2sigma(I)]	R1 = 0.0539, wR2 = 0.0959
R indices (all data)	R1 = 0.0863, wR2 = 0.1062
Largest diff. peak and hole	1.185 and -0.767 e.Å^{-3}

Table A.34. Crystal data and structure refinement for HL2$_a$PtCl$_2$

Identification code	14035
Empirical formula	C20 H26 Cl4 N2 O Pt
Formula weight	647.32
Temperature	150(2) K
Wavelength	0.71073 Å
Crystal system	Monoclinic
Space group	P2(1)/n
Unit cell dimensions	a = 22.521(4) Å α= 90°.
	b = 9.2593(16) Å β= 104.091(3)°.
	c = 22.696(4) Å γ = 90°.
Volume	4590.3(14) Å^3
Z	8
Density (calculated)	1.873 Mg/m^3
Absorption coefficient	6.593 mm^{-1}
F(000)	2512
Crystal size	0.29 x 0.16 x 0.14 mm^3
Theta range for data collection	1.14 to 27.00°.
Index ranges	-28<=h<=28, -11<=k<=11, -28<=l<=28
Reflections collected	37653
Independent reflections	10013 [R(int) = 0.0638]
Completeness to theta = 27.00°	100.0 %
Absorption correction	Empirical
Max. and min. transmission	0.831 and 0.571
Refinement method	Full-matrix least-squares on F^2
Data / restraints / parameters	10013 / 0 / 515
Goodness-of-fit on F^2	0.968
Final R indices [I>2sigma(I)]	R1 = 0.0369, wR2 = 0.0573
R indices (all data)	R1 = 0.0546, wR2 = 0.0612
Largest diff. peak and hole	1.201 and -0.942 e.Å^{-3}

Table A.35. Crystal data and structure refinement for **HL2$_c$PtCl$_2$**

Identification code	16033
Empirical formula	C19 H23 Br Cl2 N2 O Pt
Formula weight	641.29
Temperature	150(2) K
Wavelength	0.71073 Å
Crystal system	Monoclinic
Space group	P2(1)/c
Unit cell dimensions	a = 8.7813(19) Å $\alpha= 90°$.
	b = 30.520(7) Å $\beta= 116.633(4)°$.
	c = 8.849(2) Å $\gamma = 90°$.
Volume	2119.9(8) Å^3
Z	4
Density (calculated)	2.009 Mg/m^3
Absorption coefficient	8.767 mm^{-1}
F(000)	1224
Crystal size	0.34 x 0.30 x 0.06 mm^3
Theta range for data collection	1.33 to 27.00°.
Index ranges	-11<=h<=11, -38<=k<=38, -11<=l<=11
Reflections collected	17638
Independent reflections	4611 [R(int) = 0.1074]
Completeness to theta = 27.00°	99.7 %
Absorption correction	Empirical
Max. and min. transmission	0.831 and 0.302
Refinement method	Full-matrix least-squares on F^2
Data / restraints / parameters	4611 / 0 / 240
Goodness-of-fit on F^2	0.937
Final R indices [I>2sigma(I)]	R1 = 0.0451, wR2 = 0.0886
R indices (all data)	R1 = 0.0643, wR2 = 0.0942
Largest diff. peak and hole	2.290 and -1.363 e.Å^{-3}

Table A.36. Crystal data and structure refinement for **HL3$_a$PtCl$_2$**

Identification code	16040
Empirical formula	C20 H26 Cl4 N2 O Pt
Formula weight	647.32
Temperature	150(2) K
Wavelength	0.71073 Å
Crystal system	Triclinic
Space group	P-1
Unit cell dimensions	a = 9.263(4) Å α= 108.546(7)°.
	b = 10.430(4) Å β= 92.071(7)°.
	c = 13.113(5) Å γ = 100.821(7)°.
Volume	1173.5(8) Å^3
Z	2
Density (calculated)	1.832 Mg/m^3
Absorption coefficient	6.448 mm^{-1}
F(000)	628
Crystal size	0.28 x 0.20 x 0.15 mm^3
Theta range for data collection	1.65 to 26.00°.
Index ranges	-11<=h<=11, -12<=k<=12, -15<=l<=16
Reflections collected	9232
Independent reflections	4546 [R(int) = 0.0957]
Completeness to theta = 26.00°	98.6 %
Absorption correction	Empirical
Max. and min. transmission	0.831 and 0.507
Refinement method	Full-matrix least-squares on F^2
Data / restraints / parameters	4546 / 30 / 258
Goodness-of-fit on F^2	0.927
Final R indices [I>2sigma(I)]	R1 = 0.0567, wR2 = 0.1030
R indices (all data)	R1 = 0.0874, wR2 = 0.1168
Largest diff. peak and hole	1.903 and -1.833 e.Å^{-3}

Table A.37. Crystal data and structure refinement for [(**HL2ₐ**)₂NiBr][Br]

Identification code	15022
Empirical formula	C39 H50 Br2 Cl2 N4 Ni O2
Formula weight	896.26
Temperature	150(2) K
Wavelength	0.71073 Å
Crystal system	Triclinic
Space group	P-1
Unit cell dimensions	a = 10.8476(19) Å α= 106.261(3)°.
	b = 14.421(2) Å β= 99.019(4)°.
	c = 14.686(2) Å γ = 103.862(3)°.
Volume	2078.6(6) Å^3
Z	2
Density (calculated)	1.432 Mg/m^3
Absorption coefficient	2.555 mm^{-1}
F(000)	920
Crystal size	0.31 x 0.22 x 0.05 mm^3
Theta range for data collection	1.49 to 26.00°.
Index ranges	-12<=h<=13, -17<=k<=17, -17<=l<=18
Reflections collected	14977
Independent reflections	7906 [R(int) = 0.1336]
Completeness to theta = 26.00°	96.7 %
Absorption correction	Empirical
Max. and min. transmission	0.862 and 0.470
Refinement method	Full-matrix least-squares on F^2
Data / restraints / parameters	7906 / 0 / 461
Goodness-of-fit on F^2	0.826
Final R indices [I>2sigma(I)]	R1 = 0.0837, wR2 = 0.1525
R indices (all data)	R1 = 0.2046, wR2 = 0.1935
Largest diff. peak and hole	1.167 and -1.016 e.Å^{-3}

Table A.38. Crystal data and structure refinement for $(HL2_b)_2NiBr_2$

Identification code	16123
Empirical formula	C44 H60 Br2 N4 Ni O2
Formula weight	895.49
Temperature	150(2) K
Wavelength	0.71073 Å
Crystal system	Monoclinic
Space group	P2(1)/c
Unit cell dimensions	a = 16.753(4) Å $\alpha = 90°$.
	b = 16.793(4) Å $\beta = 101.562(6)°$.
	c = 16.149(4) Å $\gamma = 90°$.
Volume	4451.3(19) Å^3
Z	4
Density (calculated)	1.336 Mg/m^3
Absorption coefficient	2.270 mm^{-1}
F(000)	1864
Crystal size	0.19 x 0.09 x 0.08 mm^3
Theta range for data collection	1.73 to 26.00°.
Index ranges	-20<=h<=20, -20<=k<=20, -19<=l<=19
Reflections collected	34571
Independent reflections	8743 [R(int) = 0.1139]
Completeness to theta = 26.00°	99.9 %
Absorption correction	Empirical
Max. and min. transmission	0.831 and 0.624
Refinement method	Full-matrix least-squares on F^2
Data / restraints / parameters	8743 / 0 / 492
Goodness-of-fit on F^2	0.730
Final R indices [I>2sigma(I)]	R1 = 0.0473, wR2 = 0.0598
R indices (all data)	R1 = 0.0972, wR2 = 0.0671
Largest diff. peak and hole	0.503 and -0.639 e.Å^{-3}

Table A.39. Crystal data and structure refinement for $(HL2_c)_2NiBr_2$

Identification code	16130
Empirical formula	C40 H50 Br4 Cl4 N4 Ni O2
Formula weight	1138.99
Temperature	150(2) K
Wavelength	0.71073 Å
Crystal system	Triclinic
Space group	P-1
Unit cell dimensions	a = 10.618(7) Å $\quad$ α= 74.779(11)°.
	b = 14.474(9) Å $\quad$ β= 71.594(11)°.
	c = 16.077(10) Å $\quad$ γ = 87.849(11)°.
Volume	2259(2) Å^3
Z	2
Density (calculated)	1.674 Mg/m^3
Absorption coefficient	4.241 mm^{-1}
F(000)	1140
Crystal size	0.45 x 0.11 x 0.05 mm^3
Theta range for data collection	1.38 to 25.00°.
Index ranges	-12<=h<=12, -16<=k<=17, -19<=l<=19
Reflections collected	16332
Independent reflections	7877 [R(int) = 0.0917]
Completeness to theta = 25.00°	99.0 %
Absorption correction	Empirical
Max. and min. transmission	0.862 and 0.477
Refinement method	Full-matrix least-squares on F^2
Data / restraints / parameters	7877 / 50 / 452
Goodness-of-fit on F^2	0.830
Final R indices [I>2sigma(I)]	R1 = 0.0636, wR2 = 0.1435
R indices (all data)	R1 = 0.1112, wR2 = 0.1551
Largest diff. peak and hole	1.139 and -1.324 e.Å^{-3}

Table A.40. Crystal data and structure refinement for **L3$_{b+Br}$NiBr(OH$_2$)$_2$NCMe**

Identification code	16145
Empirical formula	C24 H35 Br2 N3 Ni O3
Formula weight	632.08
Temperature	150(2) K
Wavelength	0.71073 Å
Crystal system	Triclinic
Space group	P-1
Unit cell dimensions	a = 8.596(2) Å $\quad$ α= 94.874(5)°.
	b = 10.733(3) Å $\quad$ β= 105.097(6)°.
	c = 15.470(4) Å $\quad$ γ = 95.794(7)°.
Volume	1361.7(6) Å^3
Z	2
Density (calculated)	1.542 Mg/m^3
Absorption coefficient	3.675 mm^{-1}
F(000)	644
Crystal size	0.10 x 0.07 x 0.03 mm^3
Theta range for data collection	1.92 to 26.00°.
Index ranges	-10<=h<=10, -13<=k<=13, -19<=l<=19
Reflections collected	10776
Independent reflections	5297 [R(int) = 0.1632]
Completeness to theta = 26.00°	99.0 %
Absorption correction	Empirical
Max. and min. transmission	0.862 and 0.341
Refinement method	Full-matrix least-squares on F^2
Data / restraints / parameters	5297 / 269 / 306
Goodness-of-fit on F^2	0.741
Final R indices [I>2sigma(I)]	R1 = 0.0788, wR2 = 0.1316
R indices (all data)	R1 = 0.1771, wR2 = 0.1570
Largest diff. peak and hole	0.890 and -0.992 e.Å^{-3}

**Table A.41.** Crystal data and structure refinement for [(**HL3**$_a$)$_2$NiBr]Br

Identification code	17008
Empirical formula	C38 H52 Br2 N4 Ni O4
Formula weight	847.37
Temperature	150(2) K
Wavelength	0.71073 Å
Crystal system	Monoclinic
Space group	C2/c
Unit cell dimensions	a = 19.765(9) Å α= 90°.
	b = 10.215(5) Å β= 114.480(11)°.
	c = 20.665(10) Å γ = 90°.
Volume	3797(3) Å^3
Z	4
Density (calculated)	1.482 Mg/m^3
Absorption coefficient	2.660 mm^{-1}
F(000)	1752
Crystal size	0.14 x 0.12 x 0.05 mm^3
Theta range for data collection	2.17 to 26.00°.
Index ranges	-24<=h<=24, -12<=k<=12, -25<=l<=25
Reflections collected	14593
Independent reflections	3736 [R(int) = 0.3085]
Completeness to theta = 26.00°	99.8 %
Absorption correction	Empirical
Max. and min. transmission	0.862 and 0.485
Refinement method	Full-matrix least-squares on F^2
Data / restraints / parameters	3736 / 21 / 229
Goodness-of-fit on F^2	0.792
Final R indices [I>2sigma(I)]	R1 = 0.0892, wR2 = 0.1655
R indices (all data)	R1 = 0.2632, wR2 = 0.2176
Largest diff. peak and hole	0.971 and -0.939 e.Å^{-3}

Table A.42. Crystal data and structure refinement for [(**L2_a**Pd)$_2$OH(HOAc)][PF$_6$]

Identification code	16062
Empirical formula	C44 H59 F6 N4 O9 P Pd2
Formula weight	1145.72
Temperature	150(2) K
Wavelength	0.71073 Å
Crystal system	Triclinic
Space group	P-1
Unit cell dimensions	a = 11.765(11) Å α= 62.195(13)°.
	b = 15.457(14) Å β= 81.866(15)°.
	c = 15.607(14) Å γ = 80.559(15)°.
Volume	2469(4) Å^3
Z	2
Density (calculated)	1.541 Mg/m^3
Absorption coefficient	0.838 mm^{-1}
F(000)	1168
Crystal size	0.44 x 0.24 x 0.12 mm^3
Theta range for data collection	1.48 to 26.00°.
Index ranges	-14<=h<=14, -19<=k<=18, -18<=l<=19
Reflections collected	18924
Independent reflections	9532 [R(int) = 0.1241]
Completeness to theta = 26.00°	98.3 %
Absorption correction	Empirical
Max. and min. transmission	0.831 and 0.649
Refinement method	Full-matrix least-squares on F^2
Data / restraints / parameters	9532 / 548 / 612
Goodness-of-fit on F^2	1.074
Final R indices [I>2sigma(I)]	R1 = 0.1096, wR2 = 0.2365
R indices (all data)	R1 = 0.1766, wR2 = 0.2595
Largest diff. peak and hole	2.809 and -2.056 e.Å^{-3}
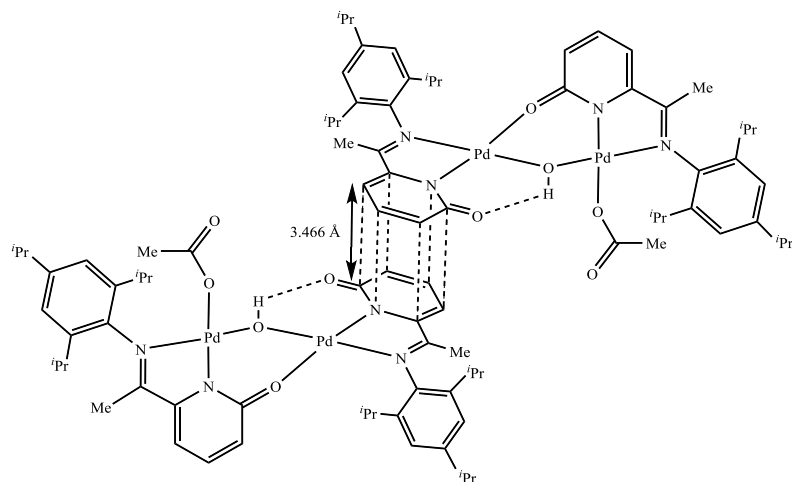
Figure A.1. π-Stacking between adjacent molecules of (**L2**$_b$Pd)$_2$OH(OAc)
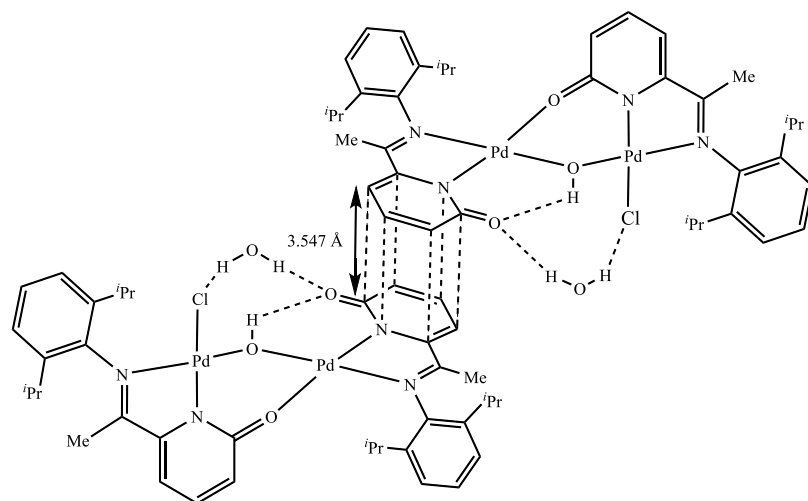
Figure A.2. π-Stacking between adjacent molecules of (**L2**$_a$Pd)$_2$OH(Cl)
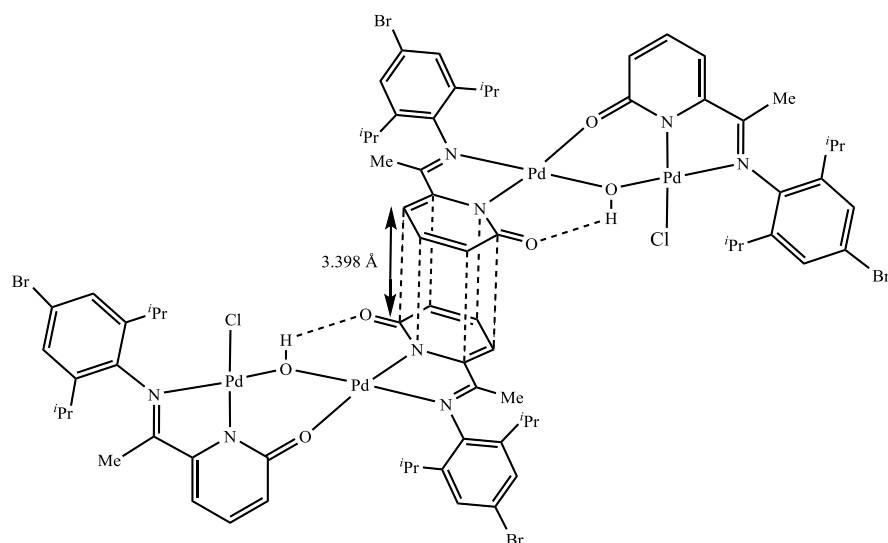
Figure A.3. π-Stacking between adjacent molecules of (**L2**$_c$Pd)$_2$OH(Cl)

Postgraduate activity

Internal Seminars

05/02/2014	Prof. Ian Baxendale, University of Durham
05/03/2014	Prof. Carl Redshaw, University of Hull
08/10/2014	Prof Gareth Williams, Durham University
03/12/2014	Prof Graham Hutchins, University of Huddersfield
12/02/2015	Professor Simon Lancaster, University of East Anglia
13/04/2015	Prof Ed Tate, Imperial College, London
04/11/2015	Prof Mike Ashford, University of Bristol
02/12/2015	Prof Duncan Wass, University of Bristol
23/03/2016	Prod. Charlotte Williams, Imperial college London
14/06/2016	Professor Ming Bao, School of Petroleum and Chemical Engineering, Dalian University of Technology
05/10/2016	Prof Steve J Archibald, University of Hull
30/11/2016	Dr. Graham Pattison, University of Warwick
01/02/2017	Dr. Ruth Webster, University of bath

Internal Symposia

- University of Leicester Department of Chemistry: One day Symposium on Catalytic C-H Functionalization 23/01/2015: Poster presentation
- University of Leicester Department of Chemistry Postgraduate Research day 04/2015: Poster presentation
- RSC Organic Division Midlands Meeting 2017, University of Leicester 5/04/2017

Poster

- 9th Saudi Student Conference-UK, Birmingham 02/ 2016: Poster presentation (Proton Responsive Pyridone-Containing *N,N,N*-Palladium(II) Pincer Complexes)
- 42th International Conference on Coordination Chemistry, Brest 3-8/07/2016: Poster presentation (Proton Responsive Pyridone-Containing *N,N,N*-Palladium(II) Pincer Complexes)